



Numerical stochastic simulation for remedial activities and risk assessment of an urban groundwater system

Dissertation

submitted to the

Department of Architecture, Civil Engineering and Environmental Sciences

University of Braunschweig – Institute of Technology

and the

Faculty of Engineering

University of Florence

in candidacy for the degree of a

Doktor-Ingenieur (Dr.-Ing.) /

Dottore di Ricerca in Risk Management on the Built Environment ^{*)}

by

Kathrin Helmholz

Born 17.03.1983

from Osterburg, Germany

2011

^{*)} Either the German or the Italian form of the title may be used.

ACKNOWLEDGMENT

This thesis is based on my research work at the Leichtweiß-Institute for Hydraulic and Water Resource Engineering (LWI) of the Technische Universität Braunschweig in the Department of Hydrology, Water Management and Water Protection during the years 2008 to 2011 within the International Graduate College 802 “Risk Management of Natural and Civilization Hazards on Buildings and Infrastructure” of the Deutsche Forschungsgemeinschaft.

First of all, I would like to thank Professor Dr. Matthias Schöniger for giving me the opportunity of this doctoral research, for his guidance and support in the pursuit and completion of this thesis. He was always ready to offer his help and advice with a sympathetic ear.

Furthermore, I would like to thank Professor Dr. Caporali from the University of Florence for agreeing to be my second reviewer of the PhD work. She had access to me at any time during my research stays in Florence. Moreover, I would like to thank her for the freedom to develop my own ideas and concepts.

In addition, thanks to Professor Dr. Peil and Professor Dr. Borri for giving me the possibility to be a member of this International Graduate College. It was an exceeding adventure and a personal gain. Special thanks go to my project-partner Tillman who tried to find a solution for formulating a groundwater risk assessment and who has had the power of endurance during the up and downs in the process of field data collection. For great collaboration and co-advicing, I would like to thank Prof. Dr. Haarstrick.

I owe great thanks to Prof. Dr. Meon who provided me the opportunity to be part of his department and his support. He was always open for questions and helpful in every possible way. My special thanks go to Karo and Marlene, the most adorable women. I think together we could feel ready to take on anything. In addition, I thank Christoph for the funny talks and his support during my trip into the programming world. Of course, I am grateful to have had the privilege of working with all the other colleagues. I would like to thank Klaus Schleicher and Detlef Duncker for their technical support, especially with the realization of field tests.

I would especially like to express my gratitude to my parents for their infinitive support of each previous project of my life. Supplementary, I am grateful to my grandparents who were always interested in my work.

Last but not least, my special gratefulness goes to Christian. You had patience within good time and bad time through the last years. The most difficult challenge was to propagate confidence in unpromising times.

ABSTRACT

Groundwater systems are under enormous hazards in urban areas. Urbanization influences the behavior and compositions of the subsurface system. This leads to adverse hydrological, aquifer quality and socio-economic effects which compromise sustainability. The European Environmental Agency (EEA) estimates a number of 100,000 polluted sites in European countries, many of them contaminated with chlorinated hydrocarbons (EEA 2005). To reduce these impacts, an application of a groundwater risk assessment management is essential.

The present dissertation contains a contribution to groundwater risk identification of an urban aquifer contaminated with chlorinated ethenes, which discharges to adjacent hydrosystems. In this process, the hydrodynamic impact on a regional chlorinated ethenes dispersal of an urban groundwater and surface water system is quantified. The aim is a determination of spatial probability of concentration occurrences isolines (spcois) on a regional scale under average and extreme conditions. The computation of the spcois is based on steady-state and transient 3D multi-species transport simulations of an unconfined aquifer.

For solving the formulated problem, an aquifer reconstruction by coupling of conventional and geo-stochastic simulations were performed to estimate parameter uncertainties. Furthermore, a Direct push technique was applied for a downscale part of the model domain to evaluate the implemented hydraulic parameters of the reconstructed subsurface model. A hydrograph analysis was performed to identify appropriate initial and boundary conditions. The calibrated multi-species transport model was subjected to a Monte Carlo simulation. Seven flow and transport-relevant parameters were ranged n-times from a probability distribution to compute spcoi of the contaminated site.

The thesis shows that hydrodynamics represent a crucial risk factor in the field of urban groundwater risk identification. Especially, the pollutant dispersal pattern is affected spatially and temporally. Even through the Monte Carlo approach, a future pollutant passage into the adjacent ecosystems could be identified including its occurrence probabilities. The PhD research is assigned to a source-pathway-receptor approach according to McKnight et al. (2010). Indeed, this approach contains a 3D multi-species transport model including different hydrological dynamics.

This approach was implemented in cooperation within the framework of the International Graduate College 802 “*Risk Management of Natural and Civilization Hazards on Buildings and Infrastructure*”.

TABLE OF CONTENT

1	Introduction	1
2	Scope of the work.....	5
3	Groundwater risk assessment formulation.....	7
4	Methodical Approach	11
4.1	Characterization of spatial and temporal process parameters	14
4.1.1	Geological parameter identification	15
4.1.2	Chemical parameter identification	24
4.2	Reconstruction Techniques of the subsurface.....	30
4.2.1	Reconstruction of the homogeneous subsurface.....	30
4.2.2	Geo-stochastic aquifer reconstruction	32
4.2.2.1	SIS Sequential Indicator Simulation.....	33
4.2.2.2	Results of the geo-stochastic heterogeneous subsurface reconstruction.....	35
4.2.3	Downscale with Hydraulic Profiling Tool (HPT)	39
4.3	Dynamic influence on the spreading pattern	42
4.3.1	Climatic data	44
4.3.2	Hydrological data	46
4.3.3	Time series in the Finite Element model.....	50
4.4	Numerical Solution method	52
4.4.1	Treatment of the free-surface.....	55
4.4.2	Numerical aspects of the Finite Element method	56
4.4.3	Time step controller description.....	56
4.4.4	Ensemble realization by application of Monte Carlo technique	58
4.5	Model development, calibration and application related to risk identification	64
4.5.1	Homogeneous multi-species groundwater model.....	65
4.5.1.1	Hydro-geological model.....	65
4.5.1.2	Initial and boundary condition of the multi-species groundwater model	67
4.5.1.3	Kinetic multi-species transport materials.....	70
4.5.2	Heterogeneous multi-species groundwater model.....	73
4.5.2.1	Hydro-geological model.....	73
4.5.2.2	Initial and boundary condition of the multi-species groundwater model	75
4.5.2.3	Kinetic Multi-species transport materials.....	76
4.5.3	Groundwater-surface water interaction related to risk identification.....	76
4.5.3.1	Type of model coupling	77
4.5.3.2	Application of the externally coupling.....	78
4.5.3.3	Coupling of the time period 12/11/2009–12/12/2010	80
4.5.3.4	Coupling of the 20-year flood (HQ ₂₀)	81
4.5.3.5	Coupling of a low flow (NQ)	84

5	Presentation of different model scenario outputs	87
5.1	Groundwater flow computation.....	88
5.2	Multi-species transport computation.....	97
5.3	Model results of probability of concentration occurrences	103
5.3.1.1	Probability isolines of the homogeneous subsurface model.....	103
5.3.1.2	Probability isolines of the heterogeneous subsurface model.....	105
5.4	Results of the groundwater – surface water interaction related to risk identification	107
5.4.1	Results of the timer period of the 12/11/2009–12/11/2010	107
5.4.2	Results of a 20-year flood (HQ ₂₀)	111
5.4.3	Results of a low flow (NQ).....	114
6	Discussion and Outlook	118
7	List of Literature	127
A	Appendix Simulation settings of the different groundwater flow and transport models	139
B	Appendix Geostochastic reconstruction technique – theoretical background.....	152
B.1	Theory of the spatial-dependent variables.....	152
B.2	Calculation of the spatial variance.....	153
B.3	Anisotropy.....	155
B.4	Histogram	155
B.5	Kriging technique	157
B.6	Pre-processing of the data set	158
C	Appendix Model scenario outputs of selected boundary conditions	165
C.1	Mass transport results of the steady-state flow and transient transport conditions	165
C.2	Mass transport results of the transient flow and transient transport conditions	166
C.3	Results of the Monte Carlo simulation of the homogeneous aquifer	169
C.4	Results of the Monte Carlo simulation of the heterogeneous aquifer.....	171

LIST OF FIGURES

Figure 1-1	2D illustration of the use of multiple data sets to constrain interpretations of geological heterogeneity at a regional site for a numerical groundwater model. The circles represent the extent of validity of each single information source. Source: Wingle et al. (1997), modified.	3
Figure 1-2	Overview of the case of damage of the urban contaminated groundwater system. The bordering ecosystems lake and river at the west side of the investigation area are of particular importance.....	4
Figure 3-1	Applied source-pathway-receptor concept of a groundwater risk assessment with corresponding fundamental aspects and work steps including data collection, exposure assessment and toxicity assessment, which leads into a risk characterization. The considered aspects of this approach are data collection, an exposure assessment and a risk characterization to provide a support for decision makers.....	8
Figure 4-1	Schematic illustration of the used aquifer models and their applications for a risk identification.	12
Figure 4-2	Hydro-geological system description and upscaling for a reconstruction of a structure model on different scales. Hard information of the laboratory and local scale must be regionalized by using interpolation techniques or geo-stochastic simulations to construct a balance region including storage and volume flows.	13
Figure 4-3	Schematic vertical geological cross section profile (drilling profile B8, B6 and B7) of the investigation area.	15
Figure 4-4	Definition of 3D anisotropic conductivity. Modified rotation definition of Eulerian angles in 3D (Diersch, 2009).	17
Figure 4-5	Left side: Regional model area. Application of hydraulic conductivities by use of slug&bail tests at selected wells. Right side: downscale model area. The hydraulic conductivities result from a Direct push method, so-called "Hydraulic Profiling Tool (HPT)". The outcome is a detail knowledge of the hydraulic conductivity distribution of the subsurface and a precise geological layer-configuration. The element size of each model is set by means of parameter assignment.....	19
Figure 4-6	Measured hydraulic conductivities of the model domain by slug&bail test at selected wells. This hydraulic conductivity can be seen as an integral over the complete borehole depth. The result is that the measured K_F -value is an average estimated parameter from different hydro-geological layers. Therefore, an application of Direct push method at the downscaled area (cf. figure 4-5) was performed.....	19

Figure 4-7	Picture A) shows the transfer coefficient Φh^{in} as colmation layer parameter of a river bed for inflowing conditions. The surface water streams into the aquifer system. The exfiltration of groundwater into a river through the colmation layer is shown in picture B). Characterized by the transfer rate Φh^{out} . Source: Diersch, 2009, modified. C) Surface water model area with the area of transfer rate validity derived from the soil sampled of the colmation layer (yellow domain).....	21
Figure 4-8	Sampling of the colmation layer. Extraction of the material by use of liner technique.....	22
Figure 4-9	Grading curves of the three colmation layer samples with corresponding K_f -value.	23
Figure 4-10	Causes for velocity variations at different investigated scales. Micro-dispersion is dominant at the pore scale. The hydraulic profiling technique shows small scale macro dispersion. An aquifer realization exhibits a large-scale macro-dispersion.....	27
Figure 4-11	Degradation chain of chlorinated ethenes; degradation is assumed as first-order kinetic. Source: Greis et al. (2011).....	28
Figure 4-12	Schematic view of the geological borehole data transfer from point information of the stratigraphy to regional layer structures by use of Inverse Distance interpolation. Visualized with Visual MODFLOW.	31
Figure 4-13	Area of the hydro-geological model. The extension from north to south is 750 m and from east to west 680 m. The complete model has an area of 0.4 km ²	32
Figure 4-14	Histogram of a coded indicator data set. The indicator portion is denoted with percentage. The line represents the cumulative distribution function of the indicator classes.	36
Figure 4-15	Fifth aquifer-realization of the reconstructed parameter field. Classified into four indicator groups. The reconstructed parameter field is implemented in the heterogeneous subsurface approach. Red: indicator 1, green: indicator 2, turkey: indicator 3 and blue: indicator 4 (cf. table 4-6).....	37
Figure 4-16	Probability of occurrence of most frequently generated indicator pro cell from 100 realizations for a range of 35% up to 50% (above) and 70% up to 85% (below).	38
Figure 4-17	Illustration of the percentage probability occurrence of the indicators 1 – 2.	38
Figure 4-18	Illustration of the percentage probability occurrence of the indicators 3 – 4.	39
Figure 4-19	Illustration of the Direct push method for a hydraulic profiling. Source: Kensas Geological Survey.....	40
Figure 4-20	Hydraulic profile cross section with corresponding K_f -values ($<10^{-5}$ - $>10^{-3}$ ms ⁻¹) and the resulting hydro-geological cross section with electric conductivity.....	41

Figure 4-21	Downscaled numerical hydro-geological structure model of the investigation domain by use of 12 HPT profiles. Cross section view of the layer configuration through the model area from HPT9 to HPT3 in groundwater flow direction.	42
Figure 4-22	Dynamic aspects of a time-dependent groundwater simulation. Illustration of the individual volumes of a groundwater balance equation. Differentiation between time varying parameters (t) like groundwater subsurface inflow or groundwater recharge, which are defined as time-varying function in the numerical model and numerical calculated parameters like groundwater discharge or groundwater outflow into rivers or lakes.	43
Figure 4-23	Precipitation, evaporation and snow height of Braunschweig (source: DWD) from 12/11/09-16/01/11. Based on this measured values the groundwater recharge was calculated by a degree-day method and defined in the groundwater model in from of a time-varying function.	44
Figure 4-24	Land cover and assignment of groundwater recharge with database associated menu in the groundwater model. Spatial data like groundwater recharge are linked by an ESRI shape file with attribute data. The linking is controlled via ID's of single spatial elements. Each ID is integrated in the Finite Element model as a time-varying function or parameter.	45
Figure 4-25	Recorded groundwater and river water levels of the model area from 12/11/09–16/01/11. The dynamic data are necessary as time-dependent boundary conditions of the transient groundwater model and for the model calibration.	46
Figure 4-26	Schematic illustration of effluent and influent hydraulic conditions between river and groundwater level of the investigation area depending on climatic events (snowmelt, groundwater recharge and precipitation).	47
Figure 4-27	Relationship between groundwater and river water level of the observed area from 23/09/2010–16/01/11.	48
Figure 4-28	Diagram of groundwater tables from daily measurements between 12/11/2009–12/11/2010 of well SB1, Nr.1, B16 and B1.	48
Figure 4-29	Evolution of the relationship between groundwater table of well SB1 and B16 and the river water table in a flood event resulting from snowmelt event (19/02/2010-13/03/2010).	49
Figure 4-30	Fluid-Flux time-varying function [md^{-1}] for the transient model. The 1 year hydrograph is defined as 2 nd Neumann boundary conditions (fluid flux) with a cyclic occurrence of 70 years (simulation period).	50
Figure 4-31	Surface water time varying function [unit m.a.s.l. d^{-1}] for the transient model. The 1 year hydrograph is defined as 3 rd Cauchy boundary conditions (transfer) with a cyclic occurrence of 70 years (simulation period).	51
Figure 4-32	Groundwater recharge time-varying function [unit $10^{-4} \text{ mm d}^{-1}$] for the transient model. The 1 year hydrograph is defined as inflow on top with a cyclic occurrence of 70 years (simulation period).	52

Figure 4-33	Moving mesh BASD technique of parameter adaption applied to 3D free-surface. Example of a contaminated groundwater system with different groundwater table increase situations caused by precipitation, subsurface inflow or bank filtration. At the beginning of the simulation the contamination is located in the saturated zone. The consequent of groundwater level increase and mesh adaption is the concentration achievement. Diersch, 2009, modified.	55
Figure 4-34	Comparison between CPU times and number of time steps of a cross-sectional vertical groundwater problem with triangle mesh, which is fully unstructured and locally refined in a layered geometry for a PCG and SAMG equation solver. The SAMG solver is superior to PCG because PCG requires more iteration. The CPU time of SAMG is three times smaller than for PCG. Diersch, 2009, modified.	56
Figure 4-35	Predictor-corrector time step scheme for transient flow simulation with adaptive time stepping.	57
Figure 4-36	Performed workflow of the thesis including Monte Carlo simulation by use of the geo-stochastic program UNCERT and the numerical simulation program FEFLOW. The combination of these two techniques is a generation of spatial probability concentration occurrence isolines (spco).	59
Figure 4-37	Density function of the Gaussian distribution of the generated random variables of the hydraulic conductivity, porosity, longitudinal and transversal dispersivity, sorption and reaction rate.	61
Figure 4-38	Density function of the Gaussian distribution with standard deviation and confidence interval as well as the derivation of the 2σ standard derivation.	62
Figure 4-39	Communication architecture of the Rubens-Cluster of the University of Siegen.	62
Figure 4-40	Application workflow of the creation of probability concentration occurrence isolines by use of a Monte Carlo simulation including a range of seven selected parameters (upper illustration). This example shows exemplarily the development of a DCE probability isoline after 50 a and 70 a.	63
Figure 4-41	Overview of the different generated groundwater transport models and the coupled groundwater-surface water model.	64
Figure 4-42	Horizontal boundary of the investigation area with hard data information from drilling profiles (red points) in the Finite Element model. Right side: Reconstruction of the homogeneous aquifer after a petrographic approach. ...	65
Figure 4-43	Geological cross section of the homogeneous subsurface body with hydraulic conductivity and corresponding porosity for each geological substrate.	66
Figure 4-44	Groundwater table map of the homogenous groundwater model based on measurements of the 12/11/2009. Interpolation by Ordinary Kriging technique. Right side: groundwater recharge map with differentiation between covered and free surface.	67

Figure 4-45	Time-dependent groundwater recharge assignment of the homogenous and heterogeneous groundwater transport model. ID 2 represents the area where groundwater recharge occurred with the calculated time-varying function. ID 1 represents an area where the surface is compacted, no inflow on top is assumed.	68
Figure 4-46	Defined steady-state flow boundary conditions of the homogeneous groundwater model. Left side, lake water level as Dirichlet boundary conditions and river water level as Cauchy boundary conditions. Right side, groundwater subsurface inflow as Neumann boundary condition.	69
Figure 4-47	Defined transient flow boundary conditions of the homogenous groundwater model. Left side, lake water level as constant Dirichlet boundary condition and river water level as time-varying Cauchy boundary conditions. Right side, groundwater subsurface inflow as time-varying Neumann boundary condition.	69
Figure 4-48	Transport boundary condition of the transient multi-species homogenous and heterogeneous groundwater model. Implementation of a time-varying mass boundary in layer 5-6 in the homogenous model and layer 7-10 in the heterogonous model.	70
Figure 4-49	Distribution of the longitudinal dispersivity in the homogenous multi-species transport model. The longitudinal dispersivity belongs to the layer-related parameters and is applied for all species.	71
Figure 4-50	Feflow Reaction Kinetics Editor for precompiled rate expression of the degradation-type kinetics for PCE. Modified. Source: Diersch, 2009.	73
Figure 4-51	Horizontal boundary of the investigation area with hard data information from drilling profiles (red points) in the Finite Element model. Right side: Reconstruction of the heterogeneous aquifer with a constant layer thickness of 1 m orientated by the DTM.	74
Figure 4-52	Schematic representation of the decoding of the geo-stochastic generated parameter fields into discrete hydraulic conductivity values for an aquifer-realization.	74
Figure 4-53	Heterogeneous subsurface and geological cross section of the groundwater body with geo-stochastic generated hydraulic conductivity and corresponding porosity for each geological substrate.	75
Figure 4-54	Distribution of the discrete longitudinal dispersivity based on a geo-stochastic generated parameter field.	76
Figure 4-55	Operation mode of an external coupling using the example of two connected nodes. M represents the model results, BC boundary condition and t the simulation time, modified. Source: Becker, 2010.	78
Figure 4-56	Flux-limiting infiltration from a river bed formulated by a maximum flux constraint $Q_{max}(t)$. Source: Diersch, 2009.	79

Figure 4-57	Schematic illustration of the groundwater-surface water model coupling of the investigation area. The coupling is operated by use of the 3 rd boundary condition (Cauchy-type) in the groundwater model. This boundary type represents a transfer between river and aquifer.....	79
Figure 4-58	Discharge hydrographs of the gauge station „Groß Schwülper“ and „Harxbüttel“ from the 12/11/2009–12/11/2010 and the calculated discharge of the gauge station „Heizkraftwerk Mitte“.....	80
Figure 4-59	Boundary conditions of the 1D surface water model (MIKE11). Inflow boundary condition represents a discharge hydrograph from 12/11/09–12/11/10 and downstream condition is defined as a water level hydrograph of the river.	81
Figure 4-60	Maximum discharge values from 1926–2006 of the gauge station “Groß Schwülper”.	82
Figure 4-61	Recurrence intervals of the gauge station “Groß Schwülper” based on the statistical analysis of 50 maximum discharge values from 1956–2006.....	82
Figure 4-62	Discharge hydrographs of the gauge station „Groß Schwülper“ and „Harxbüttel“ from the 12/11/2001–12/11/2002 and the calculated discharge of the gauge station „Heizkraftwerk Mitte“. This discharge hydrographs represent a calculated HQ ₂₀	83
Figure 4-63	Boundary conditions of the 1D surface water model (Mike11). Inflow boundary condition represents a discharge hydrograph from 12/11/2001–12/11/2002 and downstream condition is defined as a water level hydrograph of the gauge station “Heizkraftwerk Mitte”.	83
Figure 4-64	Discharge hydrographs of the gauge station „Groß Schwülper“ and „Harxbüttel“ from the 12/11/2000–12/11/2001 and the calculated discharge of the gauge station „Heizkraftwerk Mitte“. This discharge hydrographs represent a calculated NQ.	84
Figure 4-65	Boundary conditions of the 1D surface water model (Mike11). Inflow boundary condition represents a discharge hydrograph from 12/11/2000–12/11/2001 and downstream condition is defined as a water level hydrograph of the gauge station “Heizkraftwerk Mitte”.	85
Figure 5-1	Computed groundwater level isolines of the homogeneous and heterogeneous steady-state groundwater flow model with corresponding Scatter Plot of the measured and computed hydraulic heads.	89
Figure 5-2	Water budget of the homogeneous subsurface model of steady-state groundwater flow conditions.	90
Figure 5-3	Fluid flux mass balance of the homogeneous steady-state groundwater flow model with percentage of the boundary conditions for inflow and outflow.	91
Figure 5-4	Water budget of the heterogeneous steady-state groundwater flow model.	91
Figure 5-5	Fluid flux mass balance of the heterogeneous steady-state groundwater flow model with percentage of the boundary conditions for inflow and outflow.	92

Figure 5-6	Groundwater hydrographs of observation well B16 and SB1 from the 12/11/2009-12/11/2010. Comparison between computed (blue) and groundwater levels (red) of the transient homogeneous groundwater flow models and illustration of water level differences.	93
Figure 5-7	Fluid flux mass balance of the homogeneous transient groundwater flow model with percentage of the boundary conditions for inflow and outflow.	94
Figure 5-8	Groundwater hydrographs of observation well B16 and SB1 from the 12/11/200-12/11/2010. Comparison between computed (blue) and groundwater levels (red) of the transient heterogeneous groundwater flow models and illustration of water level differences.	95
Figure 5-9	Fluid flux mass balance of the heterogeneous transient groundwater flow model with percentage of the boundary conditions for inflow and outflow.	97
Figure 5-10	Comparison of computed and measured pollutant concentrations (PCE, TCE, DCE and VC) of the homogeneous model for steady-state flow and transient transport conditions. Source: Greis et al., 2011.	98
Figure 5-11	Comparison of the measured and computed PCE mass concentration of the homogeneous steady-state flow and transient transport model by variation of the diffusion coefficient. Source: Greis et al., 2011.	99
Figure 5-12	Comparison between measured and computed PCE mass concentration of the homogeneous steady-state flow and transient model by variation of hydraulic conductivity. Source: Greis et al., 2011.	100
Figure 5-13	Correlation of measured and computed results for TCE mass concentration at several observation wells; error bars indicate range of TCE concentration in the Monte Carlo simulation. Source: Greis et al., 2011.	100
Figure 5-14	Computed contaminant isolines (1.0 mg l^{-1} and 0.1 mg l^{-1}) of the homogeneous and heterogeneous steady-state flow and transient transport model for PCE, TCE, DCE and VC.	101
Figure 5-15	Computed 0.05 mg l^{-1} concentration isolines of the transient homogeneous and heterogeneous multi-species transport model for 50 a and 70 a simulation time.	102
Figure 5-16	Computed 80% PCE and TCE probability of concentration isolines of the homogeneous subsurface model of 50 a and 70 a simulation time based on a Monte Carlo simulation.	104
Figure 5-17	Computed 80% DCE and VC probability of concentration isolines of the homogeneous subsurface model of 50 a and 70 a simulation time based on a Monte Carlo simulation.	104
Figure 5-18	Computed 80% PCE and TCE probability of concentration isolines of the heterogeneous subsurface model of 50 a and 70 a simulation time based on a Monte Carlo simulation.	106
Figure 5-19	Computed 80% DCE and VC probability of concentration isolines of the heterogeneous subsurface model of 50 a and 70 a simulation time based on a Monte Carlo simulation.	107

Figure 5-20	Result of the coupled groundwater-surface water model for the homogeneous transient model for 1 year simulation time (12/11/2009-12/11/2010). The figure displays the computed river water level (blue) and groundwater level (red) with the corresponding computed groundwater exfiltration and river bank filtration (transfer, black).....	108
Figure 5-21	Result of the coupled groundwater-surface water model for the heterogeneous transient model for 1 year simulation time (12/11/2009-12/11/2010). The figure displays the computed river water level (blue) and groundwater level (red) with the corresponding computed groundwater exfiltration and river bank filtration (transfer, black).....	109
Figure 5-22	Comparison between the homogeneous and heterogeneous model concerning to the calculated transfer for 1 year simulation time.....	110
Figure 5-23	Comparison between computed transfer and measured daily river water level of the homogeneous groundwater model for the time period 12/11/2001–12/11/2002 which represents a HQ ₂₀ conditions.....	111
Figure 5-24	Fluid flux mass balance of the homogeneous transient groundwater flow model with percentage of the boundary conditions for inflow and outflow. Simulation of HQ ₂₀ conditions.....	112
Figure 5-25	Comparison between computed transfer and measured daily river water level of the heterogeneous groundwater model for the time period 12/11/2001–12/11/2002 which represents a HQ ₂₀ conditions.....	112
Figure 5-26	Fluid flux mass balance of the heterogeneous transient groundwater flow model with percentage of the boundary conditions for inflow and outflow. Simulation of HQ ₂₀ conditions.....	113
Figure 5-27	Comparison between computed transfer and measured daily river water level of the homogeneous groundwater model for the time period 12/11/2000–12/11/2001 which represents a NQ conditions.....	114
Figure 5-28	Fluid flux mass balance of the homogeneous transient groundwater flow model with percentage of the boundary conditions for inflow and outflow. Simulation of NQ conditions.....	115
Figure 5-29	Comparison between computed transfer and measured daily river water level of the heterogeneous groundwater model for the time period 12/11/2000–12/11/2001 which represents a NQ conditions.....	115
Figure 5-30	Fluid flux mass balance of the heterogeneous transient groundwater flow model with percentage of the boundary conditions for inflow and outflow. Simulation of NQ conditions.....	116
Figure 5-31	Results of the 3 different hydrological dynamic scenarios of the coupled homogeneous and heterogeneous groundwater-surface water models including an risk interpretation for the bordering ecosystems based on effluent and influent conditions.	117

Figure 6-1	Evaluation of spatial probability of 0.5 mg/l DCE concentration occurrences for an advective transport to adjacent hydrosystems based on a Monte Carlo simulation approach with different hydrological boundary conditions (b.c., cf. chapter 4.5) and temporal & spatial assignment of groundwater recharge. Calibrated computed hydraulic heads with available observation wells.	126
Figure A-1	First order degradation equation for the used species (PCE, TCE, DCE and VC) of the transport models. Implementation in the Finite Element program via a kinetic reaction editor.	150
Figure A-2	First order degradation equation for the used species (ethane and Cl) of the transport models. Implementation in the Finite Element program via a kinetic reaction editor.	151
Figure B-1	Parameter used to calculate semi-variogram. Source: England et al. (1988).	154
Figure B-2	Shape of the spherical, exponential, Gaussian and Hole-effect model equations. Source: (Wingle et al. 1997). Modified.	154
Figure B-3	Illustration of the histogram of the input parameter of indicator class	158
Figure B-4	Illustration of the histogram of the input data (blue) and the geo-stochastic generated realization number five (red) as well as the percentage deviation. Source: (Nienstedt 2011).	159
Figure B-5	Finite Element mesh of the investigation area and corresponding discretization of 770 m x 760 m of the geo-stochastic interpolation mesh.	160
Figure B-6	Experimental indicator variogram in horizontal and vertical direction for indicator 1 and 2.	161
Figure B-7	Experimental indicator variogram in horizontal and vertical direction for indicator 3 and 4.	161
Figure B-8	Probability of occurrence of the most frequency generated indicator pro grid element from 100 realizations for the range 35% up to 85%.	163
Figure B-9	Demonstration of the probability of indicator 1, 2, 3 and 4 from 100 Monte Carlo simulations with a probability of occurrence of at least 25% and at least 65%.	164
Figure C-1	Contaminant isolines (0.5 mg/l ⁻¹ and 0.05 mg/l ⁻¹) of the homogeneous and heterogeneous steady-state flow and transient transport model for PCE, TCE, DCE and VC.	165
Figure C-2	Computed 1.0 mg/l ⁻¹ concentration isolines of the transient homogeneous and heterogeneous multi-species transport model for 50 a and 70 a simulation time.	166
Figure C-3	Computed 0.5 mg/l ⁻¹ concentration isolines of the transient homogeneous and heterogeneous multi-species transport model for 50 a and 70 a simulation time.	167

Figure C-4	Computed 0.02 mg/l ⁻¹ concentration isolines of the transient homogeneous and heterogeneous multi-species transport model for 50 a and 70 a simulation time.....	168
Figure C-5	Computed 50% PCE and TCE probability of concentration isoline of the homogeneous subsurface model of 50 a and 70 a simulation time based on a Monte Carlo simulation.	169
Figure C-6	Computed 50% DCE and VC probability of concentration isoline of the homogeneous subsurface model of 50 a and 70 a simulation time based on a Monte Carlo simulation.	169
Figure C-7	Computed 90% PCE and TCE probability of concentration isoline of the homogeneous subsurface model of 50 a and 70 a simulation time based on a Monte Carlo simulation.	170
Figure C-8	Computed 90% DCE and VC probability of concentration isoline of the homogeneous subsurface model of 50 a and 70 a simulation time based on a Monte Carlo simulation.	170
Figure C-9	Computed 50% PCE and TCE probability of concentration isoline of the heterogeneous subsurface model of 50 a and 70 a simulation time based on a Monte Carlo simulation.	171
Figure C-10	Computed 50% DCE and VC probability of concentration isoline of the heterogeneous subsurface model of 50 a and 70 a simulation time based on a Monte Carlo simulation.	171
Figure C-11	Computed 90% PCE and TCE probability of concentration isoline of the heterogeneous subsurface model of 50 a and 70 a simulation time based on a Monte Carlo simulation.	172
Figure C-12	Computed 90% DCE and VC probability of concentration isoline of the heterogeneous subsurface model of 50 a and 70 a simulation time based on a Monte Carlo simulation.	172

LIST OF TABLES

Table 4-1	Literature values of the hydraulic conductivity for different substrate types of a porous media and the derived values for the numerical groundwater model.	18
Table 4-2	Calculated transfer rates of three sampled layers with corresponding thickness and hydraulic conductivity.	23
Table 4-3	Longitudinal and transversal dispersivity for the geological layer of the Finite Element transport model. Investigated by Greis (2011).	27
Table 4-4	First order kinetic reaction rate for different species (PCE, TCE, DCE and VC) in the Finite Element model. Investigated by Greis (2011).	28
Table 4-5	Linear sorption coefficients of the multi species. Investigated by Greis (2011).	29
Table 4-6	Classification of the substrates of the geological profiles into four indicator classes for the hydraulic conductivity.	36
Table 4-7	Parameter of the adapted variogram models as well as the calculated root-mean-square deviation and anisotropy factor. Investigated by Nienstedt (2011).	37
Table 4-8	Degree-day factor a_d in mm/(°Cd) for different vegetation covers after Maniak (1997) with basis temperature $T_b = 0^\circ\text{C}$	45
Table 4-9	Adapted hydraulic conductivities in x-, y- and z-direction for the Finite Element groundwater model of the model area with appendant storativities of each layer.	66
Table 5-1	Statistical error parameters of the steady-state groundwater flow simulation.	89
Table 5-2	Statistical error parameters of the transient groundwater flow simulation.	97
Table A-1	Model setup of the homogeneous steady-state flow transient transport groundwater model.	140
Table A-2	Model setup of the heterogeneous steady-state flow and transient transport groundwater model.	142
Table A-3	Model setup for the homogeneous transient flow transient transport groundwater model.	144
Table A-4	Model setup of the heterogeneous transient flow transient transport groundwater model:	146
Table A-5	Model setup of the transient surface water model.	148

LIST OF ABBREVIATIONS

a	Year
a_d	Degree-day factor
AMG	Algebraic Multigrid
α_L / α_T	Average interstitial velocity (longitudinal and transversal)
α	Phase indicator
BASD technique	Best-Adaption-to-Stratigraphic-Data technique
b.c.	Boundary condition
BF_{River}	Bank filtration
β_L / β_T	Longitudinal and transversal dispersivity of porous media
CHC	Chlorinated hydrocarbons
C_{eq}	Equilibrium solute concentration
C_i	Value of the field variable at a node
C_R	Courant Number
C_k^α	Concentration of species k of α -phase
d	Colmation layer thickness
DCE	Dichlorethene
D_L / D_T	Dispersion (longitudinal and transversal)
D_k^α	Tensor of hydrodynamic dispersion of species k
$D_{d_k}^\alpha$	Coefficient of molecular diffusion of species k of f -phase
EC	Electrical conductivity
F_O	Neumann criterion
$GW_{Discharge}$	Groundwater discharge
$GW_{Recharge}$	Groundwater recharge
$GW_{Subsurface}$	Groundwater subsurface
$GW_{Outflow}$	Groundwater outflow into a river
h	Hydraulic head
h_1^R, h_2^R	Prescribed boundary values of hydraulic head h
HPT	Hydraulic Profiling Tool
HQ ₂₀	20-year Flood
I	Indicator
K	Hydraulic conductivity (tensor)
K_f	Hydraulic conductivity
K_0^{in}	Colmation layer conductivity
K_H	Henry distribution coefficient
$k_{1,...,n}$	Sorption coefficient (HENRY)

k_m	Bulk rate constant
m	Node number of the mesh
m.a.s.l.	Meter above sea level
MAE	Mean average error
MCs	Monte Carlo simulation
n_{eff}	Effective (drainable / fillable) porosity
N_i	Interpolation function
N_r	Number of reaction
NQ	Low Flow
PCE	Tetrachlorethene
P	Precipitation
P_e	Peclét Number
Q_i	Groundwater discharge component
Q_k^α	Zero-order nonreactive production term of species k
$\Phi_h^{in} / \Phi_h^{out}$	Directional coefficient of in-transfer and out-transfer
Φ_h	Transfer coefficient
Ω	Problem domain
pdf	Density function
RMSE	Root mean squared error
ΔR	storage
r_r	Rate of reaction
R_k	Bulk rate of chemical reaction of species k
SIS	Sequential Indicator Simulation
spcoi	Spatial probability concentration occurrence isoline
TCE	Trichlorethene
T_b	Basis temperature
T_L	Air temperature
V	Darcy velocity
VC	Vinyl chloride
z_c	Cut-off value
μ	Standard deviation
$\Delta x / \Delta y$	Investigation dimension
Δz	Aquifer thickness

1 Introduction

In numerical studies, e.g. Natarajan et al. (2010), Clement et al. (2000), Zheng et al. (2008), Prommer et al. (2002) and Mao et al. (2006), a growing number of transport models have been developed for solving complex multi-species transport problems in porous media regarding to the dynamic movements of the fluid phase in the saturated and unsaturated zone, and their characteristic processes in the subsurface.

One of the mostly used groundwater model beside the Finite Element method program *FEFLOW 6.0x* (Wasy GmbH, Berlin) is the program *MODFLOW* (Modular three-dimensional Finite-Difference ground-water model) of the U.S. Geological Survey (1988). This program package developed by Harbaugh and McDonald (1996) is used to describe and forecast the behavior of groundwater. In the last years, numerous scientists e.g. Vilhelmsen et al. (2011), Faunt et al. (2011), Carroll et al. (2009), enhanced the open source code and combined *MODFLOW* with several program packages. Each program attends to the specific characterization of the aquifer system. Zheng (1990) developed a transport model for simulation of advective, dispersion and chemical reaction of dissolved constituents in an aquifer with *MT3D* (Modular 3-Dimension Transport model). *MT3D* is commonly used in contaminant transport modeling and remediation assessment studies. Wang and Zheng (1997) presented the application of *MT3D* for a typical two-dimensional pump-and-treat example to determine the minimum pumping needed to contain an existing contamination plume. Another three-dimensional model *PHT3D*, based on *MODFLOW / MT3DMS* for simulating multicomponent transport in porous media is presented in Appelo et al. (2010). This program can handle the broad range of equilibrium and kinetic reactive processes, including aqueous complexity, mineral precipitation and ion exchange. Johnson et al. (2006) introduced the application of *RT3D* (Reactive Transport in 3-Dimensions) to model field-scale natural attenuation at multiple sites for modeling chlorinated solvents in context of an environmental management strategy that relies on a variety of attenuation process to degrade contaminants. *RT3D* provides several pre-defined packages for biodegradation of oxidisable contaminants consuming one or multiple electron acceptors and for sequential decay chain-type reactions of chlorinated hydrocarbons. Essaid and Bekins (1997) designed the two-dimensional model *BIOMOC* (a multi-species solute-transport model with biodegradation) to simulate zero-order or first-order approximations of biodegradation rates, the growth and decay of several microbial populations performing the transformations and the limitation of microbial growth by lower biomass inhibition. Jang (2005) documented the numerical studies with *TechFlow^{MP}*, a multiphase multi-species contaminant fate and transport analysis system based on a Galerkin Finite Element method. The aim was to investigate the fate and multiphase flow and transport

of volatile organic compounds (VOC) in the subsurface environment, biological transformations of contaminants and in-situ air sparging (IAS).

For solving the multi-species transport equation in this thesis the Finite Element subsurface flow and transport simulation system *FEFLOW 6.0x* was selected. A significant advantage of *FEFLOW 6.0x* for complex geological aquifer structures are the treatment of the free-surface by a so-called BASD (Best-Adaption-to-Stratigraphic Data) technique. In consideration of a Finite Element discretization, it provides an application of a flexible mesh generator, which enables the possibility to implement add-ins like river, lakes and wells (ASCII shp.-file) into the mesh. An adaptive time-step control allows an optimal calculation of long-term simulation with hydrological and chemical dynamic events. Furthermore, the degradation of the chlorinated hydrocarbons was defined and implemented with the integrated *FEMATHEd* editor which offers the opportunity to set different degradation types into the multi-species transport model.

The establishment of a multi-species transport model is based on a multiple data set to constraint interpretations of geological, hydro-geological and hydraulic heterogeneity as well as hydrological and chemical dynamics of the aquifer and bordering ecosystems at a regional site. Figure 1-1 presents the essential data and information source for a numerical groundwater model. Different types of information (borehole data, hydraulic data, chemical data, stratigraphic data etc.) from different sources and contents have to be incorporated. Figure 1-1 points out the individual significance and extent of validity (circles) of each information. However, this information content is failure afflicted because of imprecise data collection or interpretation. Each groundwater model has to attempt to cover the individual information and the best possible solution is an integrated interpolation. Chapter 4 describes the parameter identification, which is necessary to combine all essential information to a complete system, which is transferred into a Finite Element model. The important demand consists in the discretization Δx and Δy (investigation dimension) and Δz (thickness, represented by the stratification). A further challenge regards to the problem of scale¹ transfer. Each information of the research area has its own temporal or spatial scale. Scheibe et al. (2007) refer that it has not been practical or possible to translate detailed knowledge at small scales into reliable predictions of field-phenomena. The multiple scales of the individual information have its own characteristics, which must be determined and comprehend. Techniques must be used to directly and adaptively couple across the model scales to solve the problem of scale transfer. Large-scale phenomena are influenced by processes occurring at smaller scales, the result is to find a compromise, by use of an intelligent parameter identification, to simulate processes at the smallest scales for a domain of engineering significance.

¹ Meaning the temporal and spatial unit at which information is available or required.

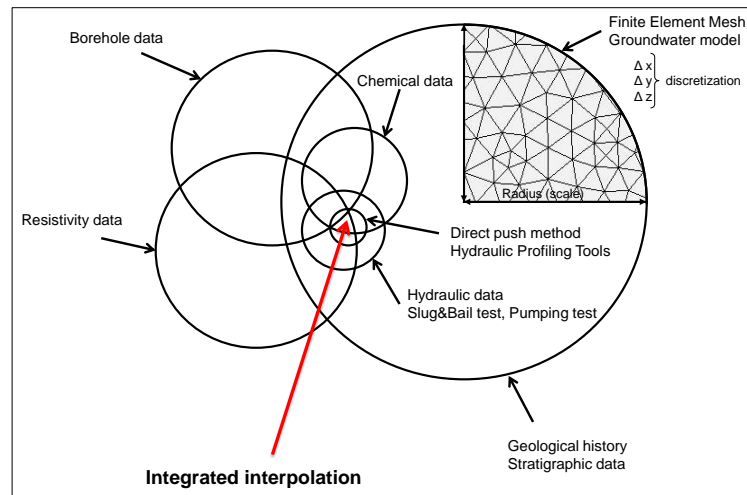


Figure 1-1 2D illustration of the use of multiple data sets to constrain interpretations of geological heterogeneity at a regional site for a numerical groundwater model. The circles represent the extent of validity of each single information source. Source: Wingle et al. (1997), modified.

All collected data of the selected investigation area were determined by field tests. The geological history of the investigation domain was aligned by borehole data. Direct push method like the hydraulic profiling tool (HPT) were used to identify the hydraulic characterization of the urban aquifer. Secondary, slug&bail tests were utilized to calibrate the hydraulic measured field data of the HPT technique. Several observation wells were fitted with divers to record the dynamic of the groundwater table. Observation wells were sampled to investigate the chemical behavior of the contamination. Climatic data for calculating the groundwater recharge were selected by the DWD (Deutscher Wetterdienst Braunschweig). Moreover, they were used to generate different scenarios by use of dynamic boundary conditions. The groundwater recharge was assigned by interpretations of landuse maps. In addition, the bordering ecosystems were investigated regarding to their hydraulic connection and dynamic. The integrated available data provide a wide range of hydro-geological interpretation alternatives. One goal must be to combine all data sets (hard data and soft data like expert knowledge) to find the best possible solution population (Wingle et al., 1997).

However, the geological and hydro-geological data (hard data) which provides the basis for aquifer modeling is dissatisfying during a planning and implementation phase of a groundwater risk assessment. These aquifer models are used as prediction tools and it is indispensable to quantify the data hole. One opportunity to counteract the small data set is a special data pre-processing as well as geo-stochastic calculation-algorithms. Therefore, equiprobable realizations of subsurface parameter fields can be generated from a small data set. These realizations are integrated as an input parameter in the numerical groundwater model. Due to the small range of hard information, soft data must be added to reconstruct the subsurface parameter fields.

Furthermore, uncertainty predictions of the reconstructed aquifer body concerning the underground heterogeneity can be quantified. Based on the realization, probabilities of model uncertainties can be identified before the numerical simulations. In addition, to conventional quality criterion like numerical stability and the comparison of computed and measured data a prediction of the hydro-geological quality is possible.

The presented procedural method of this thesis is executed for an urban contaminated groundwater system in Braunschweig (Low Saxony). The investigation area is located in the northern part of the city and has an area of 0.4 km². A former chemical cleaning company caused a contamination by polynuclear aromatic hydrocarbons (PAH) and chlorinated hydrocarbons (CHC) which is located at the east side of the investigation area. The concentration maximum amounts 40,000 µg l⁻¹. Detailed technical investigations with direct and indirect techniques were instructed by the Environmental Agency.

The contaminated aquifer borders to two different ecosystems (river, lake) which are hydraulically connected (cf. figure 1-2). The commissioned investigations have shown that the groundwater flow is directed to the bordering ecosystem because of the hydraulic gradient. Concerning a risk assessment, this investigation area provides the best requirements to combine numerical and stochastic methods to generate probability of concentration occurrences (spco) of pollutants. The influence of dynamic boundaries on hydrocarbon degradation in groundwater flow direction, a risk analysis by use of spco and the identification of reconstruction uncertainties are taken into account.

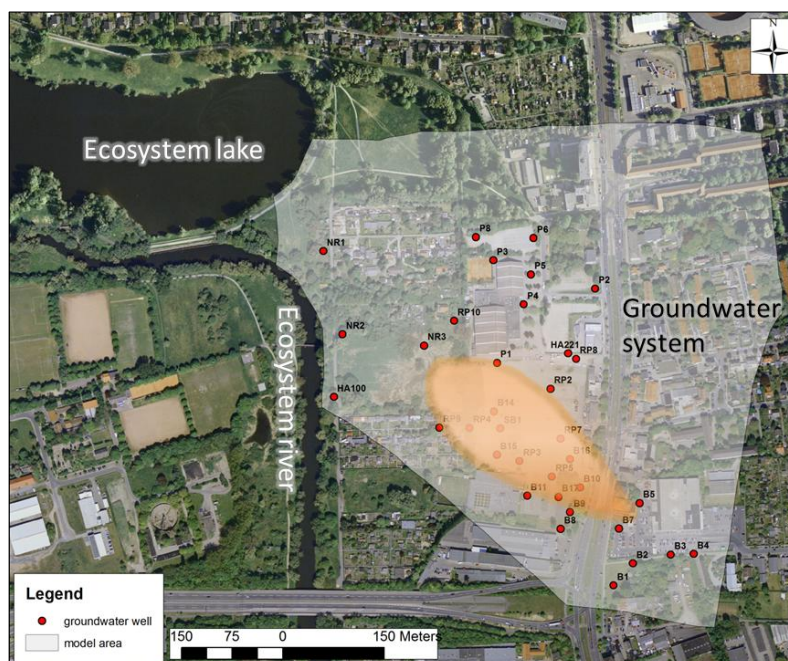


Figure 1-2 Overview of the case of damage of the urban contaminated groundwater system. The bordering ecosystems lake and river at the west side of the investigation area are of particular importance.

2 Scope of the work

The motivation of this thesis is related to a description and prediction of a chlorinated hydrocarbon (CHC) contamination genesis in an urban area (Braunschweig, Lower Saxony). Stochastic and numerical methods are applied to analysis, description and prediction of this regional case of damage. The necessary input parameters originate from the investigation area and were collected by several field campaigns.

The objective of the thesis is the detection of spatial probability concentration occurrences (spco) of the existent contaminants in the subsurface and the nearby hydro-systems involving hydrological dynamics and groundwater-related processes.

The spco of the several pollutants in the groundwater system or bordering hydro-systems is based on a multitude of numerical realizations of flow and transport simulations by use of stochastic generated continuous parameter fields and subsurface structures by a definition of average and extreme hydrological conditions regarding to groundwater recharge by actual infiltrated precipitation, subsurface inflow and interaction with surface water. The hydrological consideration of the different dynamic aspects is of particular importance in regard to spatial mobility of the contamination in the aquifer.

The present research pursues the approach to determine large-scale spreading pattern of a complex CHC contamination by use of measured parameters for a regional scale. For the reconstruction of the geological aquifer structure, two different approaches were performed and compared. The first approach is an aquifer layer-configuration on a traditional interpretation of drilling profiles with a subsequent interpolation of the hard information (borehole data) of the elevation of different aquifer layers. The second reconstruction approach is based on a conditional Sequential Indicator Simulation, which operates similarly with the hard information of the drilling profiles. This geo-stochastic structure analysis was calibrated with a selected area of the model domain by use of a Hydraulic Profiling Tool (HPT) in cooperation with the company geo-log GmbH (Braunschweig) to evaluate the hydraulic behavior of the subsurface soil. Hence, a scale transfer during the subsurface reconstruction is included.

The target of the geo-stochastic analysis after the approach of Journel (1983) is the quantitative and qualitative description of the spatial geological structure for the implementation into the Finite Element mesh. Furthermore, a characterization of the spatial correlation of the hydraulic- and transport-relevant parameters for a stochastic Monte Carlo approach for generating computation-ensembles (cooperation with the *University of Siegen, Department of Information Systems*, 300 CPU cluster) is taken into account. An identification of spco for selected contaminants and mass concentrations results from the application of a

Monte Carlo method to create n-aquifer-realizations with modified input parameters and parameter fields. Two flow material parameters (hydraulic conductivity and porosity) and five transport material parameters (longitudinal and transversal dispersion, reaction rate, sorption and molecular diffusion) were ranged.

Within the framework of the International Graduate College 802 “Risk Management of Natural and Civilization Hazards on Buildings and Infrastructure”, a contribution for decision support systems in terms of a risk identification is provided by application of an urban contaminated groundwater system. The chemical and transport parameter as well as the reaction kinetic equations of the case of damage were determined by a research partnership with the *Institute of Biochemical Engineering* (TU Braunschweig, T. Greis). The dissertation of T. Greis is focused on the biological-chemical aspects concerning a health risk by contaminated groundwater, whereas this thesis is targeted on the additional benefit of geo-stochastic generated ensembles under average and extreme hydrological conditions. The focus of this thesis is the presentation of a compatible procedural combination of hydro-geological and engineering methods by use of reinforced physical models to quantify spatial probability of concentration occurrences of a regional contaminated urban aquifer under different climatic and hydrological scenarios.

Especially, an optimal selection of data information for the numerical groundwater model setup will be pointed out. The present research demonstrates explicit aspects of an interdisciplinary information theory, which builds the fundament of multi-species transport simulation.

3 Groundwater risk assessment formulation

The aim of this chapter is to classify the ecological risk and the integration of the thesis content into the risk assessment framework

The description and analyzing of groundwater risk is relatively new. Several definitions and terminologies were created but differ from each other, which leads to ambiguities. Christensen et al. (2003) stated that fundamental terms are associated with description and characterization of chemical, biological and physical processes leading from risk source to possible consequences / effects. The Royal Society (1992) published a report about the terminology and definitions related to risk management. They defined risk as “the probability that a particular adverse occurs during a stated period of time, or results from a particular challenge” (Royal Society, 1992). According to the Royal Society, a risk assessment includes:

- a) a hazard identification, in which all outcomes potentially leading to harm to humans are analyzed,
- b) an estimation of the magnitude of the consequences,
- c) an assessment of probability of the outcomes and
- d) a risk evaluation, where the results from the first three points are evaluated.

According to Lawrence et al. (2001), the risk assessment of this thesis is based on a source-pathway-receptor approach. The pathway provides the means or route for contamination to reach the receptor. In this present case, the natural pathway is given by the complex aquifer structure in which the groundwater movement builds the transport media. Trolborg (2010) highlights that a given source can only be result in a risk if a complete pathway-linkage exists between the source and the receptor. Subsurface contamination is a hazard, which may be a source of risk if toxic materials reach receptors by various pathways. These facts are given by the selected investigation area.

The investigated contamination plume on a regional scale is closely directed to two ecosystems, a lake and river system. Hydrological field investigations have shown that both ecosystems are in hydraulic connection with the adjacent contaminated aquifer.

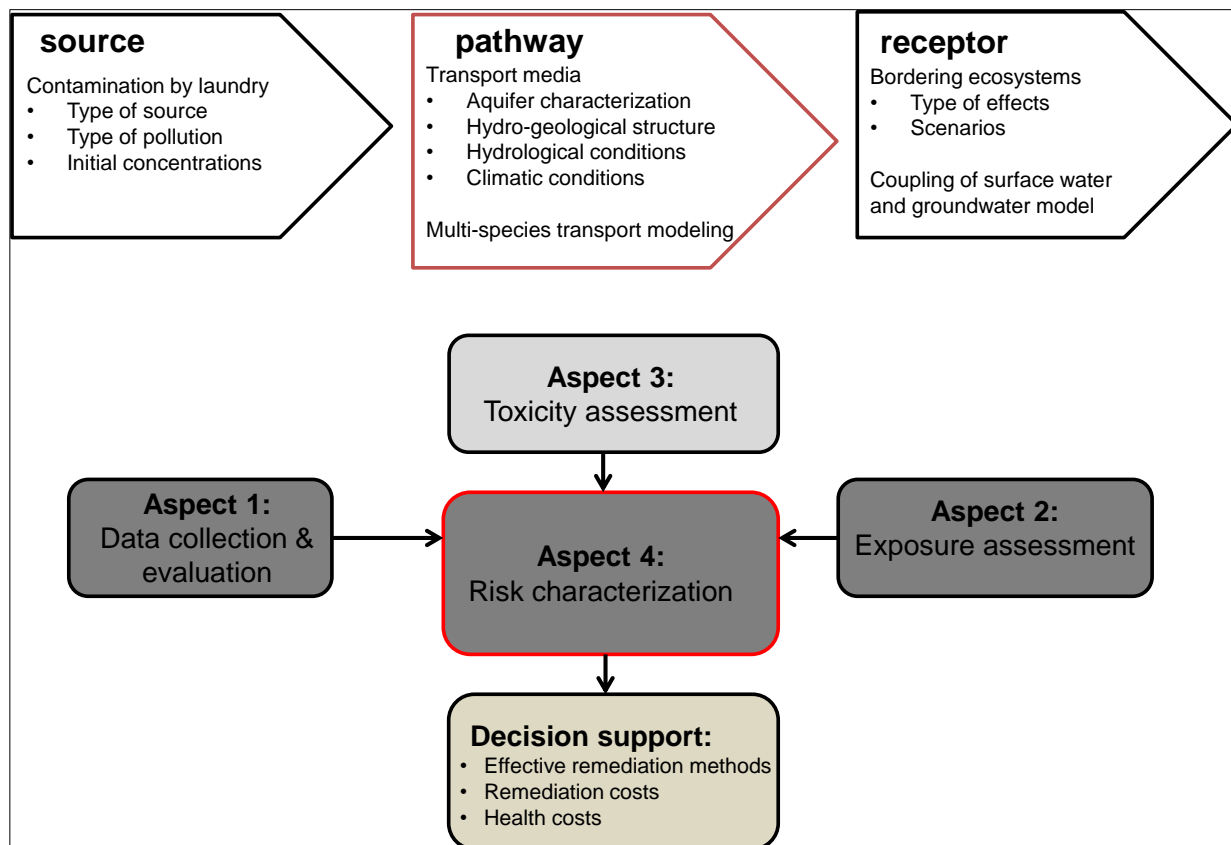


Figure 3-1 *Applied source-pathway-receptor concept of a groundwater risk assessment with corresponding fundamental aspects and work steps including data collection, exposure assessment and toxicity assessment, which leads into a risk characterization. The considered aspects of this approach are data collection, an exposure assessment and a risk characterization to provide a support for decision makers.*

Corresponding to the US EPA (2010) the evaluating of the risk in this work is related to an ecological risk assessment approach. The evaluation is focused on how likely it is that the environment may be impacted as a result of exposure to one or more environmental stressors. In this study, the source is represented by chemical groundwater pollution caused by a laundry. The environments under stress are the bordering ecosystems.

Fergusom et al. (1998) created a fundamental concept of contaminated land risk assessment. His approach is the basis for the applied groundwater risk identification of this thesis. The approach includes the following general methodological aspects:

1. Data collection and evaluation. This data collection is aimed at a source characterization, in which data about the contamination source and information about how the contamination will behave in the future are collected. This includes a study of the soil and aquifer properties affecting the dispersion of the contamination. A field investigation phase is attached with physical sampling. Subsequent, a hazard identification must be performed including the physical-chemical characterization.

2. Exposure assessment. Process of estimation the magnitude, frequency and duration of exposure that may occur due to contact with contamination media have to analyzed. This involves the identification of receptors, an evaluation of exposure pathways and a development of quantitative estimates to determine the exposure concentration and the amount of contaminated media taken in by the receptor over time. A typical requirement of this approach is the application of flow and transport models.
3. Toxicity assessment. This topic deals with the process of estimating exposure-response-relationships. The aim is to determine what the adverse effects are at different exposure level.
4. Risk characterization. This aspect connects the results of the first three aspects. The outcome of the risk characterization must be a presentation how these risks are assessed and state where assumptions and uncertainties exist.

Figure 3-1 represents the used groundwater risk assessment strategy of this approach. The fundamental aspects are composed of appropriate parameter identification (cf. chapter 4) and an exposure assessment regarding to the chemical substances (cf. chapter 5). This intended a groundwater risk characterization including identities of potential contamination occurrences in the future (cf. chapter 5.3). Fundamental estimations of environmental receptors, which are perhaps under stress, can be declared. The risk characterization obtains a knowledge base for decision makers and stakeholders to calculate remediation strategies, remediation-, health - and environmental costs (Lemming et al., 2010). In-Situ remediation, soil excavation and monitoring can be performed optimally. Furthermore, the application of geo-stochastic methods allows an uncertainty estimation of the aquifer reconstruction. A reconstruction uncertainty identification is required due to the fact that all further transport simulations are depended on this reconstructed aquifer. The presented PhD work is motivated to provide a contribution of a compatibility analysis of an urban contaminated aquifer according to Nasiri et al. (2007). The challenge is the identification of the most compatible remediation strategy for an individual contaminated site. Expert systems and an adapted site-risk assessment will be presented to facilitate a decision support process.

In summary, all four aspects of a risk assessment are used as a framework for the implementation of a groundwater risk assessment of a regional CHC contaminated urban catchment. However, the main focus of this thesis is concentrated on the source-pathway-receptor part of the risk assessment, especially on an optimal information theory and a numerical prognosis model. In this connection, the risk assessment is founded on the use of data from field investigation to characterize the source and pathway. This leads to a forecast of pollutant impact and concentrations on groundwater to the point of receptor. Aspect 3 is excluded in this thesis. The priority is to establish a more effective way to constrain a multi-

species transport model to enhance its accuracy for a risk assessment. The following chapters introduce the methodological approach for developing a contribution of a groundwater risk assessment based on a numerical-stochastic optimized transport model.

Method for quantifying uncertainty in risk assessments

In the past, numerous researchers e.g. Wang et al. (2002), Feyen et al. (2005), Kinzelbach et al. (2002), Refsgaard et al. (2007), Waler et al. (2003) have worked in the field of quantifying uncertainties in model simulations.

According to Trolborg (2010), two groups of model calibration exist. Group 1 is an uncertainty analysis modeling without historical data. Group 2 is related to an uncertainty risk modeling involving historical data. Beven (2007) underlines that the output of the risk assessment depends on the chosen input values and the model assumptions regarding model structure, parameter values and boundary conditions. In addition, this presented risk approach of groundwater contamination and prediction is based without being able to calibrate or condition the multi-species transport model against historical time series. Therefore, the output of the transport model was evaluated by conducting a sensitivity analysis and a Monte Carlo simulation (MCs).

The MCs is an accepted technique to estimate parameter uncertainties during a groundwater flow and transport modeling. For example, Brown and Heuvelink (2007) developed a software tool for assessing and simulating uncertain environmental variables based on a Monte Carlo method. Blasone (2007) estimates input parameter uncertainty by use of sensitivity analysis through a MCs. The estimation is focused on changing of model output by varying the input parameters.

The MCs provides the opportunity to generate n-output values constituting a random sample from the probability distribution over the output induced by the input (Bekesi et al., 1999). By use of a standard statistical procedure, a probability of an output value (e.g. mass concentration) can be computed. Because of the computational requirement, Monte Carlo is not often applied with complex models of environmental systems (Isukapalli et al., 1998). However, it seems to be the only technique capable of estimating uncertainties in highly non-linear and complex groundwater systems to solving practical problems (Bright et al., 2002).

The reason for an application of the MCs in the field of a groundwater risk identification is based on the complete definition of the range of each uncertain parameter and it is straightforward to implement.

4 Methodical Approach

This chapter presents the methodical approach to develop a multi-species transport model, which describes the storage and volume flows as well as the contaminants behavior in the aquifer. The case of damage can only be prognosticated when all system-relevant processes and parameters are analyzed and interpreted. But often, the hydro-geological, hydrological and chemical parameters are heterogeneous and unknown. Furthermore, the available lithological parameters are unable to fully describe the real parameter distribution. Before application to field-models, these groundwater models must be filled with specific data for a satisfying calibration. The goal is a correlation between the model solution of piezometric head and solute concentration with limited collected field observation data. A judicious adjustment of selected flow and transport parameters as well as the description of their importance is documented in this methodical approach. Each presented methodical procedure is aimed to execute groundwater risk estimation based on the computing of probability of concentration occurrences (spco) for a selected urban polluted aquifer.

For a groundwater risk treatment two multi-species transport models which differ in the subsurface reconstruction were subjected to MCs for the generation of spco. The differentiation of the aquifer reconstruction is reasonable in the flow and transport parameter allocation. A homogeneous subsurface reconstruction is referred to a uniform allocation of input parameter for each geological layer in the Finite Element mesh. In contrast, by use of the geo-stochastic simulation of flow and transport parameter fields, a heterogeneous subsurface is created. The input data inside a geological layer are varied for each mesh node of the Finite Element model. The steady-state and transient calibrated two different multi-species transport models are the basis for the Monte Carlo simulation. Moreover, the interaction between the bordering ecosystem river and groundwater is taken into account by coupling the groundwater models with a 1D-surface water model. The model coupling is essential to detect the hydraulic system-connection between the river and aquifer and therefore a potential mass transfer among this ecosystem. However, the investigation of the interaction is restricted on the hydraulic-induced dynamic volume flows of the boundary conditions. A specified consideration of the colmation layer² respective to the geo-chemical conditions, which have an influence on the contamination degradation, is neglected.

² Colmation describes the process of sealing of a water body caused by sedimentation of deposits and suspended particles. The colmation layer is located on the top of the water body and has a thickness between 0.1-1 m and a reduced hydraulic conductivity.

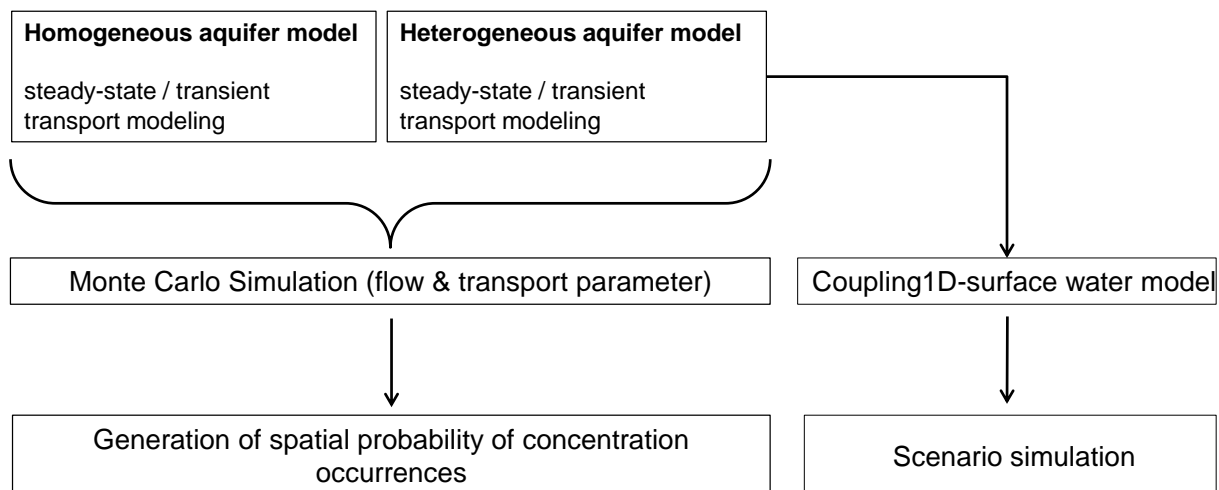


Figure 4-1 Schematic illustration of the used aquifer models and their applications for a risk identification.

The following listed work steps were performed to establish a risk identification of the selected complex urban contaminated aquifer:

1. Information or rather model parameter identification. Hydraulic field experiments, chemical laboratory tests and Direct push method afford the assembly of the hydro-geological structure model. Measured dynamic field data and climatic, hydrological data reflect the processes in the subsurface and are integrated in the Finite Element model as initial and boundary conditions. A further problem is the scale reflection during a numerical groundwater flow and mass simulation. In this connection, a development of space-oriented approach based on graduated system classification is an accepted technique to include all relevant scale-dependent process. The scale transfer between the observation scale and model scale involves an applied research and a downscaling. A downscaling is operated when an input parameter is not available on the model scale (Bierkens et al., 2000). The model downscaling was necessary to validate the complex hydro-geological structure and hydraulic parameters of the numerical downscaled groundwater model.

By means of interpolations techniques and geo-stochastic 3D interpolations, the point information from sediment cores can be regionalized on a macro-scale. The combination of practical detailed subsurface field data collection (Direct push method) and the geo-stochastic analysis of generated hydraulic and transport parameter fields build an optimal procedure.

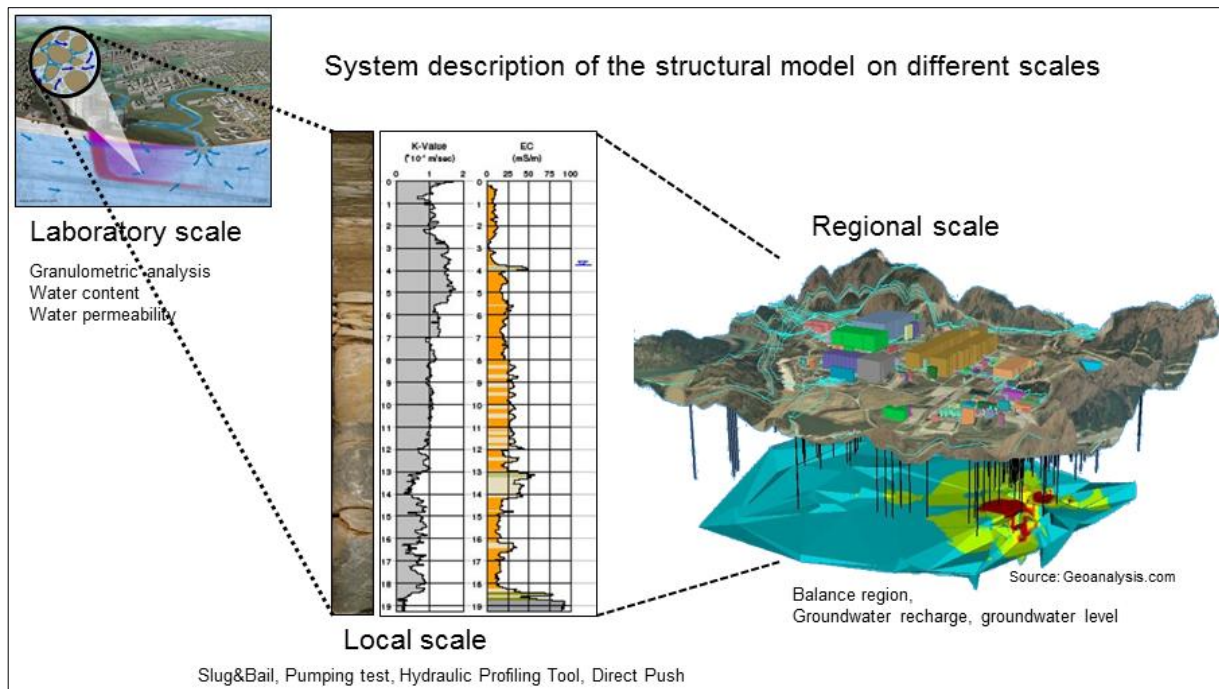


Figure 4-2 Hydro-geological system description and upscaling for a reconstruction of a structure model on different scales. Hard information of the laboratory and local scale must be regionalized by using interpolation techniques or geo-stochastic simulations to construct a balance region including storage and volume flows.

2. The numerical model selection regarding to the target-orientated problem. A target-oriented problem definition and concerted data provide the basis of a task assignment of a dynamic numerical flow and transport simulation. In the field of groundwater management and remediation, numerical models are considered as essential planning instruments. The complex hydraulic and hydro-geological processes in steady-state and transient models can only be computed by implementation of data sets which are necessary for solving the partial flow and transport differential equation. The transfer from a structural model into a numerical model requires the reconstruction of the hydro-geological aquifer model by interpretation of geological drilling profiles. Condition flow parameters can be divided into three groups. Initial conditions must be defined with measured hydraulic heads. Aquifer parameters like hydraulic conductivities, porosities and transfer rates must be investigated by field and laboratory tests. Furthermore, the specification of boundary conditions demands a time series measurement of groundwater, surface water and climatic events. During a mass transport simulation chemical, physical and bio-chemical data of the contaminant must be detected. Corresponding kinetic reaction equations have to formulate in the model.

-
3. The reconstruction of the subsurface structure by use of geo-stochastic interpolation method (3D SIS Sequential Indicator Interpolation) to quantify and qualify uncertainties of the hydro-geological structure model. The estimation of uncertainties of the parameter adjustment also leads to a risk valuation regarding to the reconstruction. Domains inside the groundwater model with a high uncertainty of parameter assignment must be taken into account in connection with an identification of appearance concentration pattern.
 4. Risk identification based on the generation of probabilities of concentration occurrences of selected compounds by use of a Monte Carlo simulation.

The target of the presented procedure is an optimal analysis and holistic treatment of a groundwater-case of damage in an urban area without focusing on a definite process. All system-significant dynamic processes and spatial parameter, which contribute a pollutant disposal in the subsurface are equal, treated in terms of a process identification and description. The result of the documented procedure provides a contribution for a site characteristic remedial strategy and a groundwater risk assessment.

4.1 Characterization of spatial and temporal process parameters

The application of multi-species transport models has been established at many hazardous contaminated sites. The reconstructed groundwater model represents simplified version of the real-world system that approximately simulates the relevant excitation-response relation depending on time and space of the real groundwater system. The simplification is introduced as a set of assumptions and identifications, which express the characterization of the system and those features of its behavior that are relevant to the problem under investigation (Bear et al., 1992). These assumptions relate to the geometry of the boundaries of the investigated area, the type of matrix comprising the aquifer (porosity, hydraulic conductivity, anisotropy, heterogeneity), the groundwater flow profile (groundwater head, gradient, groundwater recharge, climatic data), the flow regime (interaction), the contaminant properties (molecular diffusion, longitudinal and transversal dispersivity, sorption, reaction rate) and the flow and transport initial and boundary conditions. The outcome is a conceptual model which describes the natural aquifer with its temporal and spatial variability based on field-data, climatic data and chemical data collection. The following chapter presents the relevant temporal and spatial parameters, which constitute the individual characteristic of the investigated urban aquifer.

4.1.1 Geological parameter identification

Drilling profiles

A groundwater flow and transport model depends on the geological and hydraulic data interpretation and preparation. The 3D geological layer-configuration is established on drilling profiles. The layer-configuration provides the architectural frame adapted from hard information (borehole information with coordinates) of the Finite Element groundwater model. Spatial-related data like material, hydraulic conductivities and porosity fill-out this structure.

Figure 4-3 shows the schematic geological cross section of the reference area created by drilling profiles. Ten geological layers are defined for the homogeneous subsurface and 14 for the heterogeneous subsurface (cf. chapter 4.2). Middle sand and fine sand are the dominant substrates.

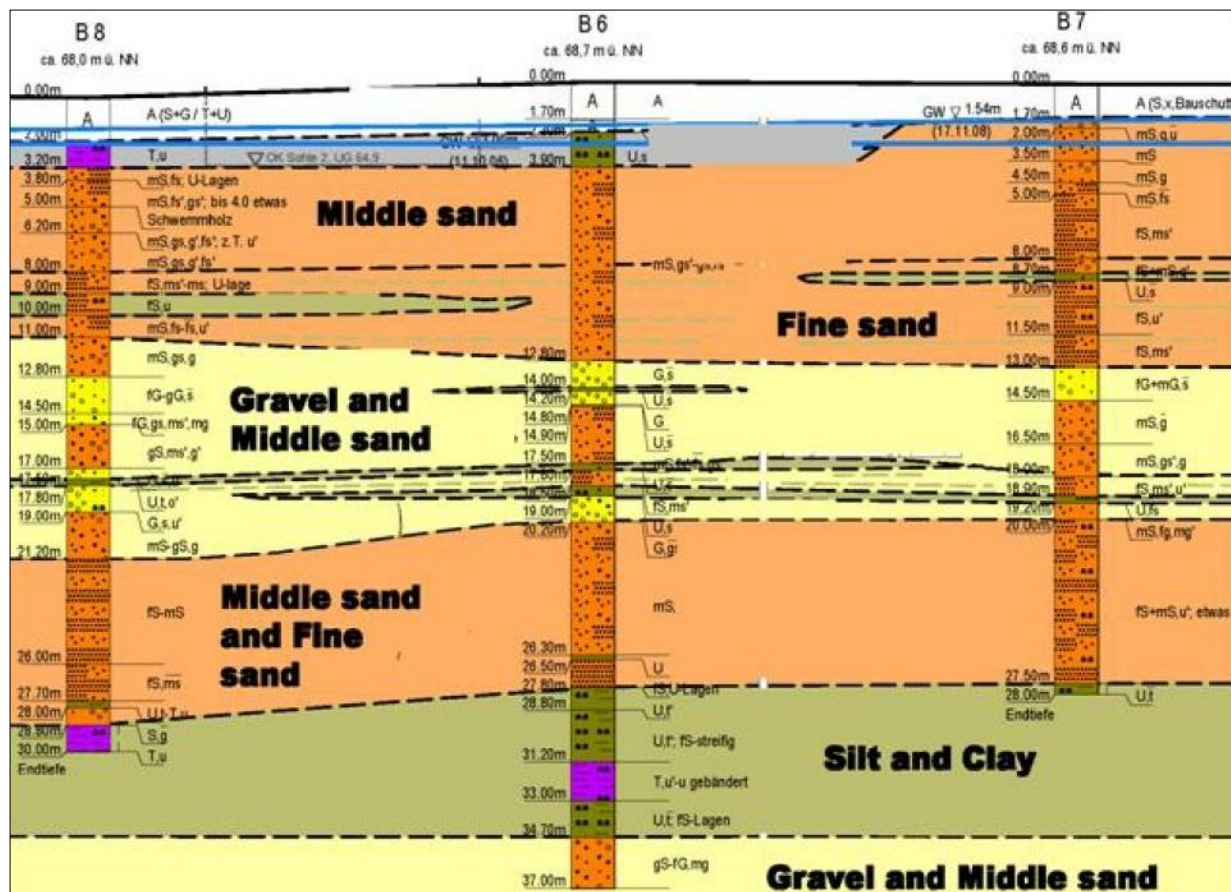


Figure 4-3 Schematic vertical geological cross section profile (drilling profile B8, B6 and B7) of the investigation area.

Saturated hydraulic conductivity

Mathematical equations have to be defined to solve the 3D groundwater flow and transport equation. The first aspect is the description of the physical processes by using the continuity equation. The essential force, which influences the groundwater flow in a saturated media, is the gravitational force. Thereby, the hydraulic head indicates the hydrostatic pressure and the location to a relative reference level. Further important parameters for a 3D density-independent saturated groundwater simulation are water density, gravitationally acceleration, storage coefficient and the location elevation. The hydraulic conductivity, which describes the ease with which water flows through a saturated porous media, is integrated as a permeability tensor. The configuration of the fluid phase in the media and the fluid property influenced the hydraulic conductivity. This variable reflects the flow resistance of the media and the internal friction of a fluid.

In case of an anisotrop aquifer, the hydraulic conductivity is differentiated in x-, y- and z-direction (cf. figure 4-4) and cannot be assumed as a scalar. In comparison to an isotrop aquifer, the hydraulic conductivity is a scalar. In general, porous mediums are anisotrop where the anisotropy is caused by layer stratigraphy. It is assumed that the geological layers are aligned in a horizontal direction, which forces a higher conductivity in horizontal than in vertical direction. In an isotrop media the conductivity is in each spatial direction equal and the water transport is parallel to hydraulic head gradient.

3-dimensional groundwater flow equation of an isotrop media with K as scalar:

$$\vec{v} = -K \nabla h \quad \text{with } \vec{v} = \begin{pmatrix} v_x \\ v_y \\ v_z \end{pmatrix} \quad \text{and } \nabla h = \begin{pmatrix} \frac{\partial h}{\partial x} & \frac{\partial h}{\partial y} & \frac{\partial h}{\partial z} \end{pmatrix}^T \quad \text{Eq. 4-1}$$

3-dimensional groundwater flow equation of an anisotropy media with K as tensor:

$$\vec{v} = -\mathbf{K} \nabla h \quad \text{with } \mathbf{K} = \begin{pmatrix} K_{xx} & K_{xy} & K_{xz} \\ K_{yx} & K_{yy} & K_{yz} \\ K_{zx} & K_{zy} & K_{zz} \end{pmatrix} \quad \text{Eq. 4-2}$$

\vec{v}	Darcy velocity	$[\text{ms}^{-1}]$
h	Hydraulic head	$[\text{m}]$
K	Hydraulic conductivity	$[\text{ms}^{-1}]$

The equation 4-1 and 4-2 show that the hydraulic conductivity is a special-related parameter, which is varied inside the aquifer in x-, y- and z-direction. According to Metherrón (1965), it is a space-dependent data (cf. chapter 4.2.2). The hydraulic conductivity parameter was used for the generation of parameter fields via a Sequential Indicator Simulation.

Additionally, a differentiation between confined and unconfined aquifer systems must be carried out because the storage coefficient differs. In case of a confined groundwater system, the storage coefficient is a function of the aquifer compressibility. Moreover, the groundwater movement and changing water-saturated volume must be considered for an unconfined aquifer. Therefore, the storage coefficient must be replaced by the effective porosity n_{eff} :

$$\text{div } K \nabla h + q = n_{eff} \frac{\partial h}{\partial t} \quad \text{Eq. 4-3}$$

The effective porosity was subjected to a 3D SIS to generate geo-stochastic parameter fields.

The groundwater flow equation resulted in the flowing formulation for an unconfined aquifer:

$$\frac{\partial}{\partial x} \left(K_x \frac{\partial h}{\partial x} \right) + \frac{\partial}{\partial y} \left(K_y \frac{\partial h}{\partial y} \right) + \frac{\partial}{\partial z} \left(K_z \frac{\partial h}{\partial z} \right) + q = n_{eff} \frac{\partial h}{\partial t} \quad \text{Eq. 4-4}$$

One of the most important problems during a hydro-geological groundwater modeling is the inhomogeneous distribution of the hydraulic conductivity. After Aeschbach-Herting (2005/2006), the hydraulic conductivity is approximately log-normally distributed. The outcome of this is that not K but $\log(K)$ follows a normal distribution. As a result, K is varying over several ranges what induced relevant problems during a groundwater modeling.

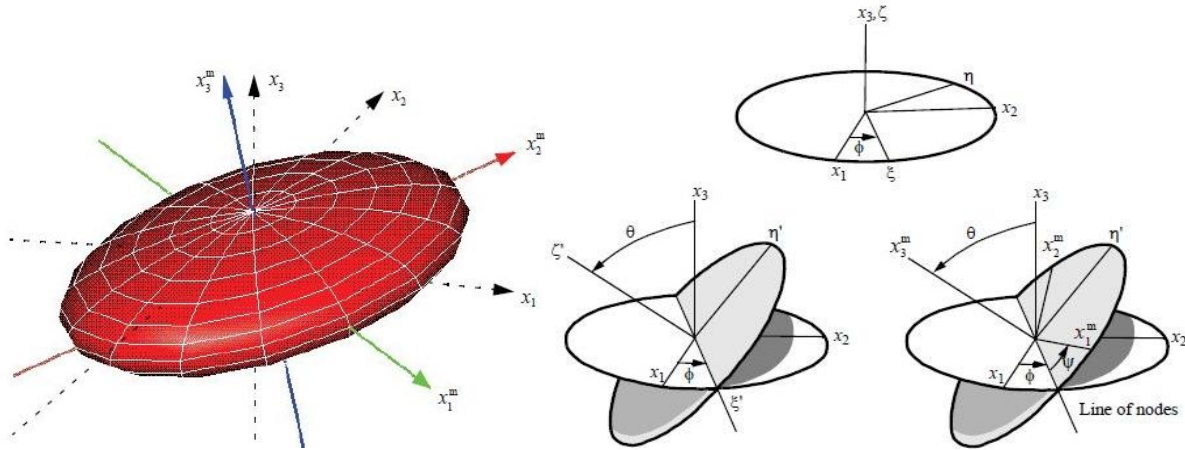


Figure 4-4 Definition of 3D anisotropic conductivity. Modified rotation definition of Eulerian angles in 3D (Diersch, 2009).

Respective values for a specific material type were measured by slug&bail test³ and compared with literature values. Both reconstructed aquifer models were defined by an anisotropy. Table 4-1 presents the implemented K_f -values in the Finite Element groundwater model. These values afford the adjustment of the hydraulic conductivity of each layer of the homogeneous

³ Abrupt artificial induced change of the hydraulic gradient between well and aquifer by a prompt groundwater level increase is defined as slug test. The opposite process – prompt decrease of groundwater level at the well is called bail test.

subsurface model and for each node involving the space-direction. For the heterogeneous aquifer model, the generated anisotropic distributed parameter fields were imported.

Table 4-1 Literature values of the hydraulic conductivity for different substrate types of a porous media and the derived values for the numerical groundwater model.

Substrate	Hölting and Coldewey (2005) [ms⁻¹]	AG Bodenkunde (1982) [ms⁻¹]	Used hydraulic conductivities [ms⁻¹]
Clay	<10 ⁻⁹	1.16 * 10 ⁻⁴ – 4.63 * 10 ⁻⁴	0.25 * 10 ⁻⁴
Silt	10 ⁻⁵ – 10 ⁻⁷	1.16 * 10 ⁻⁴ – 4.63 * 10 ⁻⁴	0.25 * 10 ⁻⁴
Fine sand	10 ⁻⁴ – 10 ⁻⁵	4.63 * 10 ⁻⁴ – 1.16 * 10 ⁻³	2.5 * 10 ⁻⁴
Rubble	-	-	2.5 * 10 ⁻⁴
Middle sand	10 ⁻³ – 10 ⁻⁴	1.16 * 10 ⁻³ – 3.47 * 10 ⁻³	12 * 10 ⁻⁴
Coarse sand	ca. 10 ⁻³	>3.47 * 10 ⁻³	12 * 10 ⁻⁴
Gravel	10 ⁻¹ – 10 ⁻²	-	25 * 10 ⁻⁴
Stones	-	-	25 * 10 ⁻⁴

The hydraulic conductivity values resulted from field test and were modified by literature values of “Ad-Hoc-Arbeitsgruppe Boden der Geologischen Landesämter und der Bundesanstalt für Geowissenschaften und Rohstoffe der Bundesrepublik Deutschland, 1996”.

A smaller part of the investigation area (downscale area, figure 4-5) is used to detect a detail reproduction of the hydraulic conductivity to evaluate the determined and tested hydraulic conductivity values, which were regionalized for the complete model domain. The reason for that area is constituted in the high contaminant concentration. In situ testing of hydraulic conductivity is performed by injecting water under a specified flow rate into the aquifer. A detail description of the HPT technique is given in chapter 4.2.2.

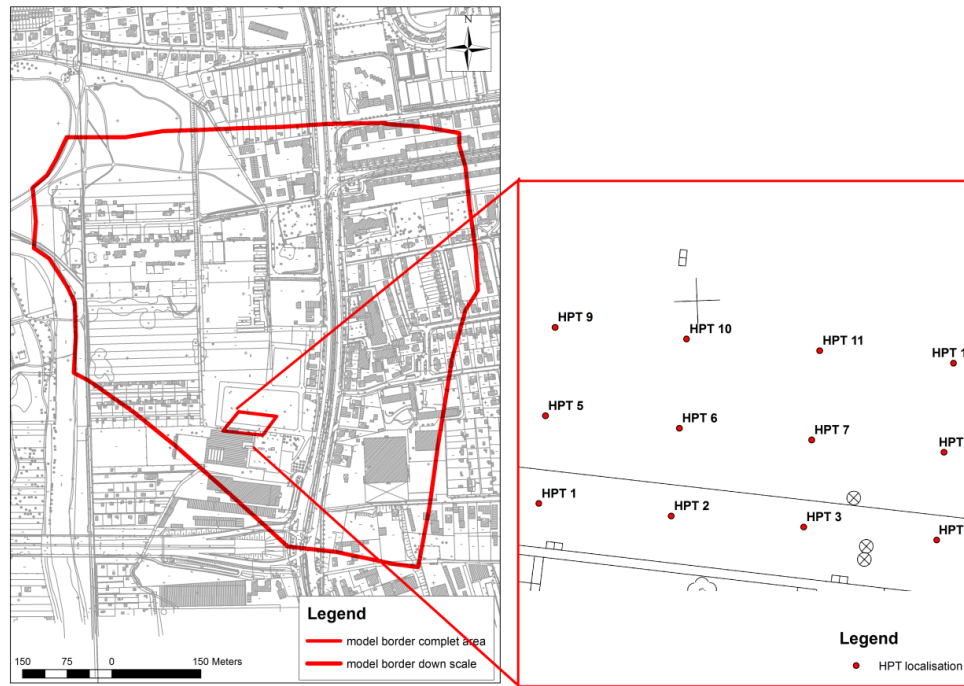


Figure 4-5 Left side: Regional model area. Application of hydraulic conductivities by use of slug&bail tests at selected wells. Right side: downscale model area. The hydraulic conductivities result from a Direct push method, so-called “Hydraulic Profiling Tool (HPT)”. The outcome is a detail knowledge of the hydraulic conductivity distribution of the subsurface and a precise geological layer-configuration. The element size of each model is set by means of parameter assignment.

Slug & Bail Test Reference area					HPT ΔK_f downscaled area
$\int_0^t K_f \cdot dz$					
Well	K_f value Hvorslev* [ms ⁻¹]	K_f value Bouwer-Rice* [ms ⁻¹]	Transmissivity [ms ⁻¹]	Range [m]	K_f value [ms ⁻¹]
Nr.1	$2.03 \cdot 10^{-3}$	$1.20 \cdot 10^{-3}$	$1.02 \cdot 10^{-3}$	1.69	
Nr.2	$1.80 \cdot 10^{-3}$	$1.14 \cdot 10^{-3}$	$1.02 \cdot 10^{-3}$	1.54	
P11	$1.18 \cdot 10^{-3}$	$8.20 \cdot 10^{-4}$	$4.50 \cdot 10^{-3}$	1.51	
HA100	$2.73 \cdot 10^{-3}$	$1.85 \cdot 10^{-4}$	$1.48 \cdot 10^{-3}$	1.58	
B14	$2.22 \cdot 10^{-6}$	$1.59 \cdot 10^{-6}$	$4.61 \cdot 10^{-5}$	2.06	
SB1	$1.41 \cdot 10^{-7}$	$8.33 \cdot 10^{-8}$	$3.14 \cdot 10^{-6}$	1.87	
B 11a	$8.50 \cdot 10^{-6}$	$6.41 \cdot 10^{-6}$	$1.86 \cdot 10^{-4}$	4.80	
B 8b	$4.52 \cdot 10^{-5}$	$3.31 \cdot 10^{-5}$	$1.04 \cdot 10^{-3}$	6.72	
B16	$3.20 \cdot 10^{-6}$	$2.41 \cdot 10^{-6}$	$6.98 \cdot 10^{-5}$	2.12	
B1	$6.35 \cdot 10^{-5}$	$1.06 \cdot 10^{-5}$	$2.06 \cdot 10^{-3}$	2.36	
RP5	$5.00 \cdot 10^{-6}$	$2.96 \cdot 10^{-6}$	$8.88 \cdot 10^{-5}$	1.80	

- Bouwer-Rice: incomplete well, free or half-confined aquifer
- Hvorslev: free aquifer

Figure 4-6 Measured hydraulic conductivities of the model domain by slug&bail test at selected wells. This hydraulic conductivity can be seen as an integral over the complete borehole depth. The result is that the measured K_f -value is an average estimated parameter from different hydro-geological layers. Therefore, an application of Direct push method at the downscaled area (cf. figure 4-5) was performed.

The resulting hydraulic conductivities were measured every 1 cm by a HPT technique. Due to the detail record of the K_f values, a pictured form of illustration was chosen (cf. figure 4-6). In contrast to the slug&bail method the K_f -value can be measured for each geological layer. Hence, the advantage of the HPT is precise centimeter determination of the K_f -values in z-direction.

An in-line pressure sensor measures the pressure response of the soil to water injection. The pressure response identifies the relative ability of soil to transmit water. Both pressure and flow rate are logged versus depth. Afterwards, a conclusion can be made from the recorded pressure to a substrate. In general, the higher the electrical conductivity value, the smaller the grain size and vice versa. One aim of the HPT technique is to help target zones of geological and hydraulic interest, minimizing the number of soil and water samples required to develop a site conceptual model (Geoprobe Systems, 2007).

Transfer rate

One important aspect during a groundwater risk assessment is the research of the interaction between groundwater and surface water, because both components are not isolated from each other. Thus, a contamination of one ecosystem affects the other. An understanding of the variety of interactions in relation to climatic, landform, geology and biotic factors is necessary. A systematic analysis of interaction across and between surface water bodies is needed to advance conceptual and modeling of groundwater and surface water systems, which must include multidimensional analysis, interface hydraulic characterization and spatial variability. The result is a site-to-region regionalization approach (Sophocleous, 2002). Several field studies of riverbank filtration with respect to dynamic river-aquifer interaction were carried out in the Rhine region. Schubert (2002) highlighted the hydraulic aspects between Rhine River and adjacent aquifer system, which caused fluctuated concentrations of dissolved compounds in the groundwater. Therefore, the dynamic behavior of the river water level and the colmation layer property influence the flow and transport phenomena and the water quality of both systems.

A decisive parameter to reproduce river-aquifer interaction in numerical groundwater models is the transfer rate Φ . It is composed of the hydraulic conductivity of the colmation layer and the colmation layer thickness. A detailed representation of saturated river-aquifer interaction for gaining/losing rivers in regional models using river and aquifer coefficients can be found in Rushton (2007).

The transfer is implemented in the Finite Element model as a formulation of 3rd kind Cauchy boundary conditions based on a relation between the reference value h_2^R on the boundary portion and the hydraulic head h to be computed at the same place. In case of transient

conditions, the reference hydraulic head can be time-dependent $h_2^R = h_2^R(t)$. Generally, two different kinds of inflowing Φ_h^{in} and outflowing Φ_h^{out} conditions are possible. The boundary condition becomes impervious if $\Phi_h \equiv 0$. The opposite case is a very large value $\Phi_h \rightarrow \infty$. Therefore, the 3rd kind of Cauchy boundary condition is reduced to a Dirichlet-type (1st kind) (Diersch, 2009). For inflowing conditions of the transfer coefficient is defined as:

$$\Phi_h \rightarrow \Phi_h^{in} (h_2^R > h) \quad [d^{-1}] \quad \text{Eq. 4-5}$$

The riverbed is clogged by a layer thickness d and a conductivity of K_0^{in} . The model boundary represents the inner border of the colmation layer because the K_0^{in} is smaller than the aquifer conductivity K . The flux through the colmation layer can be calculated from the Darcy equation:

$$q \approx -K_0^{in} \frac{\Delta h}{\Delta l} = -K_0^{in} \frac{h_2^R - h}{d} \quad [md^{-1}] \quad \text{Eq. 4-6}$$

The Φ_h^{in} for a vertical, horizontal unconfined aquifer is estimated as:

$$\Phi_h^{in} \approx \frac{K_0^{in}}{d} \quad [d^{-1}] \quad \text{Eq. 4-7}$$

Φ_h^{out} can be calculated analog. In case of infiltration the coefficients Φ_h^{in} and Φ_h^{out} differ. The conductivities of the colmation layer become depart from that of the exfiltration $K_0^{in} \neq K_0^{out}$.

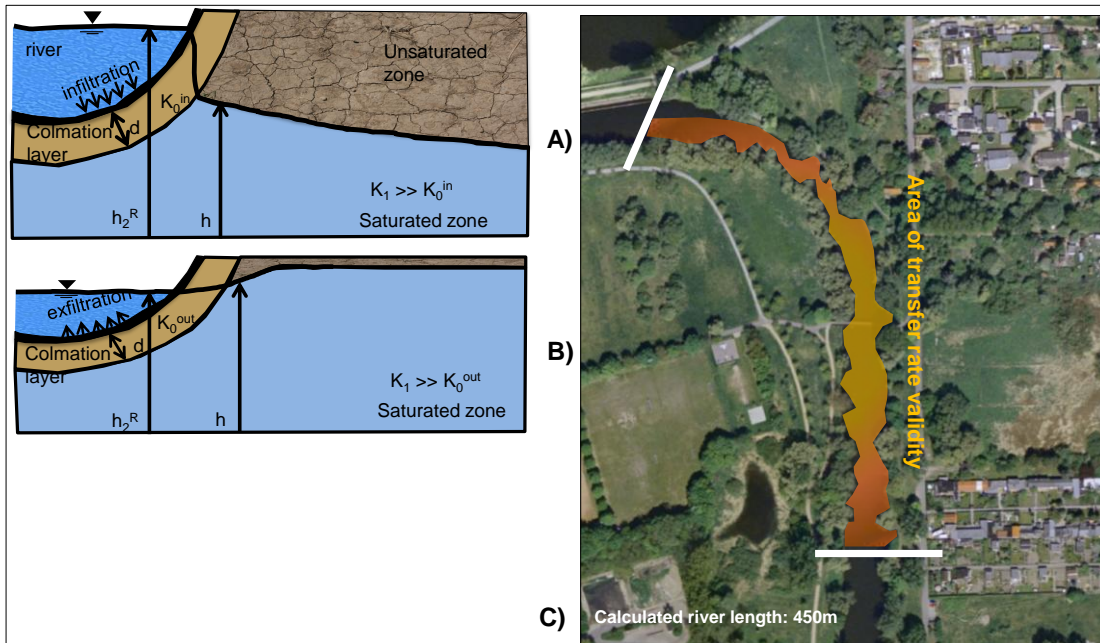


Figure 4-7 Picture A) shows the transfer coefficient Φ_h^{in} as colmation layer parameter of a river bed for inflowing conditions. The surface water streams into the aquifer system. The exfiltration of groundwater into a river through the colmation layer is shown in picture B). Characterized by the transfer rate Φ_h^{out} . Source: Diersch, 2009, modified. C) Surface water model area with the area of transfer rate validity derived from the soil sampled of the colmation layer (yellow domain).

Several research papers on the interaction mechanisms of stream-aquifer systems caused by hydraulic conditions were taken into account in the last years. Blaschke et al. (2003) documented the analysis of clogging processes in hyporheic interstices of an impounded river depending on flood events. They pointed out that the exchange of contaminants between rivers and aquifers is closely related to the hydraulics of the stream-aquifer system. Different types of clogging layers are presented with their thicknesses and corresponding hydraulic conductivities. The hydraulic conductivities vary by more than five orders of magnitude ($1 \cdot 10^{-3} \text{ ms}^{-1}$ – $5 \cdot 10^{-8} \text{ ms}^{-1}$). Song et al. (2010) analyzed the variability of streambed vertical hydraulic conductivity with depth along the Elkhorn River by use of *in situ* falling-head standpipe parameter tests. The investigation referred to two connected layers and resulted in an average thickness of 59.5 cm/29.3 cm and a hydraulic conductivity of $26.6 \text{ md}^{-1}/16.1 \text{ md}^{-1}$. Schälchli (1992) investigated the clogging of coarse gravel river beds by fine sediments from the Langeten River by use of a steel frame method and a freeze core sampler. Six layers were analyzed to a depth of 0.45 m with hydraulic conductivities between $1.1 \cdot 10^{-3}$ – $4.8 \cdot 10^{-5} \text{ ms}^{-1}$ after Krumbein & Momk. Birk (2006) studies the impact of high-stage events on riverbed scour and hydraulic conductivity. Riverbed seepage meter spanned two orders of magnitude with values ranging from 0.0076 md^{-1} to 0.82 md^{-1} .

For this approach, a sampling of the colmation layer was performed to analyze the transfer rate of the reference area. The extraction of the colmation layer material was executed by a closed Liner System. The sampling was performed depth-oriented. Afterwards, a granulometric analysis and determination of the hydraulic conductivity was taken into account for several samples (cf. figure 4-8). A transfer rate was calculated based on the analyzed K-value and the colmation layer thickness



Figure 4-8 Sampling of the colmation layer. Extraction of the material by use of liner technique.

Three samples were examined to determine streambed hydraulic conductivity at three different places along the river. The extracted samples were investigated in laboratory tests after DIN 18130. Figure 4-9 shows the grading curve of the three colmation layer samples for different depths with corresponding K_f -value.

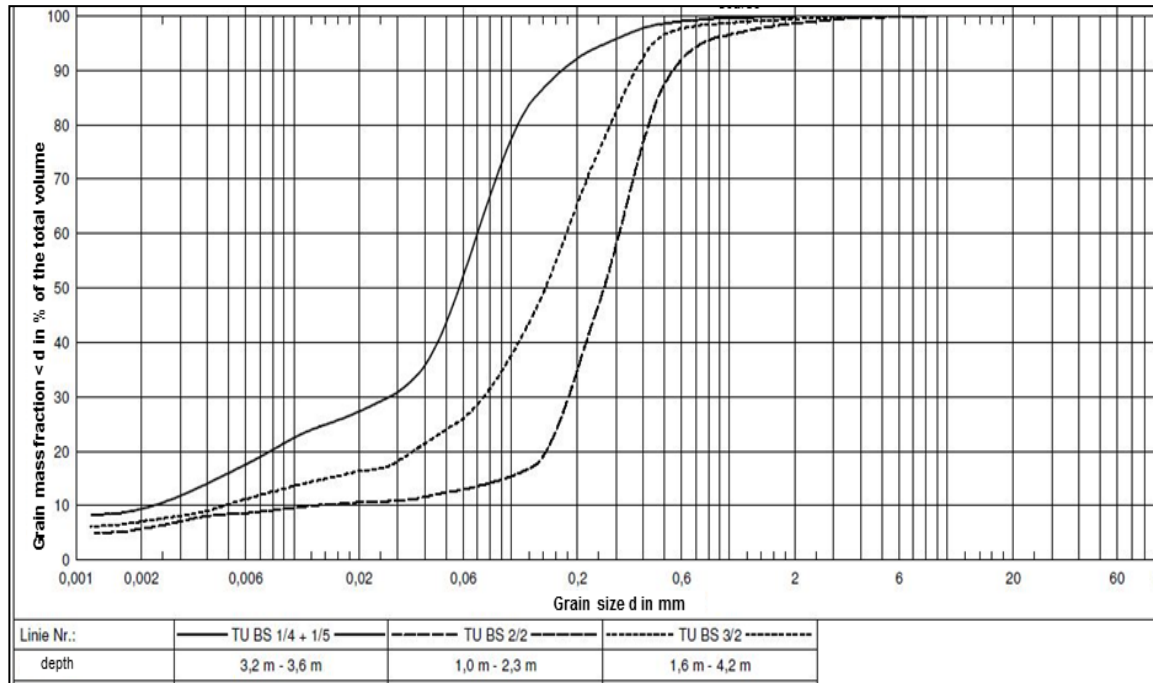


Figure 4-9 Grading curves of the three colmation layer samples with corresponding K_f -value.

The resulted transfer rates are represented in table 4-2 and were calculated by equation 4-7.

Table 4-2 Calculated transfer rates of three sampled layers with corresponding thickness and hydraulic conductivity.

Sample	Depth [m]	Thickness [m]	Hydraulic conductivity [ms^{-1}]	Transfer rate [1d^{-1}]
1	3.2 – 3.6	0.4	$4.8 \cdot 10^{-8}$	$10.36 \cdot 10^{-4}$
2	1.0 – 2.3	1.3	$1.7 \cdot 10^{-5}$	$11,298 \cdot 10^{-4}$
3	1.6 – 4.2	2.6	$2.9 \cdot 10^{-7}$	$96.36 \cdot 10^{-4}$

The three calculated transfer rates were used for the flow simulation. Only the first three layers of the groundwater flow model were assigned with the transfer rate. The in and out transfer were defined with equal values under the assumption of similar effluent and influent conditions.

The results of the flow simulations have shown that the selected transfer coefficients are too low and consequently the hydraulic conductivity, as well. After multiple simulations runs, the best parameter fit for the transfer rate was given with $6 \cdot 10^2 1\text{d}^{-1}$. This equates to a hydraulic conductivity of $3.5 \cdot 10^{-4} \text{ms}^{-1}$. The modification of the transfer rate had a positive effect on the quality of the simulation results.

Porosity

To simulate specific discharge in the aquifer, the advective transport needs to be converted to seepage velocities by dividing local values of effective porosity (Andermann et al., 2003). For the transport simulation, only the part of total porosity contributing to fluid flow, and thus to advective transport, is relevant. This so-called effective porosity can be seen in table 4-9. For each substrate, an effective porosity was derived from Pannike et al. (2006). Depending on the porous media properties only a part of the pore volume – effective or drainable void – i.e. effective porosity n_{eff} results in an effective discharge. The effective porosity can be approximately calculated by the MAROTZ equation (Koch et al., 2003/2004):

$$n_{eff} = 0.462 + 0.045 * \log K_f \quad \text{Eq. 4-8}$$

The porosity was used as a space-dependent variable. Based on the Sequential Indicator Simulation a heterogeneous parameter field was generated.

4.1.2 Chemical parameter identification

Due to their desirable properties (volatile, highly stable, non-flammable), chlorinated ethenes like tetrachloroethene (PCE) have been widely used as degreasing agents in dry cleaning processes in the past, for example in laundries, metalworking or automotive industries. The chloroethenes, tetrachloroethene, trichloroethene (TCE), dichloroethene (DCE) and vinyl chlorid (VC) were detected in the groundwater of the investigation area as a result of non-professional disposal of sewage water of a laundry. Several chlorinated hydrocarbons researches have shown that biological activities in groundwater induce a degradation of these compounds. In combination with remediation activities like pump and treat procedure a significant cleaning of subsurface water can be gained. However, a successful decontamination can only be provided if the chemical and biological behavior of the compounds and microorganisms in the aquifer are analyzed. Bradley (2000) refers that under reducing conditions, aquifer microorganisms reduce PCE and TCE to the daughter products DCE and VC.

A first order degradation kinetic was implemented for each step of the consecutive reaction chain (cf. figure 4-11). It was assumed that no by-products (e.g. trans-DCE) are formed and that PCE is the only primary pollutant (all other chlorinated ethenes are metabolites from degradation of PCE). Further, no gas emission from soil was presumed.

All chemical parameters of the reference area were determined by the project partner Tillman Greis (Institute Biochemical Engineering, ibvt). Parameters like dispersion, diffusion, sorption and degradation rates were taken from different publications (Clement et al., 1998), (Alvarez-Cohen et al., 2001), (Azizian et al., 2007), (Schaerlaekens et al., 1999), (Benekos et al., 2007),

(Noell, 2009), (Mulligan et al., 2004). However, it was necessary to choose an appropriate parameter set from the whole range listed in the citations. For instance, reaction constants in literature differ from each other by up to three orders of magnitude dependent on soil type and other environmental conditions like redox potential (Wiedermeier et al., 1998). Preliminary simulations were performed in order to identify an appropriate parameter range for the Finite Element model. The transport and reaction parameters used in the multi-species model are listed in the following section. This set of parameters was identified to deliver the best fit regarding simulated and measured concentrations. To optimize the chemical parameter set, a Monte Carlo simulation was performed by the project partner.

The total error of a model is calculated:

$$\text{Error}_{\text{absolute}} = \frac{C_{\text{measured}} - C_{\text{computed}}}{\text{mass well}}^2 \quad \text{Eq. 4-9}$$

For the optimization each mass error was standardized on the primary model:

$$\text{Error}_{\text{standatrdized}} = \frac{\text{well } C_{\text{measured}} - C_{\text{computed}}^2}{\text{mass well } C_{\text{measured}} - C_{\text{primary model}}^2} \quad \text{Eq. 4-10}$$

Four MCs with 1,200 runs were simulated. The best multi-species model of a MCs was used as an initial model for further Monte Carlo simulation. In this process, the standard deviation were set smaller step by step ($0.5 * \mu \rightarrow 0.25 * \mu \rightarrow 0.15 * \mu \rightarrow 0.1 * \mu$).

Molecular Diffusion

According to Grathwohl (1992), the molecular diffusion of contaminants in sand, gravel as well as clay and silt is a limiting factor during decontamination of soil and aquifer pollution. Furthermore, it caused long time remediation activities in practice. The molecular diffusion describes the mass transport based on the thermal proper motion of the molecule or atoms and leads to an equilibrium inside of a fluid. Physical-chemical properties of diffuse substances and the media influence the diffusion coefficient. A falling pressure and density plus a rising temperature effect an increase of the diffusion coefficient (Weber, 2002). A diffusion coefficient equal to $10^{-9} \text{m}^2 \text{s}^{-1}$ means, that for a decrease in concentration equal to $1 \text{ mgm}^{-3} \text{m}^{-1}$ per second, 10^{-9}mg of solute will migrate through an area equal to 1 m^2 in the direction opposite to the concentration gradient. A global molecular diffusion coefficient of $50 * 10^{-9} \text{m}^2 \text{s}^{-1}$ was set in the multi-species transport model for each species and layer.

Longitudinal and transversal dispersion

The small-scale variations in groundwater velocities are responsible for characteristic spreading of a solute. A transport model must include the description of the spreading. According to Rausch et al. (2005), the prediction of contaminant transport based on the average velocity at the representative elementary volume (REV) scale fails to capture the spreading of contaminants caused by the small-scale variations. With respect to the measurable average velocity, the hydrodynamic dispersion must be taken into account to honor the microscopic velocity. The dispersion is a local-scale or pore-scale phenomenon. In general, the pore-scale dispersion plays a greater role than the molecular diffusion. Velocity variation in heterogeneous aquifers causes greater variations in contaminant velocities. This turns into a greater dispersion compared to laboratory values, which lead to contamination migration over distances ranging from millimeters to decimeters. The velocity variation at a scale larger than the pore size scale is defined as macro-dispersion. Macro-dispersion is the dominant process at larger scales (cf. figure 4-10). A relation between laboratory- and field test with an impact on the scale-dependent dispersion is documented in Gelhar et al. (1992), Schulze-Makuch (2005), Pickens et al. (1981) and Neuman et al. (2003). Dispersion is larger in groundwater flow direction (longitudinal dispersion) than in direction perpendicular to it (transverse dispersion). The transversal dispersivity is assumed 10 to 20 times smaller than the longitudinal dispersivity.

The longitudinal and transversal dispersion coefficients can be expressed as the product of an intrinsic aquifer property, the dispersivity, and the intrinsic of flow field. For a uniform velocity, the dispersion coefficients are given by:

$$D_L = \alpha_L u \quad \text{and} \quad D_T = \alpha_T u \quad \text{Eq. 4-11}$$

D_L / D_T	Dispersion (longitudinal and transversal)	$[m^2s]$
α_L / α_T	longitudinal and transversal dispersivity	$[m]$
u	velocity	$[ms^{-1}]$

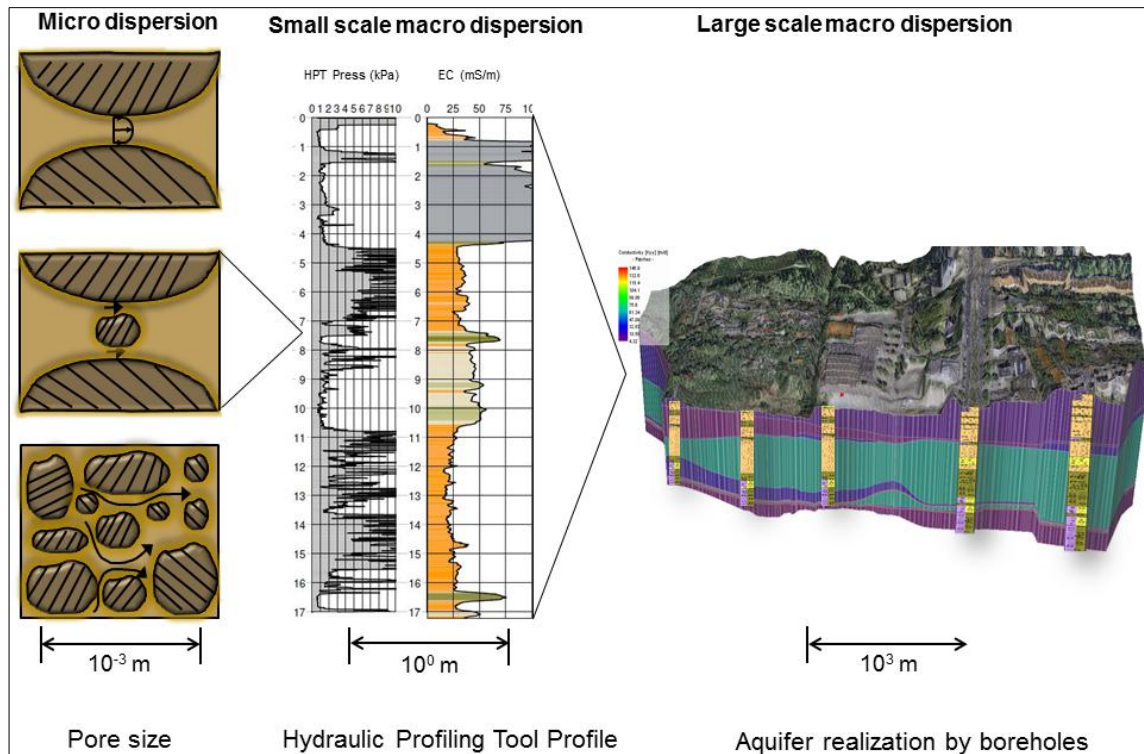


Figure 4-10 Causes for velocity variations at different investigated scales. Micro-dispersion is dominant at the pore scale. The hydraulic profiling technique shows small scale macro dispersion. An aquifer realization exhibits a large-scale macro-dispersion.

In dependence on John (2006) and Gelhar et al. (1992), different longitudinal and transversal dispersivities were tested for the large model scale. The used values of the multi-species transport model are documented in table 4-3.

In addition, the longitudinal and transversal dispersivity given in table 4-3 were subjected to the geo-stochastic reconstruction technique for a heterogeneous parameter field generation.

Table 4-3 Longitudinal and transversal dispersivity for the geological layer of the Finite Element transport model. Investigated by Greis (2011).

material type	geological layer	longitudinal dispersivity [m]	transversal dispersivity [m]
Rubble	1 layer	8.8	1.98
Silt	2 layer	6	1.35
Fine sand	3 layer	8	1.8
Middle sand	4 layer	7.6	1.71
Fine sand	5 layer	8	1.8
Coarse sand	6 layer	10	2.25
Middle sand	7 layer	7.6	1.71
Fine sand	8 layer	8	1.8
Coarse sand	9 layer	10	2.25
Silt	10 layer	6	1.35

Reaction rate

A sequential biodegradation of chlorinated hydrocarbons follows a series of chain reactions (cf. figure 4-11). Only reductive processes afford a degradation of PCE under methanogenic or sulfate-reducing concentrations. Commonly, these conditions dominate in the saturated zone.

PCE has been shown to be reductively dechlorinated to ethane by sequential dechlorination through the intermediates TCE, cis-DCE and VC. PCE is resistant to aerobic metabolism and its dechlorination intermediates can be cometabolized aerobically. Commonly, they accumulate under anaerobic environmental conditions. The dechlorination of the intermediates appears to be rate limiting in the reductive dechlorination of PCE (Flynn et al., 2000). A particular consequence for remediation of PCE is the accumulation of VC. VC is the most toxic and carcinogen of the chlorinated ethenes.

An anaerobic first-order degradation kinetic was implemented for each step of the consecutive reaction chain (cf. figure 4-11) for the multi-species reaction model. In numbers of papers, e.g. Fetter (2001) and Praamstra (1996), the first-order is adequate for describing reductive dechlorination. It is assumed that no by-products are formed and that PCE is the only primary pollutant (all other chlorinated ethenes are metabolites from degradation of PCE). Further, no gas emission from soil was presumed.

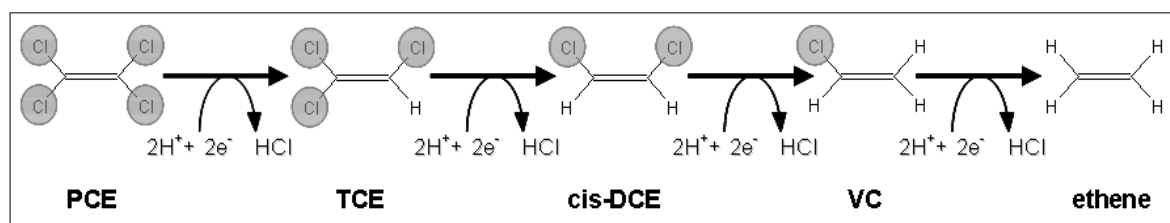


Figure 4-11 Degradation chain of chlorinated ethenes; degradation is assumed as first-order kinetic. Source: Greis et al. (2011).

The chemical reaction rates for the investigated compounds are given in table 4-4. This parameter is important to estimate how the reaction occurs. That factor defines the change in the concentration of a reactant or a product with time.

Table 4-4 First order kinetic reaction rate for different species (PCE, TCE, DCE and VC) in the Finite Element model. Investigated by Greis (2011).

species type	reaction rate [10^{-4} /s]
PCE	$5.0 \cdot 10^{-5}$
TCE	$1.0 \cdot 10^{-4}$
DCE	$5.0 \cdot 10^{-6}$
VC	$1.2 \cdot 10^{-4}$

Linear Sorption

Sorption is often the prior process controlling the behavior of contaminants in subsurface. It can be defined as the interaction of contaminant with the soil matrix. The sorption process can be divided into adsorption and absorption. The term sorption is used in a generic way to encompass both phenomena (Piwoni et al., 1990). Chemical and physical characteristic of the contaminant, compositions of the subsurface and fluid media control the interaction of a contaminant and the soil matrix. The chlorinated ethenes belong to organic contaminants, which are nonpolar species.

The sorption of the multi-species transport model was defined by the isotherm equation after *HENRY*. The *HENRY* law is based on a linear relationship between the loading of the sorbent and the equilibrium concentration of the solute. A sorbent is the contamination that is adhered aquifer matrix. The sorbed amount of a mass pro unit sorbent (a_{eq}) is proportional to the equilibrium concentration of the solute (C_{eq}) and is dependent on the so-called *HENRY*-coefficient (K_H):

$$a_{eq} = K_H \cdot C_{eq} \quad \text{Eq. 4-12}$$

K_H *HENRY* Distribution coefficient $[\text{lg}^{-1}]$

The *HENRY* distribution coefficient is the proportion of the loading of the sorbents and the equilibrium concentration of the solute. A selection of *HENRY* coefficients for metals and organics at different sorbents can be found in (Spitz et al., 1996). Table 4-5 documented the used linear sorption coefficients of the multi-species transport model.

Table 4-5 *Linear sorption coefficients of the multi species. Investigated by Greis (2011).*

species type	sorption [-]
PCE	4.0
TCE	4.0
DCE	2.0
VC	1.0

4.2 Reconstruction Techniques of the subsurface

Requirements for a numerical flow and mass simulation are a knowledge of the aquifer stratigraphic and lithology. Therefrom, the material parameter and their spatial distribution can be deduced. In most cases, the reconstruction of the hydro-geological underground structures based on point data from drilling profiles. Consequently, the regional 3D aquifer realization is subjected to uncertainty factors. However, the quantitative and qualitative requirements for the data set of a numerical mathematical groundwater modeling are sophisticated. Usually, the data availability for regional groundwater models turns out to be difficult because the input parameters are often not available for a regional scale. Generally, borehole information provide the so-called hard information e.g. hydraulic conductivities or porosity of the aquifer at one point of the investigation area. These hard pieces of information are subjected to regionalization techniques by using interpolation methods, which leads to uncertainties in the accuracy of the model parameterization. Abbot et al. (1996) highlighted that the construction of the geological model is a straightforward process based in the degree of details depends on the amount of existing data. Christensen et al. (1998) demonstrated that the hydro-geological parameter uncertainty is reflected in the uncertainty of a predicted stream flow gains. Three different subsurface reconstruction techniques were used to create a flow and transport model. The first reconstruction contains geological layers, which are regionalized by a common interpolation technique. This created model will be classified as the “homogeneous” groundwater model. A further reconstruction of the same aquifer is performed by a geo-stochastic indicator simulation – the heterogeneous model. The third reconstruction of the investigation area is executed by downscaling. This downscale model contains the hydro-geological structure, which was determined by a hydraulic profiling tool. Hydraulic Profiling Tool is a system to evaluate the hydraulic behavior and allow a 3D characterization of the aquifer in a high detail degree. On this smaller investigation area, remediation activities are planned on the basis of the detailed groundwater model.

4.2.1 Reconstruction of the homogeneous subsurface

The first development of the hydro-geological model reconstruction is oriented to the numerical Finite Element model. A configuration of geological layers and material changes as well as the geometric relation has to be defined to implement the stratigraphic information. The geometry of the 3D aquifer model is built up by drilling profiles interpretation (cf. figure 4-12). With regard to a regional model the borehole information (hard data) are analyzed by use of interpolation technique. The hard data points represent the topography and the discontinuities between the stratigraphic units to refine the vertical spatial discretization.

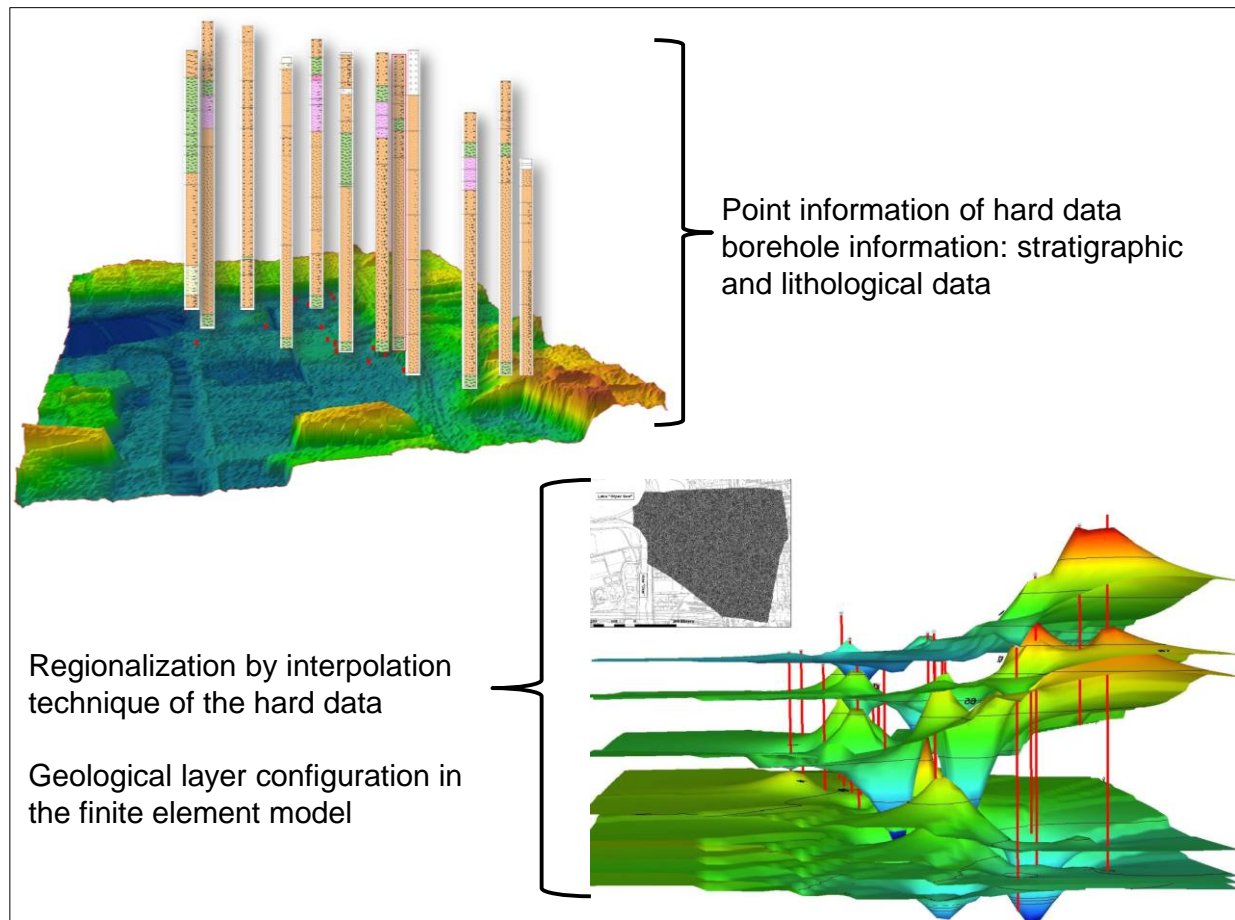


Figure 4-12 Schematic view of the geological borehole data transfer from point information of the stratigraphy to regional layer structures by use of Inverse Distance interpolation. Visualized with Visual MODFLOW.

The used drilling profiles were provided by the GGU (Gesellschaft für Grundbau und Umwelttechnik mbH) and the Environmental Agency of Braunschweig. The produced hydro-geological model consists of ten geological layers. The sequence of the sediment layers is recurrent. A classification in rubble, silt, middle sand, fine and coarse sand was conducted (cf. chapter 4.1.1)

The hard point data were regionalized with Inverse Distance Weighting via prepared model files. In addition, four neighboring points were set for the interpolation. The vertical and horizontal dimension of the structure model is specified by the model area geometry, (cf. figure 4-13) and the Finite Element mesh, which provides the geometric border of the model domain.

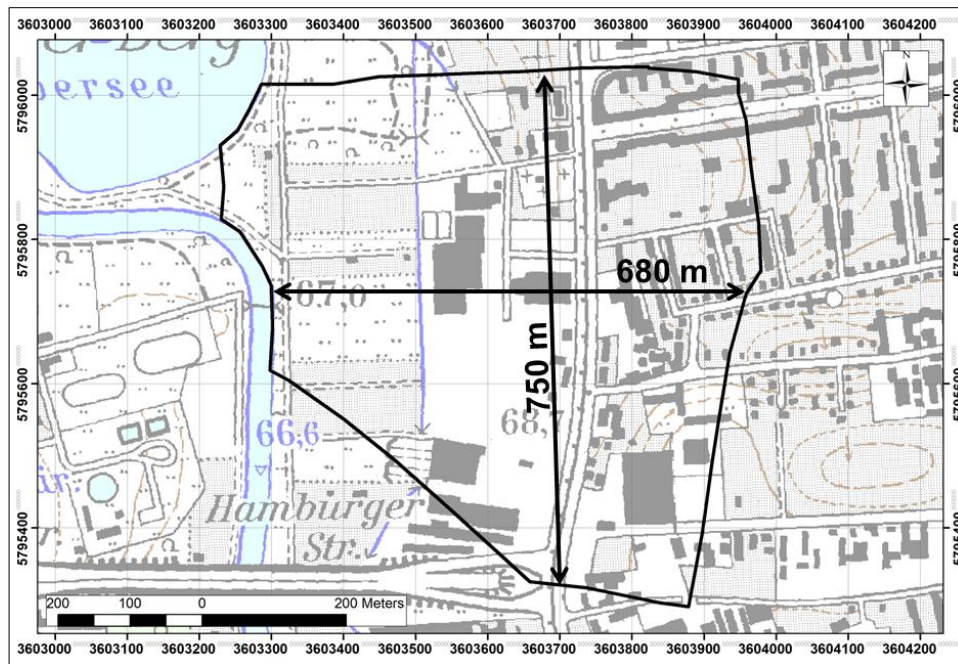


Figure 4-13 Area of the hydro-geological model. The extension from north to south is 750 m and from east to west 680 m. The complete model has an area of 0.4 km².

The vertical construction is orientated on the hydro-stratigraphic units. Impermeable layers are in focus because of their function as stratigraphic level. Especially in a depth of ten meters, the silt layer divides the groundwater body into two aquifers. The maximum vertical extraction is defined by the problem task. It is given that the silt layer functioned as an aquiclude, as a result the contaminants are detected just in the first aquifer.

4.2.2 Geo-stochastic aquifer reconstruction

The geo-stochastic aquifer reconstruction refers to a heterogeneous subsurface construction. The geological layer configuration is based on the same database described in chapter 4.2.1. Conventional regionalization methods were used to reconstruct the homogeneous aquifer. These conventional techniques do not afford a quantification of uncertainties of interpolated hydro-geological model input parameters. Accordingly, a groundwater model is established and calibrated without knowledge which subsurface areas include uncertainties of parameter distribution and assignment.

Often, the hydro-geological aquifer structure based on point information (hard data), but most subsurface environments are too complex, even a plethora of information is not sufficient to resolve the distribution of the aquifer properties which influence the flow and transport conditions. The 3D geo-stochastic estimation method provides an opportunity to complete process understanding (Kitanidis, 2003). Goovaerts (1997) accented that geo-stochastic

techniques are used to identify uncertainties of unknown parameters through the generation of alternative realizations that honor the data and reproduce aspects of patterns of spatial dependence.

The realization of the geo-stochastic treatment of the subsurface parameter set was computed by the software package *UNCERT* (Wingle et al., 1997) of the Colorado School of Mines (Colorado) which is based on the Geostatistical Software Library *GSLIB*, (Deutsch et al., 1998). The aim of the geo-stochastic method application is the generation of spatial parameter fields based on 35 hard data from drilling profiles. For this purpose the 3D conditioned Sequential Indicator Simulation (SIS, (Gómez-Hernández et al., 1990) is applied. Uncertainties regarding the probability of occurrence of the interpolated parameter can be quantified through the generation of equiprobable multiple-realizations. An exemplary realization was used to provide the basis for the reconstruction of the heterogeneous subsurface aquifer. The quantification of the input parameter by using a geo-stochastic interpolation method allows an uncertainty identification of the parameter fields before the numerical model will be started. Different from other research topics, this approach represents the implementation of measured and calculated hydrological, hydro-geological and metrological input parameters of a real regional contaminated urban groundwater system.

4.2.2.1 SIS Sequential Indicator Simulation

The conventional geological layer configuration based on a drilling profile analysis in which the point information of the hydro-geological data is interpolated over the model area by use of current interpolation method (Kriging or Akima). The determination of the layer thickness and layer morphology is derived from the substrate distribution. This results into certain drawbacks. One disadvantage applies to the interpolation of hard information, which varies over several orders of magnitude (e.g. hydraulic conductivity). In case of a poor database, this leads to a high parameter uncertainty. Furthermore, the quality of the geological layer configuration cannot be quantified.

The SIS method was applied to interpolate data which are distributed over a large range in a three dimensional medium in consideration of their spatial distribution. Thereby, the petrographic differentiated input parameters are graduated into different classes dependent on the hydraulic conductivity. Afterwards, a spatial distribution of the indicator parameters is calculated. The SIS includes an integrated Monte Carlo simulation for calculating equiprobable multiple-realizations which are used to identify certainties of indicator probability of occurrences and consequently of the coded hydro-geological parameter.

Several problems can occur if the input data contains an inclined distribution or outlier during a data interpolation. The data manipulation by using a data transformation (logarithmic calculus) or outlier elimination results in a loss of structural aquifer properties. Journel (1983) presented an indicator approach for the first time. This non-parametric method enables the avoidance of interpolation errors. According to Schafmeister (1999), two different indicator approaches can be consulted. The qualitative description or data classes can be defined as state variable. The location x is deemed: if a defined condition or value is appeared, the indicator variable gets the value 1 - if not - the indicator variable will be assigned by 0:

$$I_{x;V} = \begin{cases} 1, & \text{if } x \in V \\ 0, & \text{otherwise} \end{cases} \quad \text{Eq. 4-13}$$

I indicator

V Defined condition or value

The implementation of threshold values (cut-off-values) enables the transformation of the distribution of a variable of an indicator type into indicator variables:

$$I_{x;z_c} = \begin{cases} 1, & \text{if } z(x) \leq z_c \\ 0, & \text{otherwise} \end{cases} \quad \text{Eq. 4-14}$$

z_c Cut-off value

The measurement z of an attribute at a defined location u_i is termed as datum. From this, it follows that no uncertainties for $z(u_i)$ are available and therefore a binary indicator probability of occurrence is existent. The calculation of the spatial variance of the indicator-coded data set takes place analogous to the common variography. The following equation is used:

$$\gamma_{z_c}(h) = \frac{1}{2} E [I_{z_c}(x+h) - I_{z_c}(x)]^2 \quad \text{Eq. 4-15}$$

An indicator-semi-variogram must be calculated for each value in case of use of multiple cut-off values. Furthermore, for each used cut-off an individual indicator-semi-variogram and an individual Kriging-system of equation must be solved. The indicator transformation is not completely reversible. Hence, only conclusion can be drawn for value-domains but not for an exact value.

The application of a SIS demands a special pre-processing of the indicator-coded input data (cf. appendix B). First of all a 3D-interpolation mesh was discretized by a specific depth (cf. appendix B.6). The coded indicator values are implemented into the mesh elements according to location after easting, northing and depth. The outcome is that the mesh elements are conditioned before the simulation starts. A random start value and the first indicator to be investigated are selected in the total interpolation mesh. Afterwards, a search-ellipse around

the element is created for the interpolation of the indicator of start element. The radius is calculated from the average value of the horizontal and vertical range of the indicator-variogram. All mesh elements, which are inside the search-ellipse and allocated by an indicator, obtain a local cumulative distribution function. Below, a random number from the interval $[0, 1]$ is calculated and the indicator will be generated dependent on the random value and the local cumulative distribution function. In case of a smaller random value is less than the portion of the first indicator class the mesh element gets the number 1. Accordingly, the mesh cell will be interpolated and the actual indicator of this cell, which is to be investigated, will be assigned. In case of a major random number, the mesh cell becomes the number 0. This means the mesh cell is already interpolated but no indicator is defined. Thus, all mesh elements are defined by a 1 or 0. If all cells are interpolated the next indicator will be used. All mesh elements, which already contain an indicator, were used for calculation the cumulative distribution function in addition to the cells, which are defined by the input data set. Cells, which are covered by an indicator, are skipped. The SIS ends when each mesh cell of the total interpolation cell contains an interpolated indicator.

Equiprobable multiple-realizations were generated based on a MC simulation of the SIS. Each realization has a different start value. This results in diverse ways through the total interpolation mesh. According to Hattermann (1998) and Nienstedt (2011), the individual realizations have an identic histogram and indicator-variogram corresponding to the original data but they differ in detail. Realizations with locations of a high information density are similar in comparison to location with a low information density. A comparison of 100 realizations shows locations where an indicator occurs more frequently than on other locations. The probability of an indicator occurrence for a point results from the percentage of the most frequently occurring indicator. Wingle et al. (1997) accented that the probability of indicator occurrence conducted to a quantification of interpolation uncertainties which leads to reconstruction errors and consequently to simulation results uncertainties.

4.2.2.2 Results of the geo-stochastic heterogeneous subsurface reconstruction

Four different hydro-geological spatial parameter fields were generated on the basis of the SIS. This parameter fields (hydraulic conductivity, porosity, longitudinal and transversal dispersivity) were integrated into the heterogeneous subsurface model. 35 drilling profiles were used as hard input information. The geological profiles were digitized with major and secondary mixture portion by using the software *Geodin 6.1* (Fugro Consult GmbH, 2009).

Four indicator classes are used for the SIS to code the discrete hydro-geological parameter values (cf. table 4-6).

Table 4-6 *Classification of the substrates of the geological profiles into four indicator classes for the hydraulic conductivity.*

Substrate	Indicator class	conductivity
Clay, silt	1	Low
Fine sand, rubble	2	Medium
Middle sand, coarse sand	3	High
Gravel, stones	4	Very high

The coding of the substrate data set was based on the conductivity property of the single substrates. By reason that the porosity, longitudinal and transversal dispersivity are material properties of the aquifer the distribution and assignment of this parameters are derived from the conductivity distribution. The indicators were replaced by the discrete parameters.

A special pre-processing was necessary to define the coded indicator data set for the SIS. The first step was the characterization of the distribution of the indicator data set by use of a histogram and cumulative distribution function (cf. figure 4-14).

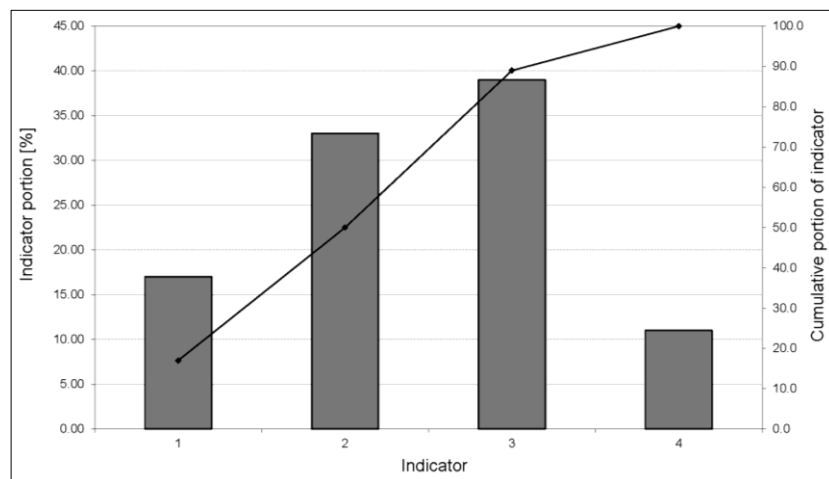


Figure 4-14 *Histogram of a coded indicator data set. The indicator portion is denoted with percentage. The line represents the cumulative distribution function of the indicator classes.*

Figure 4-14 shows that the class 2 and 3 are the dominant substrates portions of the investigation area. This suggests a medium up to high hydraulic conductivity.

The second step was the quantification of the spatial data correlation through the generation of experimental variogram and the adaption of a variogram function. A variogram in horizontal and vertical direction were calculated for each indicator (cf. appendix B.6).

The calculated parameter range, anisotropy factor, sill and nugget as well as the root-mean-square deviation of the model function of the indicator variograms are shown in table 4-7. The model function must be used for all horizontal and vertical variogram to calculate the necessary anisotropy factor.

Table 4-7 Parameter of the adapted variogram models as well as the calculated root-mean-square deviation and anisotropy factor. Investigated by Nienstedt (2011).

Indicator	Direction	Range	Sill	Nugget	MSE	Anisotropy factor
1	horizontal	174.0	0.04	0.10	$2.91 \cdot 10^{-4}$	116
	Vertical	1.5	0.04	0.09	$2.66 \cdot 10^{-4}$	
2	Horizontal	180.0	0.08	0.16	$1.30 \cdot 10^{-4}$	120
	Vertical	1.5	0.10	0.13	$4.60 \cdot 10^{-4}$	
3	Horizontal	324.0	0.01	0.06	$1.42 \cdot 10^{-4}$	25.3
	Vertical	12.8	0.11	0.05	$7.34 \cdot 10^{-4}$	
4	Horizontal	300.0	0.01	0.06	$1.89 \cdot 10^{-4}$	142.8
	Vertical	2.1	0.36	0.42	$9.84 \cdot 10^{-3}$	

The average value of the variogram correlation length provides the basis of the search-radius of the SIS. The horizontal search-radius is detected with 245 m and the vertical one with 5 m.

100 aquifer parameter field realizations are generated by use of SIS on the basis of the indicator parameters, search-radius, anisotropy factor and the cumulative distribution function (table 4-6 and table 4-7). Exemplarily, the fifth realization was selected for the aquifer parameter fitting. Figure 4-15 shows the used aquifer-realization differentiated into four indicator classes.

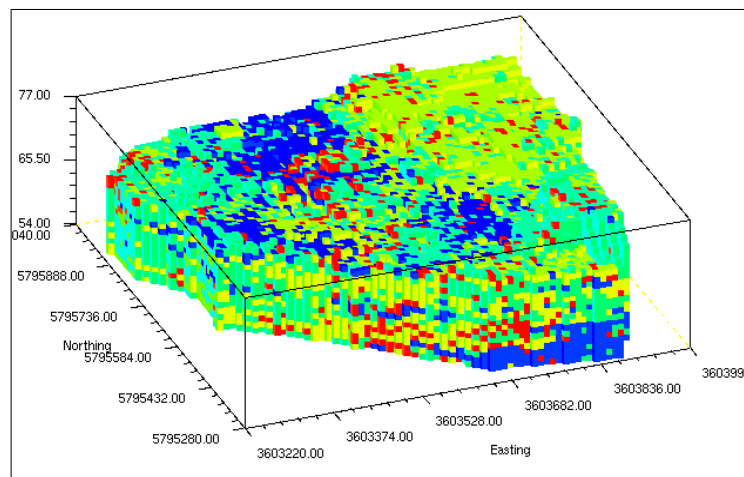


Figure 4-15 Fifth aquifer-realization of the reconstructed parameter field. Classified into four indicator groups. The reconstructed parameter field is implemented in the heterogeneous subsurface approach. Red: indicator 1, green: indicator 2, turkey: indicator 3 and blue: indicator 4 (cf. table 4-6).

The quantification of the uncertainties of the indicator class probability of occurrences was performed by 100 MCs of the reconstructed aquifer-realization.

Figure 4-16 illustrates the percentage probability of occurrence of the most frequently generated indicator.

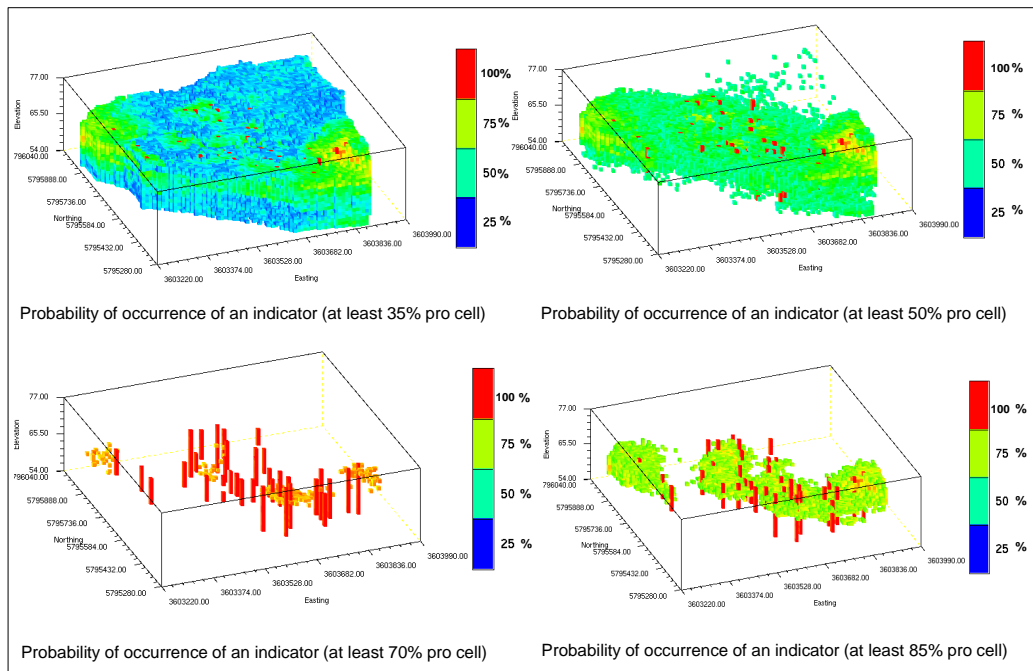


Figure 4-16 Probability of occurrence of most frequently generated indicator pro cell from 100 realizations for a range of 35% up to 50% (above) and 70% up to 85% (below).

A conclusion for which the indicator is documented through the visualized probabilities of occurrence in figure 4-16 cannot be taken. Therefore, figure 4-19 represents the probability of occurrence for each indicator based on 100 aquifer-realizations by using MCs. Figure 4-17 and figure 4-18 include two illustrations of one indicator. The left pictures present the probability of occurrence with at least 25%. The right pictures show the probability of occurrence with at least 65%.

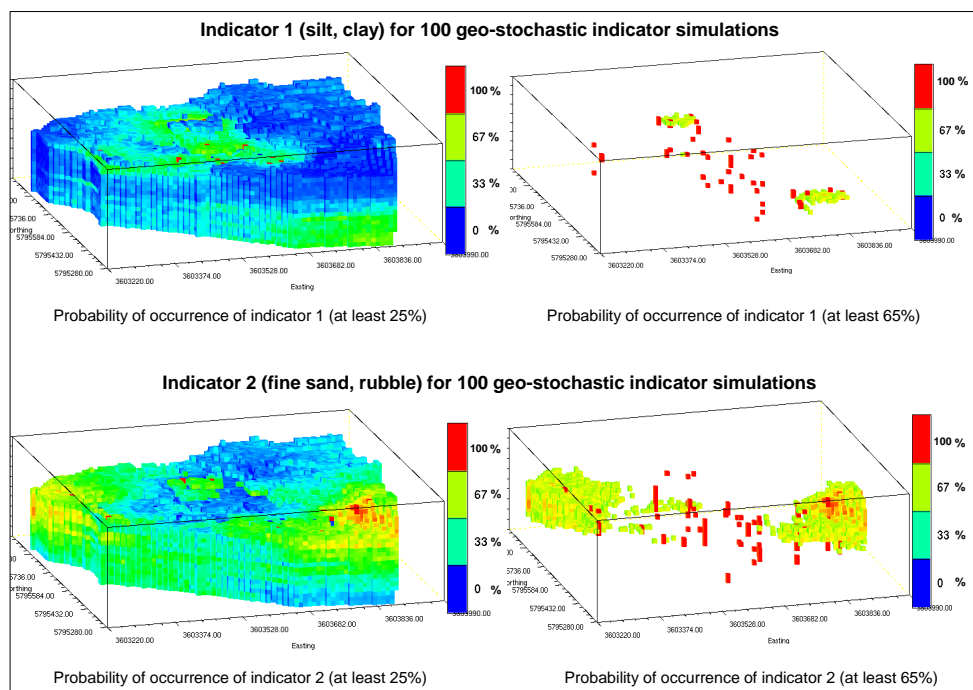


Figure 4-17 Illustration of the percentage probability occurrence of the indicators 1 – 2.

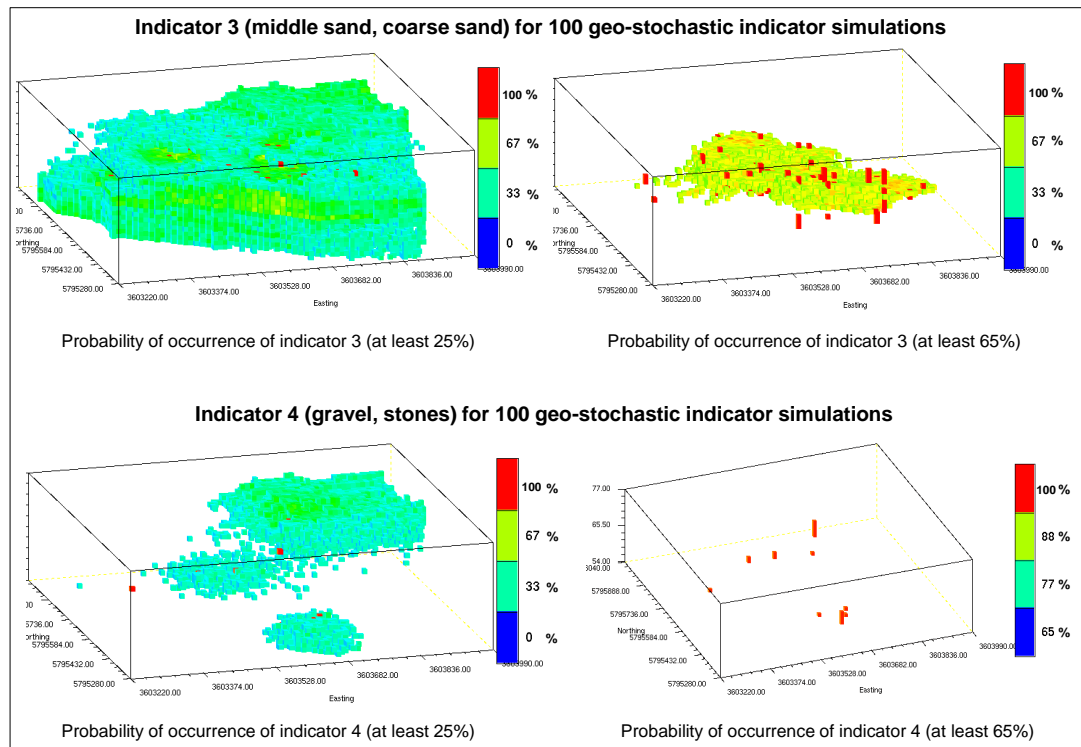


Figure 4-18 Illustration of the percentage probability occurrence of the indicators 3 – 4.

4.2.3 Downscale with Hydraulic Profiling Tool (HPT)

Direct push methods (hydraulic profiling tools) offer the opportunity to get a detailed view of the hydraulic characteristic of the contaminant aquifer. A small area with the highest contaminant concentrations of the investigation area was selected to apply the HPT technique regarding to a detail site characteristic and compatible remediation strategy. The downscaled model of the observed area is supposed to evaluate the generated and assumed hydraulic data. Conventional reconstructions of the aquifer parameter allow “tolerated” uncertainties due to the hydro-geological model set. Even if a contaminant transport takes place, a best possible reconstruction of potential pathways must be taken into account. Especially, the qualities of hydraulic and chemical investigation control the quality of the case of loss quantity. Moreover, the result of the collected data has an influence on decisions concerning remediation strategies. With regard to a groundwater risk assessment, which is targeted at an exact assignment of potential risk factors and elements, cost-efficient hazard identification, must be considered. One of the main important parameters to figure out potential pathways in the aquifer is the hydraulic conductivity. Previous hydraulic conductivities definitions were based on slug&bail or pumping tests. Both techniques have their disadvantages. Slug&bail test provides K_f -value just over the whole filter cascades. Therefore, a layer differentiation gets lost. In contrast, pumping tests are improper if a contaminant groundwater system is investigated. In most cases, the disposal of contaminated groundwater is much more

expensive than the complete remediation. Direct push methods afford fast investigations, more measurement points than the above-mentioned techniques and spatial differentiated K_f -values.

The functionality of hydraulic profiling tools can be referred in Geoprobe Systems (2007) (cf. figure 4-19). Hydraulic Profiling Tool is a system manufactured to evaluate the hydraulic behaviour of subsurface soil. The tool is advanced through the subsurface while water is injected at a constant rate through a screen on the side of the probe. An in-line pressure sensor measures the pressure response of the soil to water injection. The pressure response identifies the relative ability of a soil to transmit water. Both pressure and flow rate are logged versus depth.

In situ testing of hydraulic conductivity is performed by injecting water under a specified flow rate (ca. 300 ml min^{-1}) into the aquifer. The water flows into the layers in an easier or heavier way, depending on the hydraulic properties of the media. The interpretation provides in a preliminary stage a relative profile of hydraulic conductivity. A Wenner array is integrated into the HPT probe and allows the user to collect soil electrical conductivity (EC) data for lithological interpretation.

By means of several slug tests the results are site-specific translated into absolute values of hydraulic conductivity. The HPT system may be used to direct other investigation methods, such as soil and groundwater sampling and slug testing. HPT pressure response and EC data can help target zones of geologic and hydraulic interest, minimizing the number of soil and groundwater samples required to adequately develop a site conceptual model. Running the HPT and EC logs simultaneously provides independent confirmation of one log against the other for lithological characterization. An illustration of the HPT application is shown in figure 4-19.

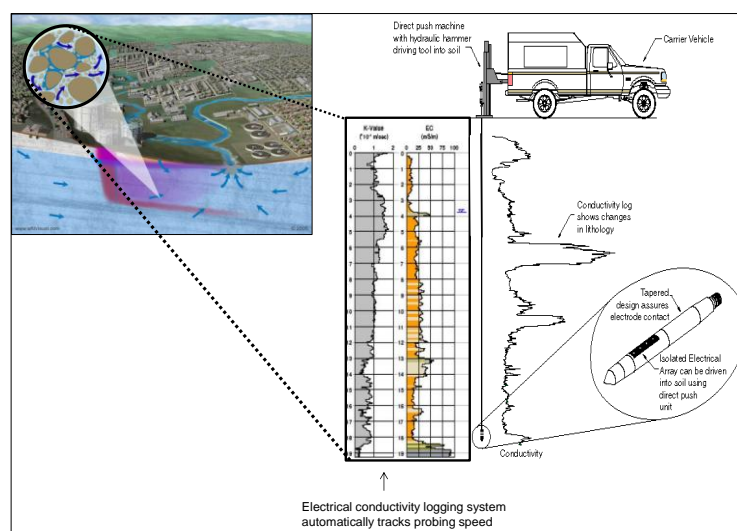


Figure 4-19 Illustration of the Direct push method for a hydraulic profiling. Source: Kansas Geological Survey.

The geological underground reconstruction of the smaller area is based on the recorded K_f -values of the Direct push method. Every 10–15 m a HPT sonde was pushed into the underground to get an investigation area raster of 45 m x 20 m with 12 HPT points (cf. figure 4-5). Based on this performed technique the geological layers were defined for the aquifer containing the hydraulic properties. The outcome is a detailed reconstructed geomorphological aquifer construction (cf. figure 4-20) and a precise record of the site characteristic hydraulic conductivities.

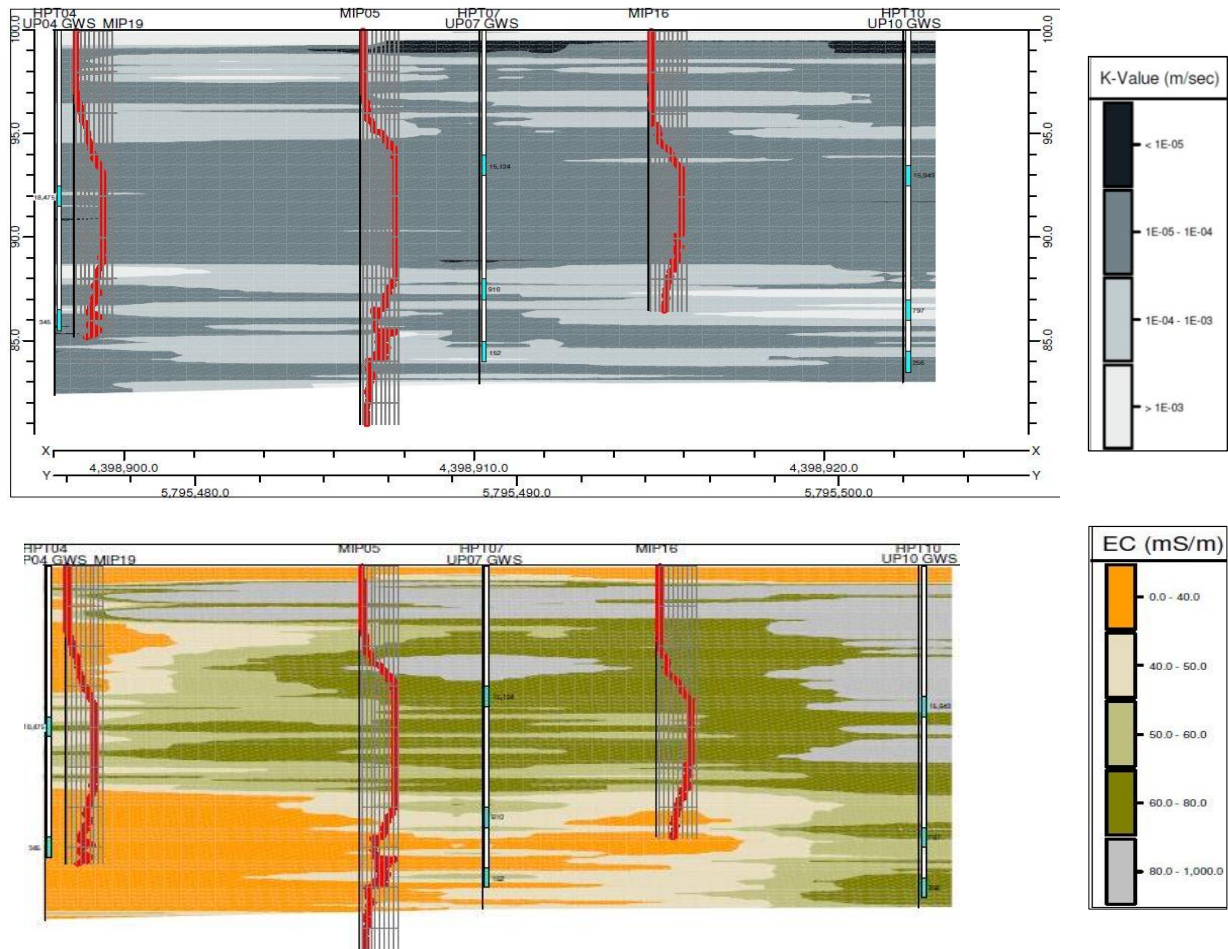


Figure 4-20 Hydraulic profile cross section with corresponding K_f -values ($<10^{-5}$ - $>10^{-3} \text{ ms}^{-1}$) and the resulting hydro-geological cross section with electric conductivity.

The numerical downscaled groundwater flow model was validated based on the determined HPT conductivities. Figure 4-21 illustrates the hydro-geological cross section view through the downscaled model developed from the HPT profiles.

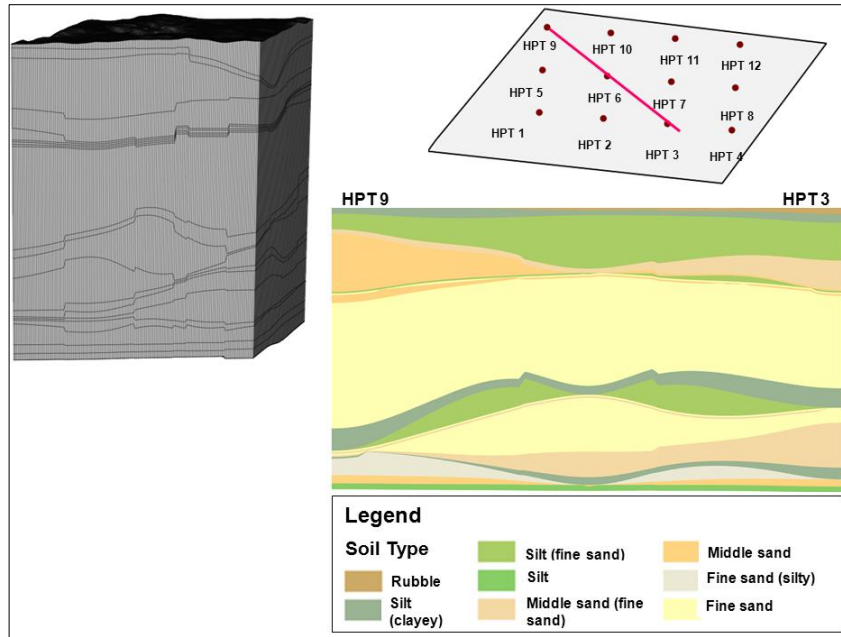


Figure 4-21 Downscaled numerical hydro-geological structure model of the investigation domain by use of 12 HPT profiles. Cross section view of the layer configuration through the model area from HPT9 to HPT3 in groundwater flow direction.

4.3 Dynamic influence on the spreading pattern

The consequences of a multi-species transport in subsurface can only be estimated by an observation of dynamic impacts of the ecosystem which is under investigation. This includes the phenomenological analysis of time series to characterize the physical and chemical properties of an aquifer. The most important part is represented by the measurement of water cycle components and their statistical analysis. Just a detail measure of hydrological events in form of closed time series ensured a reproduction of a dynamic model. The objective of time-dependent modeling is the calculation of water volume and mass balances in assumption of future developments, to record the best possible groundwater system dynamic. A fundamental basis of an estimation of volume and storage is a detailed measurement of the temporal groundwater flow and transport processes.

The analysis of the system impulse responses of varying time series allows a loss assessment and examination of major factors influencing the flow and transport dynamic. The most important groundwater dynamic is represented by hydraulic head variations. Hydraulic heads have to be measured in observation wells to study the general behavior of the groundwater system and to monitor impacts scenarios. In additions, significant effects like precipitation, evapotranspiration and snowfall must be recorded to calculate the transient groundwater recharge. The analysis and interpretation of the time series variability enables the derivation of relationships among hydrological-hydraulic processes. A further important variable in this context is the river water table. Climatic events, including drought season and rainy season,

affected the behavior of the river and ground water level decrease or increase. Both phenomena caused a typical mass concentration occurrence in the contaminated aquifer. Hydraulic processes like river bank filtration and groundwater exfiltration lead in effluent and influent conditions which can be responsible for the mass transfer. Furthermore, an investigation of varying time-series regarding to correlation aspects is necessary to identify system-relevant dynamic processes. The dynamic aspects of a time-dependent transport modeling are illustrated in figure 4-22. It shows exemplarily the groundwater volume exchange and the relation between the aquifer system and surface water as well as subsurface inflow and outflow. Measured or calculated time series like daily areal groundwater recharge, subsurface inflow, transfer and hydraulic heads are integrated in the numerical Finite Element groundwater model as dynamic boundary and initial conditions to calculate transient groundwater flow and mass transport. Furthermore, the use of dynamic variables allows the simulation of quantities of fluid and contamination masses, which enter or leave the model domain.

The observation of the contamination plume was performed by several groundwater sampling and focused on the measurement of PCE, TCE, DCE and VC, redox potential, nitrate, sulfate, iron, manganese, sodium, calcium, potassium, magnesium and chloride.

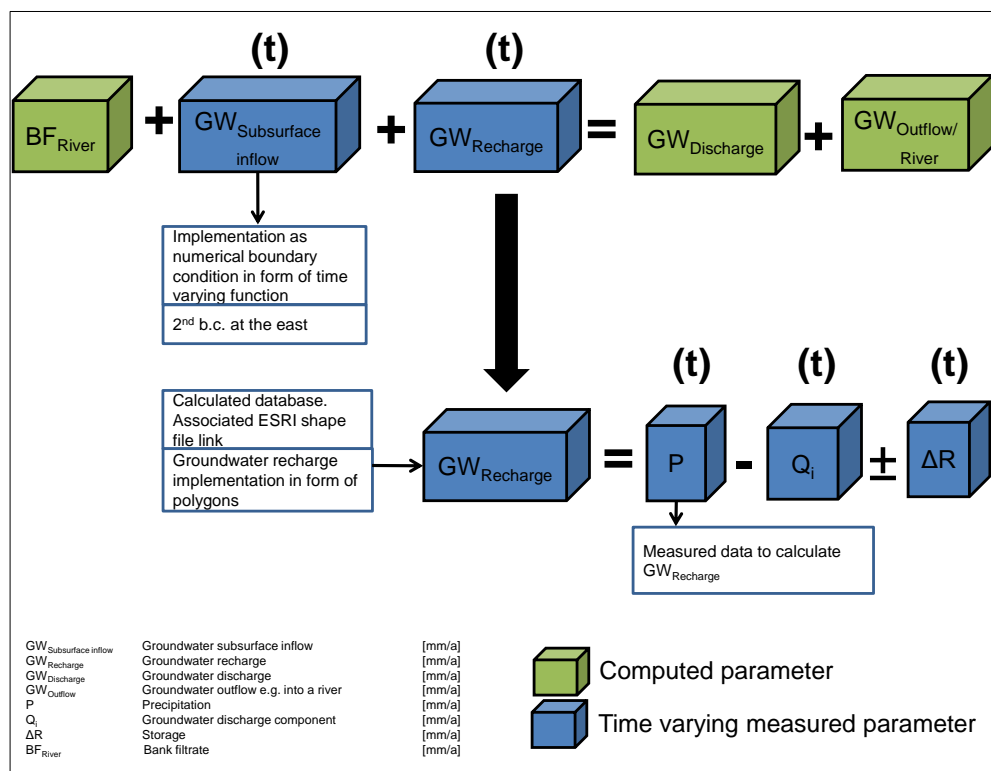


Figure 4-22 Dynamic aspects of a time-dependent groundwater simulation. Illustration of the individual volumes of a groundwater balance equation. Differentiation between time varying parameters (t) like groundwater subsurface inflow or groundwater recharge, which are defined as time-varying function in the numerical model and numerical calculated parameters like groundwater discharge or groundwater outflow into rivers or lakes.

4.3.1 Climatic data

To specify the transient transport model of the investigation area, different climatic and hydrological parameters were determined. Overall, a period of 431 days (12/11/2009 – 16/01/2011) was taken into account. Figure 4-23 shows the climatic events for precipitation, snow, evaporation and groundwater recharge of Braunschweig from the “Deutscher Wetterdienst (DWD)”.

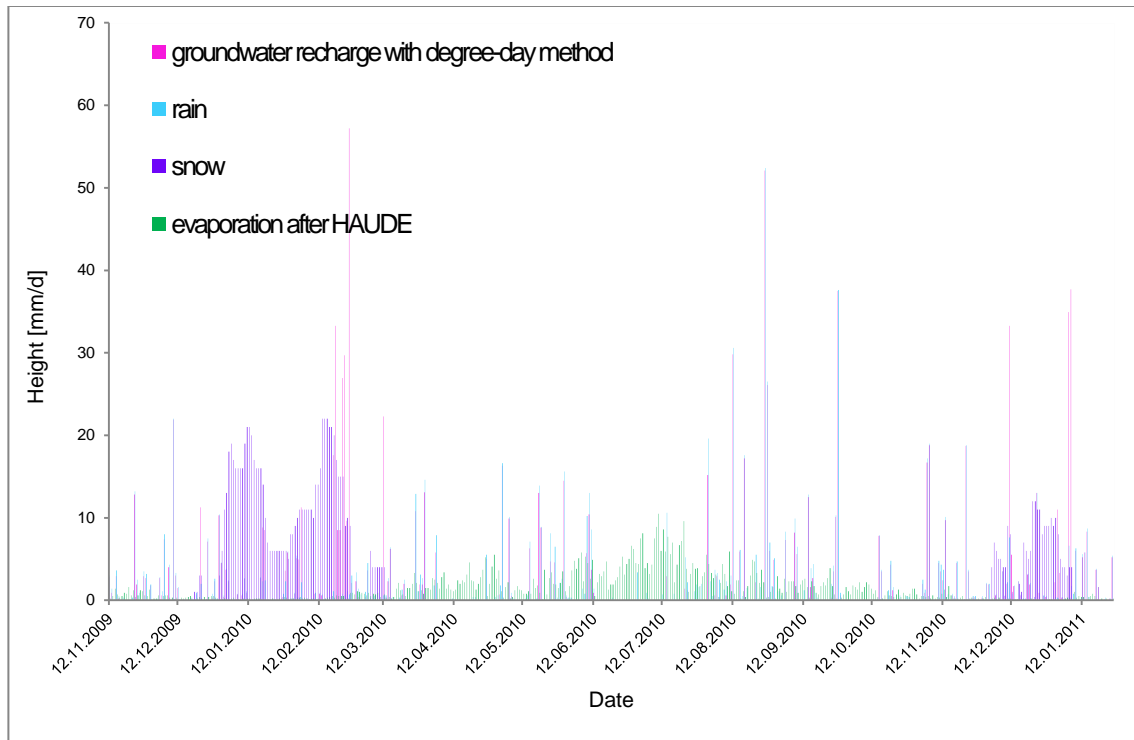


Figure 4-23 Precipitation, evaporation and snow height of Braunschweig (source: DWD) from 12/11/09-16/01/11. Based on this measured values the groundwater recharge was calculated by a degree-day method and defined in the groundwater model in from of a time-varying function.

The groundwater recharge is an area-related property, which must be implemented in a time-dependent groundwater model as an actual infiltration into the model area from the top. In the process of groundwater recharge definition it has to be note that the land cover (use) has an influence on the infiltration behavior. One possibility to include the land cover as well as groundwater recharge by snowmelt is the degree-day method:

$$M_d = a_d T_L - T_b \text{ mmd}^{-1} \quad \text{Eq. 4-16}$$

a_d Degree-day factor or snowmelt factor e.g. $4 < a_d < 8$ (table 4-8) [mm/°C]

T_L Air temperature, average value of the day period with positive values [°C]

T_b Basis temperature, generally 0°C [°C]

The air temperature is used for the calculation of the potential snowmelt rate, which is composed of the sum of the daily average value of the positive temperature and a degree-day factor. The basis for the degree-day factor is the numeral coverage of the sensible heat flow by the heat transfer coefficient and the temperature difference between air and snow layer. After Maniak (1997), the daily snowmelt rate alternate for uncovered surface between 3 and 10 $\text{mmd}^{-1}\text{K}^{-1}$.

Table 4-8 Degree-day factor a_d in $\text{mm}/(^{\circ}\text{Cd})$ for different vegetation covers after Maniak (1997) with basis temperature $T_b = 0^{\circ}\text{C}$.

Vegetation cover	a_d
Uncovered surface	4 ... 7
Open deciduous forest with low coniferous forest portion	3 ... 4.3
Coniferous forest or dense mixed forest	1.5 ... 2.3
Dense coniferous forest	1 ... 1.5
High mountains, glacier	> 6

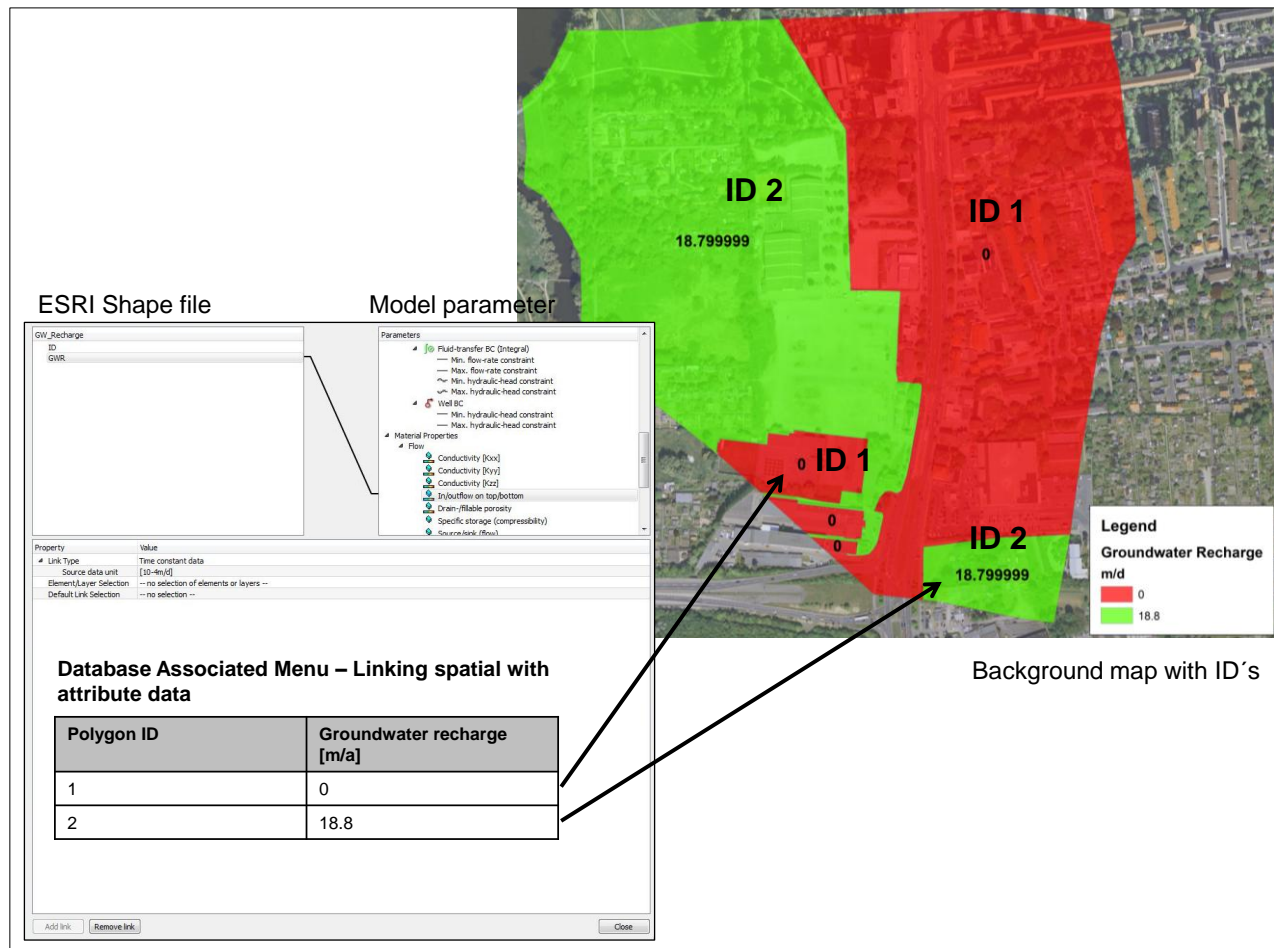


Figure 4-24 Land cover and assignment of groundwater recharge with database associated menu in the groundwater model. Spatial data like groundwater recharge are linked by an ESRI shape file with attribute data. The linking is controlled via ID's of single spatial elements. Each ID is integrated in the Finite Element model as a time-varying function or parameter.

4.3.2 Hydrological data

Even if an aquifer is connected with bordering hydro-systems it is important to understand the dynamic of both ecosystems. Especially, the effluent and influent hydraulic conditions must be taken into account regarding to a contaminant transport. The colmation layer plays a special role because it is the hydraulic barrier between the river and groundwater level.

The temporal variation of the hydrological parameters like groundwater level and river water level in dependency of climatic events were recorded by several data loggers distributed over the investigation area. Figure 4-25 shows the daily recorded groundwater and river water hydrographs of selected wells.

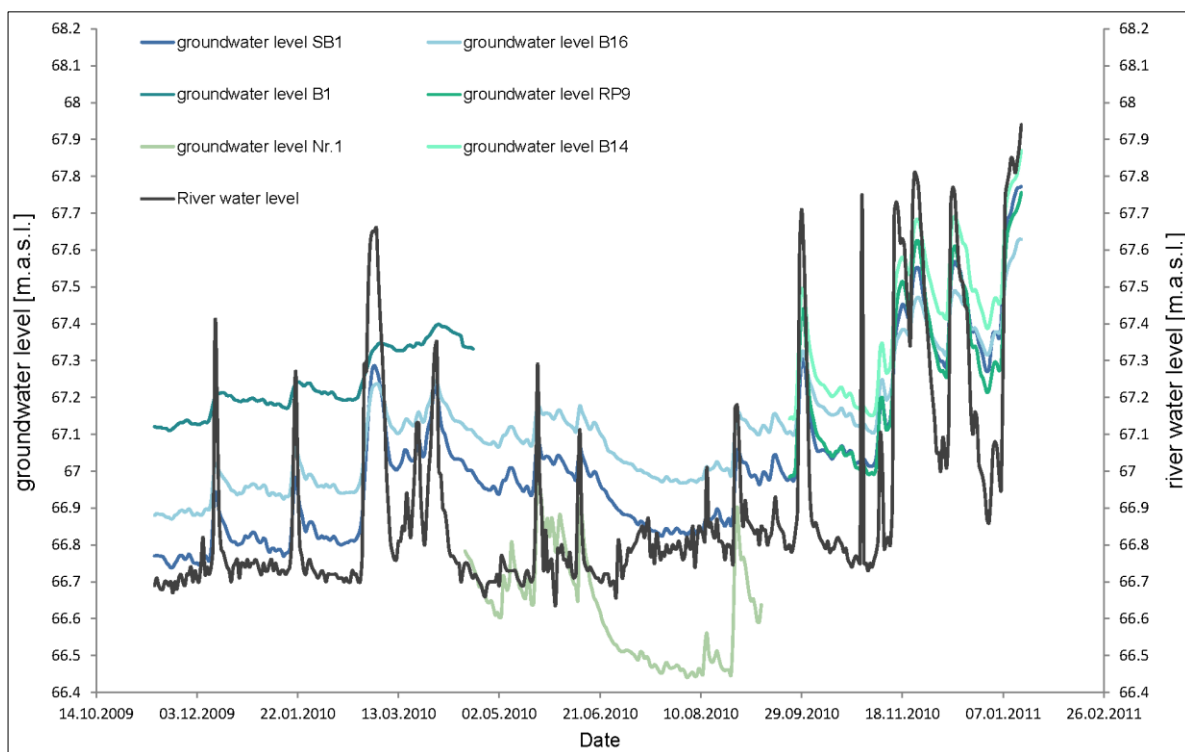


Figure 4-25 Recorded groundwater and river water levels of the model area from 12/11/09–16/01/11. The dynamic data are necessary as time-dependent boundary conditions of the transient groundwater model and for the model calibration.

The investigated groundwater and river water level provide a typical surface-groundwater interaction. In drought season (summer, winter) the groundwater level is above the river water level. On the contrary, in wet season the water table is below the river water level. Due to this fact, different dynamic conditions were developed to analyze their impacts on the pollutant dispersal

The groundwater level as well as the river water level is used as initial and boundary conditions. In both steady-state and transient simulations, initial hydraulic head is reference as

hydraulic head in time step 0. The groundwater hydrograph was additionally used to calculate a Neumann boundary condition (fluid-flux) for the east model border.

Groundwater and surface water can be closely linked, each contributes to the other. That interaction plays an important role for the catchment (Becker, 2010). The figure 4-26 gives an overview of two interaction categories for the observed model area.

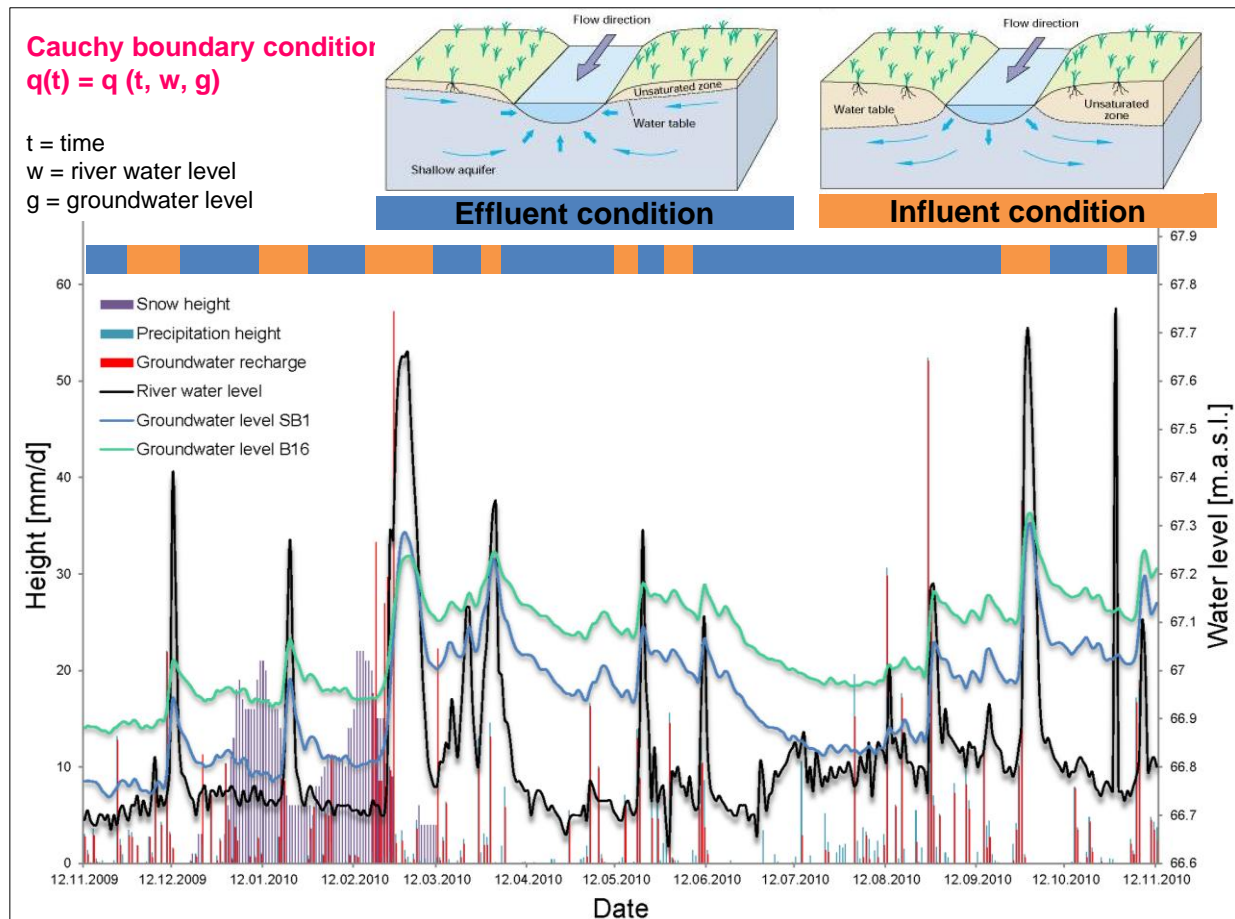


Figure 4-26 Schematic illustration of effluent and influent hydraulic conditions between river and groundwater level of the investigation area depending on climatic events (snowmelt, groundwater recharge and precipitation).

Most commonly, groundwater contributes to a stream (effluent condition). During extreme value events (e.g. snowmelt or intense rain), the conditions invert to influent processes where the river water level is above the groundwater level. The river water flows from the stream bed through a porous media to recharge the groundwater. A seasonal cycle of climatic events is crucial for the interaction. In regard to a contaminant flow and transport model that effect must be considered. Depending on the colmation layer property the interaction can be bidirectional.

Another opportunity to research the hydraulic connection between the aquifer system and gaining stream is an arrangement of the correlation between ground- and surface water table (cf. figure 4-27). In addition, conclusion of integrated contaminant transport can be made.

The impact of a rapid groundwater reaction on system inputs and its resulting influence of the flow conditions are documented in Herrmann et al. (1992).

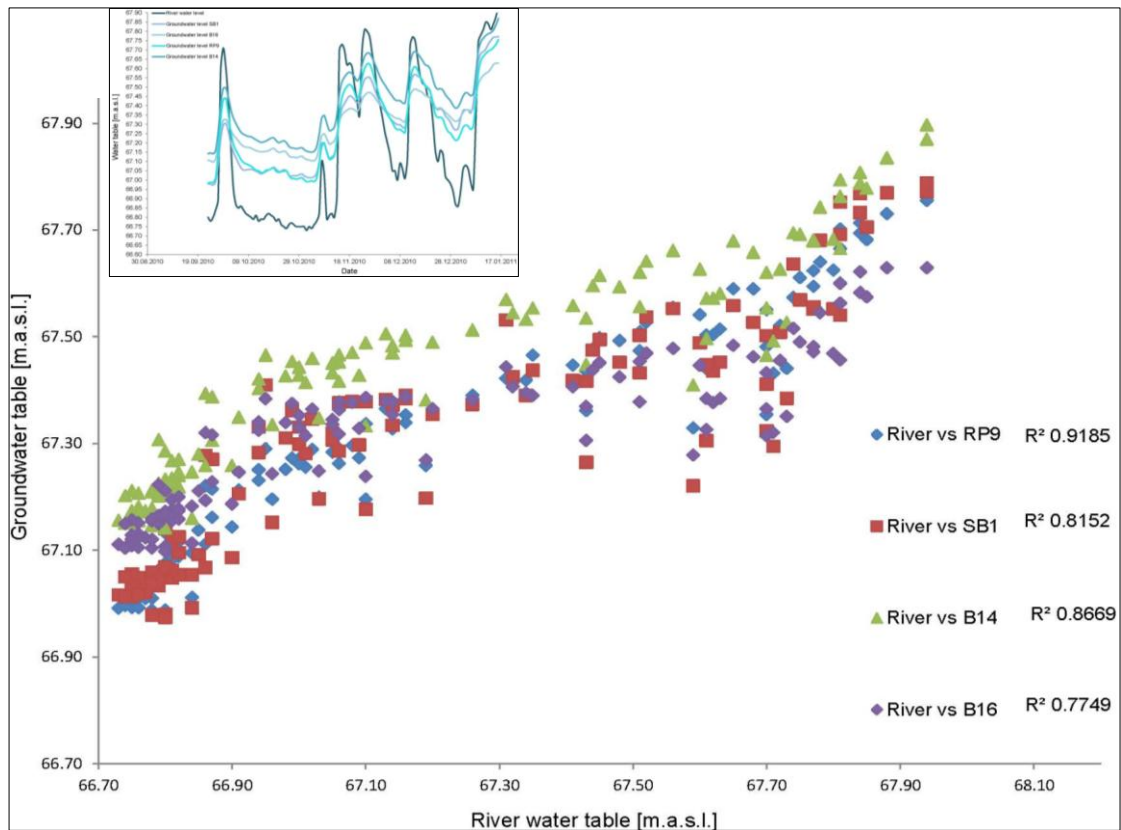


Figure 4-27 Relationship between groundwater and river water level of the observed area from 23/09/2010–16/01/11.

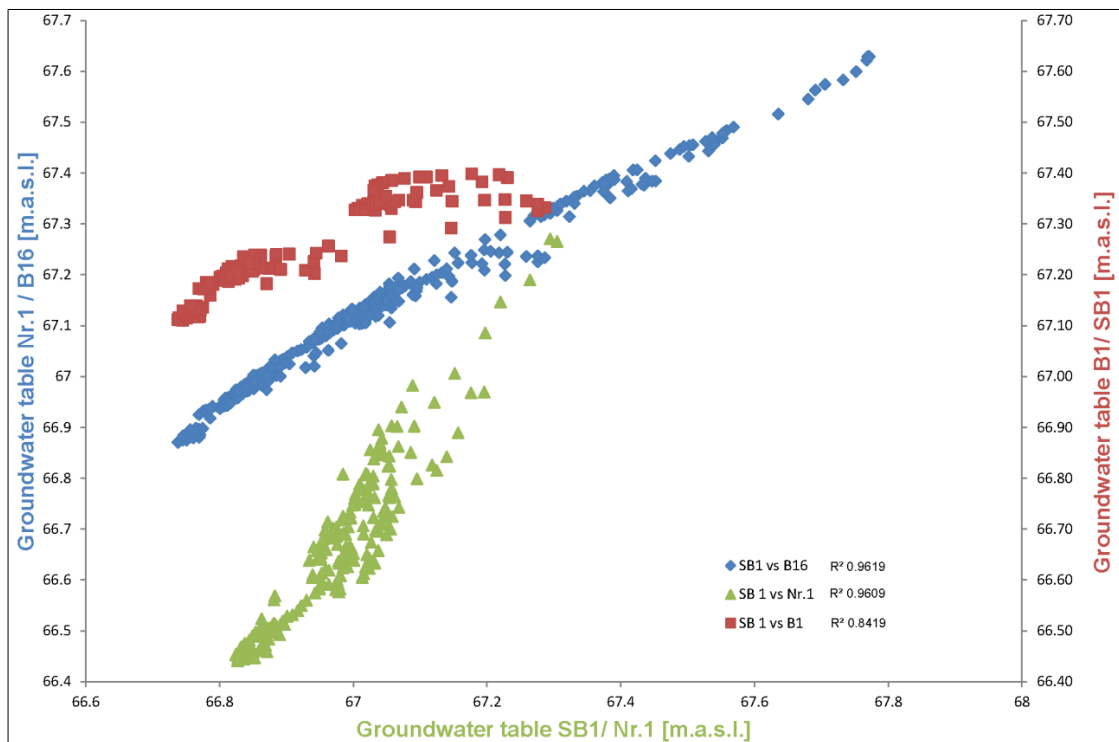


Figure 4-28 Diagram of groundwater tables from daily measurements between 12/11/2009–12/11/2010 of well SB1, Nr. 1, B16 and B1.

Figure 4-28 exemplarily shows the daily groundwater tables of SB1, B1, B16 and Nr.1 for one year plotted against each other. A significant linear correlation is identifiable between SB1 and Nr.1 as well as SB1 and B16. Nr.1 is located closed to the bordering river. B16 is installed on the middle of the reference area. The throughout constant elevation difference allows the conclusion that the flow conditions respond to a hydraulic gradient from east to west. An existence of hydraulic potential between those wells is proven. Furthermore, the diagram can be consulted to interpret climatic events, which have an influence on the groundwater recharge. The hydraulic dynamic on an inflow on top event at each well is linear.

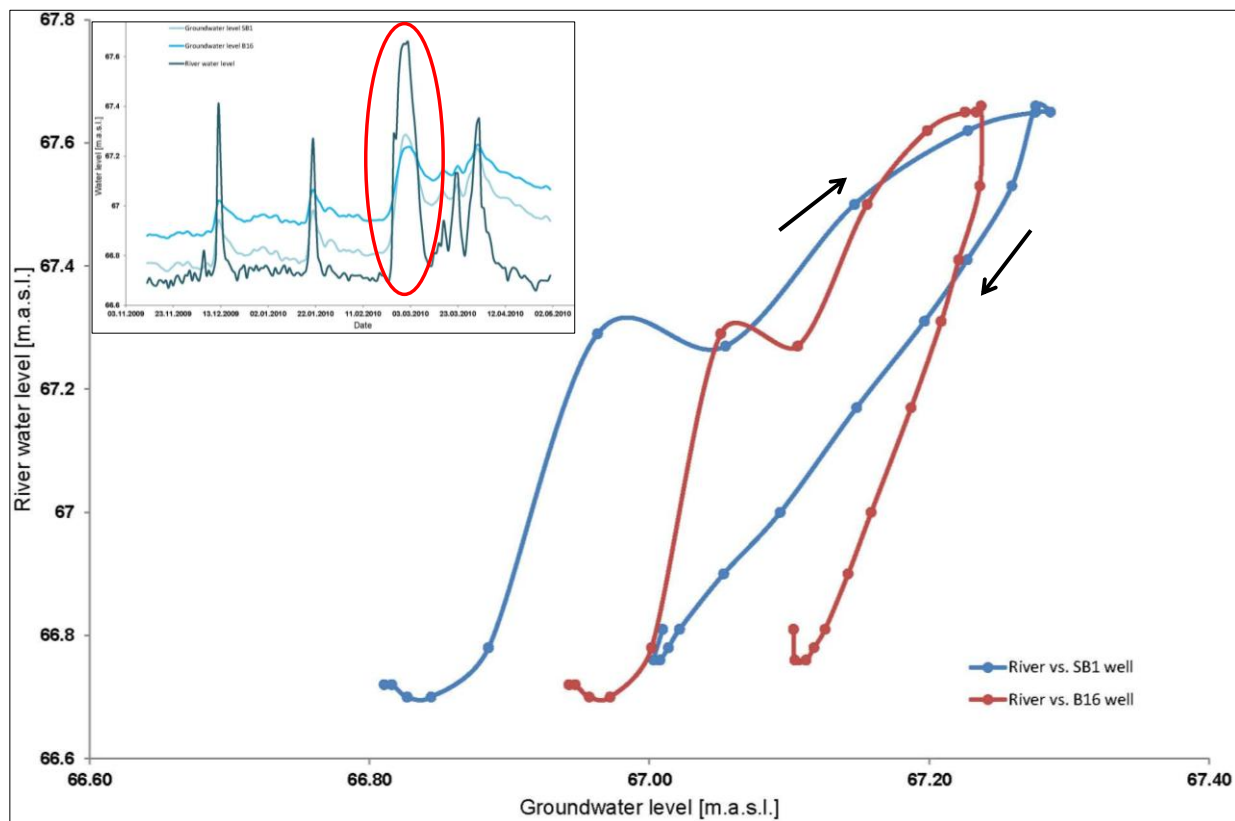


Figure 4-29 Evolution of the relationship between groundwater table of well SB1 and B16 and the river water table in a flood event resulting from snowmelt event (19/02/2010-13/03/2010).

The time series analysis of the ground- and surface water table has shown a hysteresis effect during flood events resulting from snowmelt or groundwater recharge caused by an intense rain. Figure 4-29 represents such a hysteresis loop for a flood event from 19/02/2010 - 13/03/2010 caused by snowmelt for groundwater table of well B16 and SB1 depending on the river water table. Both wells show a hydraulic dynamic interaction between the ground- and river water table. While the river water table is increased, the increase of groundwater table reacts with a short time delay. Influent conditions are adjusted. After the flood event, the opposite case takes place. The groundwater table is higher than the river water table, so-called effluent conditions level out.

4.3.3 Time series in the Finite Element model

A time and spatial-dependent flow and mass transport simulation assume a model area and model time discretization to solve the partial flow and transport equation. Therefore, the spatial parameter distribution and boundary condition type and location must be known. The prepared times series in form of groundwater and surface water hydrographs are integrated in the transient FEM model as time-varying functions. All time series were recorded for one year to represent a hydrological year. The initial time step (t^0) is the 12/11/09 with a time length of 25,550 days. Because of the short time period of one year, the varying-time functions were set as cyclic recurrent. Figure 4-30 represents the groundwater hydrograph of the transient flow model as 2nd Neumann boundary condition. A further central importance has the surface water level of the bordering river ecosystems. There are two general opportunities to describe the influence of the surface water table in the groundwater model. The first way is the definition of a 3rd Cauchy boundary condition (transfer), if the aquifer and river are under normal conditions (average water level) (cf. figure 4-31).

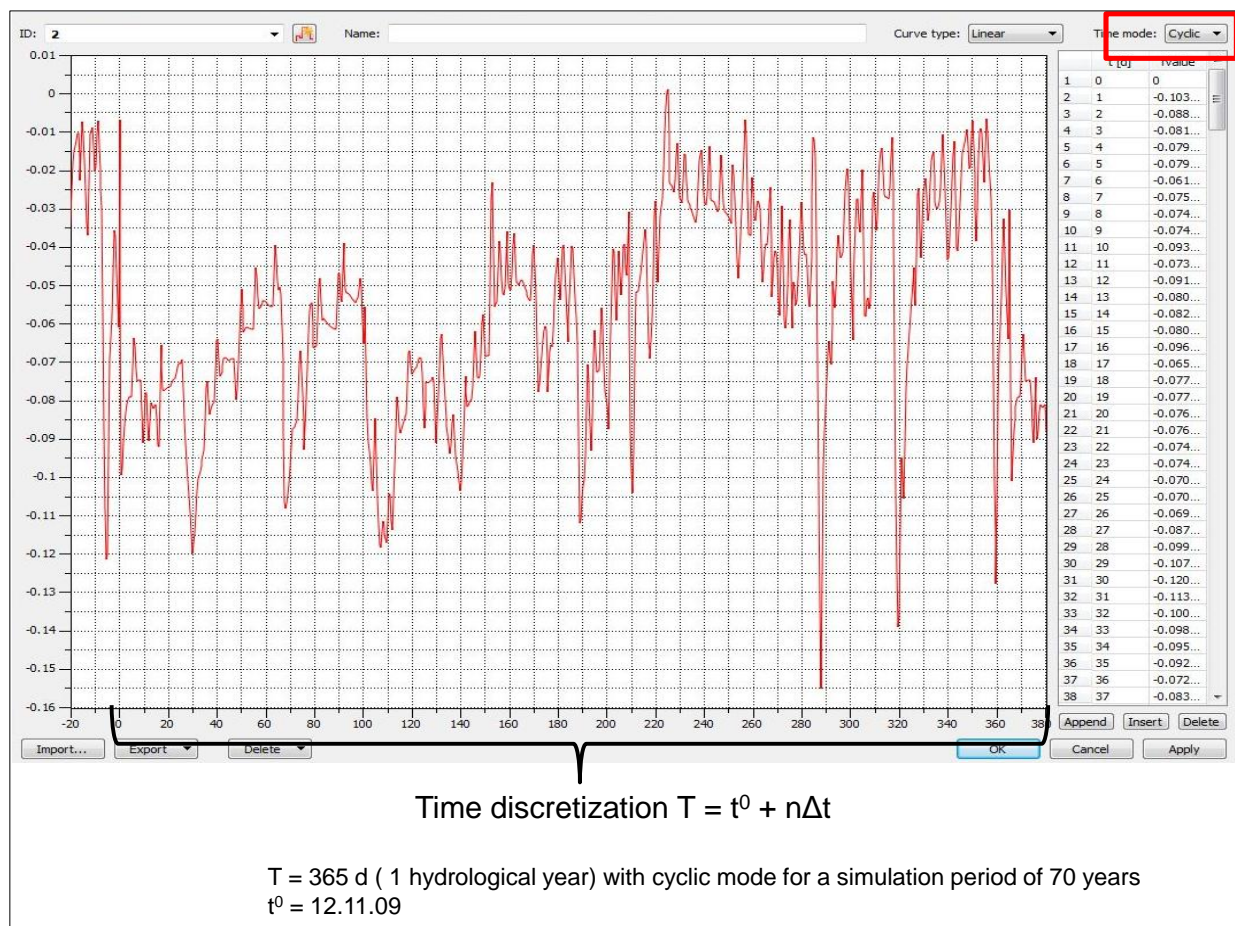


Figure 4-30 Fluid-Flux time-varying function [m d^{-1}] for the transient model. The 1 year hydrograph is defined as 2nd Neumann boundary conditions (fluid flux) with a cyclic occurrence of 70 years (simulation period).

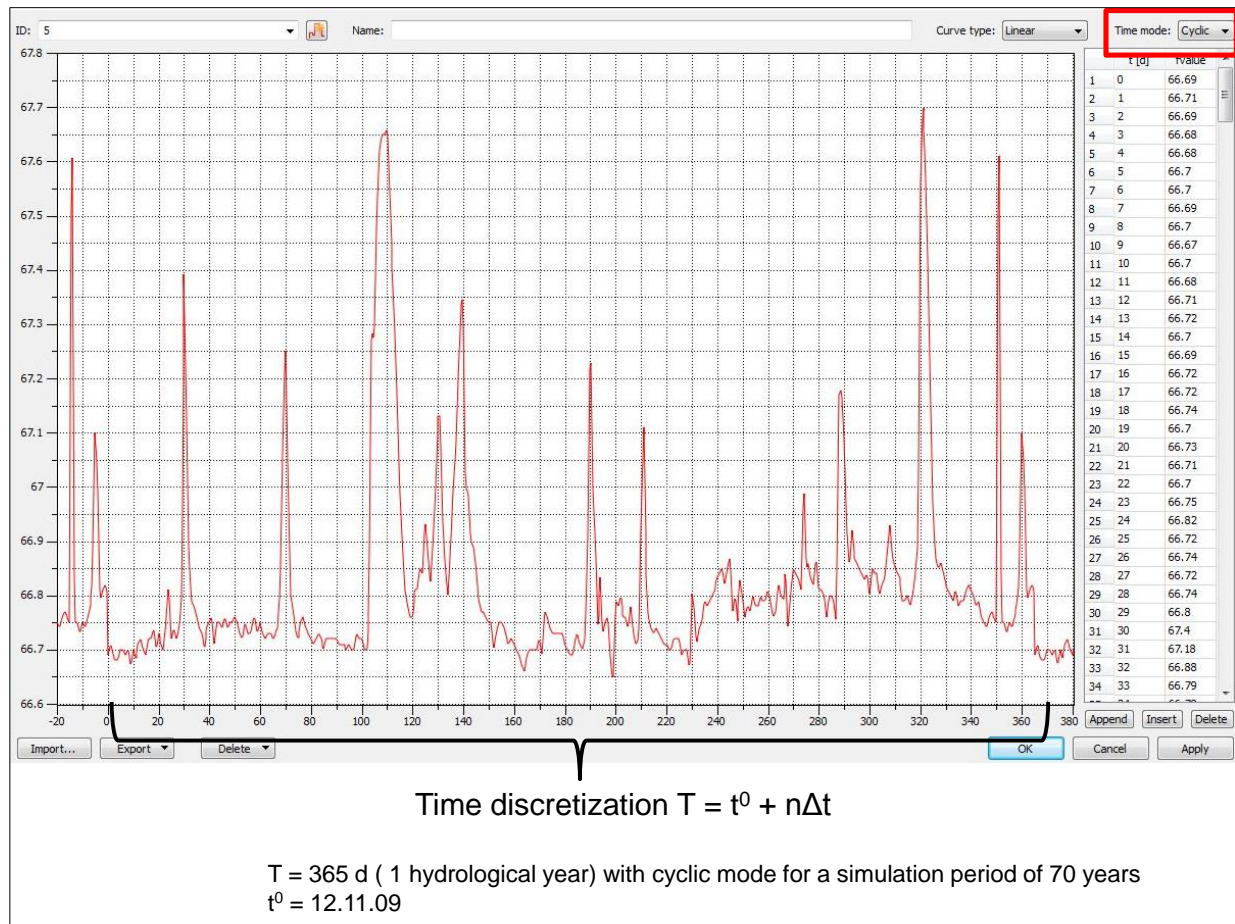


Figure 4-31 Surface water time varying function [unit m.a.s.l. d^{-1}] for the transient model. The 1 year hydrograph is defined as 3rd Cauchy boundary conditions (transfer) with a cyclic occurrence of 70 years (simulation period).

Another way is the coupling of both ecosystems by an interface between the groundwater and surface water. In this thesis, the coupling is used to simulate different scenarios like flood events to identify the interaction regarding to a risk situation and the impact degree on the water exchange volume.

The time-dependent infiltration is defined as a groundwater recharge time-varying function with the same conditions as the groundwater and surface water time discretization (cf. figure 4-32). This parameter was set on the top of the model. During the simulation, the flows will be applied to the corresponding layers.

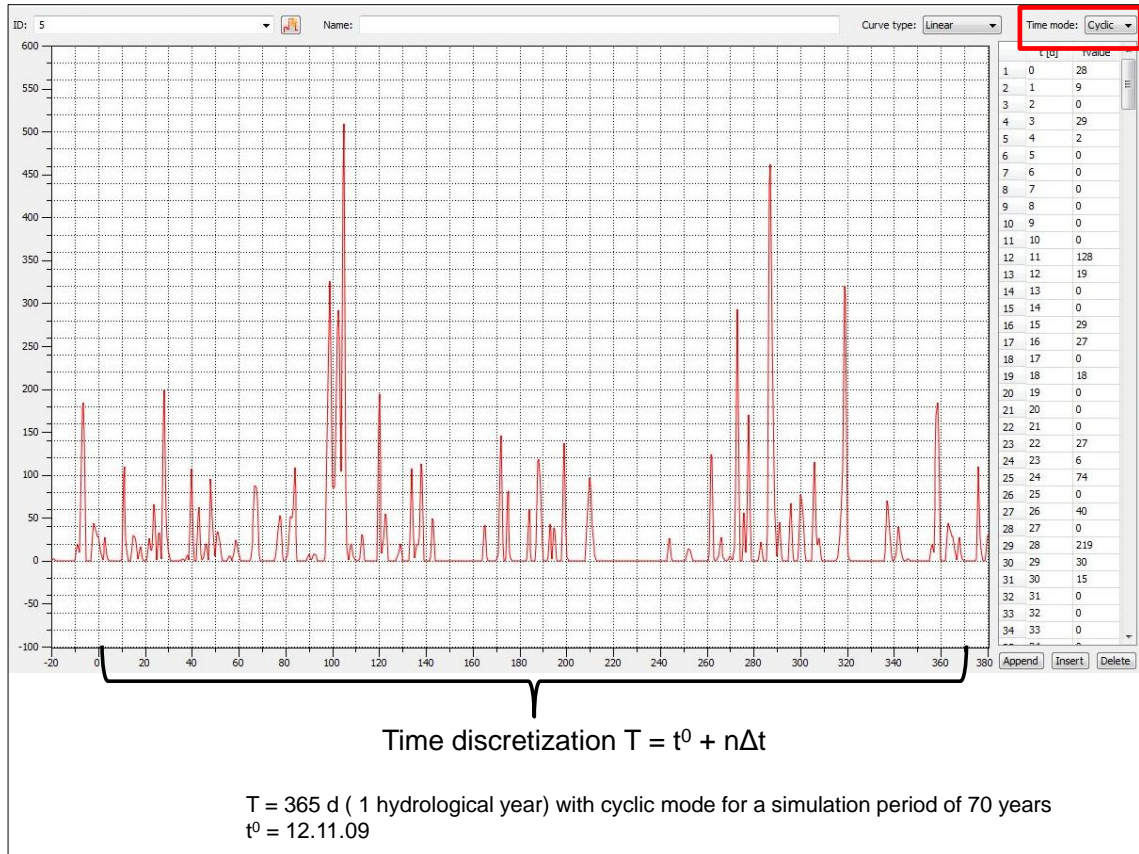


Figure 4-32 Groundwater recharge time-varying function [unit $10^{-4} \text{ mm d}^{-1}$] for the transient model. The 1 year hydrograph is defined as inflow on top with a cyclic occurrence of 70 years (simulation period).

4.4 Numerical Solution method

The groundwater flow and transport calculation is operated by a Finite Element method software tool, which was tested for diverse benchmarks.

Istok (1989) accented several advantages for using Finite Element method in the field of flow and transport problems. The method is qualified especially for heterogeneous, anisotropic aquifers with complex geological structures and irregular boundaries.

The Finite Element method, like the Finite Volume method is based on a linear approximation of the unknown hydraulic head and concentration c_i , using approximation function $N_i(x,y,z)$ (Rausch et al., 2005):

$$C_{x,y,z} = \sum_{i=1}^m c_i N_i(x,y,z) \quad \text{Eq. 4-17}$$

N_i Interpolation function

c_i (unknown) Values of the field variables at the node

m Number of nodes in the mesh

The *integral formulation* leads to a system of algebraic equations that can be solved for the hydraulic head and mass concentrations at each node of the Finite Element mesh. The *method of weighted residuals* is a general approach to derive the *integral formulation*. This method is based on an approximation solution to the boundary or initial value problem. A residual occurs at each node when the approximation solution is substituted into the governing differential equations. The weighted average of the residuals for each node is forced to equal zero:

$$\int_{\Omega} W(x,y,z) R(x,y,z) d\Omega = 0 \quad \text{Eq. 4-18}$$

$W(x,y,z)$	Weighting function
Ω	Problem domain
R	Residual due to the approximation solution

The Finite Element method is used to solve the advective-dispersive transport equations for mass concentrations. The transport advective phenomenon often becomes dominant which leads to the failure of the numerical technique or numerical instabilities. Numerical difficulties could be overcome for multi-species transport problems by using upwinding techniques such as the streamline-upwind *Petrov-Galerkin* (SUPG) to stabilize the numerical solution. The *Petrov-Galerkin* least square (PGLS) Finite Element method appears for tackling advective-dominant flow and transport processes at variably saturated conditions (Diersch, 2009). The Galerkin method assumes that the test function is equal to the approximation functions that have already been defined. A detail description of the *Petrov-Galerkin* method can be reviewed in (Diersch, 2009).

The combined effects of transport and diffusion are lead to numerical oscillations. The *Peclet* number P_e , which represents the ration of transport versus diffusion effects, governs the advection-diffusion equation. A dominant diffusion process results in a low value of P_e . On the contrary, a high value of P_e implies an advective transport. Huyakorn (1977) documented typical cases and examples of severe numerical oscillations. The typical P_e element equation is given by:

$$P_e = \frac{v h}{D} \leq 2 \quad \text{Eq. 4-19}$$

v	Macroscopic phase (pore) velocity
h	Representative element length
D	Dispersion

Weatherill et al. (2004) propose the use of several problems of unstable steady-state convection with variable fluid density in porous media. The study represents grid *Peclet* numbers for five varying layer depths. With an element discretization of 2 m x 2 m and 50 m depth and a velocity of $2.3 \times 10^{-6} \text{ ms}^{-1}$ a P_e number of 1.29 was resulted. Weatherill et al. (2004) declared that a numerical stability is given by a P_e number ≤ 4 . Kolditz et al. (1998) examined variable density flow and solute transport in groundwater systems. A mesh analysis for different refinement rates is provided in this research by use of the grid *Peclet* number. The more refined the numerical mesh the smaller was the P_e number (P_e 2.5) and less numerical instabilities

The average pore velocity of the used groundwater transport model is calculated with 3.6 md^{-1} with a longitudinal dispersivity of 8.8 m and a representative element length of 4.4 m. The P_e number for the Finite Element transport model is given with 1.8. After Lege (1996), a P_e number smaller than 2 represents a parabolic character of the differential equation, which means a numerical stability, is given.

A further important parameter for describing the numerical stability is the *Courant* number C_r . The *Courant* number expresses the ratio of the distance traveled by a disturbance in one time step to length of a computational distance step. For the simplest identification of the stability, the *Courant* number must be less than or equal to 1 to ensure that the solution remains within the computational domain. Ataie-Ashtiani et al. (1999) analyzed numerical truncation errors by different *Peclet* and *Courant* numbers for a Finite Difference model for solute transport equation with first-order reaction. They figured out that an increasing of the Courant number leads to a decrease in numerical dispersion. The criterion is calculated by:

$$C_R = \frac{v \Delta t}{\Delta l} \leq 1 \quad \text{Eq. 4-20}$$

Δt Time step

Zairi et al. (2000) proposed a two-dimensional Finite Element model for pollutant migration in porous media with an implementation of the advective-dispersion equation in the numerical model and validations test by comparison analytical solutions. The simulation tests have shown that a convergent and stabile solution is observed with a Courant number between 0.25 and 2 for a Galerkin Finite Element method.

The average Δt for the transient transport simulation is given by 1d by use of an adaptive time step scheme (cf. chapter 4.4.2). Subsequent, a *Courant number* of 0.81 is obtained.

The adherence of the *Neumann criterion* assures that the concentration gradient in a Finite Element during a time step Δt can be inverted only by the diffusive or dispersive mass flow:

$$F_o = \frac{D}{\Delta l^2} \Delta t \leq \frac{1}{2} \quad \text{Eq. 4-21}$$

The resultant *Neumann number* for the transient transport simulation of the contaminated aquifer is computed with 0.4.

4.4.1 Treatment of the free-surface

A particular problem during transport simulation is the treatment of the phreatic surface. The distribution of the contaminant in the aquifer is dependent on the groundwater flow. Just by a transient groundwater level, different parts of the aquifer are saturated. In that case, the concentration c is a function of the hydraulic head h . For this reason, the surface must be considered to a free and movable mesh (cf. figure 4-33). The used groundwater model includes the adaption of the Finite Element mesh to a changeable free-surface by the BASD (best adaption to stratigraphic data) technique. According to Diersch (2009), this technique transforms and joins the model data containing the stratigraphic initial structure to a moving Finite Element mesh. Consequently, the mesh is adapted to the free-surface location. The condition leads to a non-linear boundary-value problem due to a priori unknown free-surface location. Processes have to be solved by an appropriate iterative scheme.

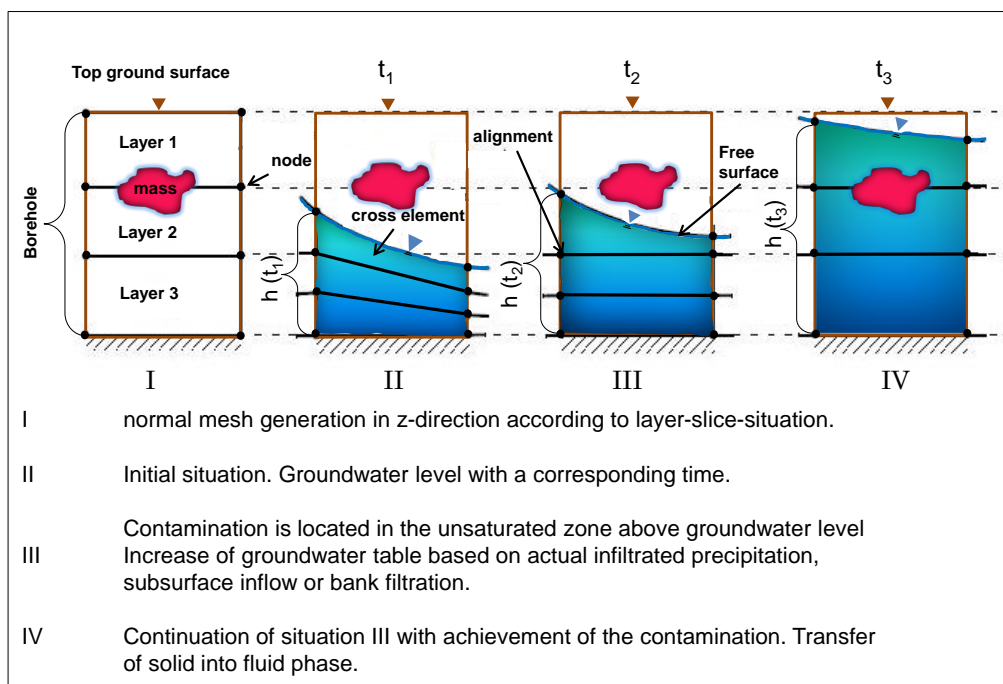


Figure 4-33 Moving mesh BASD technique of parameter adaption applied to 3D free-surface. Example of a contaminated groundwater system with different groundwater table increase situations caused by precipitation, subsurface inflow or bank filtration. At the beginning of the simulation the contamination is located in the saturated zone. The consequent of groundwater level increase and mesh adaption is the concentration achievement. Diersch, 2009, modified.

4.4.2 Numerical aspects of the Finite Element method

Another important point regarding a complex flow and mass transport simulation is the overall runtime and software memory. The use of a robust and efficient linear solver is indispensable. The Fraunhofer Institute (K. Stüben Institute for Algorithms and Scientific Computing) developed an *Algebraic Multigrid* (AMG) solution technique. An AMG is a hierarchical, matrix-based approach that operates with increasingly smaller linear systems equations. Restrictions of residuals and interpolation of corrections are transfer by a matrices construction, which is based on matrices entries. In particular, matrices on coarser levels are computed by a Galerkin principle. The AMG solution is divided into two parts (Diersch, 2009):

- a) *Setup phase*. Choosing the coarse levels and defining the transfer and the coarse-grid operator.
- b) *Solution phase*. Performance of normal multigrid cycling until a desired level of convergence is reached.

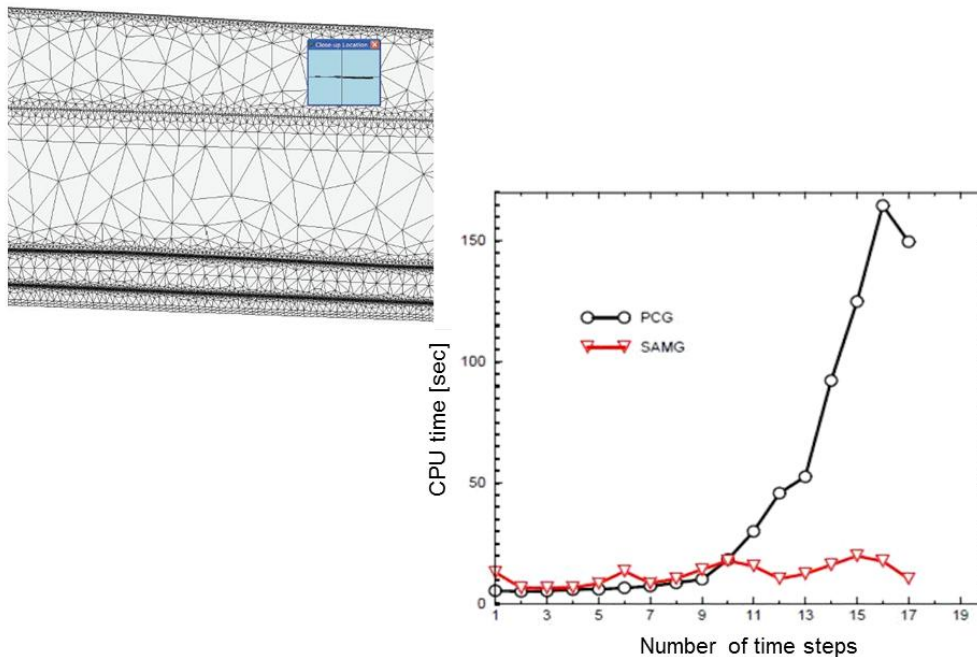


Figure 4-34 Comparison between CPU times and number of time steps of a cross-sectional vertical groundwater problem with triangle mesh, which is fully unstructured and locally refined in a layered geometry for a PCG and SAMG equation solver. The SAMG solver is superior to PCG because PCG requires more iteration. The CPU time of SAMG is three times smaller than for PCG. Diersch, 2009, modified.

4.4.3 Time step controller description

The temporal discretization and iterative solution process can cost a lot of simulation time if the time steps are not adapted to the complex flow and transport process. In general, it must be predicted which time steps are allowable with respect to the accuracy requirement. Unlike

predefined time step marching strategy fully implicit and semi-implicit two-step techniques like GLS-(Gresho-Lee-Sani) predictor-corrector time integrator with automatically controlled time stepping of first order by the *Forward Euler/Backward Euler* and of second order by the *Adams/Bashforth/Trapezoid Rule* have proven to be accurate strategies.

The performance of the nonlinear multi-species kinetic reaction transport model requests a powerful time stepping technique. It refers to an explicit forward Euler formula as the predictor and the implicit backward Euler method as the corrector. For this reason, the automatic time step control of first-order was chosen for the transient conditions. This means that at each time step the convergence tolerance directly governs the time-step size. In consideration of the simulation performance, it is a cost-effective method, because the time-step size is increased whenever possible and decreased when necessary due to the error estimates.

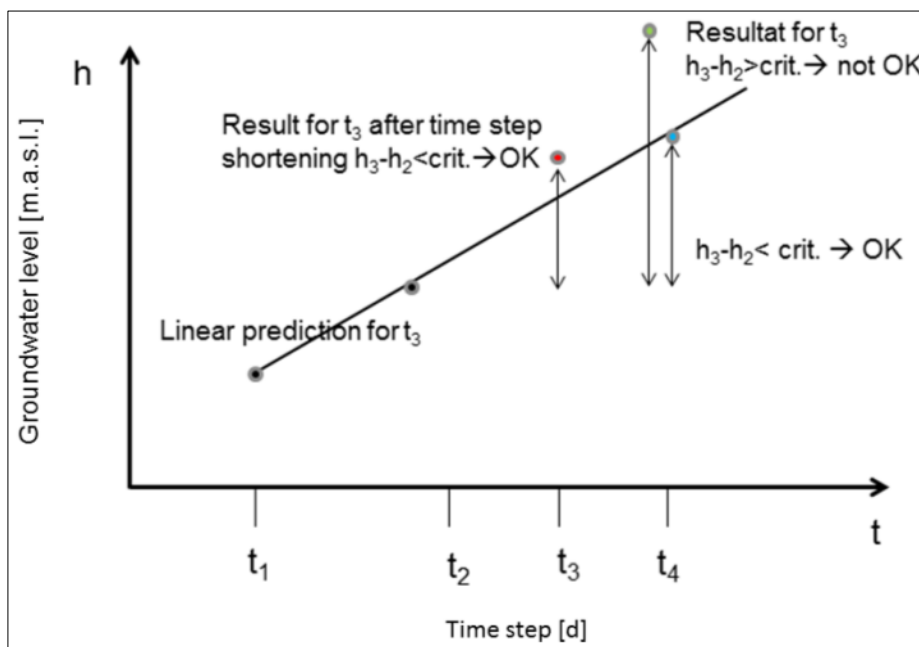


Figure 4-35 Predictor-corrector time step scheme for transient flow simulation with adaptive time stepping.

The GLS scheme is thoroughly described in Gresho et al. (1980), Diersch (1988), Wouters et al. (1987) and Diersch (1998).

The choice of the time step size Δt_n and the iteration control of the Newton scheme significantly

influence the success and the efficiency of the simulation. A fully automatic and adaptive time selection strategy is useful for the present multi-species transport problem. The aim of the predictor-corrector scheme is to monitor the solution process via a local time truncation error estimation in which the time step size is automatically varied in accordance with the temporal accuracy requirement. The time step size is increased whenever possible and decreased only if necessary. The primary variable switching strategy, which is shown (cf. figure 4-35) is based on the Newton method. This method converges by use of variable time step size if a good initial guess of the solution is available. In case of transient conditions, this is feasible with an adaption of the time step size to the evolving flow behavior. At a given time stage, a good initial guess of the solution can be obtained, which provides that the time step is sufficiently small. The required degree of convergence has to be satisfied in just one full Newton iteration

per time step (Perrochet et al., 2009). Therefore, the time discretization error δ can be used as a Newton convergence criterion for the iteration.

4.4.4 Ensemble realization by application of Monte Carlo technique

Lahkim et al. (1999) accented that a decision-making process based on a stochastic approach with consideration of natural heterogeneity of the groundwater system and the uncertainty in its flow and transport parameters lead to a distribution of possible values of exposure rather than a single value estimation. In risk assessment research concerning groundwater, there have been many studies which deal with a quantifying of exposure and risk by use of stochastic approaches. In the majority of cases, this research is restricted to a consideration and not applied in modeling. Suter (2007) emphasized the application of sophisticated tools and a wide range of data to estimate specific risks. A lot of literature is available on analytical stochastic modeling of contaminant transport in groundwater (Dagan, 1984, Riva et al., 2001, Guadagnini et al., 2003, Serrano, 1992, Hansen, 2002, Harter, 1998). The numerical stochastic simulation based on a Monte Carlo simulation (MCs) is also good developed (Fu et al., 2009, Marin, 1989, Carsel et al., 1988, Patelli, 2006, Shrestha et al., 1994). The MCS is the most used method to solve stochastic equation and represent an essential part of this thesis. Various researchers (Ndambuki et al., 2003, Baalousha, 2006, Bekesi et al., 1999 and Vovelle, 1986) deal with MCs applied to groundwater resource assessment.

However, only a minor number of researches, e.g. Hassa (2003), Shlomi (2009), Boeckenhauer et al. (2000), Figueira et al. (2001) and Saito et al. (2001), have been linked the analytical (numerical) groundwater transport modeling with a geo-stochastic exposure assessment for a real contaminated site.

This thesis presents a stochastic methodology based on a classical MCs for exposure assessment for a numerical heterogeneous and homogeneous multi-species transport model. The challenge of this adopted approach is the use of a real regional groundwater system that contains a contamination, with degradation processes, caused by a laundry.

The classical meaning of the MCs is an application of stochastic simulations to avoid the mathematically exact description of a physical process and the solution of the necessary equation by the selection of adapted density functions (pdf) (Computational Science, 1995). In this thesis the MCs is used in a framework of groundwater modeling where the input parameter of the physical groundwater process is stochastically simulated. Subsequently, the stochastic simulations replace the probabilistic part of the partial groundwater flow and transport equation. The procedural method is consisted of solving the flow and transport

equation with deterministic parameters. Thereby, the probabilistic part is determined separated by an approximation of the stochastic processes through a multitude of simulations.




	Step 1 UNCERT/ Monte Carlo simulation	Geostochastic reconstruction of the investigated aquifer based on hydraulic conductivity and effective porosity parameter = Parameter uncertainty identification
	Step 2 Feflow/ Monte Carlo simulation	Monte Carlo simulation of the calibrated model (step 1) Including dynamic of the boundary conditions (ID's) Variation of chemical and hydraulic parameters = spatial probabilities of concentration occurrences
	Step 3 Spco isolines Outcome	Risk identification + model result quantification by quantification of model input data sets

Figure 4-36 Performed workflow of the thesis including Monte Carlo simulation by use of the geo-stochastic program UNCERT and the numerical simulation program FEFLOW. The combination of these two techniques is a generation of spatial probability concentration occurrence isolines (spco).

The MCs is used in two different approaches in the present research (cf. figure 4-36). The first approach is the use of MCs concerning the investigation of hydro-geological properties in form of probabilities of occurrences of an indicator (cf. chapter 4.2.2) by use of Sequential Indicator Simulation. The outcome is a parameter uncertainty identification by a geo-stochastic reconstruction of porosity, hydraulic conductivity, longitudinal and transversal dispersivity parameter fields. Baalousha (2006) assumed that the hydro-geological properties of an aquifer may vary significantly in time and space, and thus cannot be treated in a deterministic way. The most limited factor during a groundwater modeling is the poor data documentation. In a majority of cases, only a few measurement points are available for an aquifer characterization. Ndambuki et al. (2003) accent that the material forming aquifers vary enormously spatially and that it is not clear how optimal management strategies designed deterministically perform in an environment of uncertainty. One opportunity to counteract the limited data set during a groundwater management is a special pre-processing as well as a geo-stochastic calculation algorithm. Equiprobable realizations of flow and transport parameter fields can be generated from a small data set of borehole information by use of conditional SIS, which provides a means of representing the variability of observed in nature. Wingle et al. (1997) observe that

conditional simulation does not produce a best estimate of reality, but it yields equiprobable models with characteristics similar to those observed in reality.

The second use of MCs in this thesis is an application with a concern to simulate 80 realizations of the calibrated homogenous and heterogeneous transient multi-species transport models (cf. figure 4-36). The heterogeneous groundwater model consists of the geo-stochastic generated porosity, hydraulic conductivity, longitudinal and transversal dispersivity parameter fields. The aim is a simulation of spco of both types of models. Afterwards, a comparison between both transports models, which are varying in the degree of hydro-geological details, is considered. The true conditions in the contaminated area can be approximated by the obtained range of contamination extents in the MCs.

The primary aim is to demonstrate the feasibility of using MCs to perform spco by using a statistical description via random fields with a given statistical structure. Kolyukhin et al. (2005) acknowledged that random fields provide a useful mathematical framework for representing disordered heterogeneous media in theoretical and computational studies. Existing studies on this field mainly focus on the assessment of hydraulic or transport-related parameters. Only very few papers deal with the whole spectrum of contaminant transport including estimation of uncertainty in an appropriate manner (Ling et al., 2007). In this research a MCs for heterogeneous contaminated urban aquifer, including sensitivity analysis of flow, transport and reaction parameters is presented unlike in most research where the heterogeneity is neglected through the use of parameterization of local scale models with experimental data.

The first step was a sensitivity analysis using variation of the single input parameters. This analysis was used to identify the range of stochastical parameter variation for the MCs. The model random variables for the MCs were chosen to be in the range of σ of the results identified by the sensitivity analysis (~68 % of the generated values in the interval, cf. figure 4-38). Stochastically independent, Gaussian distributed random variables were generated with Mathworks Matlab 2009b.

Two flow parameters (porosity and hydraulic conductivity) and five transport parameters (longitudinal and transversal dispersivity, reaction rate, molecular diffusion and sorption) of a multi-species reactive transport model were subjected to a parameter variation (cf. chapter 4.5.1.3). This six parameters were randomly generated by a normal distribution with an expectation of 1 and standard deviation of 0.2. Figure 4-37 shows the density function of the Gaussian distribution of the generated variables. Hence, 80 independent multi-species transport model variants were calculated. The results of the 80 flow and transport models were stochastically analysed to generated probability of concentration occurrences of the pollutants.

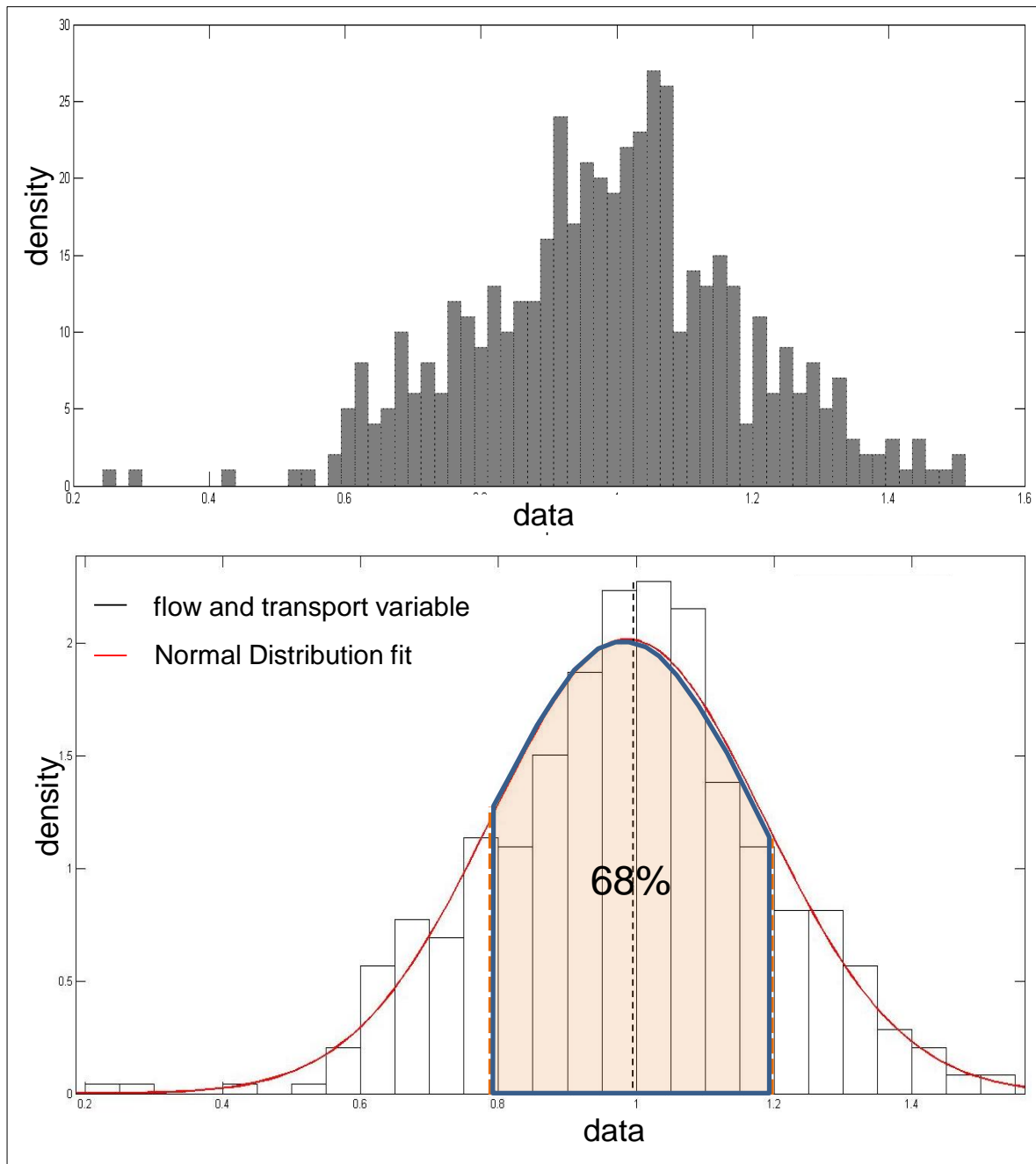


Figure 4-37 Density function of the Gaussian distribution of the generated random variables of the hydraulic conductivity, porosity, longitudinal and transversal dispersivity, sorption and reaction rate.

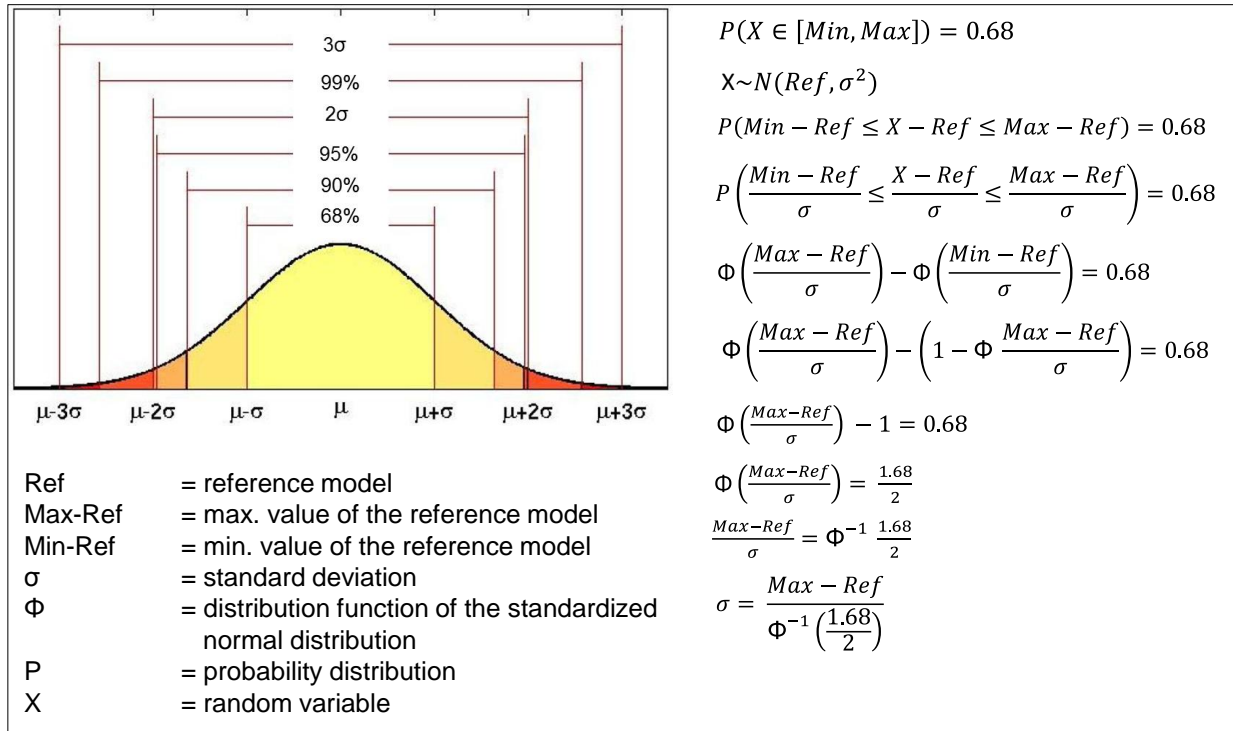


Figure 4-38 Density function of the Gaussian distribution with standard deviation and confidence interval as well as the derivation of the 2σ standard deviation.

The MCs were calculated in cooperation with the University of Siegen (Informatics Systems Institute) with the LINUX High-Performance Computing (HPC) Cluster “Rubens” with a parallel processing algorithm. Through the parallel performances on multi CPUs an economy of calculation time is achieved. Inside of the cluster, a superior node (*Master*) adapts the overall system administration. A few special configured nodes (*Storage Nodes*) administrate the central loading and storage of data. All residual nodes (*Worker*) of the cluster are used for the

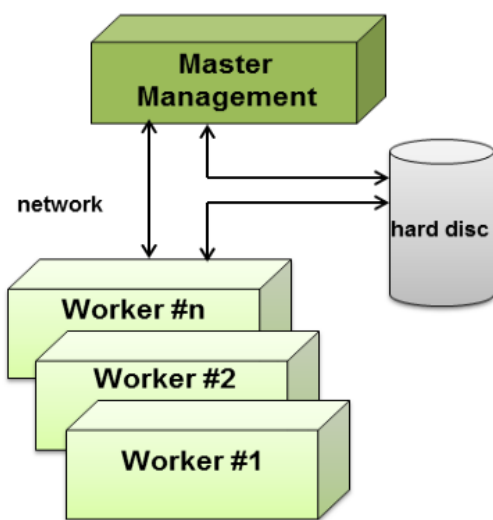


Figure 4-39 Communication architecture of the Rubens-Cluster of the University of Siegen.

actual calculation. Figure 4-39 shows the general communication architecture of the Rubens-Cluster, which only admits a direct communication between the *Master* and *Worker* via the network. A direct communication or exchange of data between single *Workers* is impossible and must be operated via the *Master*. The *Workers* have a direct access to the *Storage Nodes* of the cluster to save and store data.

A total number of 150 nodes are available inside the Rubens-Cluster with 2 Single-Core AMD Opteron CPUs (2 or rather 2.8 GHz) and 2 or rather 4 GB RAM per node. For the multi-species transport simulations, 40 nodes a 2 CPUs were used with a parallel computation of the software *FEFLOW* 6.0x. The

simulation time of the homogeneous transport model is 10 days and for the heterogeneous model 14 days per simulation run.

Subsequent to the MCs the 50%, 80% and 90% frequency of occurrence of 1 mg l^{-1} , 0.5 mg l^{-1} , 0.2 mg l^{-1} , 0.1 mg l^{-1} and 0.01 mg l^{-1} , 0.001 mg l^{-1} and 0.005 mg l^{-1} for PCE, TCE, DCE and VC were calculated at each Finite Element node of the multi-species transport model for generating the probability of concentration occurrences. Figure 4-40 shows the application flow of the analysis. This example presents the calculation of DCE at one Finite Element node after 50 a and 70 a simulation time. The principle is based on a count of a selected threshold concentration value of a certain probability.

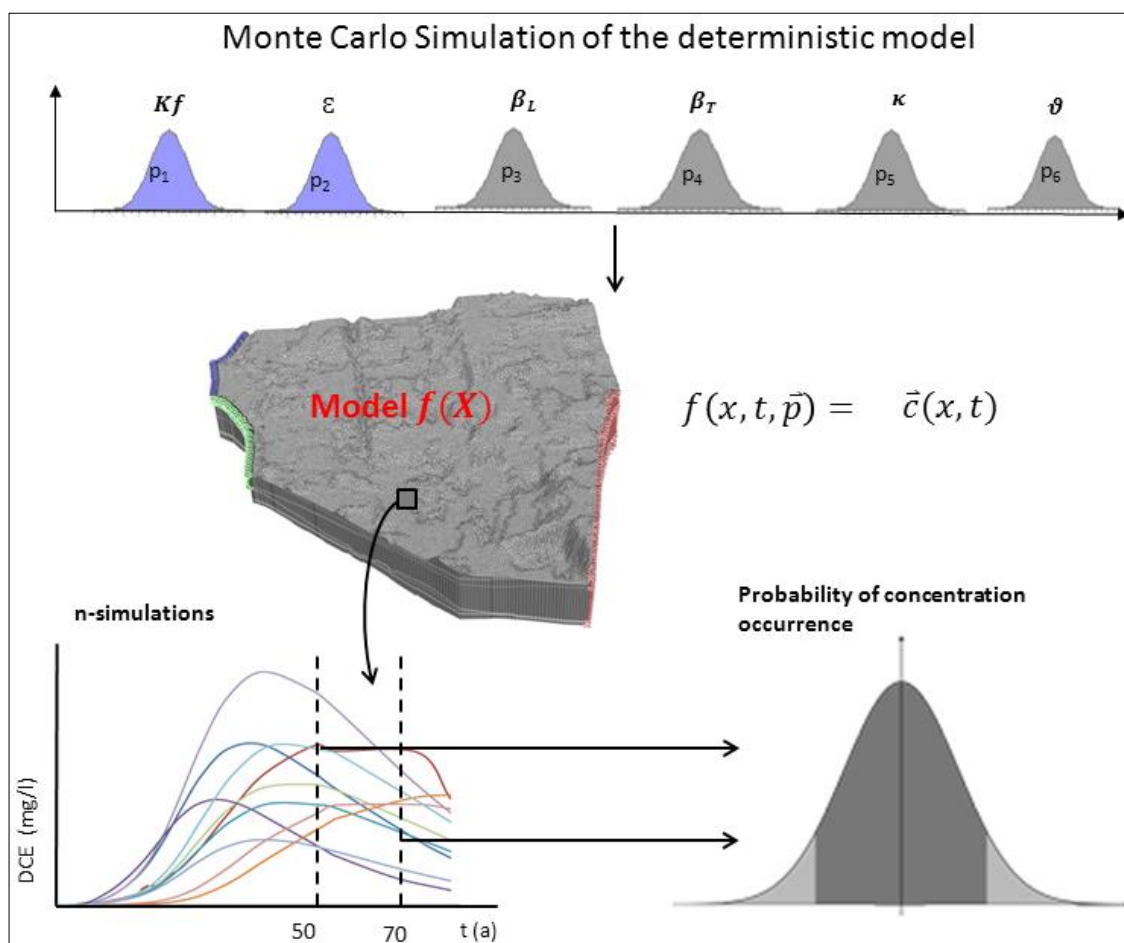


Figure 4-40 Application workflow of the creation of probability concentration occurrence isolines by use of a Monte Carlo simulation including a range of seven selected parameters (upper illustration). This example shows exemplarily the development of a DCE probability isoline after 50 a and 70 a.

4.5 Model development, calibration and application related to risk identification

In this section two model setups for two different subsurface reconstructions (cf. chapter 4.2), of the same investigation area, are explained. Four different groundwater models were established and evaluated (cf. figure 4-41). Two selected groundwater models are presented exemplarily in this chapter. Both calibrated models were treated by MCs to generate spatial probabilities of mass concentration occurrences for detect high probability contamination concentration and development of a remedial strategy.

Furthermore, a coupled groundwater-surface water model is presented to identify the importance of water exchange between both ecosystems according to a mass transport. Different hydrological extreme value scenarios were simulated by use of dynamic boundaries.

All numerical parameter settings can be found in the appendix A.

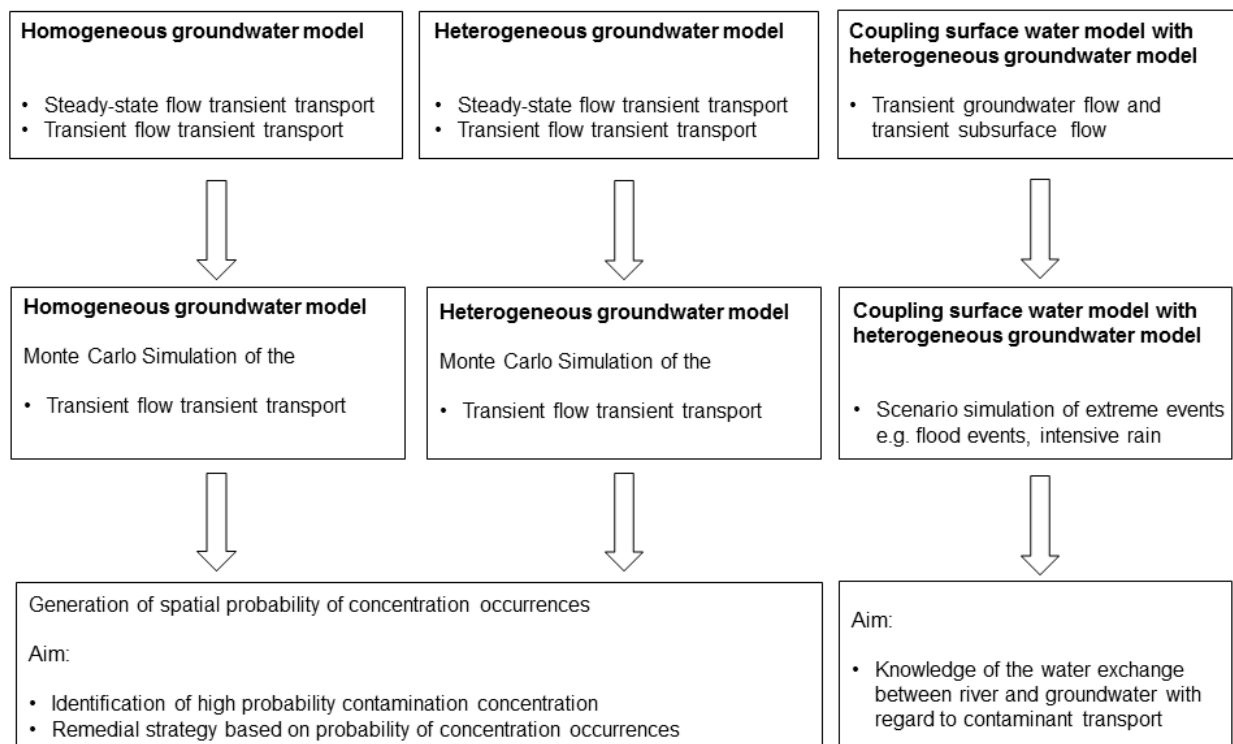


Figure 4-41 Overview of the different generated groundwater transport models and the coupled groundwater-surface water model.

4.5.1 Homogeneous multi-species groundwater model

4.5.1.1 Hydro-geological model

The hydro-geological underground reconstruction of the homogeneous aquifer is carried out by a petrographic approach. A construction of the substrate intersection is defined based on the material compound (cf. chapter 4.2.1). Figure 4-42 shows the superelement mesh⁴, which forces the geometric shape of the Finite Element model. 29 borehole information (red points) provide the basis for the 3D-layer-configuration. The layer-configuration is founded on the different substrate thicknesses at each borehole. One layer is defined by its upper and lower material border. The resulted layer chronology is documented in chapter 4.2.1.

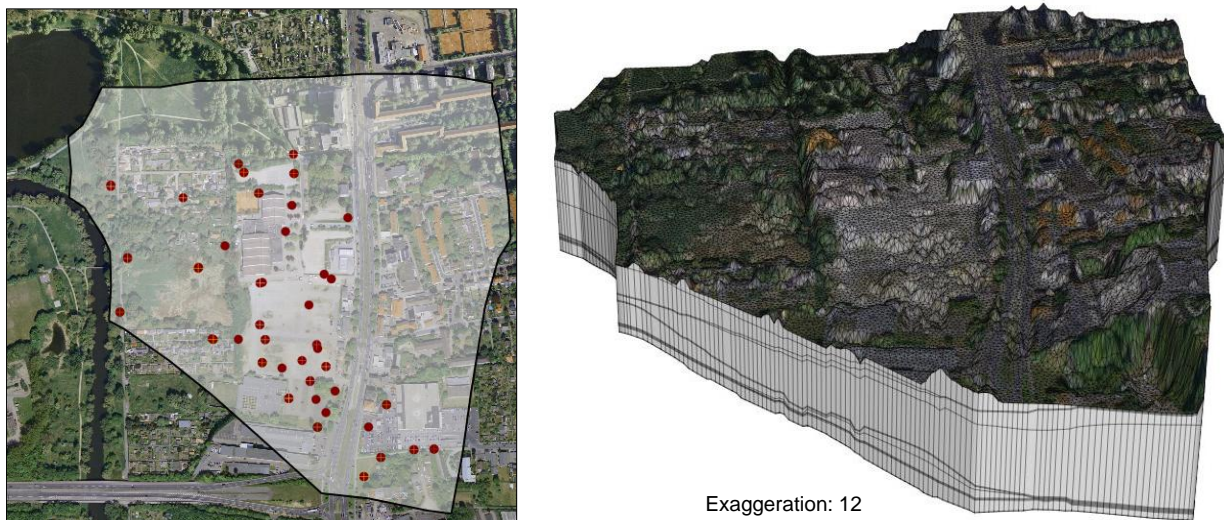


Figure 4-42 Horizontal boundary of the investigation area with hard data information from drilling profiles (red points) in the Finite Element model. Right side: Reconstruction of the homogeneous aquifer after a petrographic approach.

The flow material assignment conforms to the geological layer characterization of the homogeneous subsurface approach. The values for the hydraulic conductivity resulted from field tests and were modified by literature values of “AG Bodenkunde” (1982). In addition, the implemented values were validated by the detected HPT values (cf. chapter 4.2.3). The ratio between K_x and K_z is assumed as 1/10th after US Geological Survey (Landon et al., 2007). According to the hydraulic conductivities, the porosity was set (cf. table 4-9).

⁴ Program specific file format. Definition of the outer model boundary

Table 4-9 Adapted hydraulic conductivities in x-, y- and z-direction for the Finite Element groundwater model of the model area with appendant storativities of each layer.

material type	geological layer FEM	K _r -value x-direction 10 ⁻⁴ ms ⁻¹	K _r -value y-direction 10 ⁻⁴ ms ⁻¹	K _r -value z-direction 10 ⁻⁴ ms ⁻¹	n _{eff} [-]
Rubble	1 layer	2.5	2.5	0.25	0.3
Silt	2 layer	0.25	0.25	0.025	0.255
Fine sand	3 layer	2.5	2.5	0.25	0.3
Middle sand	4 layer	12	12	1.2	0.331
Fine sand	5 layer	2.5	2.5	0.25	0.3
Coarse sand	6 layer	12	12	1.2	0.331
Middle sand	7 layer	12	12	1.2	0.331
Fine sand	8 layer	2.5	2.5	0.25	0.3
Coarse sand	9 layer	12	12	1.2	0.331
Silt	10 layer	0.25	0.25	0.25	0.255

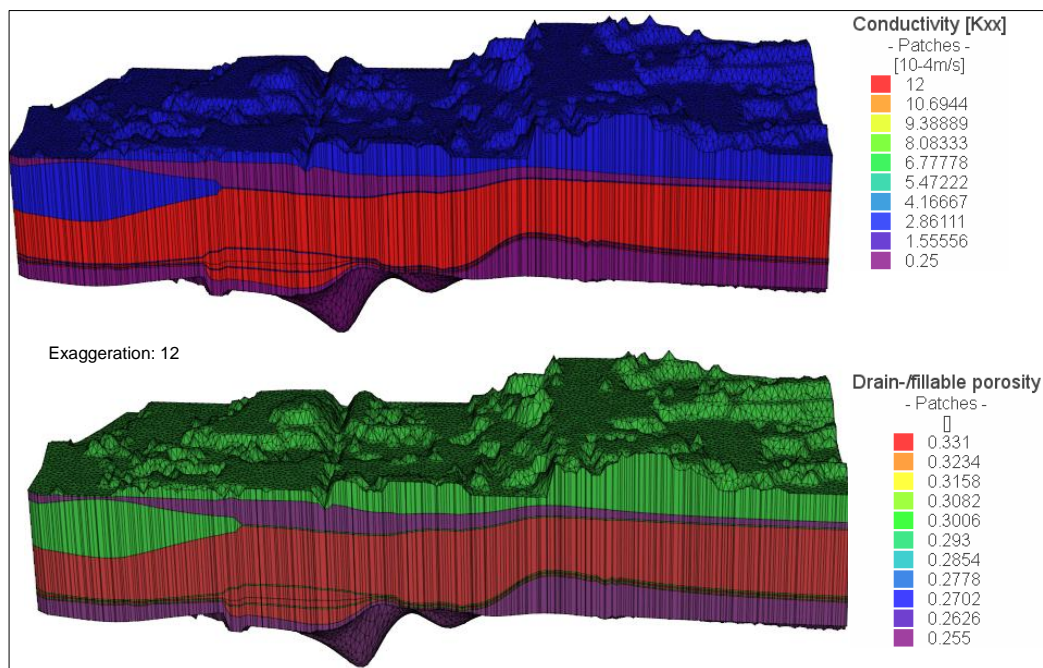


Figure 4-43 Geological cross section of the homogeneous subsurface body with hydraulic conductivity and corresponding porosity for each geological substrate.

The specified hydraulic flow material values are set as “global” values for each geological substrate in the numerical groundwater model. To that fact, all nodes of the Finite Element model, which belong to a layer, receive the same hydraulic value.

4.5.1.2 Initial and boundary condition of the multi-species groundwater model

Initial flow and transport conditions are necessary for later transient flow simulations (cf. chapter 4.3.3) flow initial conditions rely on a groundwater level measurement of the 12/11/2009.

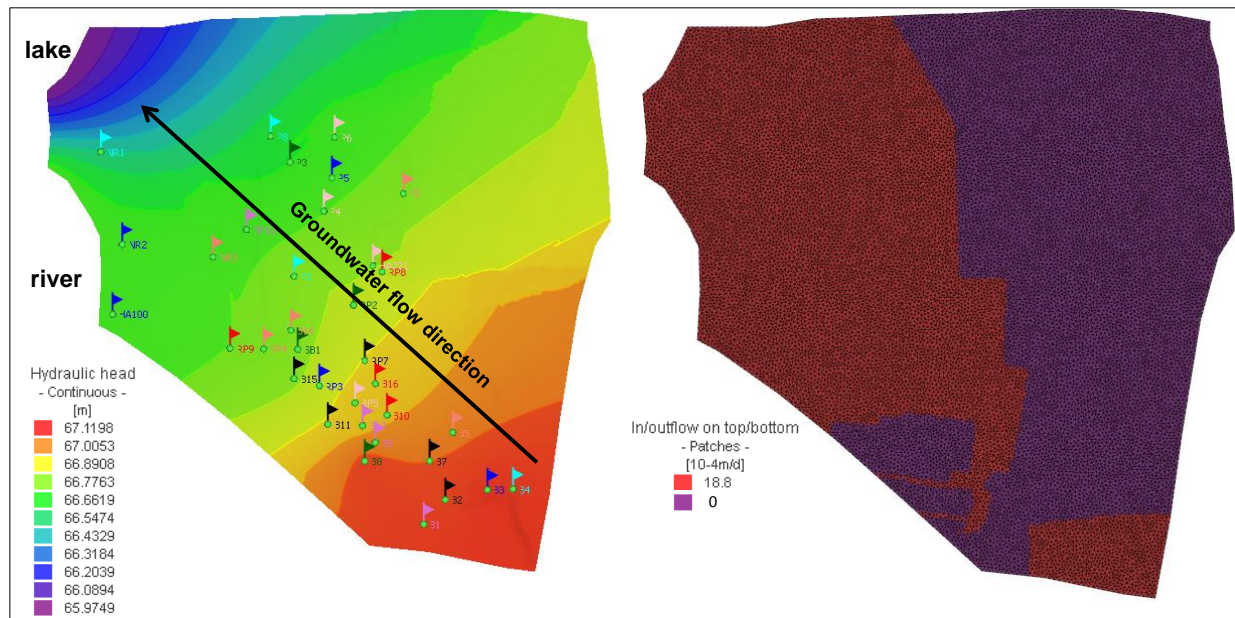


Figure 4-44 Groundwater table map of the homogenous groundwater model based on measurements of the 12/11/2009. Interpolation by Ordinary Kriging technique. Right side: groundwater recharge map with differentiation between covered and free surface.

Because of absent groundwater measurements at each well no average hydrological condition could be calculated. Therefore, the groundwater table of the 12/11/09 was used to estimate an initial groundwater level. A regionalization was realized by Ordinary Kriging method. Figure 4-44 represents the interpolated groundwater table map and the groundwater recharge distribution of the model domain. Particularly clear is that the groundwater flow is directed to the bordering ecosystems. The initial hydraulic head condition is used for all Finite Element variants, which are investigated in this thesis.

A differentiation between covered and free surface was performed to identify groundwater recharge parts of the model area. Covered areas are assumed with a value of $0 \cdot 10^{-4} \text{ md}^{-1}$ and free surface with $18.8 \cdot 10^{-4} \text{ md}^{-1}$ inflow on top. The time-dependent groundwater recharge for the transient flow model was calculated after equation 4-4. Analogous to the steady-state groundwater model the groundwater recharge values were transferred exactly to the transient groundwater model via a geo-information system (cf. figure 4-45).

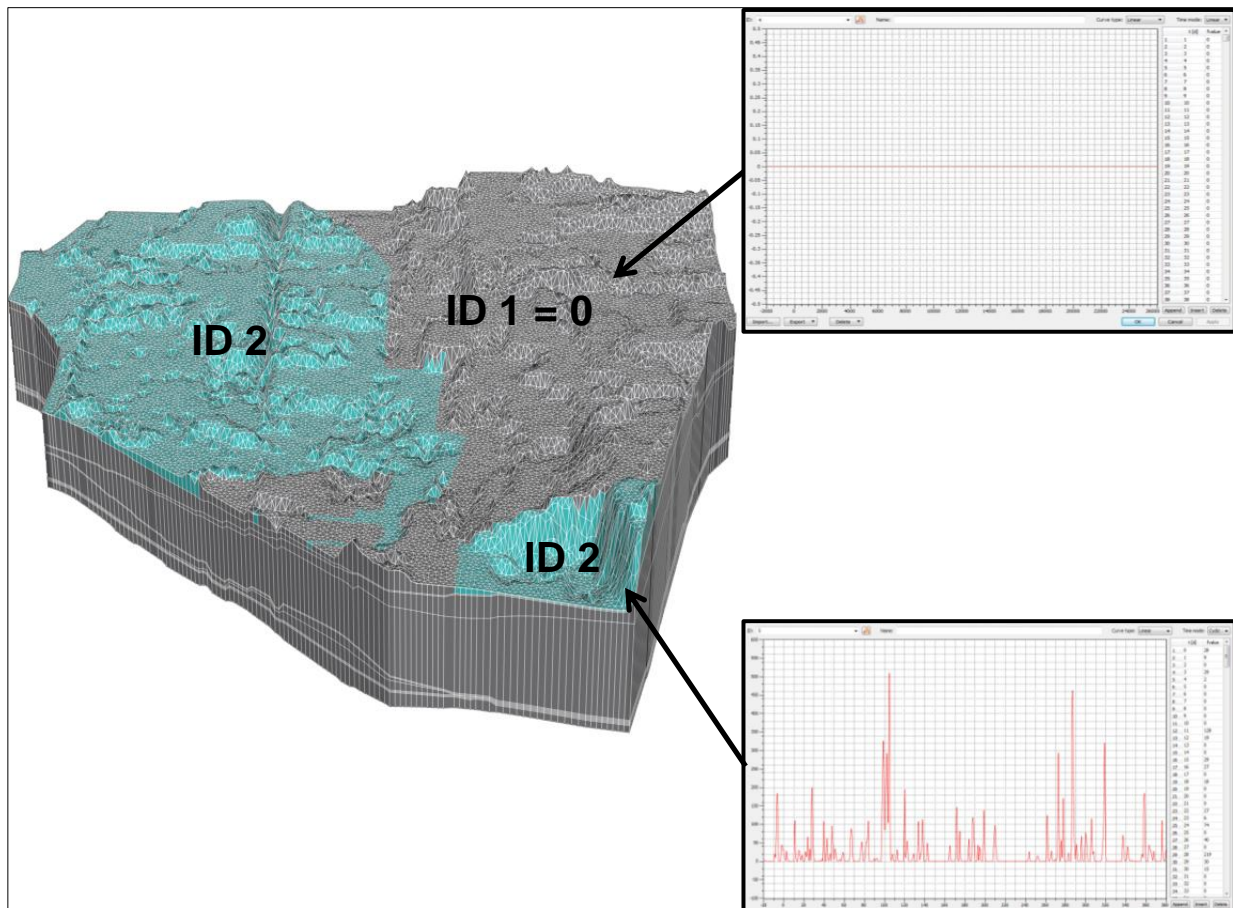


Figure 4-45 Time-dependent groundwater recharge assignment of the homogenous and heterogeneous groundwater transport model. ID 2 represents the area where groundwater recharge occurred with the calculated time-varying function. ID 1 represents an area where the surface is compacted, no inflow on top is assumed.

The initial mass condition of the contamination is defined as 0 mg l^{-1} for all nodes of the Finite Element model. It is supposed that the groundwater body contains no mass concentration before the contamination took place.

Totally, three boundary conditions (b. c.) kinds are set for the flow conditions. In case of the steady-state flow conditions, constant flow boundaries are implemented (cf. figure 4-45). On the west side of the model a constant lake water level between 65.98 and 65.89 m.a.s.l. is defined as a Dirichlet b. c. because no data were available to identify a transfer b. c. The Dirichlet b. c. was applied for all slices. In contrast, the Cauchy b. c. with 66.83 m.a.s.l. of the river water level was only set in the first three slices. Based on the assumption that the east model border represents a groundwater inflow, a Neumann b. c. with $-0.050046 \text{ md}^{-1}$ was assigned. The groundwater hydrograph of an observation well closed to the model border was used to calculate the inflow. The water volume, which streams into the groundwater model during the simulation was calculated and divided by the border area. The resulting groundwater flow velocity was placed at all slices.

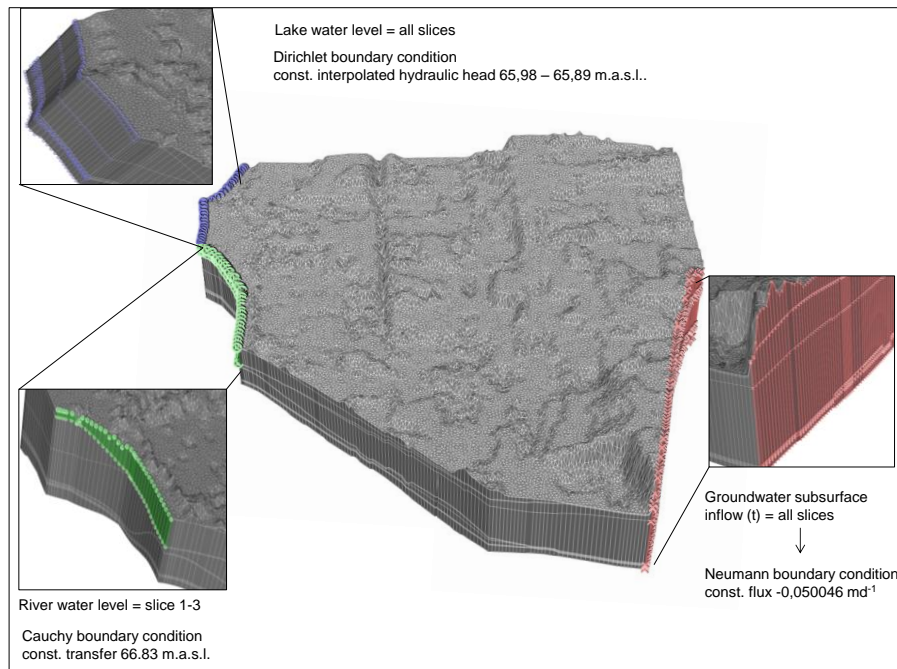


Figure 4-46 Defined steady-state flow boundary conditions of the homogeneous groundwater model. Left side, lake water level as Dirichlet boundary conditions and river water level as Cauchy boundary conditions. Right side, groundwater subsurface inflow as Neumann boundary condition.

For the transient flow conditions, the time series, which are described in chapter 4.3.3, were replaced for the constant data type (cf. figure 4-46). The lake water level subjects to no dynamic events because of an artificial water table regulation. For this reason, a constant lake water table was defined for the transient flow model.

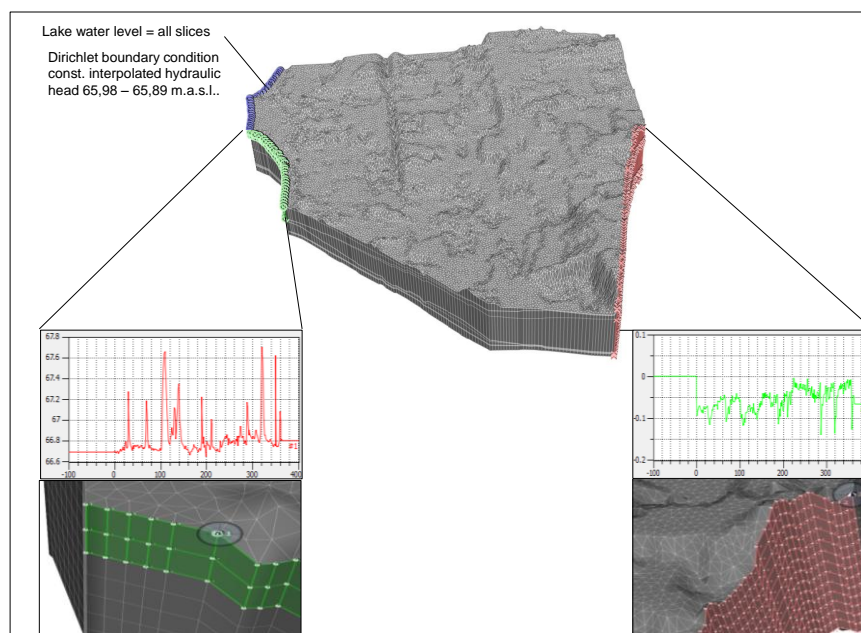


Figure 4-47 Defined transient flow boundary conditions of the homogeneous groundwater model. Left side, lake water level as constant Dirichlet boundary condition and river water level as time-varying Cauchy boundary conditions. Right side, groundwater subsurface inflow as time-varying Neumann boundary condition.

The transport boundary consideration corresponds to the sewage disposal in the 1970s. It is assumed that a continuous contamination occurred until the 1970s. The mass concentration is estimate with 160 mg l^{-1} and began to reduce during the 1970s. Further investigation carried out that the maximum concentration is located in 7-10 m depth. This relates to layer 5-6 for the homogeneous subsurface. In comparison to the homogenous transport model, the mass boundary for the heterogeneous aquifer was set in the 7-10 layers (cf. figure 4-48) because of the reconstructed layer configuration (cf. chapter 4.5.2).

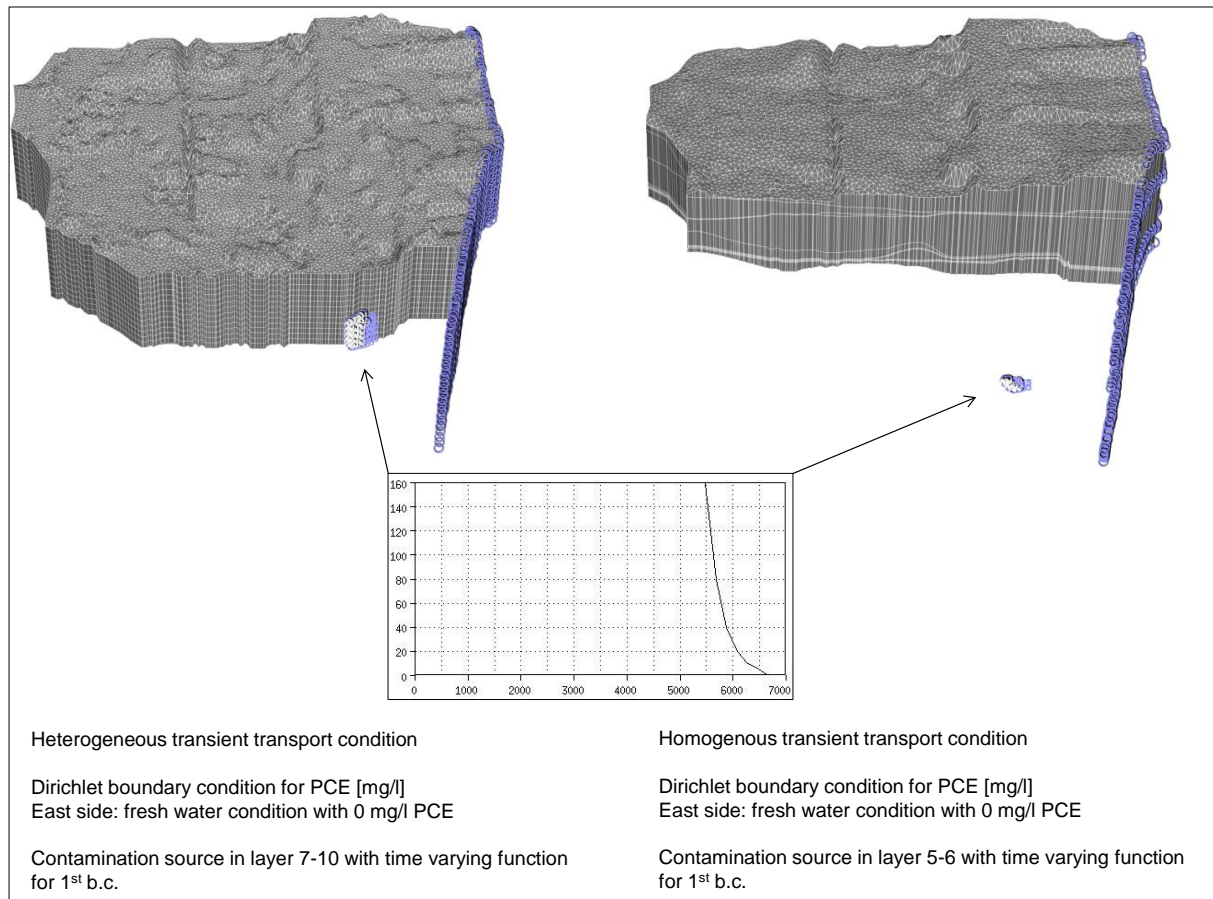


Figure 4-48 Transport boundary condition of the transient multi-species homogenous and heterogeneous groundwater model. Implementation of a time-varying mass boundary in layer 5-6 in the homogenous model and layer 7-10 in the heterogonous model.

4.5.1.3 Kinetic multi-species transport materials

The field of reactive transport modeling draws on numerous fields in environmental sciences, including hydrology, geochemistry, biochemistry, soil physics and fluid dynamics. Reactive transport modeling has a significant impact on the treatment of contaminant retardation in the subsurface.

All identified parameters (cf. chapter 4.1.2) were implemented into the homogenous transport model. In this process, a separation between layer-specific and species-specific values must be carried out. Sorption, reaction rate, molecular diffusion, porosity and the kinetic reaction

equations are species-related parameters. These values were defined as different parameters for all species and copied to all layers in the Finite Element model.

Longitudinal and transversal dispersivity are layer-related parameters. These values were determined for each geological layer and implemented as “global” values for all slices, which correspond to a geological layer. Figure 4-49 shows exemplarily the distribution of the longitudinal assignment.

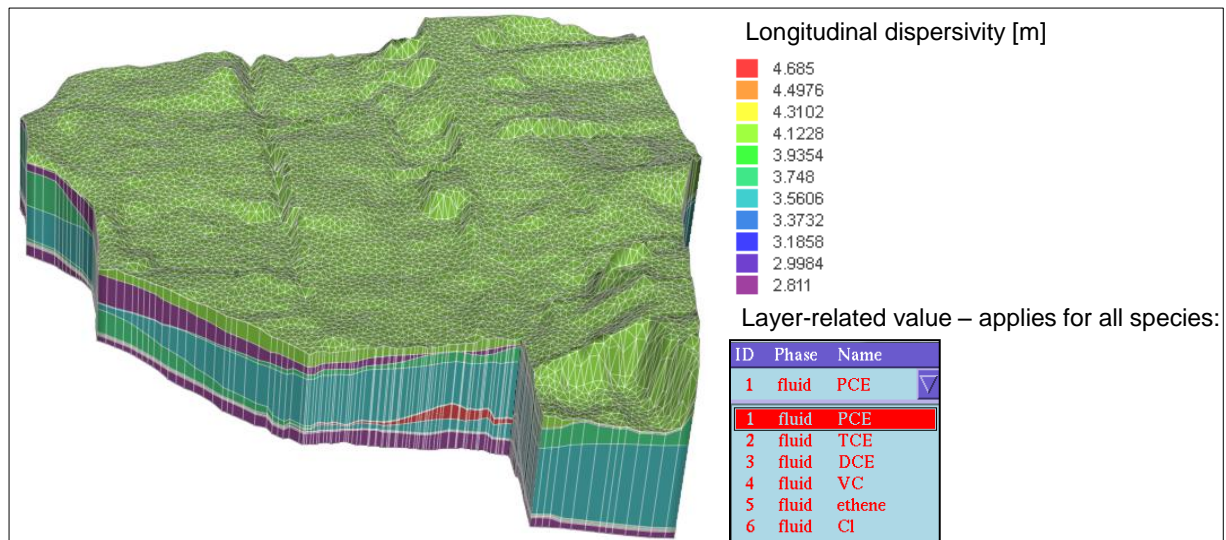


Figure 4-49 Distribution of the longitudinal dispersivity in the homogenous multi-species transport model. The longitudinal dispersivity belongs to the layer-related parameters and is applied for all species.

The mentioned chemical parameters in chapter 4.1.2 were assigned for the different multi-species types. The used degradation equations can be found in the appendix A.

The applied Finite Element model (*Feflow 6.0x*, Wasy GmbH, Berlin) provides a tool in introducing and editing reactive multi-species transport problems. The degradation equations were defined by the reactive kinetics editor (*FEMATHEd*).

A given species (contaminant) can be mobile, associated with a fluid phase, or immobile, associated with a solid phase. The contaminants used in this thesis are in a fluid phase, which leads to a subjection to advection and dispersion. The transport parameters, which are integrated in the mass conservation equation (cf. equation 4-22), are important for the MCs approach. Four parameters, longitudinal and transversal dispersion, molecular diffusion, reaction rate and sorption after *HENRY* are subjected to a stochastic treatment by use of the MCs. These parameters as well as the two flow parameters, hydraulic conductivity and porosity, were ranged by a Gaussian distribution function around an expectation value of 1 with a standard deviation 0.2 (cf. chapter 4.4.4). The parameter variation inside the flow and mass differential equations leads to a range of concentration outputs of the contaminants,

which are analyzed with a stochastic frequency of occurrence for a risk estimation of pollutants occurrence in the urban aquifer. The following represented equations are used to describe the placement of the four transport parameters, which have an impact on the contamination pattern on the field site. The mass conservation of chemical species in fluid phases of a porous media can be written in the following from:

$$\frac{\partial}{\partial t} \varepsilon_a C_k^\alpha - \nabla \cdot \boxed{D_k^\alpha} \cdot \nabla C_k^\alpha + \nabla \cdot q^\alpha C_k^\alpha - \varepsilon_a Q_k^\alpha = \boxed{R_k} \quad \text{Eq. 4-22}$$

D_k^α	Tensor of hydrodynamic dispersion of species k	$[l^2 t^{-1}]$
k	Species indicator	
Q_k^α	Zero-order nonreactive production term of α -phase	$[t^{-1}]$
q^α	$\varepsilon_a v^\alpha$, Darcy flux of α -phase	$[l t^{-1}]$
v	Pore velocity of α -phase	$[l t^{-1}]$
R_k	Bulk rate of chemical reaction of species k	$[ml^{-3} t^{-1}]$
α	Phase indicator	$[l]$
ε_a	Volume fraction of α -phase	$[l]$
C_k^α	Concentration of species k of α -phase	$[ml^{-1}]$

The hydrodynamic dispersion of the species k of the f -phase is defined as:

$$D_k^\alpha = \varepsilon_a D_{d_k}^\alpha + \beta_T q^\alpha I + \boxed{\beta_L - \beta_T} \frac{q^\alpha \otimes q^\alpha}{q^\alpha} \quad \text{Eq. 4-23}$$

$D_{d_k}^\alpha$	Coefficient of molecular diffusion of species k of f -phase	$[10^{-9} m^2 s^{-1}]$
I	Unit tensor	
β_L, β_T	Longitudinal and transversal dispersivity of porous media,	$[m]$

The rate R_k can be developed in a polynomial representation of low order (Diersch, 2009):

$$\boxed{R_k = \sum_{r=1}^N v_{kr} r_r \quad (k = 1, \dots, N)} \quad \text{Eq. 4-24}$$

N_r	Number of reaction	
r_r	Rate of reaction associated with the type of reaction r	$[10^{-4} s^{-1}]$
v_{kr}	Stoichiometric number of species k and reaction r	

The typical constitutive representation of r_r has a functional:

$$r_r = r_r(C_1^\alpha, \dots, C_N^\alpha, s_f, \varepsilon) \quad \alpha = f \text{ or } s$$

For degradation type kinetics the R_k can be written in the general form:

$$R_k = \sum_{m=1}^N k_m c_m^\alpha n_m \quad \alpha = f \text{ or } s$$

$$= k_1 (c_1^\alpha)^{n_1} + k_2 (c_2^\alpha)^{n_2} + \dots + k_N (c_N^\alpha)^{n_N}$$
Eq. 4-25

k_m ($m=1, \dots, N$) bulk rate constants, can depend on ϵ and s_f

$k_{1, \dots, n}$ Sorption coefficient (Henry) [1]

s_f Saturation referring to the fluid f -phase, in saturated media is $s_f = 1$

ϵ Porosity [1]

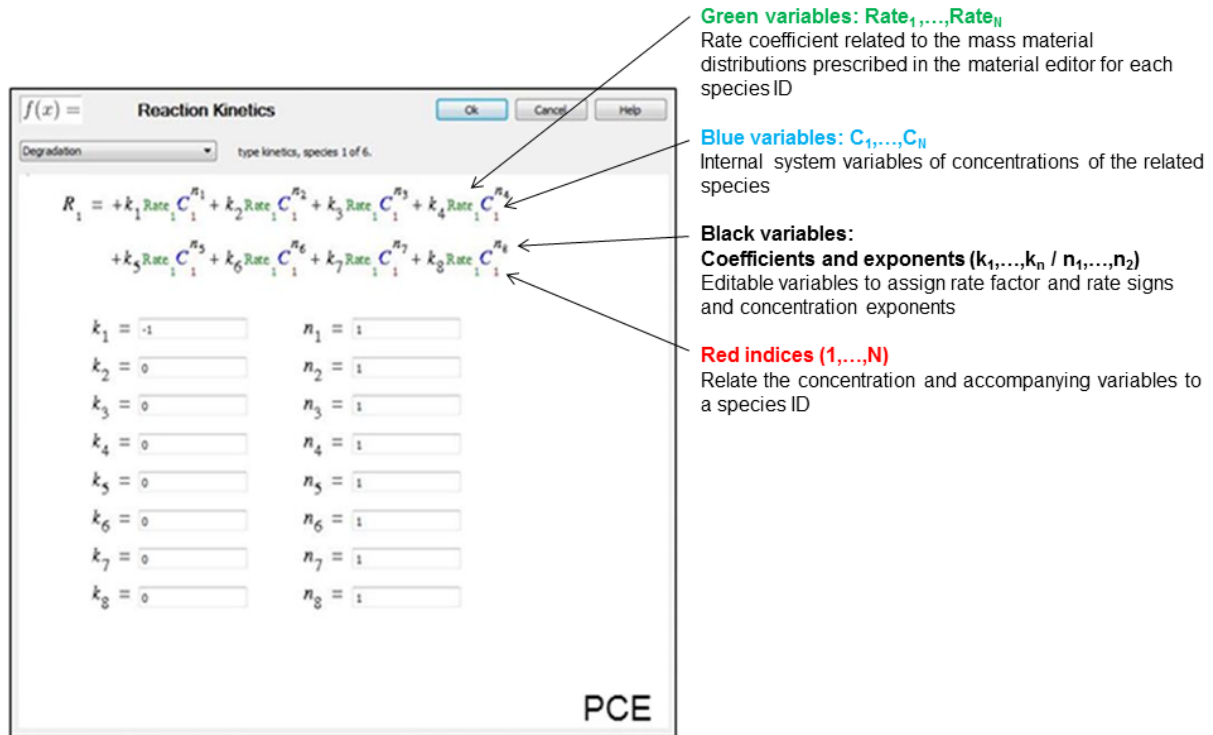


Figure 4-50 Feflow Reaction Kinetics Editor for precompiled rate expression of the degradation-type kinetics for PCE. Modified. Source: Diersch, 2009.

4.5.2 Heterogeneous multi-species groundwater model

4.5.2.1 Hydro-geological model

Based on the explained method in chapter 4.2.2 different spatial parameter fields of the hydro-geological properties were generated and implemented into the hydro-geological model. A vertical extension of an interpolation grid was designed based on the DTM and the drilling profiles. The highest point of the DTM is located in the southeastern corner of the investigation area with an elevation of 77 m.a.s.l., the deepest point is located close to the lake in the north-western corner with an elevation of 66 m.a.s.l. An elevation-difference of 11 m is the result. The groundwater observation wells have different drilling depths, therefore the amount of

available data for the Sequential Indicator Simulation is decreasing with increasing depth. Because of this fact, a depth of 53 m.a.s.l. was selected as the lowest limitation at the northwestern corner of the model area. In this depth 8 groundwater wells are still available. Moreover, this elevation value matches to the aquifer depth of the homogeneous model. The vertical discretization is carried out with a defined layer-thickness of 1 m. The layer-chronology was selected surface-parallel to the DTM (cf. figure 4-51).

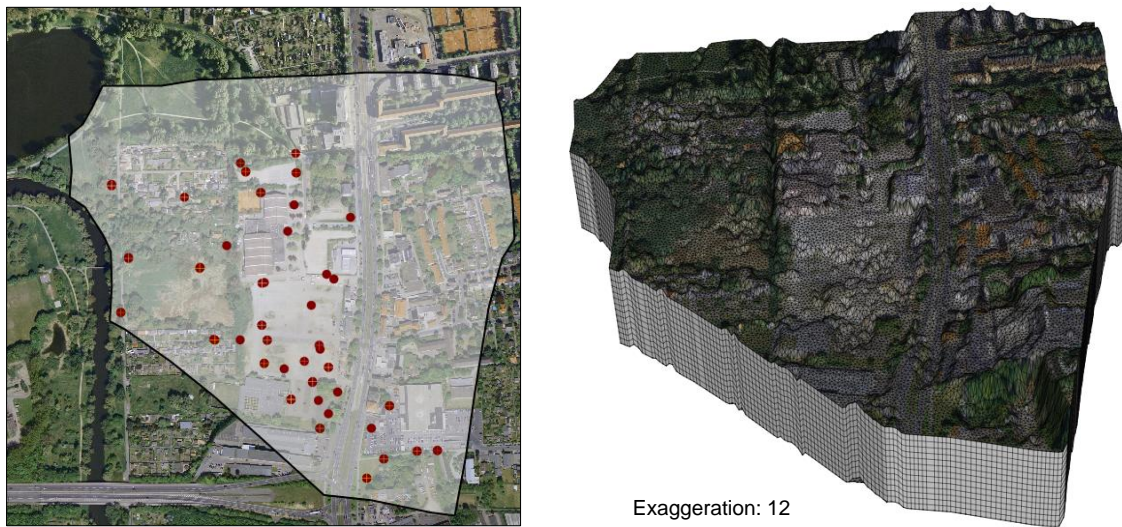


Figure 4-51 Horizontal boundary of the investigation area with hard data information from drilling profiles (red points) in the Finite Element model. Right side: Reconstruction of the heterogeneous aquifer with a constant layer thickness of 1 m orientated by the DTM.

The indicator parameter fields had to decode into real hydraulic conductivity and porosity values because the Finite Element program operates only with discrete values (cf. figure 4-52). The used values are listed in chapter 4.1.1 (cf. table 4-1). This allows an accurate assessment of uncertainties in the hydro-geological parameter identification.

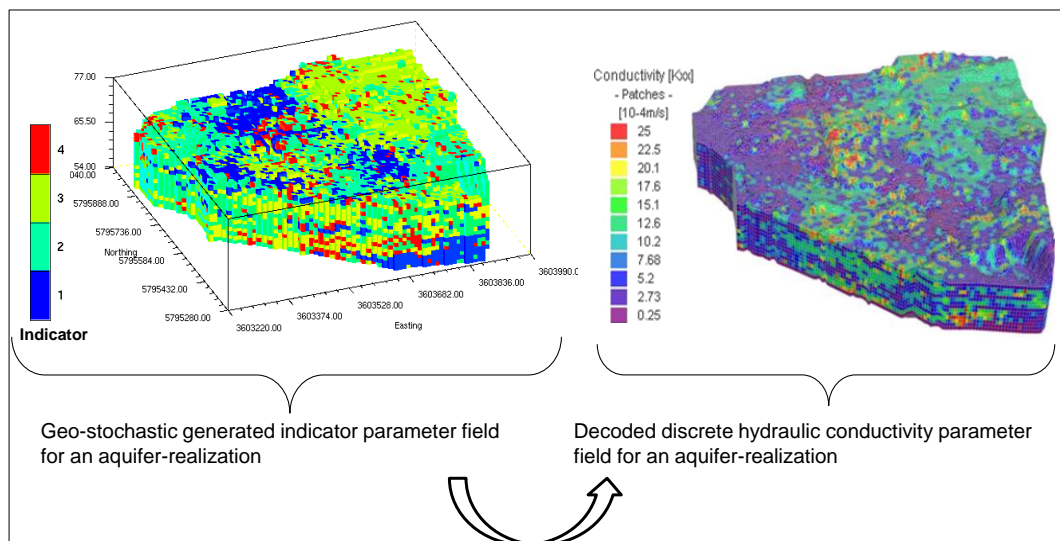


Figure 4-52 Schematic representation of the decoding of the geo-stochastic generated parameter fields into discrete hydraulic conductivity values for an aquifer-realization.

The geo-stochastic generated hydraulic conductivity and porosity parameter fields allow a differentiation of hydraulic properties inside of one geological layer. Specific prepared parameter files (trp.-file⁵) were imported for each layer. Figure 4-53 shows representatively the distribution of the hydraulic conductivity in y-direction and the corresponding porosity. In this case, an anisotropic assembly of the hydraulic conductivity was not necessary because of the heterogeneous value distribution inside a geological layer.

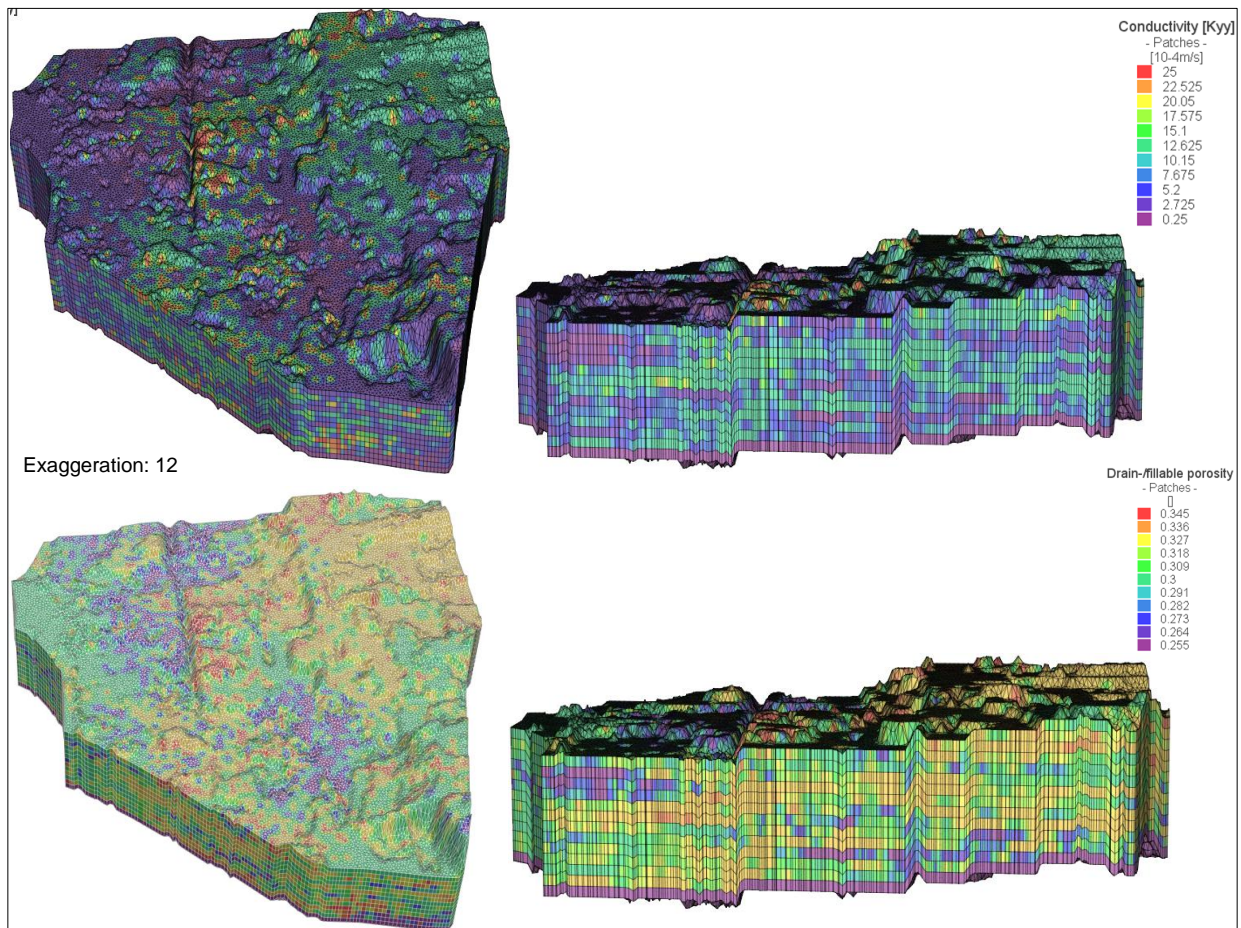


Figure 4-53 Heterogeneous subsurface and geological cross section of the groundwater body with geo-stochastic generated hydraulic conductivity and corresponding porosity for each geological substrate.

4.5.2.2 Initial and boundary condition of the multi-species groundwater model

The definition and implementation of initial and boundary conditions are related to the homogenous steady-state and transient transport model. A groundwater level measurement on the 12/11/2009 was used as initial hydraulic head conditions. The placement of the hydrological flow and chemical transport boundary conditions are mentioned in chapter 4.5.1.2.

⁵ ASCII triplet format file (X- coordinate, Y-coordinate, item) for one single attribute value.

4.5.2.3 Kinetic Multi-species transport materials

Similar to the homogenous model a differentiation between layer and species-related values were taken into account. The species-related values correspond to the used values, which are described in chapter 4.5.1.3.

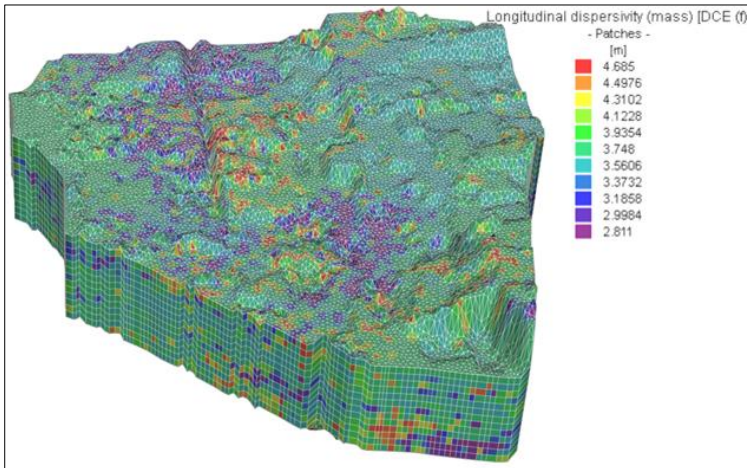


Figure 4-54 Distribution of the discrete longitudinal dispersivity based on a geo-stochastic generated parameter field.

The geo-stochastic generated parameter fields were used for the definition of the layer-related longitudinal and transversal dispersivities. Therefore, the geological substrate properties were utilized. Related to the transformation of an indicator to a hydraulic

conductivity value, the decoding of an indicator to α_L and α_T were executed. The outcome is a heterogeneous distribution of transport material parameters as a function of the geological aquifer characterization. Figure 4-54 illustrates the heterogeneous implementation of the longitudinal dispersivity of the heterogeneous aquifer.

The definition and implementation of the degradation type equation was performed with the reaction kinetic editor tool, which is described in chapter 4.5.1.3.

4.5.3 Groundwater-surface water interaction related to risk identification

Groundwater and surface water are part of a hydrological continuum (Fleckenstein et al., 2009). An integral and interdisciplinary analysis must be considered to understand the interaction of both ecosystems. Numerous flow pathways exist which influence the movement of contaminant groundwater into river water. Concerning to a contaminated water exchange between both systems the transition zone has to be investigated (cf. chapter 4.1). This zone is of particular importance regarding the water ecology, water quality and quantity. Fleckenstein et al. (2009) emphasize the necessity of high-capacity field methods and simulation tools to represent the spatial and temporal pattern of the water exchange on different scales as well as the interplay between hydraulic and water quality. In consideration of a groundwater risk management the ecological function of both ecosystems as a biotope and livelihood has be protected. Furthermore, preventive water protection including a risk assessment finally effects

a long-term and cost-efficient action in comparison to “reparation operations” (*Umwelt Bundes Amt, 2010*). The policy is responsive to potential risks and losses of water bodies by use of an integrated risk management, which links the complete range of hydrological-ecological problems by application of specific software tools and expertise.

Massmann et al. (2009) documented the importance of a good water quality condition in urban areas. The major portion of bank filtration is used for drinking water in urban areas (*EU Water Framework Directive, 2010*). In case of a groundwater contamination, the bordering river system and the bank filtration are under risk. An analysis of the effluent and influent conditions between both ecosystems is necessary to determine the spatial distribution and temporal dynamic of the exchange processes. On this basis, an estimation of potential contaminant exchange for a risk estimation will be accomplished by groundwater–surface water model coupling application.

4.5.3.1 Type of model coupling

The coupling between the groundwater model (*Feflow 6.0x*, DHI-WASY GmbH, Berlin) and the 1D surface water model (*MIKE11*, DHI-WASY GmbH, Berlin) is an externally coupled model. *Mike11* is a widely used hydrodynamic river modeling tool.

In most cases, a certain resistance between the river and groundwater body is existent. The result is a difference between the ground- and surface water level. A 3rd boundary condition type (Cauchy-type) has to define:

$$q_{n_h} \quad x_i, t = -\Phi_h \quad h_2^R - h \quad \text{for 3D and 2D vertical \& unconfined}$$

$$q_{n_h} \quad x_i, t = -\Phi_h \quad h_2^R - h \quad \text{for 2D horizontal confined}$$

$$\Phi_h = \begin{cases} \Phi_h^{in} & \text{for } h_2^R > h \\ \Phi_h^{out} & \text{for } h_2^R \leq h \end{cases} \quad \text{Eq. 4-26}$$

$$\Phi_h = \begin{cases} \Phi_h^{in} & \text{for } h_2^R > h \\ \Phi_h^{out} & \text{for } h_2^R \leq h \end{cases}$$

Φ_h, Φ_h Transfer coefficient (or transfer rate)

q_{n_h} Normal Darcy flux of fluid

q_{n_h} Vertically average normal Darcy flux of fluid

$\Phi_h^{in}, \Phi_h^{out}$ Directional coefficient of in-transfer and out-transfer 3D

$\Phi_h^{in}, \Phi_h^{out}$ Directional coefficient of in-transfer and out-transfer 2D

h_1^R, h_2^R Prescribed boundary values of hydraulic head h

The area enclosed by the Cauchy boundary nodes describes the exchange area between the surface and groundwater body. In that case, the area represents the real exchange area, which depends on both, the river profile and the water depth. That enables the investigation of the period where the groundwater drops below the bottom the river. The discharges calculated by *FEFLOW* 6.0x to the coupled boundary nodes are being exported to the *MIKE11* HPoints (calculating points of a *Mike11* network) as an additional boundary conditions (Q_base) after each time step (Diersch, 2010).

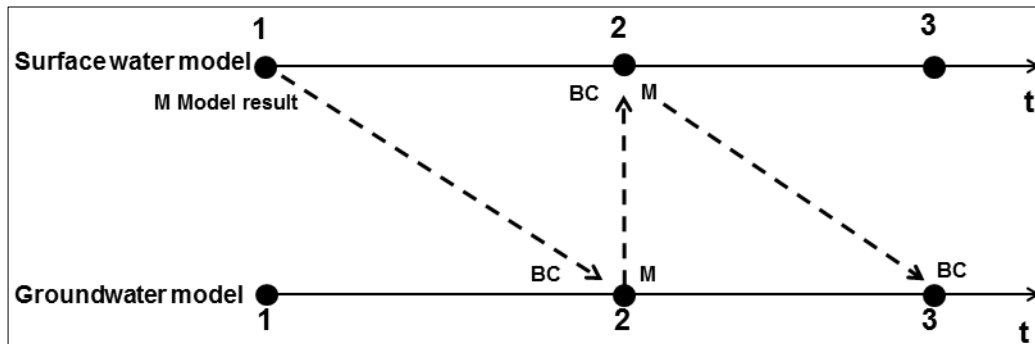


Figure 4-55 Operation mode of an external coupling using the example of two connected nodes. *M* represents the model results, *BC* boundary condition and *t* the simulation time, modified. Source: Becker, 2010.

Figure 4-55 shows the schematic operation of the external coupling. The model results of one compartment were delivered to the other one via the boundary condition. Usually, the surface water flow is calculated at first, because the groundwater flow responds afterwards. Then a calculated value of the surface model is available for the calculation of the unknown time step of the groundwater component (Becker, 2010). Examples and the mathematical-numerical solution technique for external coupling can be found in Monninkhoff (2004), Monninkhoff (2006), Partington et al. (2009), Panday et al. (2004) and Gunduz et al. (2005).

4.5.3.2 Application of the externally coupling

In this thesis, the coupling of the surface- and subsurface water model was performed to demonstrate the time-dependent dynamic processes of the investigation area. The analysis is focused on the effluent and influent conditions, which influence the stream flow direction of the groundwater and therewith a possible contamination passage through one ecosystem into the other. Based on the leakage approach after Diersch (2009) exfiltration and infiltration processes on the field scale were examined.

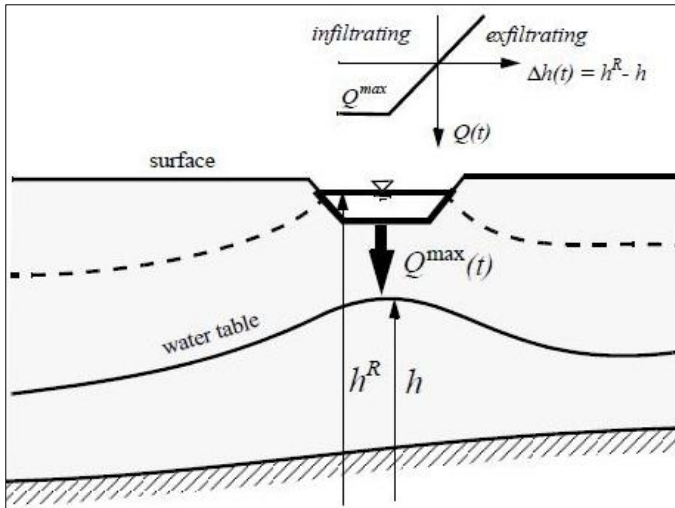


Figure 4-56 Flux-limiting infiltration from a river bed formulated by a maximum flux constraint . Source: Diersch, 2009.

The value of the transfer rate is definite by the pressure head difference between the river water table and groundwater table. The larger the pressure head difference, the higher the water amount, which is exchanged per time and area between the surface water and the subsurface. The most common leakage approach is the Darcy-approach. The transfer rate is related to the contact area, which is available for the water exchange between the surface- and groundwater body. It has the dimension of the Darcy-

velocity (ms^{-1}). Positive values represent an infiltration of the water from the river into the aquifer, negative values relate to an exfiltration process.

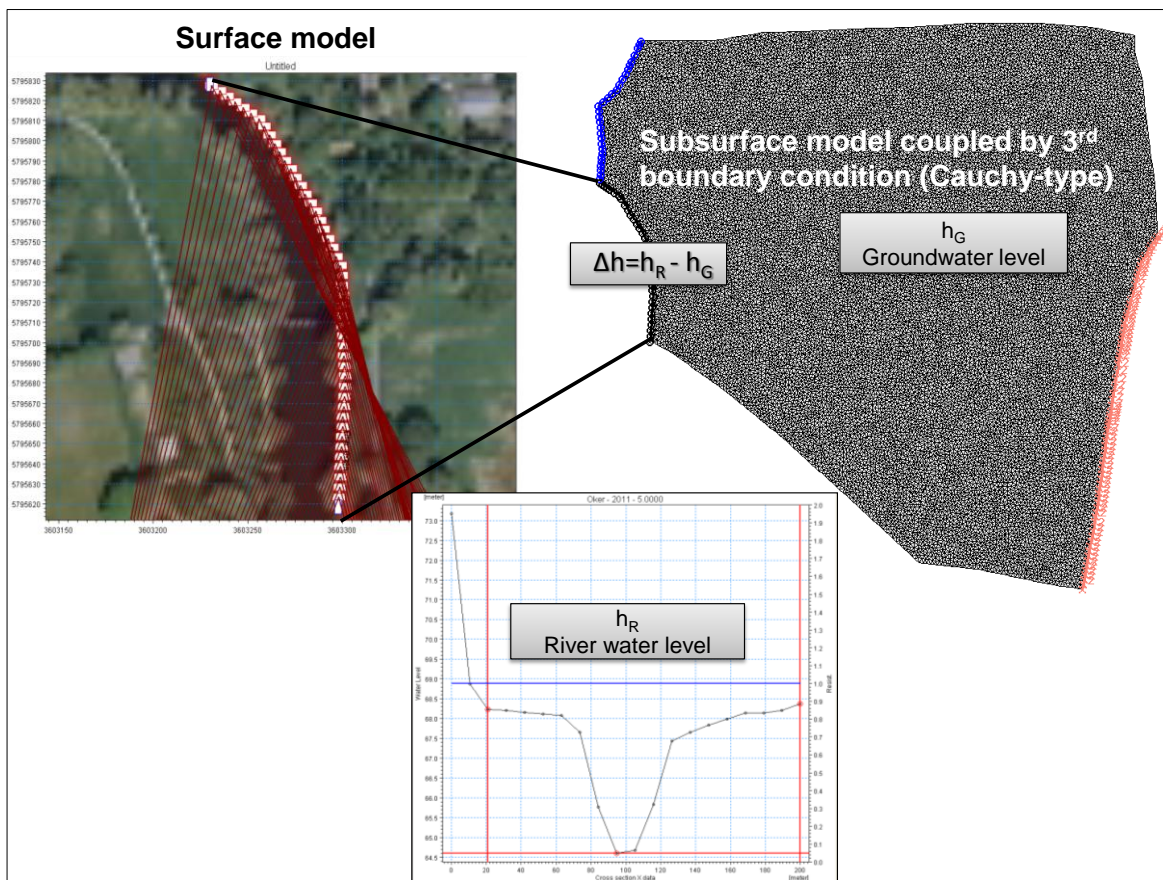


Figure 4-57 Schematic illustration of the groundwater-surface water model coupling of the investigation area. The coupling is operated by use of the 3rd boundary condition (Cauchy-type) in the groundwater model. This boundary type represents a transfer between river and aquifer.

4.5.3.3 Coupling of the time period 12/11/2009–12/12/2010

By use of *MIKE11*, a 1D surface water model was calibrated to couple the heterogeneous aquifer model (cf. chapter 4.5.2) and the homogeneous groundwater model (cf. chapter 4.5.2). The river network (cf. figure 4-57) of the 1D surface water model amounts 230 m and includes 147 river cross sections. A discharge and water level hydrograph from the 12/11/2009 - 12/11/2010 were defined for the gauge station “Heizkraftwerk Mitte” as boundary conditions in form of inflow and water level type of the surface water model. That gauge station was selected because of its spatial location to the bordering aquifer (investigation area). The selected date represents normal conditions of a hydrological year without extreme events in forms of drought seasons or flood events (HQ_{20} = 20-year flood etc.). The aim is to ascertain the water volume transfer between the aquifer and river by groundwater exfiltration and river bank infiltration under normal hydrological conditions to identify a potential contaminant transfer from the groundwater system into the river system.

A discharge hydrograph was defined as a model inflow. Because of unavailable discharge data of the gauge station “Heizkraftwerk Mitte” two further gauge stations were consulted to estimate the discharge of the “Heizkraftwerk Mitte”. By use of a discharge relation calculation between the gauge “Groß Schwülper” and “Harxbüttel”, the discharge of the “Heizkraftwerk Mitte” was estimated. The outflow of the 1D surface water model was defined by a river water level which was directly measured at the gauge “Heizkraftwerk Mitte”.

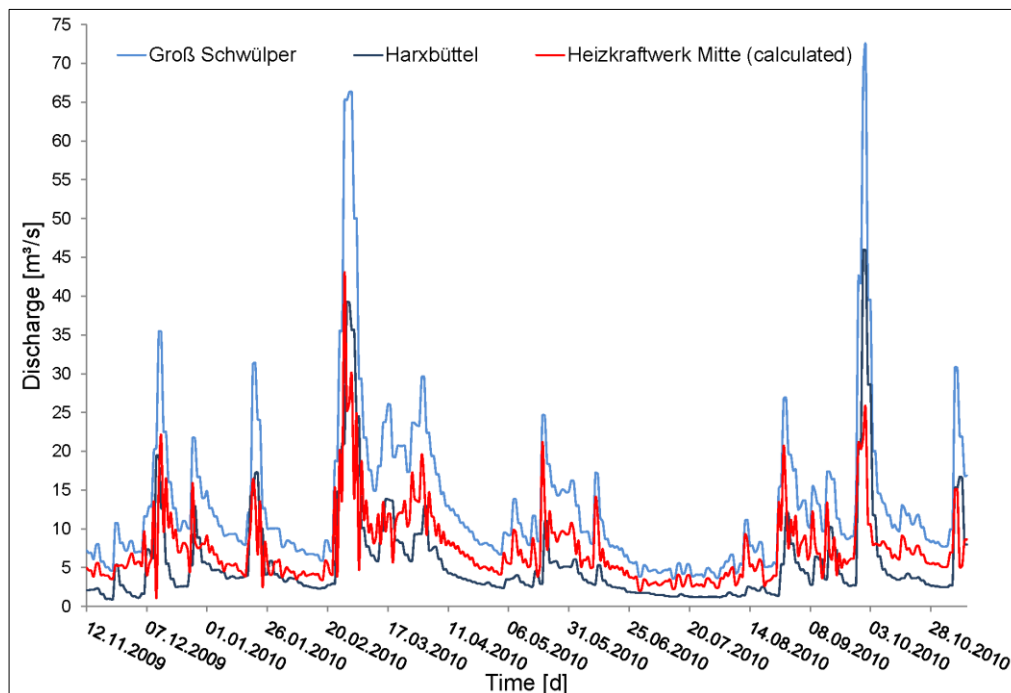


Figure 4-58 Discharge hydrographs of the gauge station „Groß Schwülper“ and „Harxbüttel“ from the 12/11/2009–12/11/2010 and the calculated discharge of the gauge station „Heizkraftwerk Mitte“.

Figure 4-59 shows the implemented boundary conditions of the 1D surface water model (*MIKE11*) from the 12/11/2009 – 12/11/2010.

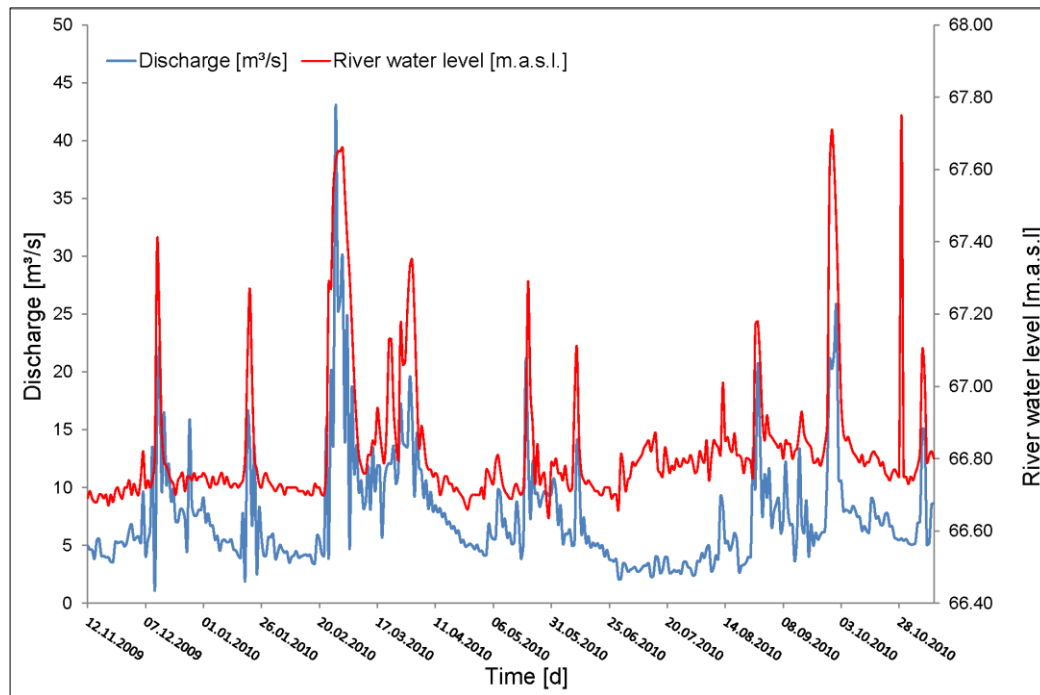


Figure 4-59 Boundary conditions of the 1D surface water model (*MIKE11*). Inflow boundary condition represents a discharge hydrograph from 12/11/09-12/11/10 and downstream condition is defined as a water level hydrograph of the river.

4.5.3.4 Coupling of the 20-year flood (HQ_{20})

With regard to a risk assessment approach, the surface–subsurface water coupling was subjected to different scenarios. The first scenario represents a 20-years flood modeling with a maximum river water level of 69.06 m.a.s.l. and a maximum discharge of $135.0 \text{ m}^3\text{s}^{-1}$ of the station “Groß Schwülper”. The statistical flood analysis was performed with the program *HQ-EX*. The maximum discharge values from the years 1956–2006 of the gauge station “Groß Schwülper” were implemented into the program. This analysis was used to identify years with extreme events.

Figure 4-60 reflects the hydrograph of the maximum discharge values from 1956 – 2006. The diagram shows that 1956 and 2002 exhibit significant flood events. Due to the fact that the river water level records of the “Heizkraftwerk Mitte” are leading back to the year 1970, the flood event of 2001 - 2002 was selected for an extreme flood event scenario.

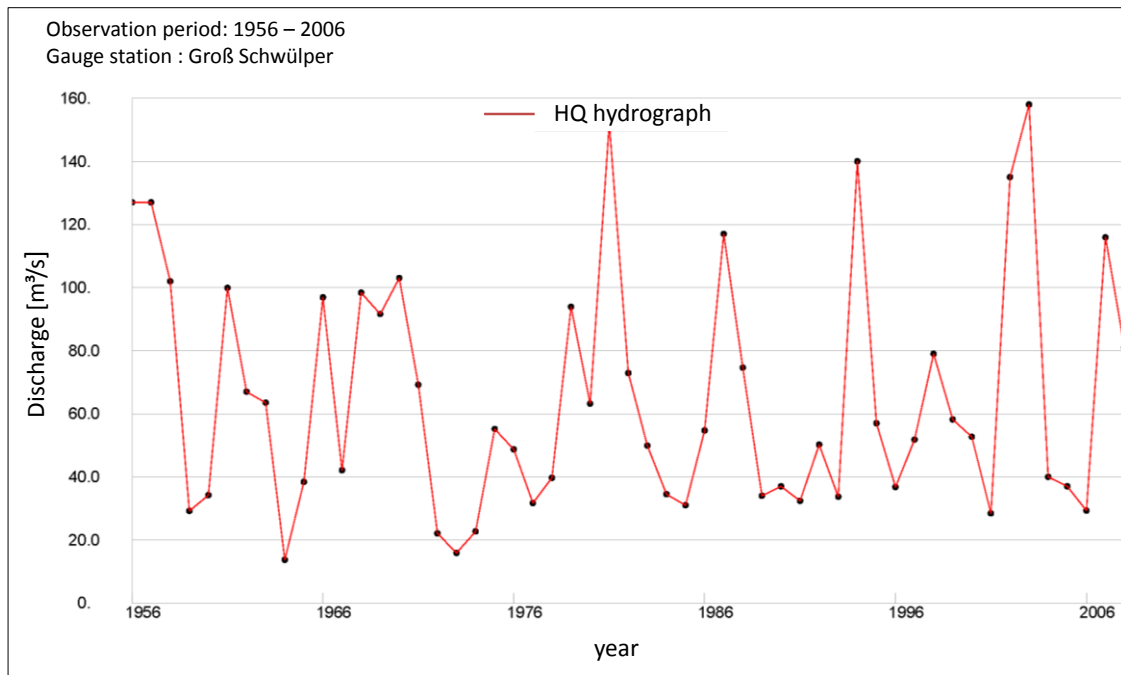


Figure 4-60 Maximum discharge values from 1926–2006 of the gauge station “Groß Schwülper”.

Figure 4-61 represents the statistically analysis of the recurrence intervals from 1956–2006 with different distribution functions and estimation methods for the gauge station “Groß Schwülper”. According the analysis, the maximum discharge value ($135.0 \text{ m}^3\text{s}^{-1}$) of the years 2001 - 2002 is related to a HQ_{20} . Based on the *HQ-EX* analysis the discharge of the “Heizkraftwerk Mitte” was calculated by the discharge relation between “Groß Schwülper” and “Harxbüttel” for the year 2001 - 2002 (cf. figure 4-62).

Observation period: 1956-2006
Gauge station: Groß Schwülper

Discharge [m^3/s]

Distribution function	Estimation method	Recurrence intervals [years]									
		2	5	10	20	25	50	100	200	500	1000
E1	MM	59.3	92.6	115.	136.	143.	163.	184.	204.	231.	252.
	MLM	58.6	90.4	112.	132.	138.	158.	178.	197.	223.	242.
	WGM	59.1	93.5	116.	138.	145.	166.	187.	209.	236.	257.
AE	MM	60.3	94.2	115.	135.	141.	159.	177.	194.	215.	230.
	MLM	56.7	98.6	138.	188.	207.	276.	367.	483.	693.	907.
	WGM	57.2	91.4	116.	141.	149.	176.	204.	234.	276.	310.
ME	MLM	54.9	93.6	121.	146.	155.	180.	205.	230.	263.	288.
LN3	MM	57.9	91.1	114.	137.	144.	167.	190.	215.	248.	274.
	MLM	55.5	91.0	118.	146.	155.	186.	218.	252.	301.	341.
	WGM	57.1	92.1	117.	141.	149.	174.	200.	227.	264.	293.
P3	MM	59.5	94.2	116.	136.	142.	161.	178.	196.	218.	234.
	MLM	56.4	92.9	118.	142.	149.	172.	195.	217.	246.	268.
	WGM	56.8	93.5	118.	142.	149.	172.	194.	215.	244.	265.
LP3	MLM	57.1	91.8	116.	139.	147.	170.	193.	216.	247.	270.
WB3	MM	59.6	95.6	117.	136.	142.	159.	174.	189.	207.	220.
	MLM	57.5	94.0	117.	139.	145.	165.	184.	201.	224.	240.
	WGM	56.2	94.1	119.	143.	150.	172.	193.	213.	239.	258.
Kleeberg/ Schumann	$c_s = 4$								205.	244.	274.

Figure 4-61 Recurrence intervals of the gauge station “Groß Schwülper” based on the statistical analysis of 50 maximum discharge values from 1956–2006.

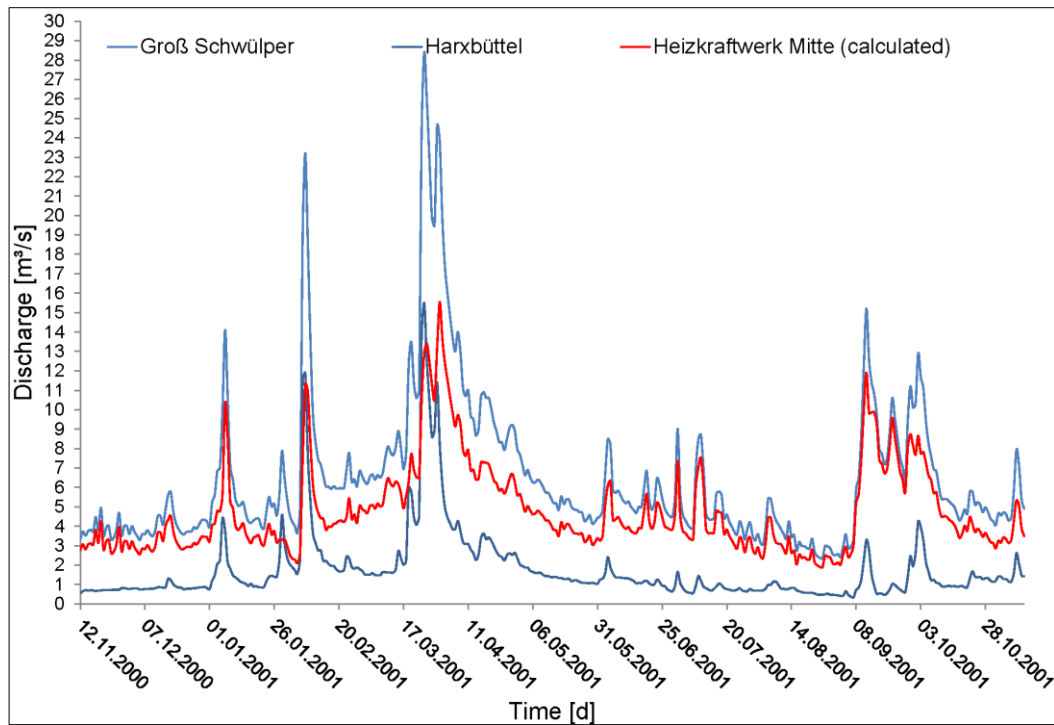


Figure 4-62 Discharge hydrographs of the gauge station „Groß Schwülper“ and „Harxbüttel“ from the 12/11/2001–12/11/2002 and the calculated discharge of the gauge station „Heizkraftwerk Mitte“. This discharge hydrographs represent a calculated HQ_{20} .

Correspondingly, the boundary conditions of the 1D surface water simulation were modified with an inflow related to the gauge “Heizkraftwerk Mitte” discharge hydrograph of 2002 and an outflow with a river water level hydrograph of 2002 (cf. figure 4-63).

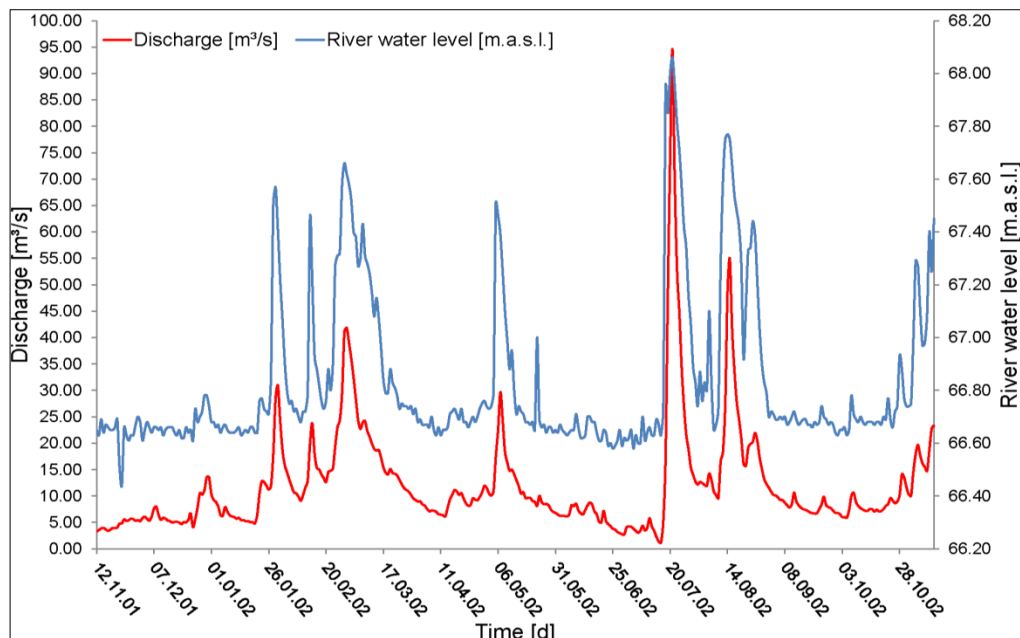


Figure 4-63 Boundary conditions of the 1D surface water model (Mike11). Inflow boundary condition represents a discharge hydrograph from 12/11/2001–12/11/2002 and downstream condition is defined as a water level hydrograph of the gauge station “Heizkraftwerk Mitte”.

4.5.3.5 Coupling of a low flow (NQ)

Another scenario modeling is related to a “drought” hydrological year in which the river water level and discharge is below normal conditions. The static analysis results shows that the time period from 12/11/2000 – 12/11/2001 represents this conditions with a maximum river water level of 66.85 m.a.s.l. and a discharge of $28.4 \text{ m}^3\text{s}^{-1}$ of the gauge station “Groß Schwülper”.

The discharge of “Heizkraftwerk Mitte” was calculated by the discharge relation between gauge station “Groß Schwülper” and “Harxbüttel” (cf. figure 4-64).

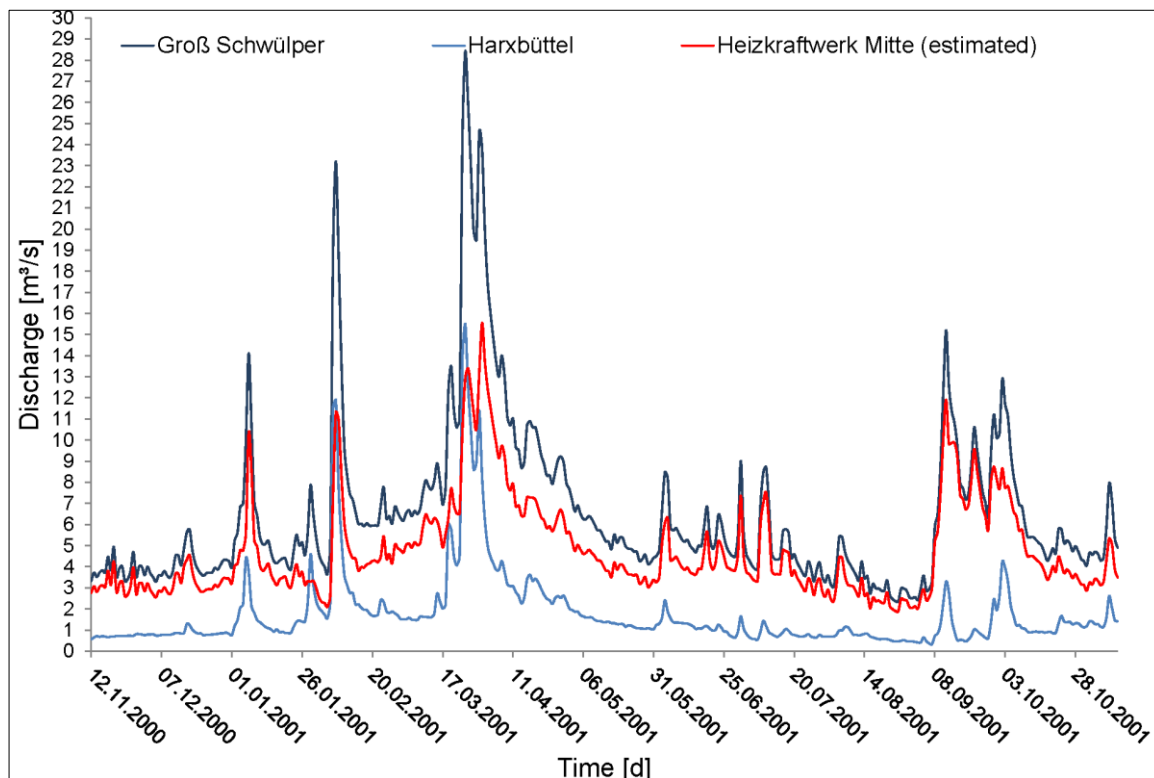


Figure 4-64 Discharge hydrographs of the gauge station „Groß Schwülper“ and „Harxbüttel“ from the 12/11/2000–12/11/2001 and the calculated discharge of the gauge station „Heizkraftwerk Mitte“. This discharge hydrographs represent a calculated NQ.

Correspondingly, the boundary conditions of the 1D surface water simulation were modified with an inflow related to the gauge “Heizkraftwerk Mitte” discharge hydrograph of 2000 and an outflow with a river water level hydrograph of 2000 (cf. figure 4-65).

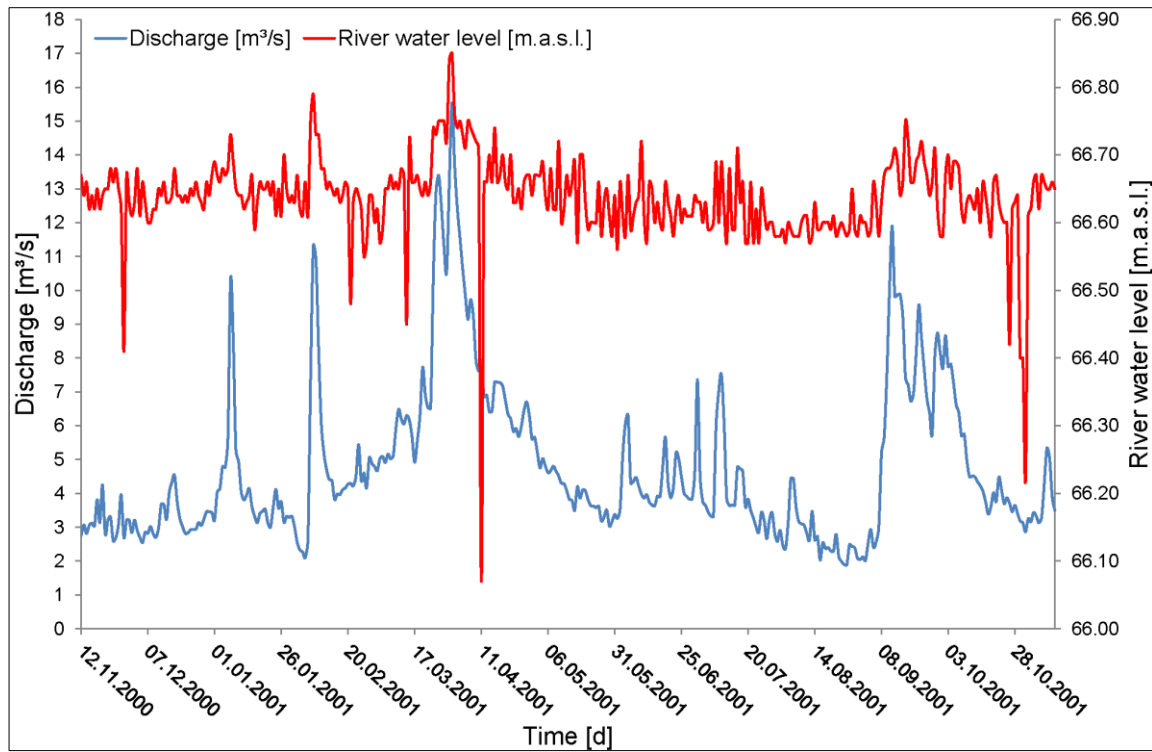


Figure 4-65 Boundary conditions of the 1D surface water model (Mike11). Inflow boundary condition represents a discharge hydrograph from 12/11/2000–12/11/2001 and downstream condition is defined as a water level hydrograph of the gauge station “Heizkraftwerk Mitte”.

5 Presentation of different model scenario outputs

This chapter presents the model results of different scenarios to investigate the influence of dynamic boundaries on transient transport simulations. At first, an overview of the calibrated steady-state and transient flow and transport simulation output is given.

The strategies for calibrating transport models are usually difficult to implement. Inaccessibility of data force the user to execute a set of assumptions. Also, this case study is characterized by restrictions in geochemical data. Only limited observation data are available for transport calibration. Groundwater samples of the investigation area were analyzed for all chlorinated ethenes and thus an effective base data set for model validation with reference data was available. The transport and reaction model was validated for model results after 50 years of simulation time. This time is considered as current contamination distribution and used for validation purposes. Thangarajan et al. (2007) have also documented an attempt to develop a transport model without concentration observation by use of inverse modeling. In addition, Barlebo et al. (1998) applied a transport model, which was calibrated only with hydraulic heads, as well.

The used transport parameters and kinetic equations were determined in cooperation with the research partner Greis (2011) and can be taken from a joint publication (Greis et al., 2011). All further model developments and multi-species transport results are based on the knowledge of this publication.

The second part of this chapter is the presentation of different dynamic scenarios by use of a numerical groundwater-surface water coupling. The results document the influence of different dynamic boundaries on the pollutant transport in a complex urban aquifer. The spatial variability and the reconstruction uncertainties of the complex aquifer could only be solved by use of a 3D geo-stochastic simulation. Moreover, a precise record of hydraulic subsurface parameters by a HPT technique leads in an adequate flow calibration. Degan et al. (1997) have already referenced the necessity of geo-stochastic tool applications during complex groundwater flow and transport simulations. Until today, the combination of geo-stochastic approaches with detailed practical field data collection exhibit a lack of utilizations in the field of dynamic risk identification.

The last section shows the results of the MCs which lead in a risk identification based on the generation of spatial probability of concentration occurrences (spco).

5.1 Groundwater flow computation

In this section the groundwater flow model results for steady-state and transient conditions, which results from the analyzed data of the investigation area (cf. chapter 4.1) and the explained model setups (cf. chapter 4.5.1, chapter 4.5.2), are described in detail. At first, the results of the calibrated flow and transport models are presented because of their relevance corresponding to the generation of probability isolines of selected contaminant concentrations for a risk assessment approach. Afterwards, the analyzed and calculated interaction relation between the aquifer and river is documented. Subsequently, the generated probability of concentration occurrences by use of the MCs is shown for the homogeneous and heterogeneous multi-species transport model.

Groundwater flow results of the steady-state conditions

Based on the defined model input parameter (cf. chapter 4.2) two different steady-state groundwater flow models for the unequal subsurface aquifer models (homogeneous and heterogeneous) were developed. The calibrated steady-state groundwater flow models provide the requisite for subsequent model increments.

The results are represented by the groundwater isopiestic lines of the homogeneous and heterogeneous steady-state model, the water balance, the comparison between computed and measured groundwater level and quality criterions.

Figure 5-1 shows the computed groundwater isolines and the scatter plot of the investigation area for the two different subsurface aquifer models. The groundwater flow of both models is directed to a bordering lake and river because of their hydraulic connection. An average groundwater flow velocity of 16.0 m a^{-1} was calculated for steady conditions. 25 observation wells were used to define the initial hydraulic heads of the model domain. The scatter plot shows the correlation between the computed groundwater level of the initial conditions and the measured groundwater levels of the observation wells. The calibration line's coefficient of determinations was determined with 0.9576 for the homogeneous flow model and 0.9547 for the heterogeneous flow model. The maximum difference between computed and measured hydraulic heads amounts to 0.33 m and the minimum difference is obtained with 0.01 m.

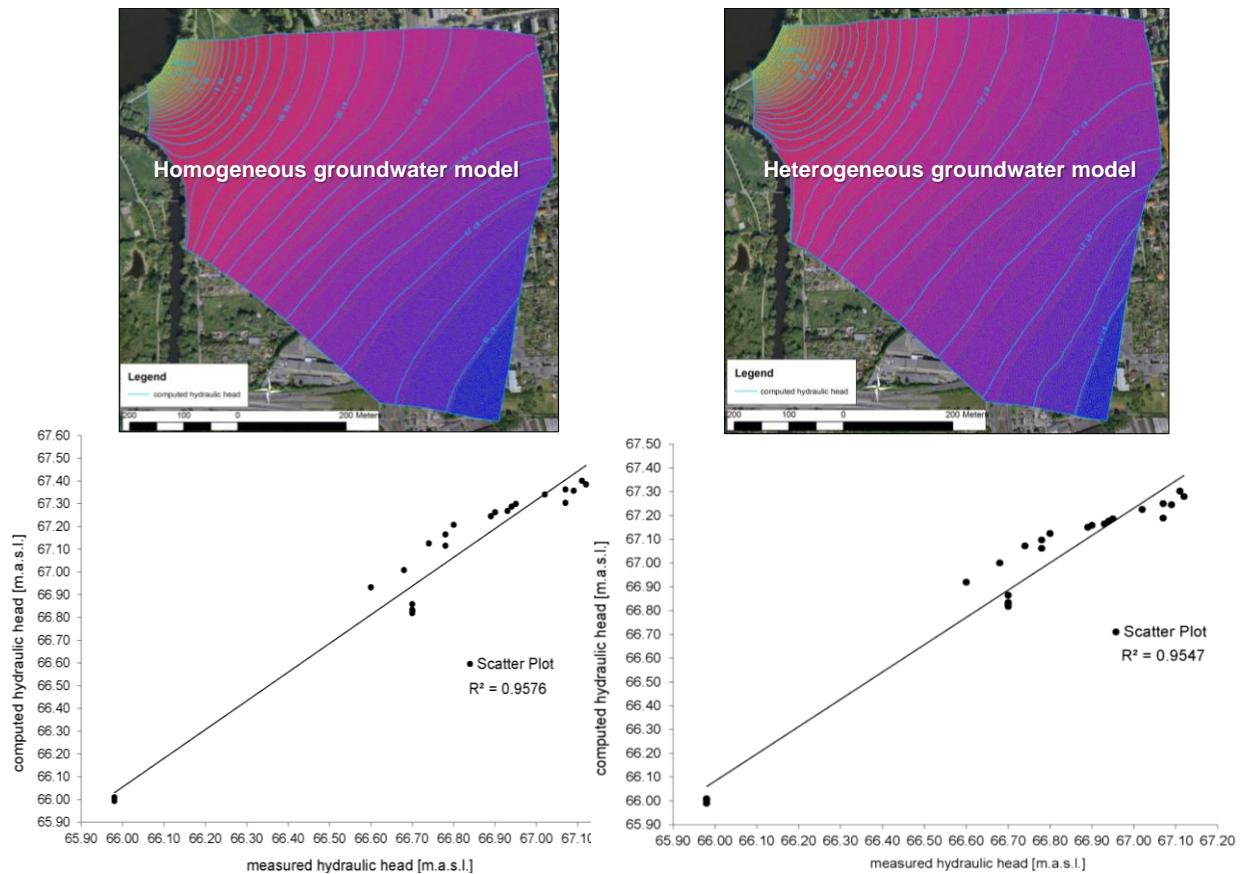


Figure 5-1 Computed groundwater level isolines of the homogeneous and heterogeneous steady-state groundwater flow model with corresponding Scatter Plot of the measured and computed hydraulic heads.

In addition to the coefficient of determination, the root mean squared error (RMSE) and the mean average error (MAE) were determined for the homogeneous and heterogeneous multi-species transport model based on the measured and computed hydraulic heads of the 25 observation wells. Table 5-1 shows the results of the error parameter calculation.

Table 5-1 Statistical error parameters of the steady-state groundwater flow simulation.

Model	RMSE [m]	MAE [m]	Correlation coefficient
Steady-state, homogeneous aquifer	0.07	0.19	0.9576
Steady-state, heterogeneous aquifer	0.07	0.19	0.9547

The water budget of the homogeneous steady-state groundwater flow model is presented in figure 5-2.

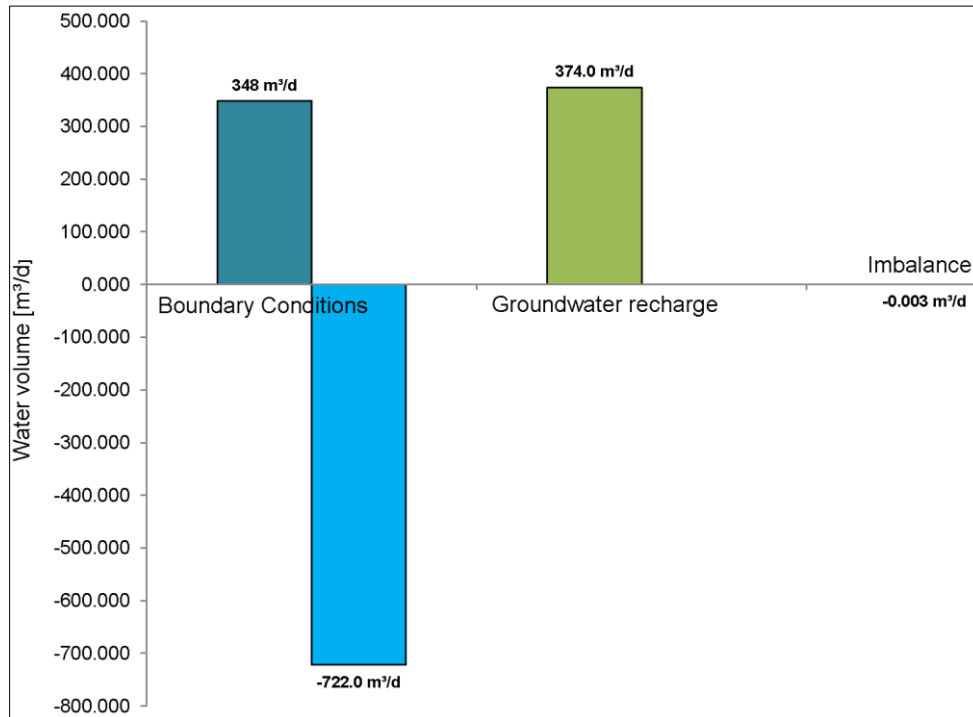


Figure 5-2 Water budget of the homogeneous subsurface model of steady-state groundwater flow conditions.

The illustration shows (cf. figure 5-2) the inflow and outflow water volume (m^3d^{-1}) of the model domain by boundary conditions, groundwater recharge and imbalance. Altogether, an inflow of $348.0 \text{ m}^3\text{d}^{-1}$ through the boundary conditions and $374.0 \text{ m}^3\text{d}^{-1}$ via groundwater recharge streams into the model. The water volume portion, which leaves the model domain by an outflow is represented by a boundary conditions water volume of $-722.0 \text{ m}^3\text{d}^{-1}$. The imbalance of the steady-state homogeneous groundwater flow model is due to $-0.003 \text{ m}^3\text{d}^{-1}$. In spite of a water volume imbalance of $-0.003 \text{ m}^3\text{d}^{-1}$, the steady-state homogeneous flow model can be assumed as calibrated because of the minor value, which has no important impact on the annual field water balance saldo.

Figure 5-3 illustrates the subdivision of the water volume of the boundary conditions and their percentage portion of the steady-state homogeneous aquifer model. The differentiation of the model inflow exhibits a percentage portion of the Dirichlet boundary condition of 16.0 % ($77.9 \text{ m}^3\text{d}^{-1}$, ecosystem lake), 31.5% ($153.0 \text{ m}^3\text{d}^{-1}$, ecosystem river) for the Cauchy boundary condition, the greatest portion is represented by the Neumann boundary condition with 52.5% ($255.0 \text{ m}^3\text{d}^{-1}$, groundwater subsurface inflow). The model outflow is dominated with 74.9% ($-541.0 \text{ m}^3\text{d}^{-1}$) by the Dirichlet b. c. and 25.1% ($-181.1 \text{ m}^3\text{d}^{-1}$) by the Cauchy b. c.

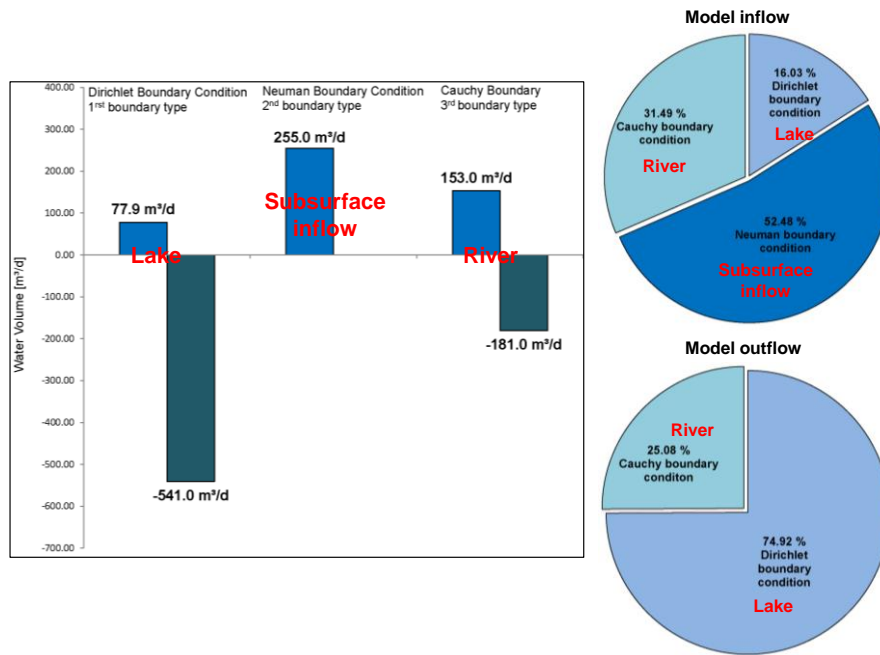


Figure 5-3 Fluid flux mass balance of the homogeneous steady-state groundwater flow model with percentage of the boundary conditions for inflow and outflow.

Figure 5-4 shows the water budget of the heterogeneous groundwater flow model including the boundary conditions, groundwater recharge and water volume imbalance. The model inflow is composed of a boundary condition water volume of $353.6 \text{ m}^3\text{d}^{-1}$ and a groundwater recharge volume of $374.0 \text{ m}^3\text{d}^{-1}$. Through the boundary condition $-727.7 \text{ m}^3\text{d}^{-1}$ water volume streams out of the model domain. An absolute imbalance water volume value of $-0.0003 \text{ m}^3\text{d}^{-1}$ was determined. Therefore, the steady-state heterogeneous flow model can be considered as calibrated as well as the homogeneous steady-state flow model.

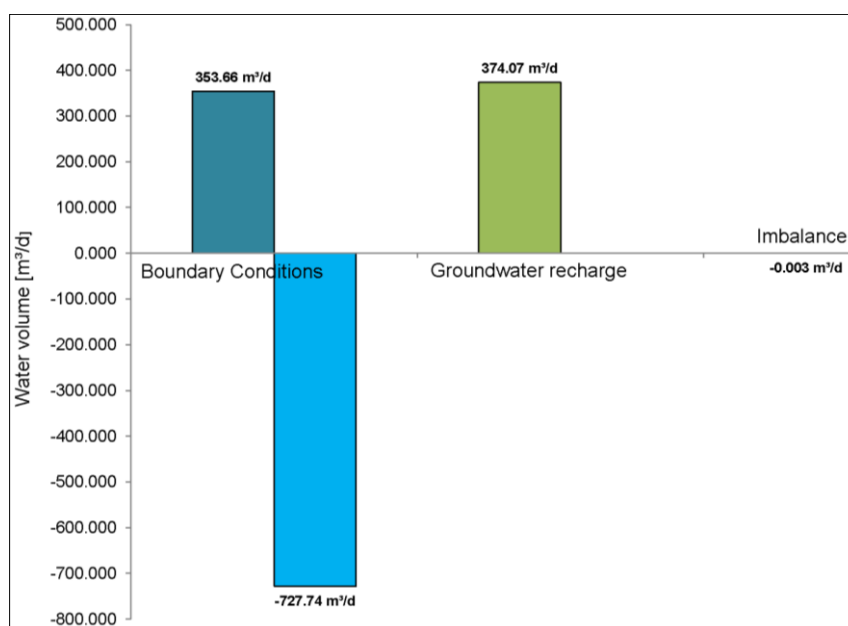


Figure 5-4 Water budget of the heterogeneous steady-state groundwater flow model.

Figure 5-5 documents the differentiation of the heterogeneous model inflow and outflow after the boundary condition types. The differentiation of the model inflow exhibits a percentage portion of the Dirichlet boundary condition of 23.1% ($81.6 \text{ m}^3\text{d}^{-1}$, ecosystem lake), 25.1% ($89.1 \text{ m}^3\text{d}^{-1}$, ecosystem river) for the Cauchy boundary condition, the greatest portion is represented by the Neumann boundary condition with 51.8% ($183.0 \text{ m}^3\text{d}^{-1}$, groundwater subsurface inflow). The model outflow is dominated with 86.37% ($-632.5 \text{ m}^3\text{d}^{-1}$) by the Dirichlet boundary condition b. c. and 13.6% ($-95.2 \text{ m}^3\text{d}^{-1}$) by the Cauchy b. c.

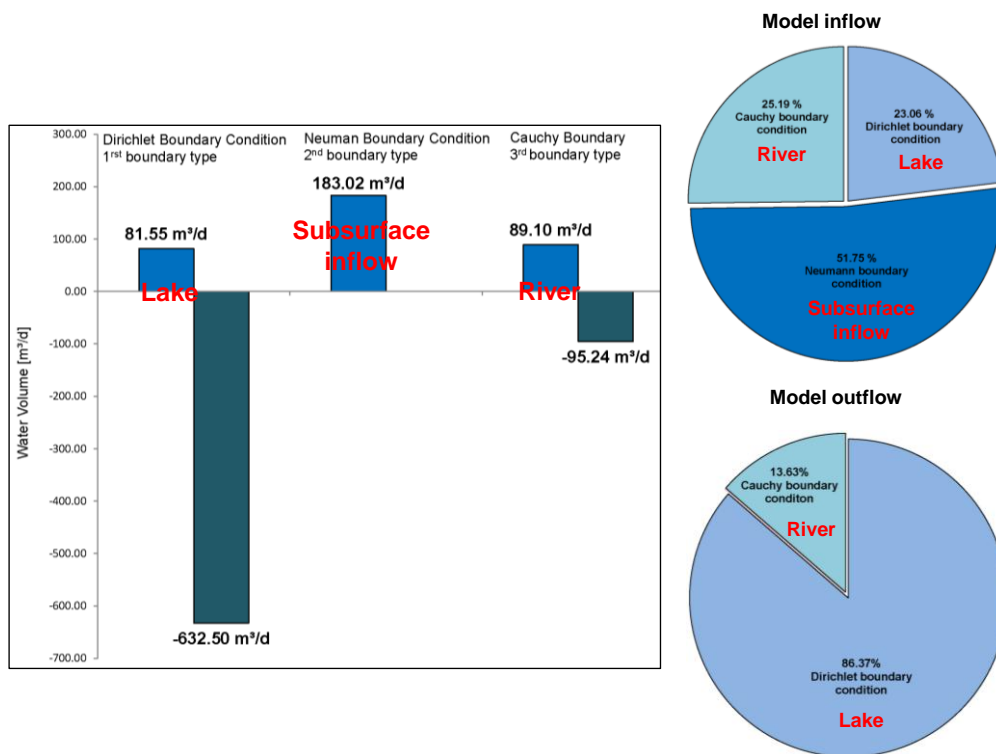


Figure 5-5 Fluid flux mass balance of the heterogeneous steady-state groundwater flow model with percentage of the boundary conditions for inflow and outflow.

Groundwater flow results of the transient conditions

The following results presentation is based on the model setup of the transient groundwater flow models, which is explained in chapter 4.5. The presentation of the results refers to unsteady climatic and hydrological conditions from the 12/11/2009 – 12/11/2010 (cf. chapter 4.3.3).

Unlike, to the steady-state conditions, a comparison between the measured and computed hydraulic heads for each time step is impossible for transient conditions. Hence, two observation wells of the model domain (SB1 and B16) were used to compare the computed and measured groundwater hydrographs. This procedural method is required to get a significance of the transient flow model calibration. Figure 5-6 presents the measured and computed groundwater hydrographs from 12/11/2009 – 12/11/2010 of SB1 and B16 with the

corresponding groundwater difference for each time step for the homogeneous aquifer. The initial groundwater level of B16 is 66.88 m.a.s.l. and cease with a value of 67.2 m.a.s.l. at the end of the period of extermination. The highest measured value is 67.33 m.a.s.l. (01/10/2010) induced by an intense rain event and the lowest value was measured with 66.87 m.a.s.l. (20/11/2009). The initial groundwater level of SB1 is 66.77 m.a.s.l. and ends with a groundwater level of 67.13 m.a.s.l. for the investigation time period. The highest groundwater level was measured on 01/10/2009 with 67.31 m.a.s.l and the lowest value with 66.74 m.a.s.l. (20/11/2009) like B16.

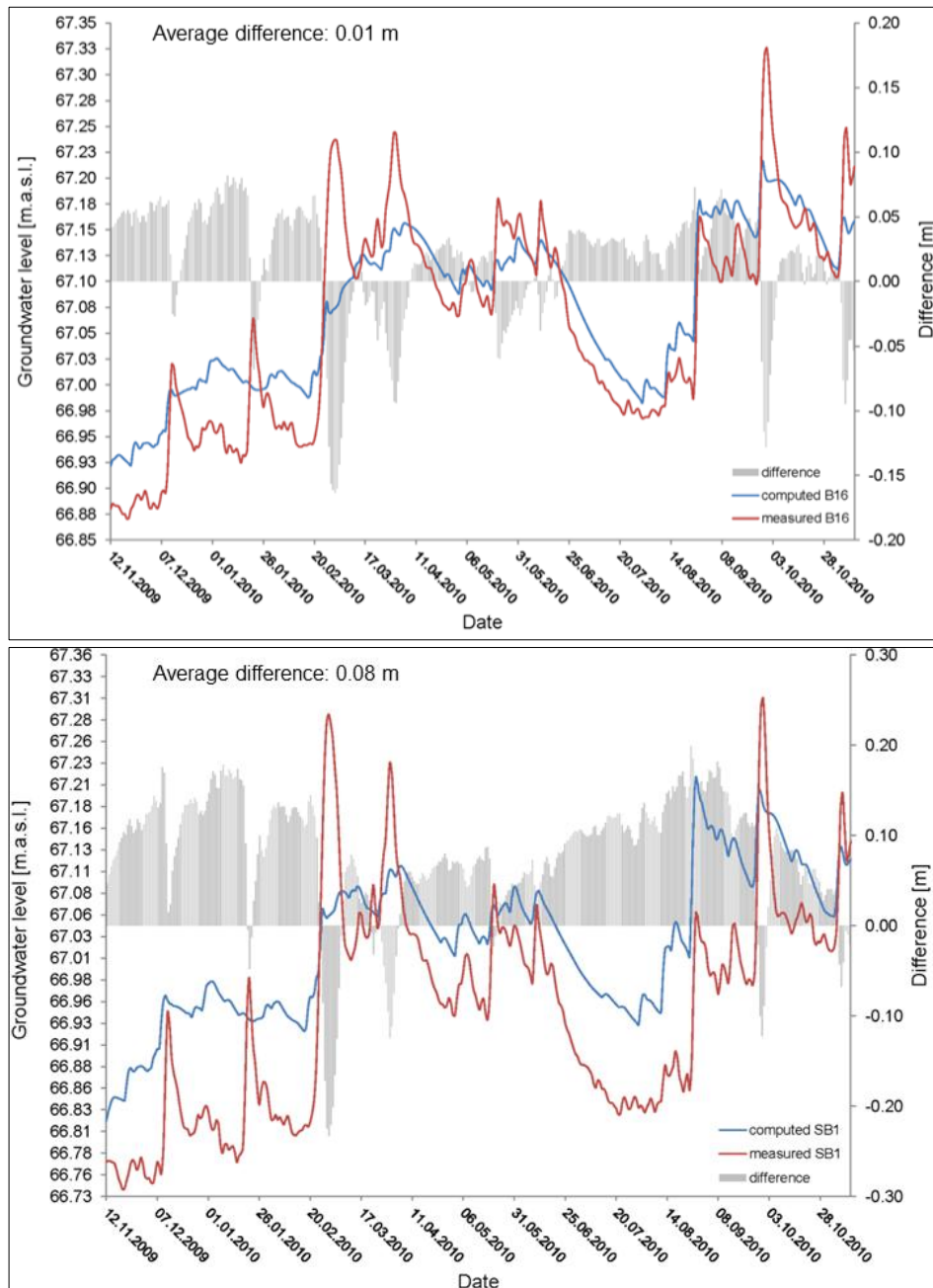


Figure 5-6 Groundwater hydrographs of observation well B16 and SB1 from the 12/11/2009-12/11/2010. Comparison between computed (blue) and groundwater levels (red) of the transient homogeneous groundwater flow models and illustration of water level differences.

The computed groundwater hydrograph of B16 starts with a value of 66.92 m.a.s.l. and increases on 67.19 m.a.s.l. at the simulation end. A comparison between the measured and computed hydrographs shows that the computed groundwater levels are above the measured values for the complete simulation time period. For each time step, in which the measured groundwater hydrograph achieves the highest groundwater value (peak), the computed value decrease below the computed levels. The average difference of the hydraulic heads is calculated with 0.01 m. Figure 5-6 detects the highest difference of -0.17 m at the 20/02/2010 and a lowest difference of zero. This value appears at multi simulation days. However, the temporal dynamic of the measured groundwater level is acceptable reflected by the computed groundwater hydrograph.

The groundwater level of SB1 at the beginning of the simulation is 66.79 m.a.s.l. and increases until the simulation end on 67.12 m.a.s.l. Moreover, this comparison of computed and measured groundwater hydrograph shows that the computed values are above the measured groundwater levels. Only during the flood events the computed groundwater level decreases below the measured value. The average difference between measured and computed groundwater levels is calculated with 0.08 m. As well as for B16, the highest difference of SB1 can be observed at the 02/03/2010 with a value of -0.25 m and the lowest difference is considered with 0.01 m for multi simulation days. Nonetheless, the temporal dynamic of the time-dependent computed groundwater hydrograph is well reproduced.

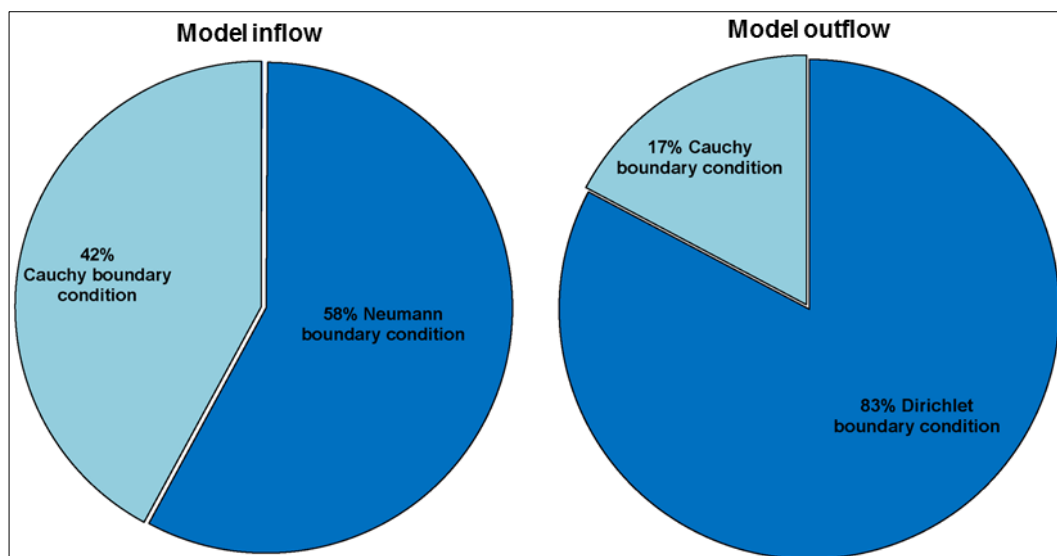


Figure 5-7 Fluid flux mass balance of the homogeneous transient groundwater flow model with percentage of the boundary conditions for inflow and outflow.

Figure 5-7 illustrates the fluid flux mass balance of the homogeneous transient groundwater flow model with the percentage of the boundary conditions for inflow and outflow. The importance of the bordering ecosystem river and lake for the transient multi-species transport is demonstrated with this figure. 42.0% (this equates $155.0 \text{ m}^3\text{d}^{-1}$) of the model inflow is

represented by the river through a Cauchy b. c. and 58.0% (this equates $213.0 \text{ m}^3\text{d}^{-1}$) of the inflow water volume is caused by subsurface inflow (Neumann b. c.). A significant model outflow is given by the lake (Dirichlet b. c.) with 83.0% ($739.0 \text{ m}^3\text{d}^{-1}$) and the river 17.0% ($154.0 \text{ m}^3\text{d}^{-1}$) Cauchy b. c.).

Figure 5-8 shows the measured and computed groundwater hydrographs for B16 and SB1 of the transient heterogeneous aquifer model.

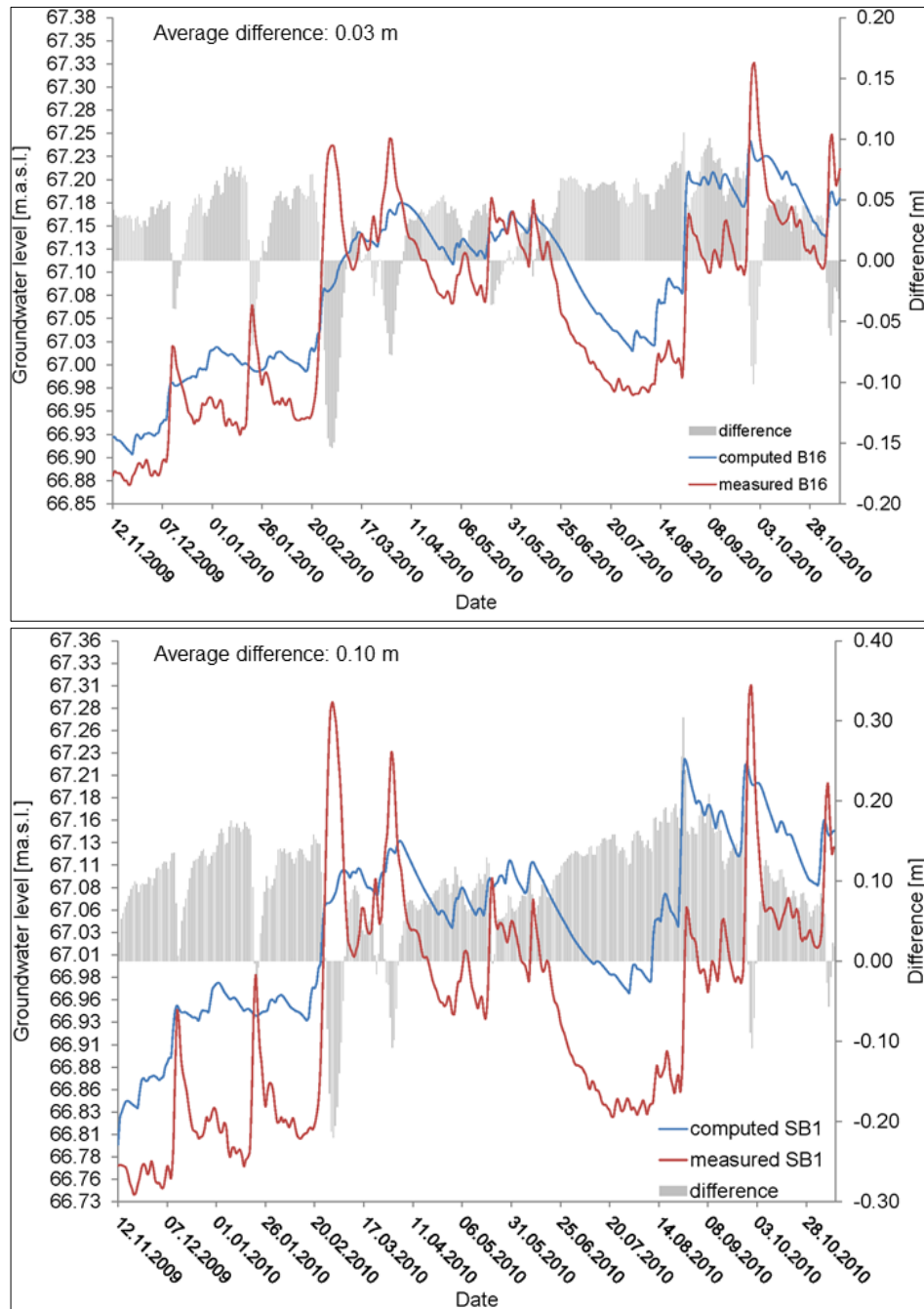


Figure 5-8 Groundwater hydrographs of observation well B16 and SB1 from the 12/11/200-12/11/2010. Comparison between computed (blue) and groundwater levels (red) of the transient heterogeneous groundwater flow models and illustration of water level differences.

The initial groundwater level of B16 is 66.88 m.a.s.l. and ceases with a value of 67.2 m.a.s.l. at the end of the period of extermination. The highest measured value is 67.33 m.a.s.l. (01/10/2010) induced by an intense rain event and the lowest value was measured with 66.87 m.a.s.l. (20/11/2009). The initial groundwater level of SB1 is 66.77 m.a.s.l. and ends with a groundwater level of 67.13 m.a.s.l. for the investigation time period. The highest groundwater level was measured on 01/10/2009 with 67.31 m.a.s.l. and the lowest value with 66.74 m.a.s.l. (20/11/2009) like B16.

The computed groundwater hydrograph of B16 starts with a value of 66.79 m.a.s.l. and increases to 67.15 m.a.s.l. at the simulation end. A comparison between the measured and computed hydrographs shows that the computed groundwater levels are above the measured values for the complete simulation time period. The average difference of the hydraulic heads is calculated with 0.03 m. Figure 5-8 detects the highest difference of -0.16 m on 02/03/2010 and a lowest difference of zero. This value appears on multiple simulation days. However, the temporal dynamic of the measured groundwater level is acceptably reflected by the computed groundwater hydrograph.

The groundwater level of SB1 at the beginning of the simulation is 66.79 m.a.s.l. and increases until the end of the simulation to 67.15 m.a.s.l. Also, this comparison of computed and measured groundwater hydrographs shows that the computed values are above the measured groundwater levels. The average difference between measured and computed groundwater levels is calculated with 0.10 m. As well as for B16, the highest difference of SB1 can be observed on 02/03/2010 with a value of -0.16 m and the lowest difference is considered with zero for multiple simulation days. Nonetheless, the temporal dynamic of the time-dependent computed groundwater hydrograph is well reproduced.

Figure 5-9 presents the differentiation between the heterogeneous model inflow and outflow based on the boundary conditions. The model inflow is composed by 68.0% subsurface inflow ($242.0 \text{ m}^3\text{d}^{-1}$ Neumann b. c.), 30.0% river water volume ($105.0 \text{ m}^3\text{d}^{-1}$ Cauchy b. c.) and 2.0% lake water volume ($7.0 \text{ m}^3\text{d}^{-1}$ Dirichlet b. c.). The most important model domain outflow is given by the lake water volume (Dirichlet b. c.) with 78.0% ($670.0 \text{ m}^3\text{d}^{-1}$) and the river water with 22.0% ($187.0 \text{ m}^3\text{d}^{-1}$).

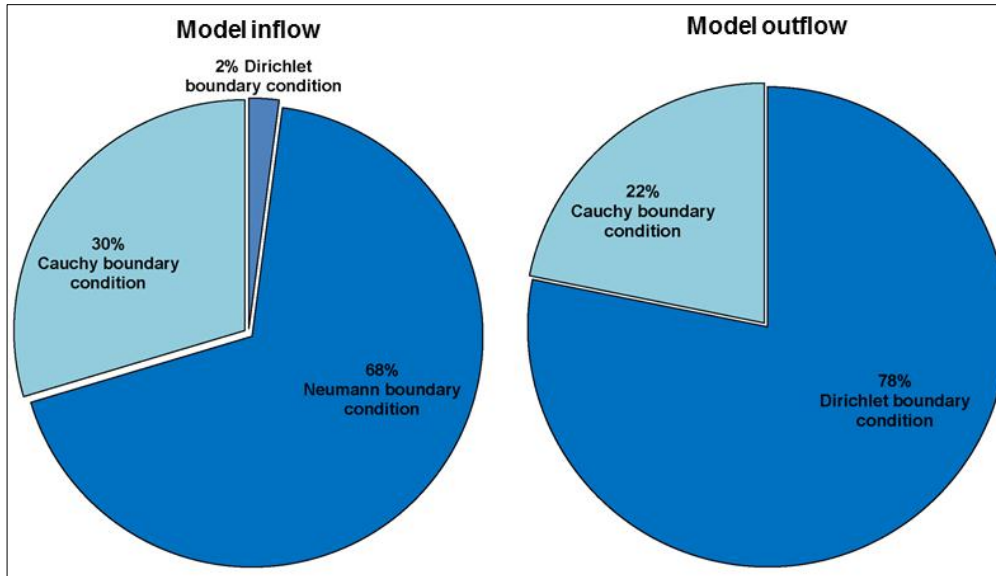


Figure 5-9 Fluid flux mass balance of the heterogeneous transient groundwater flow model with percentage of the boundary conditions for inflow and outflow.

Adjacent to the comparison of the measured and computed groundwater hydrographs, the root mean squared error (RMSE) and the mean average error (MEA) of the measured and computed groundwater levels of the 25 observation wells were calculated. The results are listed in table 5-2.

Table 5-2 Statistical error parameters of the transient groundwater flow simulation.

Model	Observation well	Statistical quality criterion	
		RMSE [m]	MAE [m]
Homogeneous aquifer	B16	0.09	0.04
	SB1	0.14	0.09
Heterogeneous aquifer	B16	0.07	0.05
	SB1	0.14	0.11

5.2 Multi-species transport computation

This section presents the simulation results of the multi-species transport (cf. chapter 4.5.1.3) for steady-state and transient transport flow conditions. Due to the fact that the contamination was caused in the 1970s a simulation period of 70 years was performed. A multi-species transport model calibration on a conventional method was impossible as a result of the unsatisfying data record of the pollutant concentration.

The first step was a definition of the reaction kinetic parameters and transport conditions for the homogeneous subsurface model. Subsequent to the transport model calibration the reaction and transport parameters were adopted for the heterogeneous model because it is assumed that the reaction conditions (pH-value, redox potential, sorption etc.) are equal.

The multi-species transport model validation of the homogeneous model was performed by taking samples of contaminated groundwater from 18 observation wells. Groundwater samples were analyzed for all chlorinated ethenes and thus a base data set for model validation with reference data was available. The transport and reaction model was validated for model results after 50 years of simulation time. This time is considered as current contamination distribution and is used for validation purposes.

Multi-Species transport results of the steady-state flow and transient transport conditions

The scatter plot of the measured and computed mass concentration of PCE, TCE, DCE and VC of the homogeneous steady-state flow and transient transport model is shown in figure 5-10. This plot exhibits acceptable agreements of the calculated and measured concentrations. The deviation of the data points from the regression line is presumed adequate in terms of accuracy.

The graphical transport model results are shown on the basis of selected mass concentration for PCE, TCE, DCE and VC with 1.0 mg/l^{-1} , 0.5 mg/l^{-1} , 0.2 mg/l^{-1} , 0.1 mg/l^{-1} and 0.01 mg/l^{-1} . This rated concentration values are retained for subsequent result presentations of the Monte Carlo simulation. The graphical analysis (cf. figure 5-14) also indicates that most of the simulated data are in conformity with measured data (cf. figure 5-10).

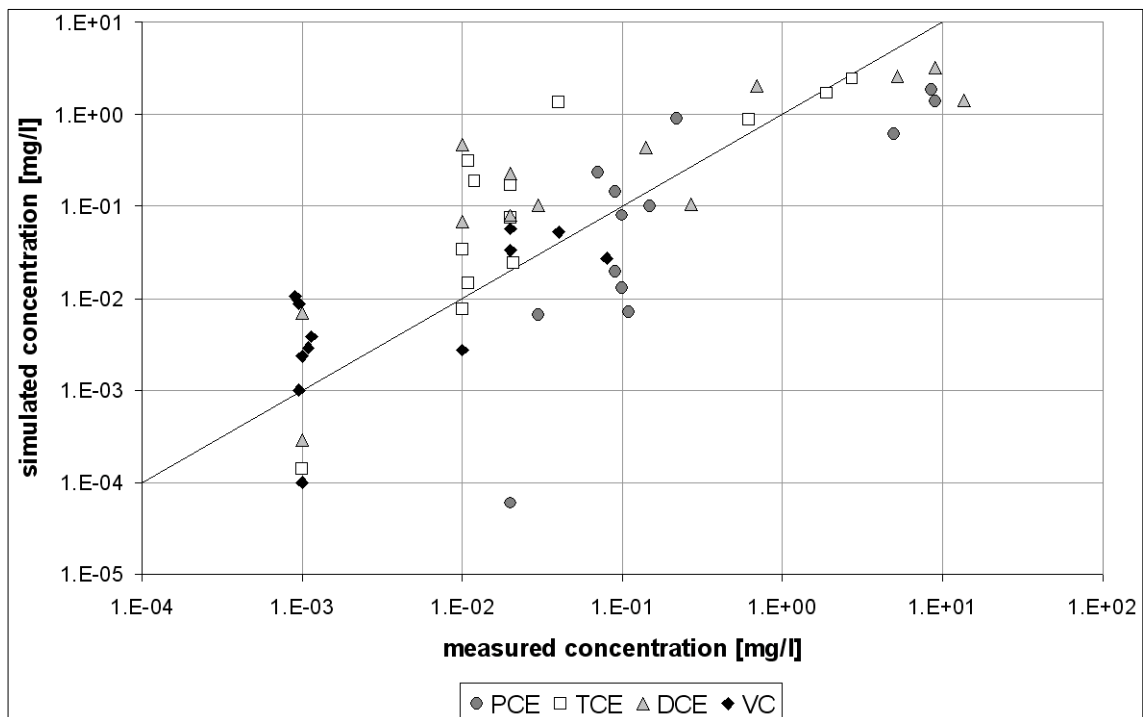


Figure 5-10 Comparison of computed and measured pollutant concentrations (PCE, TCE, DCE and VC) of the homogeneous model for steady-state flow and transient transport conditions. Source: Greis et al., 2011.

Sensitivity analysis was performed for seven important flow and transport parameters in order to evaluate their influence on the resulting concentration isolines. The tested parameters are porosity, hydraulic conductivity, longitudinal and transversal dispersivity, diffusion coefficient, reaction rate and K_d -value (linear adsorption isotherm coefficient). In summary, it was shown, that diffusion and porosity have minor influence on contaminant transport, while dispersivity, adsorption, reaction rate and hydraulic conductivity have major impact on transport behavior. Despite the large interval of variation of the diffusion coefficient ($1e^{-9}$ – $1e^{-6}m^2s^{-1}$) (cf. figure 5-11), differences in resulting contaminant concentration are negligible. On the other hand, even small changes in hydraulic conductivities ($\pm 50\%$ of the value implemented in the model) lead to extremely differing results (cf. figure 5-12) (Greis et al., 2011).

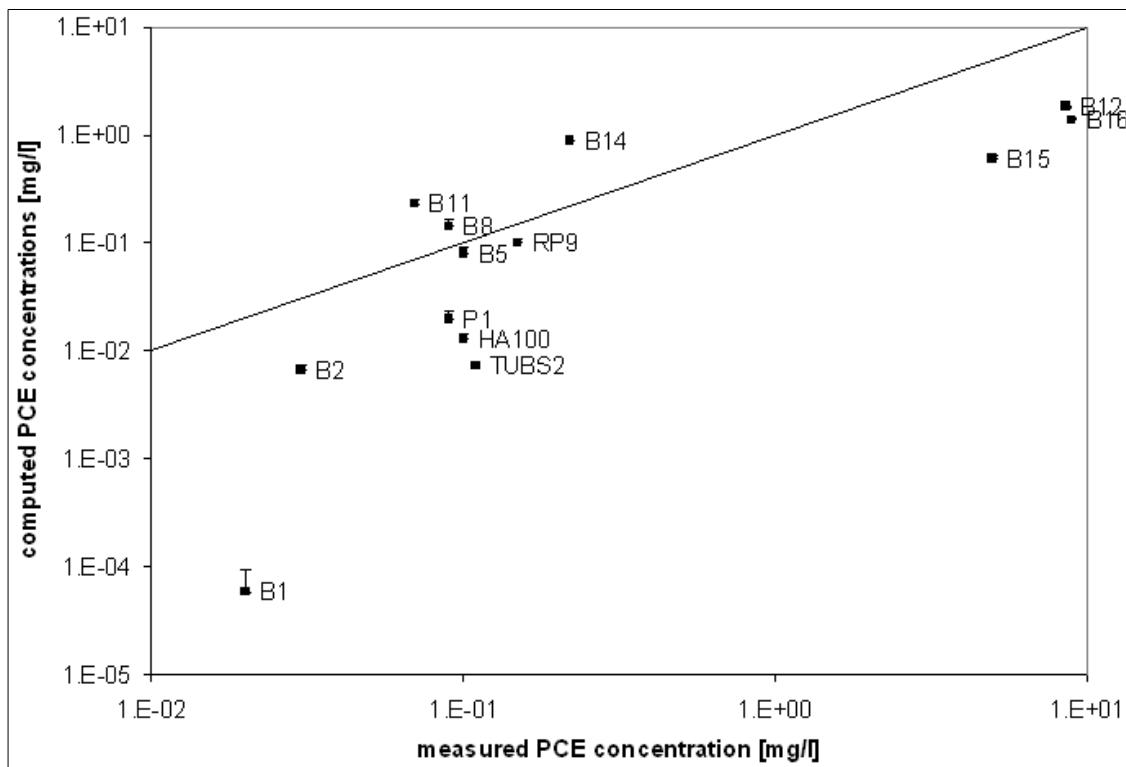


Figure 5-11 Comparison of the measured and computed PCE mass concentration of the homogeneous steady-state flow and transient transport model by variation of the diffusion coefficient. Source: Greis et al., 2011.

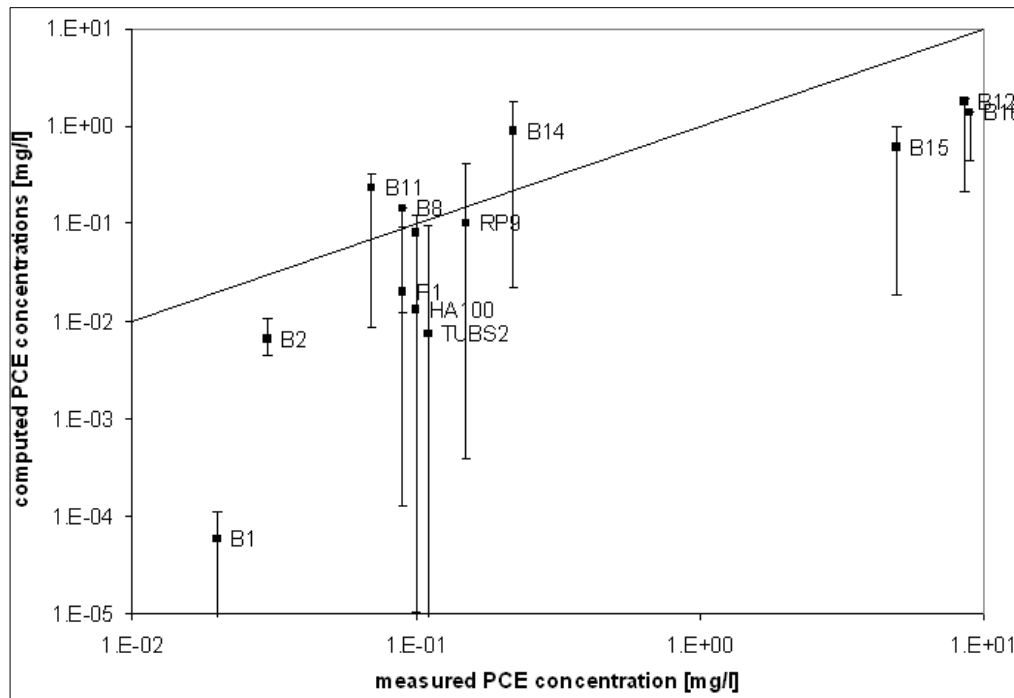


Figure 5-12 Comparison between measured and computed PCE mass concentration of the homogeneous steady-state flow and transient model by variation of hydraulic conductivity. Source: Greis et al., 2011.

Figure 5-13 shows the range of calculated concentration by Monte Carlo variation (cf. chapter 4.1.2) exemplified for TCE of the homogeneous steady-state flow and transient transport model. From this data it becomes obvious that the parameter distribution chosen for the MC approach leads to concentrations ranging over 2-3 orders of magnitude. For reasons of clarity and readability, a double-logarithmical illustration of the graph was selected.

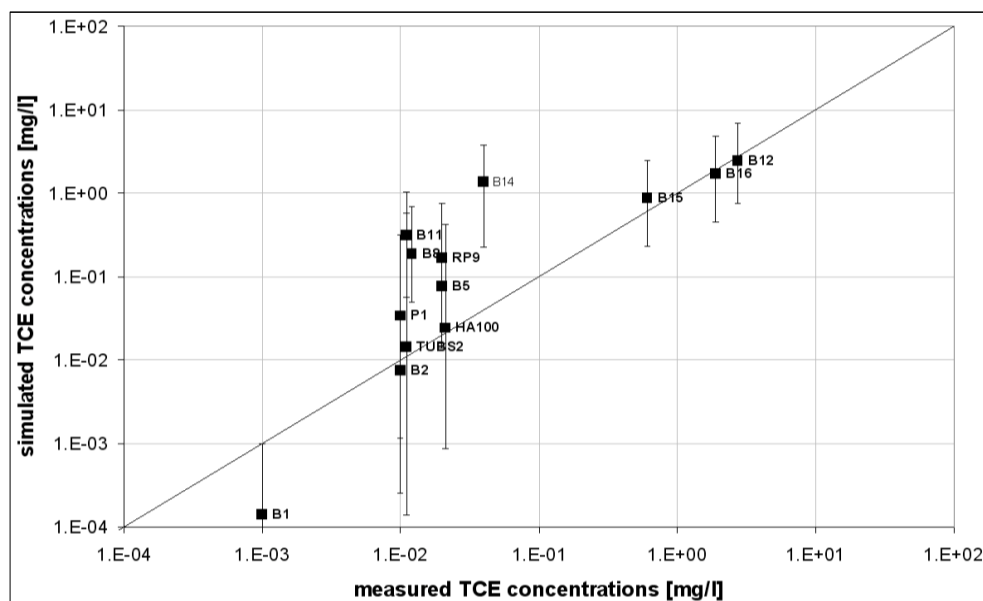


Figure 5-13 Correlation of measured and computed results for TCE mass concentration at several observation wells; error bars indicate range of TCE concentration in the Monte Carlo simulation. Source: Greis et al., 2011.

According to the graphical presented data, the selected parameter variation of the MC approach is assumed to be sufficient. Further results of the MC simulation were mainly evaluated by graphical analysis. For illustration purposes, the construction of probability isolines for different pollutant concentrations was analyzed (cf. chapter 5.3).

Figure 5-14 presents the graphical illustration and comparison of pollutant concentration threshold values of the homogeneous and heterogeneous steady-state flow and transient transport model with a simulation time of 70 years. Contaminant isolines of 1.0 mg/l^{-1} and 0.1 mg/l^{-1} are displayed for PCE, TCE, DCE and VC.

The comparing of both transport models shows that the pattern of the isolines are almost equal for 1.0 mg/l^{-1} but deviating in the extent. While, the length of the homogeneous plume amounts approximately 110 m and is concentrated closely to a building, the heterogeneous plume is spread with a length of 212 m over the whole site. Additional, the PCE and VC concentration of 1.0 mg/l^{-1} of the homogeneous aquifer is complete reduced by the degradation process. In case of the heterogeneous model, the only the PCE concentration is decomposed.

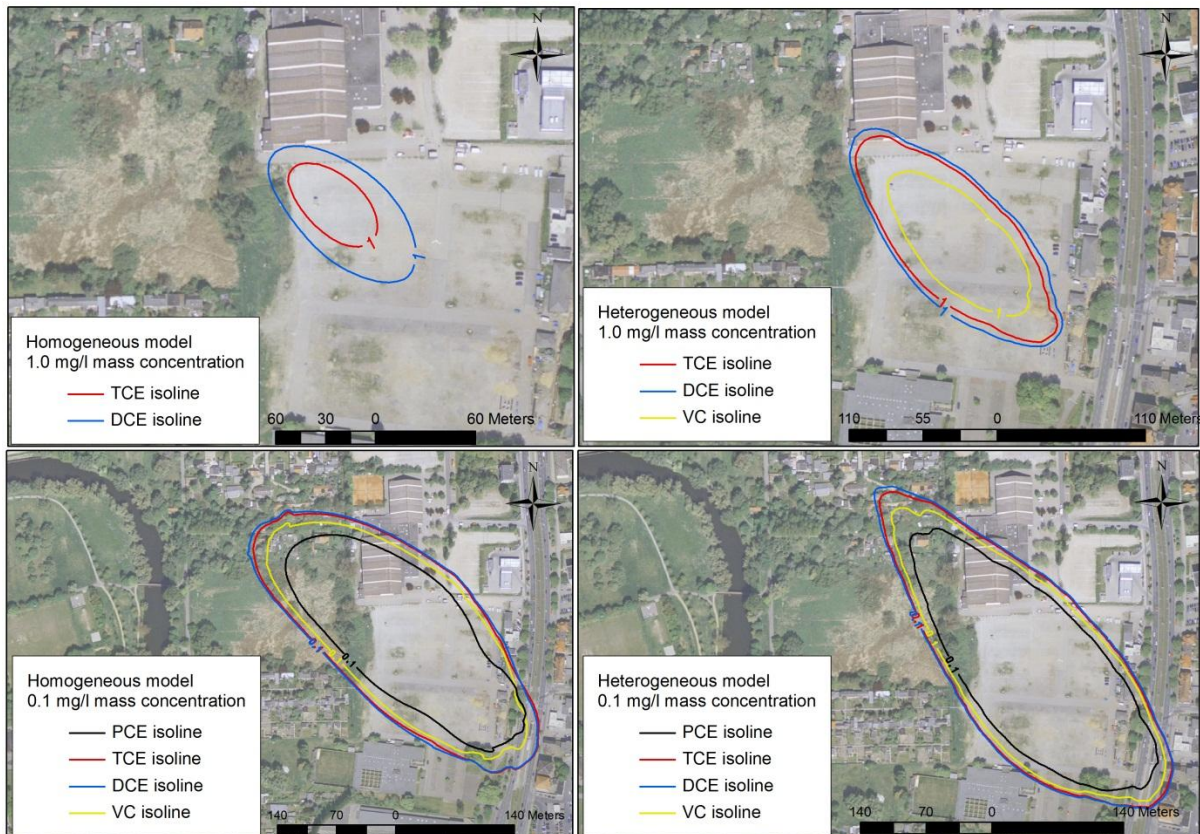


Figure 5-14 Computed contaminant isolines (1.0 mg/l^{-1} and 0.1 mg/l^{-1}) of the homogeneous and heterogeneous steady-state flow and transient transport model for PCE, TCE, DCE and VC.

The 0.1 mg/l^{-1} concentration isolines can be found in the homogeneous as well as in the heterogeneous model for PCE, TCE, DCE and VC. The lengths of the concentration isolines of

both subsurface models are nearly equal with 440 m but the pattern and the adjustment vary. While the isolines of the homogeneous model depict a more oval pattern and are directed to the bordering river, the heterogeneous isolines are directed northward to the bordering lake with a tapered front. Further analyzed concentration isolines of the different subsurface multi-species transport models for steady-state flow and transient transport condition can found in the appendix C.1.

Multi-Species transport results of the transient flow and transient transport conditions

The simulation results of the transient homogeneous and heterogeneous multi-species models are shown exemplarily for the 0.05 mg/l^{-1} mass concentration isoline because of its occurrence in each model scenario. Further concentration analysis can be found in the appendix C.2.

The model results are referred to transient flow and transport conditions, which are explained in chapter 4.5.1.2. A simulation time output for 50 a and 70 years were chosen for a data interpretation.

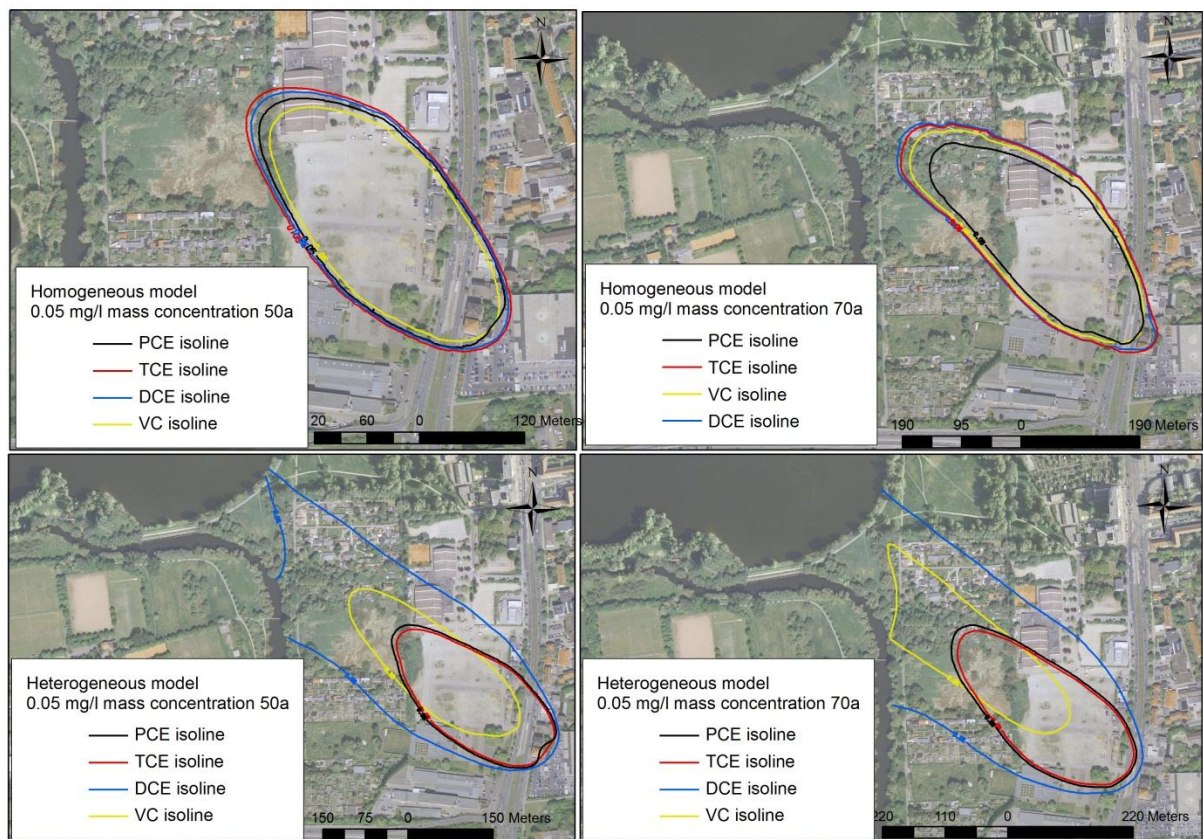


Figure 5-15 Computed 0.05 mg/l^{-1} concentration isolines of the transient homogeneous and heterogeneous multi-species transport model for 50 a and 70 a simulation time.

Figure 5-15 presents a comparison between the heterogeneous and homogeneous multi-species transport isolines by use of a threshold value of 0.05 mg/l^{-1} of PCE, TCE, DCE and VC. The simulation results are separated into 50 a and 70 a simulation time. The results show that

the spreading and the pattern of the isolines are different. Altogether, the homogeneous 0.05 mg l⁻¹ isolines of 50 a simulation time of the different pollutants are close located and pass the whole place in an oval form. On the opposite, the 0.05 mg l⁻¹ isolines of the heterogeneous model after 50 a simulation time are varied and DCE reaches the bordering river as well as the lake. Furthermore, the isolines are spatially staggered.

After a simulation time of 70 a, the 0.05 mg l⁻¹ concentration isolines of the homogeneous model are still close located except for PCE. The contamination plume is near the river system. The analysis of the heterogeneous isolines shows a further lateral spreading for DCE and VC, both concentrations reach the bordering ecosystems.

5.3 Model results of probability of concentration occurrences

This section introduces the result of the Monte Carlo simulation (cf. chapter 4.4.4). The generated spco isolines are used to estimate potential concentration accumulation areas, which results in a risk estimation for the bordering ecosystems. Moreover, these computed potential concentration occurrences can be applied during remedial activities. On the basis of the generated pollutant occurrences, an effective and a spatial target-oriented decontamination can be taken into account.

Overall, the 50%, 80% and 90% probability of exceedance of selected pollutant concentration of PCE, TCE, DCE and VC were analyzed and visualized. The following two sections exemplarily present the results of 80% probability of concentration occurrence, the 50% and 90% probabilities of isolines can be found in the appendix C3 and C.4.

5.3.1.1 Probability isolines of the homogeneous subsurface model

Figure 5-16 and figure 5-17 exemplify the results of 80% spco of selected threshold values of the homogeneous subsurface model after 50 a and 70 a simulation time.

The comparison between the computed probability isolines of PCE and TCE after 50 a shows that the isoline patterns are almost similar. The smallest part of the pollution is accompanied by 1.0 mg l⁻¹ with approx. 80 m for PCE and 30 m for TCE. In contrast, the majority of the contamination is composed by 0.001 mg l⁻¹ and 0.005 mg l⁻¹ of 130 m plume length of both species. In addition, 0.2 mg l⁻¹ and 0.5 mg l⁻¹ exhibits the same plume length of 250 m. It is noticeable that the 0.01 mg l⁻¹ mass concentration does not occur for TCE. The consideration of the 70 a simulation results shows that 0.2 mg l⁻¹ is not built for TCE. All patterns of the spco isolines exhibit a similar spread character. With 80% probability the 0.001 mg l⁻¹ PCE and TCE isolines have a plume extent of 515 m. Also, the 0.005 mg l⁻¹ and 0.01 mg l⁻¹ concentration occurrences of both species have an equal length of 430 m.

Based on the degradation process the DCE and VC concentration deviate from PCE and TCE for 50 a as well as for 70 a simulation results.

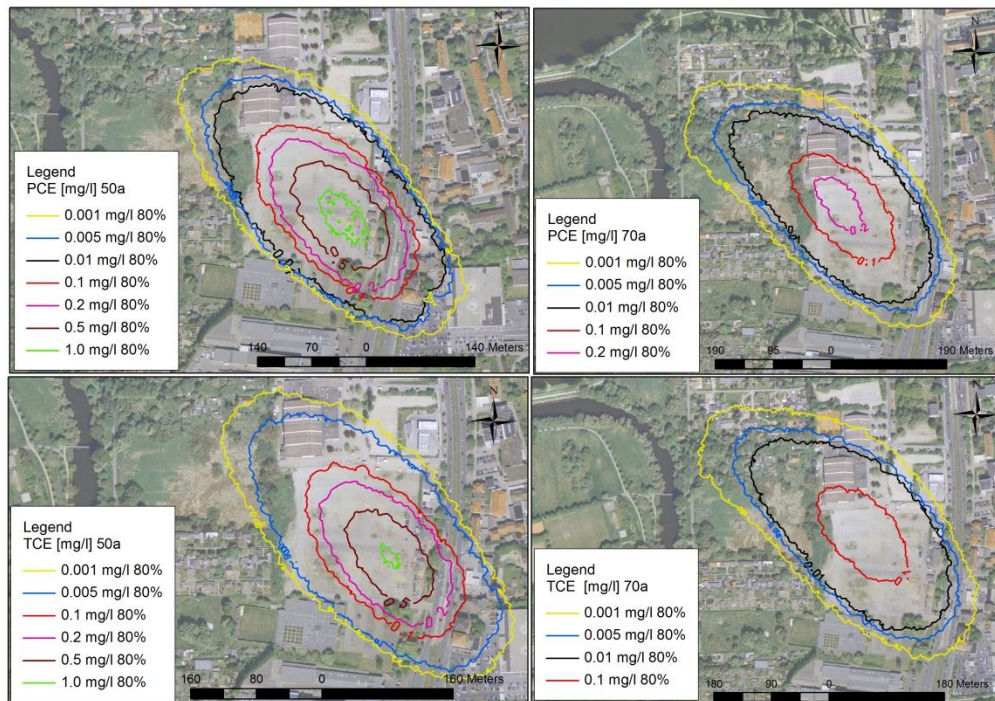


Figure 5-16 Computed 80% PCE and TCE probability of concentration isolines of the homogeneous subsurface model of 50 a and 70 a simulation time based on a Monte Carlo simulation.

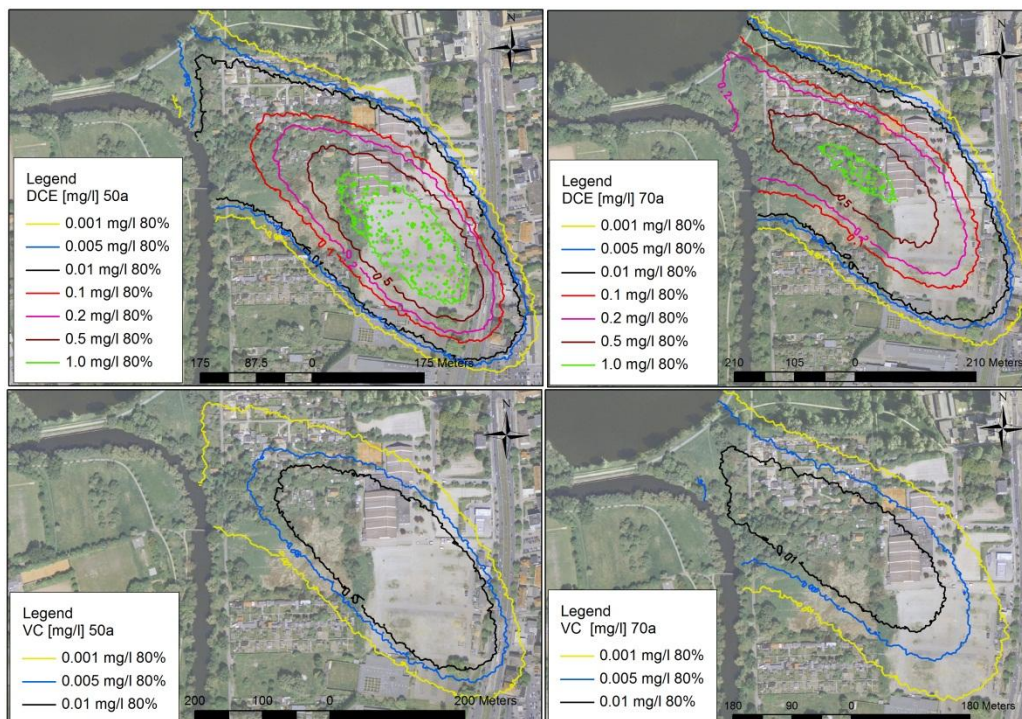


Figure 5-17 Computed 80% DCE and VC probability of concentration isolines of the homogeneous subsurface model of 50 a and 70 a simulation time based on a Monte Carlo simulation.

The computed results of DCE show that some concentrations (0.001 mg l^{-1} with 670 m, 0.005 mg l^{-1} with 720 m and 0.001 mg l^{-1} with 730 m) will reach the bordering ecosystems lake and river after 50 a simulation time with 80%. Also, the highest concentration of 1.0 mg l^{-1} has a respectable length of 265 m. 0.5 mg l^{-1} , 0.2 mg l^{-1} and 0.1 mg l^{-1} are extended to the whole place with a approx. length of 450 m. After 70 a simulation period, the contamination plume is moved forward and the plume length of 1.0 mg l^{-1} is reduced to 151 m and 0.5 mg l^{-1} to 350 m. The mass concentration of 0.01 mg l^{-1} and 0.02 mg l^{-1} reaches the lake and river with a plume length of 550 m. All remaining concentrations (0.001 mg l^{-1} , 0.001 mg l^{-1} and 0.01 mg l^{-1}) are spread forward and lateral. The most carcinogenic contaminant VC occurs after 50 a simulation run with a mass concentration of 0.05 mg l^{-1} and 0.001 mg l^{-1} and a plume length of 550 m with 80% probability. The picture shows that the river is impacted by the 0.001 mg l^{-1} probability isoline. Except for the 0.01 mg l^{-1} mass concentration, all remaining contaminants pass the bordering ecosystems with an extent of 600 m after 70 a simulation time.

5.3.1.2 Probability isolines of the heterogeneous subsurface model

Figure 5-18 and figure 5-19 exemplify the results of 80% spco of selected threshold values of the homogeneous subsurface model after 50 a and 70 a simulation time.

The comparison between the computed spco solines of PCE and TCE after 50 a shows that the isoline patterns are almost similar. The highest concentration value of 1.0 mg l^{-1} has an extent of 105 m for PCE and 65 m for TCE. The plume length of 0.1 mg l^{-1} , 0.2 mg l^{-1} and 0.5 mg l^{-1} are in the range of 170 – 260 m for both species. Lower concentration of both contaminants (0.001 mg l^{-1} , 0.005 mg l^{-1}) spread to a length of 340 – 430 m but they do not reach the bordering ecosystems. The consideration of the results after 70 a simulation time shows that the spco isolines of 1.0 mg l^{-1} and 0.5 mg l^{-1} not occur for PCE and TCE. The spreading patterns of all isolines exhibit the same characters. With 80% probability, the lower concentration of 0.005 mg l^{-1} and 0.001 mg l^{-1} of both masses resulted in a plume length between 430 – 490 m. Higher concentrations (0.2 mg l^{-1} , 0.1 mg l^{-1}) of the two pollutants reach a length of 39 – 220 m.

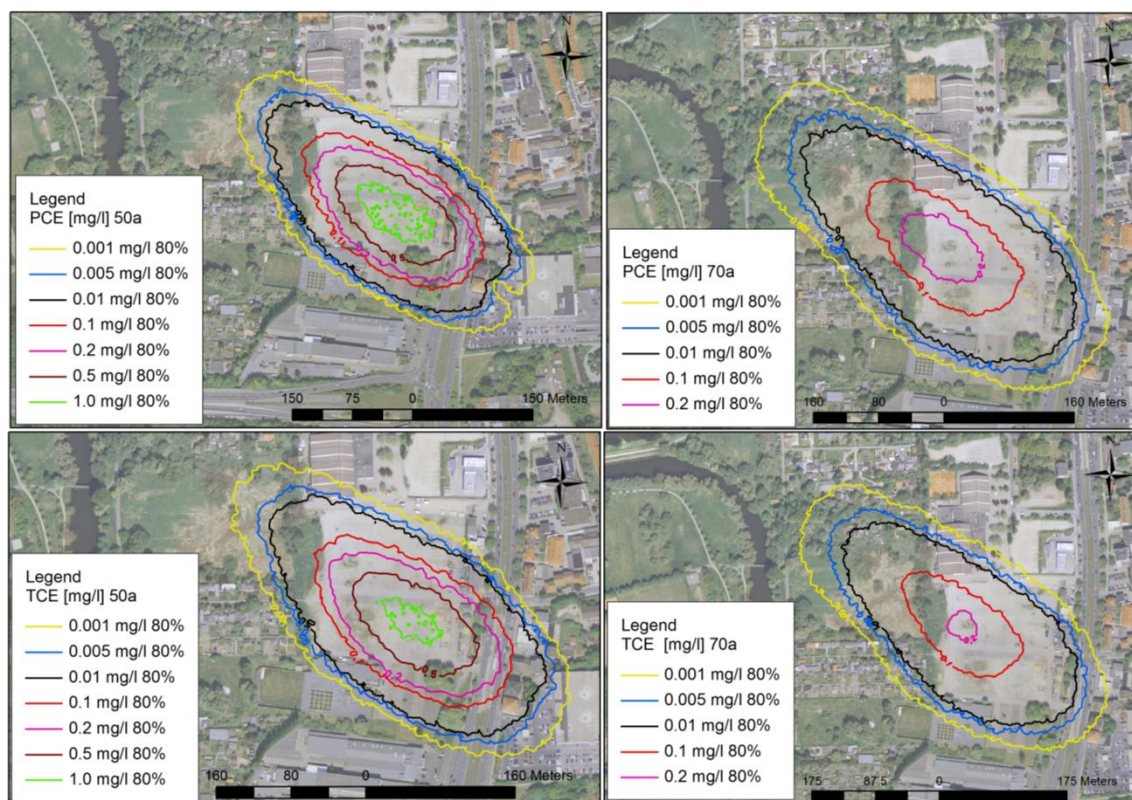


Figure 5-18 Computed 80% PCE and TCE probability of concentration isolines of the heterogeneous subsurface model of 50 a and 70 a simulation time based on a Monte Carlo simulation.

Based on the implemented degradation kinetic the DCE and VC 80% probability concentrations deviate from PCE and TCE for 50 a as well as for 70 a simulation results. Several of the selected threshold concentration values of DCE reach the adjacent ecosystems after 50 years e.g. 0.01 mg/l^{-1} of 500 m length, 0.005 mg/l^{-1} of 675 m extent and 0.001 mg/l^{-1} of 740 m spreading. Also, higher DCE concentration values (0.5 mg/l^{-1} , 0.2 mg/l^{-1}) exhibit a significant extent between 400 – 450 m. The highest spco isoline of 1.0 mg/l^{-1} resulted in a plume length of 319 m. After 70 years simulation time, the impact of the spreading is enhanced for all threshold values of DCE. Except for 1.0 mg/l^{-1} DCE concentration all remaining concentration have contact with the adjacent surface water bodies. Due to the fact that VC is the last species of the degradation chain, higher probability concentrations like 0.2 – 1.0 mg/l^{-1} are not developed after 50 years. The highest concentration is detected with 0.1 mg/l^{-1} and plume length of 206 m. Lower concentrations ($0.01 - 0.001 \text{ mg/l}^{-1}$) are computed with a spread length between 430 – 460 m. It is noticeable that 0.001 mg/l^{-1} concentration will reach the river with 80% probability. After 70 years simulation time, all computed 80% spco isolines of the most carcinogenic species VC ($0.01 - 0.001 \text{ mg/l}^{-1}$) will contact the river and lake.

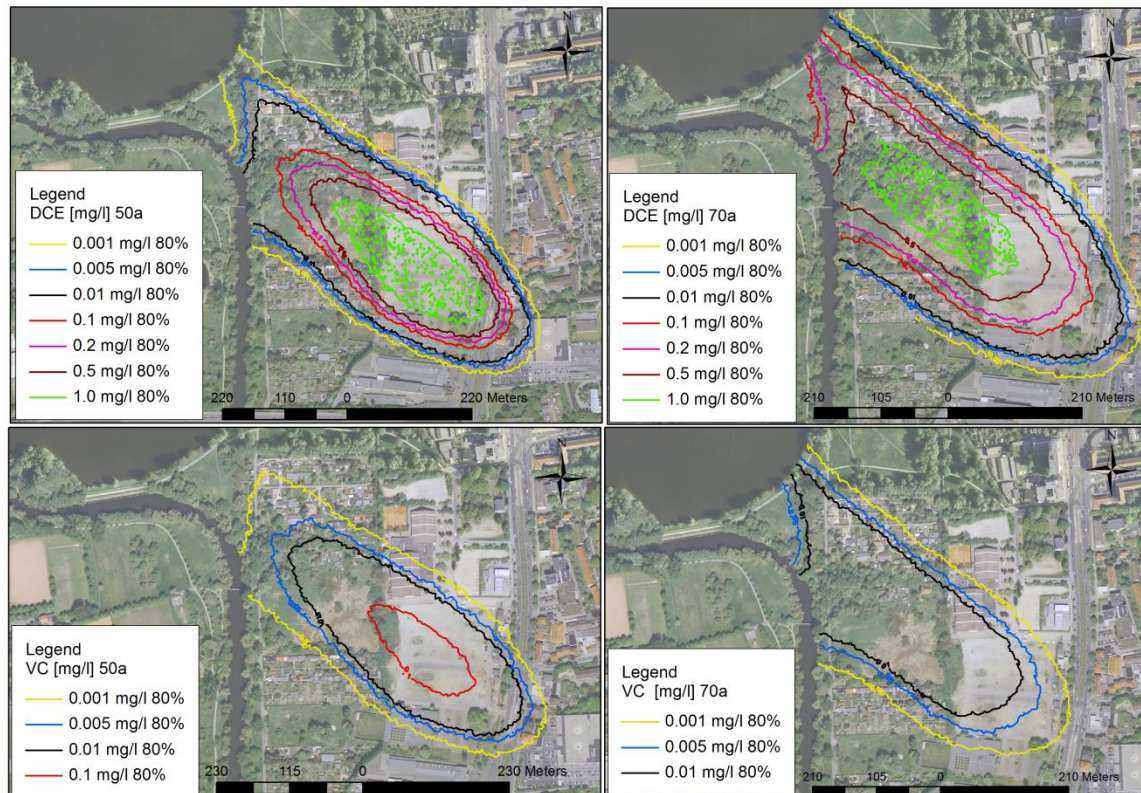


Figure 5-19 Computed 80% DCE and VC probability of concentration isolines of the heterogeneous subsurface model of 50 a and 70 a simulation time based on a Monte Carlo simulation.

5.4 Results of the groundwater – surface water interaction related to risk identification

5.4.1 Results of the timer period of the 12/11/2009–12/11/2010

This section presents the numerical results of the groundwater-surface water model coupling which is described in chapter 4.5.3. By use of the explained interface model, the groundwater simulation program *FEFLOW 6.0x* was coupled with the 1D surface water simulation program *MIKE11*. In this case study, a certain resistance of the river is observed (cf. chapter 4.1) and a 3rd type boundary (Cauchy-type) has to be used. Only this boundary type is supported by the interface to execute a model coupling regarding to the water exchange of the river system and groundwater system in order to identify a risk of contaminants passages from the groundwater into the bordering ecosystem river.

The presented figure 5-20 shows the results of the computed groundwater exfiltration and river band filtration (transfer m^3d^{-1}) of the homogeneous subsurface model and the measured groundwater level (red line) and river water level (blue line) of 350 days which equates to the simulation period from the 12/11/2009 – 12/11/2010. Negative transfer values conform to groundwater exfiltration into the river, so-called “effluent conditions” (cf. chapter 4.3.2). In most cases of the observation period, the groundwater recharges the bordering river. The highest

exfiltration values are gained during flood events and periods where the groundwater level is above the river water level. A maximum groundwater exfiltration value was calculated with $-2,056.32 \text{ m}^3\text{d}^{-1}$ (10/10/2010 = 321 d). At this day, a river water level of 66.84 m.a.s.l. and a groundwater level of 66.99 m.a.s.l. were measured. In summary, the exfiltration days of the investigation period achieve 51.0%. These effluent conditions are responsible for the mass concentration passage between the ecosystems.

Also, “influent conditions” (cf. chapter 4.3.2) can be observed for the investigation area represented by positive transfer values related to a river bank filtration. During short flood speaks, the hydraulic conditions return. The river recharges into the bordering aquifer. A maximum value of $345.6 \text{ m}^3\text{d}^{-1}$ was simulated (13/04/2010 = 141 d) during a short spring flood event during which the river water level was measured with 67.33 m.a.s.l. and the groundwater level with 67.23 m.a.s.l. All infiltration days from 12/11/2009 – 12/11/2010 result in 49.0%.

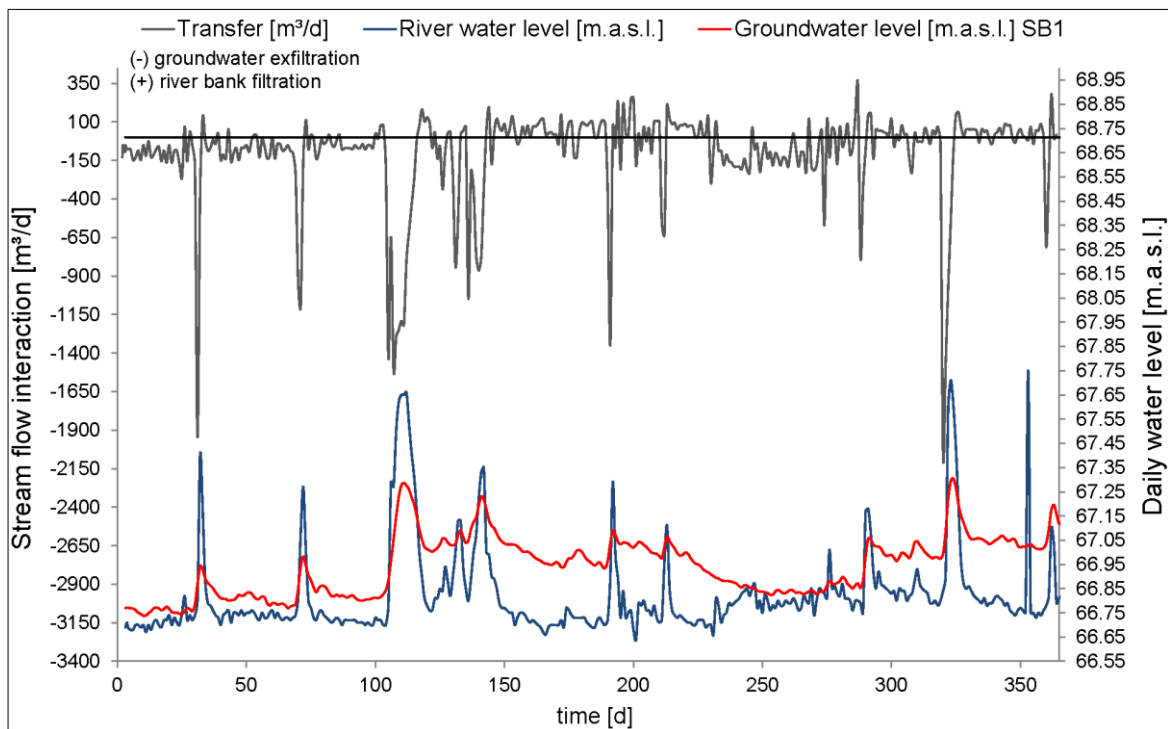


Figure 5-20 Result of the coupled groundwater-surface water model for the homogeneous transient model for 1 year simulation time (12/11/2009-12/11/2010). The figure displays the computed river water level (blue) and groundwater level (red) with the corresponding computed groundwater exfiltration and river bank filtration (transfer, black).

Figure 5-21 shows the results of the computed groundwater exfiltration and river band filtration (transfer m^3d^{-1}) of the heterogeneous subsurface model and the measured groundwater level (red line) and river water level (blue line) of 350 days, which equates to the simulation period from the 12/11/2009 – 12/11/2010. In this case, the groundwater exfiltration into the river system over the observed time period is predominated with 51.4% and leads to a

contamination transfer between both hydrosystems. The maximum exfiltration water volume is computed with $-673.9 \text{ m}^3\text{d}^{-1}$ for the 14/03/2010 (simulation day 111). On this day, a river water level of 67.65 m.a.s.l. and a groundwater level of 67.29 m.a.s.l. were measured. The recorded groundwater and river water hydrographs clearly demonstrate a spring flood event during the maximum exfiltration water volume.

The river bank filtration of the heterogeneous subsurface model occurs during the indicated time period 48.6%. The maximum transfer volume is simulated with $216.0 \text{ m}^3\text{d}^{-1}$ at the 08/06/2010 (simulation day 197) with a measured river water level of 66.73 m.a.s.l and a recorded groundwater level of 67.0 m.a.s.l. The analysis of the measured hydrographs illustrates that the groundwater level is above the river water level.

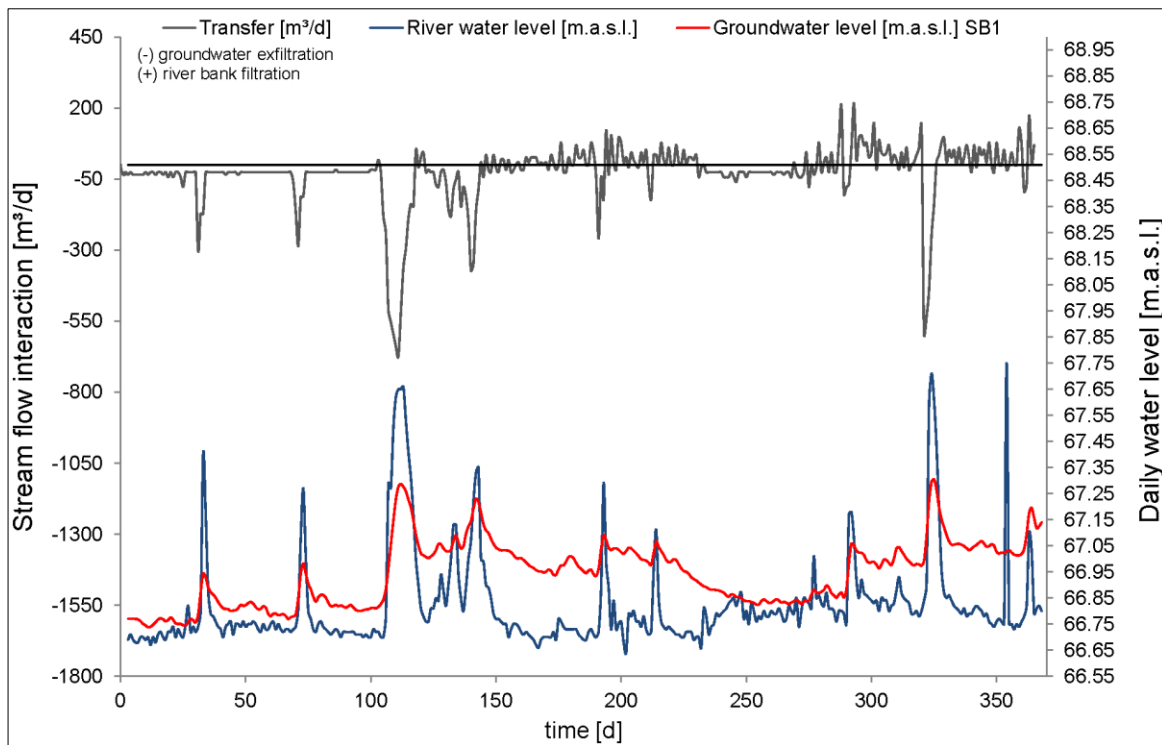


Figure 5-21 Result of the coupled groundwater-surface water model for the heterogeneous transient model for 1 year simulation time (12/11/2009-12/11/2010). The figure displays the computed river water level (blue) and groundwater level (red) with the corresponding computed groundwater exfiltration and river bank filtration (transfer, black).

Figure 5-22 documents a comparison between the homogeneous (green line) and heterogeneous (red line) subsurface models concerning to the computed transfer volumes from 12/11/2009 – 12/11/2010. The comparison of both time series reveals that the heterogeneous transfer interaction is reduced compared to the homogeneous time series.

The homogeneous model is responsive to flood events and intense rain more significant than the heterogeneous model.

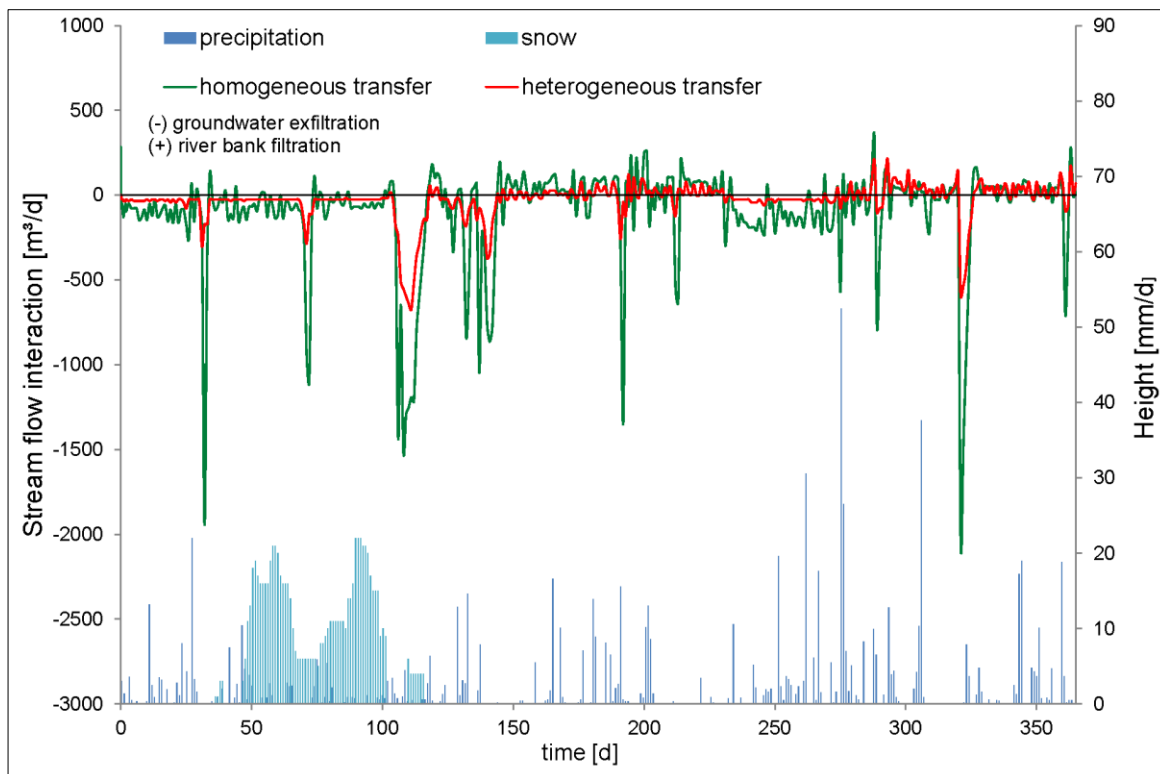


Figure 5-22 Comparison between the homogeneous and heterogeneous model concerning to the calculated transfer for 1 year simulation time.

The data analysis shows that both models react differently on extreme events. The maximum groundwater exfiltration volume of the homogeneous model is computed for the 10/10/2010 (simulation day 321), even if this date does not seem to be a hydrologically or hydraulically important event. In comparison, the maximum transfer rate from the subsurface into the river of the heterogeneous model is simulated for the 14/03/2010 (simulation day 111). This datum shows a significant hydrological event by snowmelt run-off. In consideration of the water exchange volume from the river into the aquifer, it is also a respectable difference of both models distinguishable. The maximum transfer volume of the homogeneous model is calculated for the 13/04/2010 (simulation day 141) where the river water level is above the groundwater level. The heterogeneous model exhibits the maximum calculated river bank filtration volume for the 08/06/2010 (simulation day 216) during which the river water level is higher than the aquifer water level which results into influent conditions. In summary, the homogeneous groundwater model leads to higher extent of effluent water conditions and therefor a higher risk of contaminant exchange must be assumed in comparison the the heterogeneous model.

5.4.2 Results of a 20-year flood (HQ₂₀)

Figure 5-23 shows the result of the computed stream flow interaction dependent on the measured river water level from the 12/11/2001 – 12/11/2002 of the homogeneous aquifer model. 100% of the exchange water volume belongs to river bank infiltration which equates to a positive transfer volume. In contrast, no the computed stream flow interaction is related to the groundwater exfiltration (negative transfer volume).

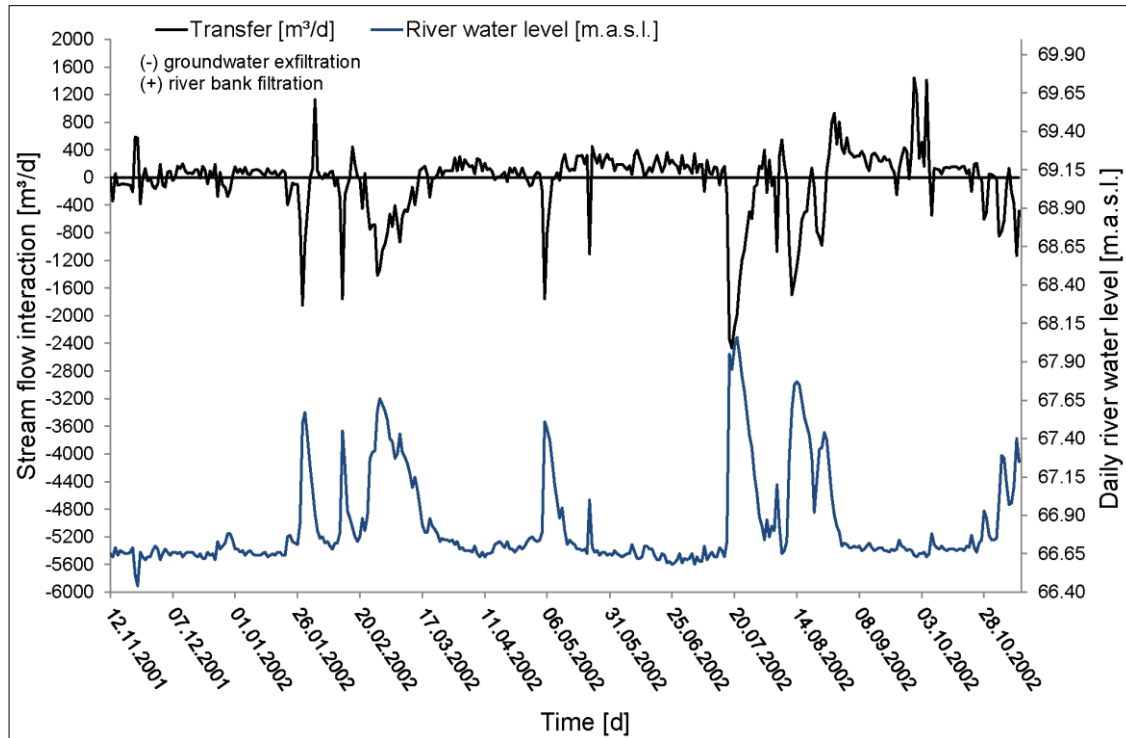


Figure 5-23 Comparison between computed transfer and measured daily river water level of the homogeneous groundwater model for the time period 12/11/2001–12/11/2002 which represents a HQ₂₀ conditions.

Figure 5-24 shows the results of the fluid flux mass balance of the boundary conditions of the homogeneous transient model of a 20-year flood conditions. The maximum water volume is represented by the Cauchy boundary condition with 1980.7 m³d⁻¹ river water inflow, which leads to 94.9% water volume inflow. The Neumann b. c. (ecosystem subsurface inflow) has a model inflow of 72.4 m³d⁻¹ (3.5% water volume). The minimum model inflow is constituted by the lake water (Dirichlet b. c.) with 33.1 m³d⁻¹, which equates to a model inflow of 1.6%. In contrast, the maximum water volume, which leaves the model is given by the lake water volume with -1205.8 m³d⁻¹ (98.4%).

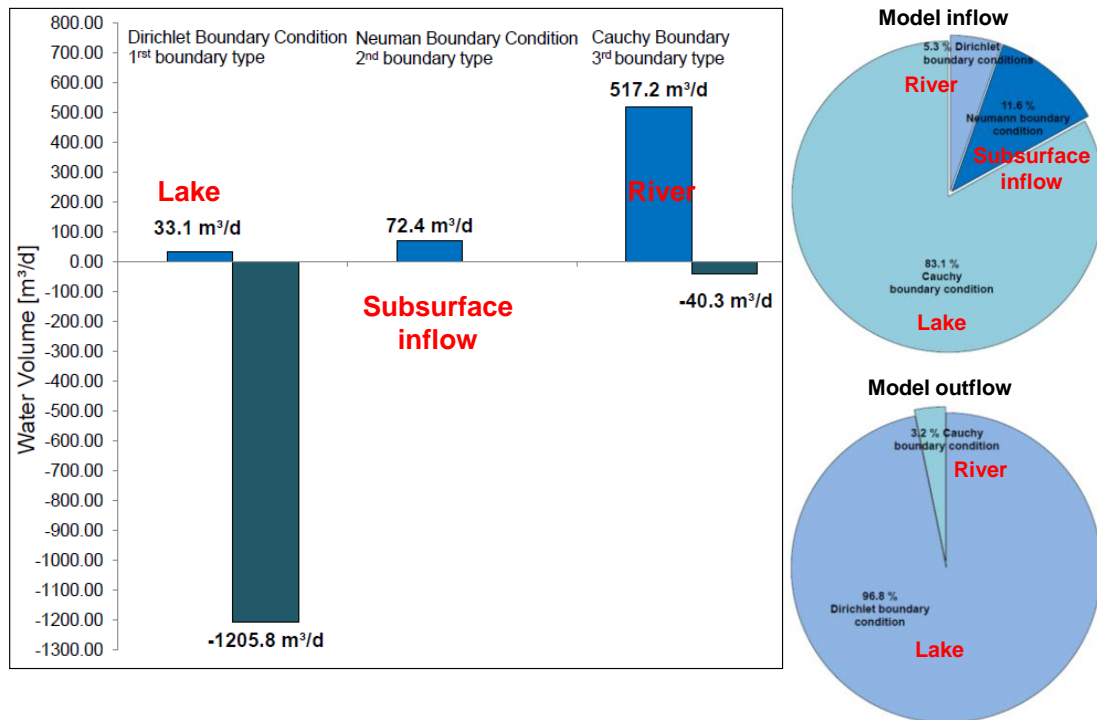


Figure 5-24 Fluid flux mass balance of the homogeneous transient groundwater flow model with percentage of the boundary conditions for inflow and outflow. Simulation of HQ₂₀ conditions.

Figure 5-25 shows the result of the computed stream flow interaction dependent on the measured river water level from the 12/11/2001 – 12/11/2002 of the heterogeneous aquifer model. 92.3% of the exchange water volume belongs to river bank infiltration which equates to a positive transfer volume. In contrast, 7.7% of the computed stream flow interaction is related to the groundwater exfiltration (negative transfer volume).

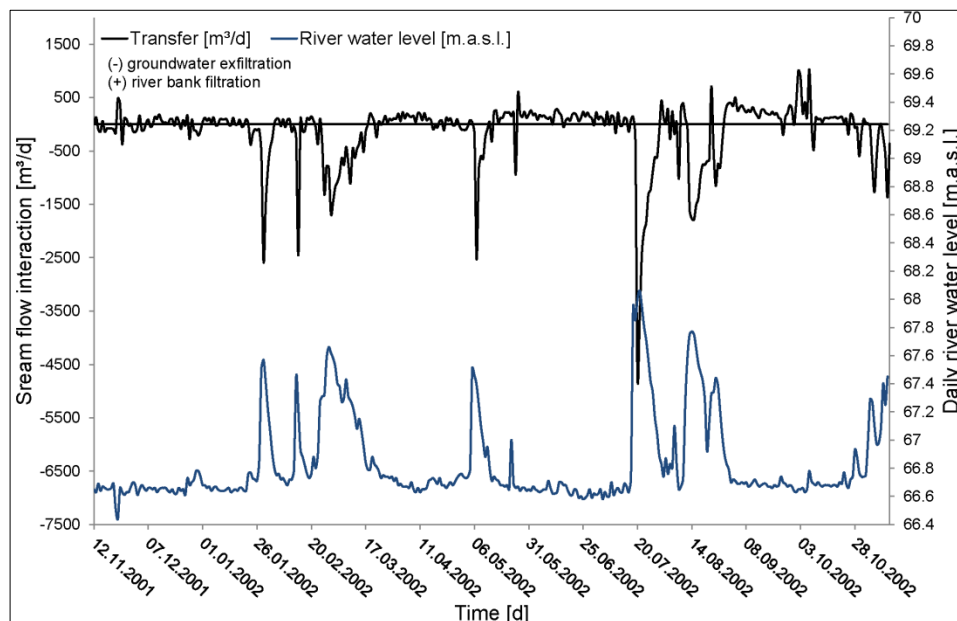


Figure 5-25 Comparison between computed transfer and measured daily river water level of the heterogeneous groundwater model for the time period 12/11/2001–12/11/2002 which represents a HQ₂₀ conditions.

Figure 5-26 shows the results of the fluid flux mass balance of the boundary conditions of the heterogeneous transient model of a HQ₂₀ conditions. The maximum water volume is represented by the Cauchy boundary condition with 410.5 m³d⁻¹ river water inflow, which leads to 62.9% water volume inflow. The Neumann b. c. (ecosystem subsurface inflow) has a model inflow of 241.4 m³d⁻¹ (37.0% water volume). The minimum model inflow is constituted by the lake water (Dirichlet b. c.) with 0.2 m³d⁻¹, which equates a model inflow of 0.04%. In contrast, the maximum water volume, which leaves the model is given by the lake water volume with -916.7 m³d⁻¹ (96.4%). The other water volume outflow is presented by the river water with an outflow of -34.2 m³d⁻¹ (3.6%).

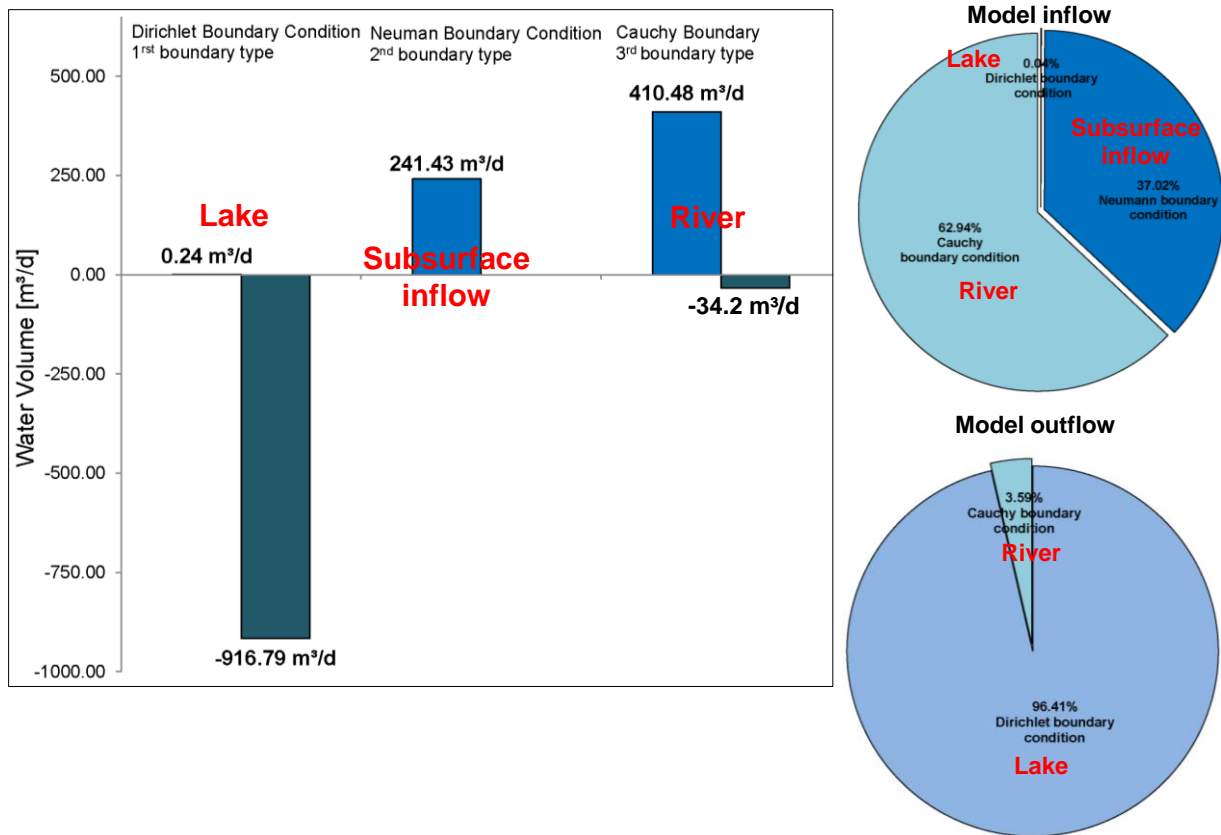


Figure 5-26 Fluid flux mass balance of the heterogeneous transient groundwater flow model with percentage of the boundary conditions for inflow and outflow. Simulation of HQ₂₀ conditions.

5.4.3 Results of a low flow (NQ)

Figure 5-27 shows the result of the computed stream flow interaction dependent on the measured river water level from the 12/11/2000 – 12/11/2001 of the homogeneous aquifer model. 12.8% of the exchange water volume belongs to river bank infiltration which equates to a positive transfer volume. In contrast, 87.2% of the computed stream flow interaction is related to the groundwater exfiltration (negative transfer volume).

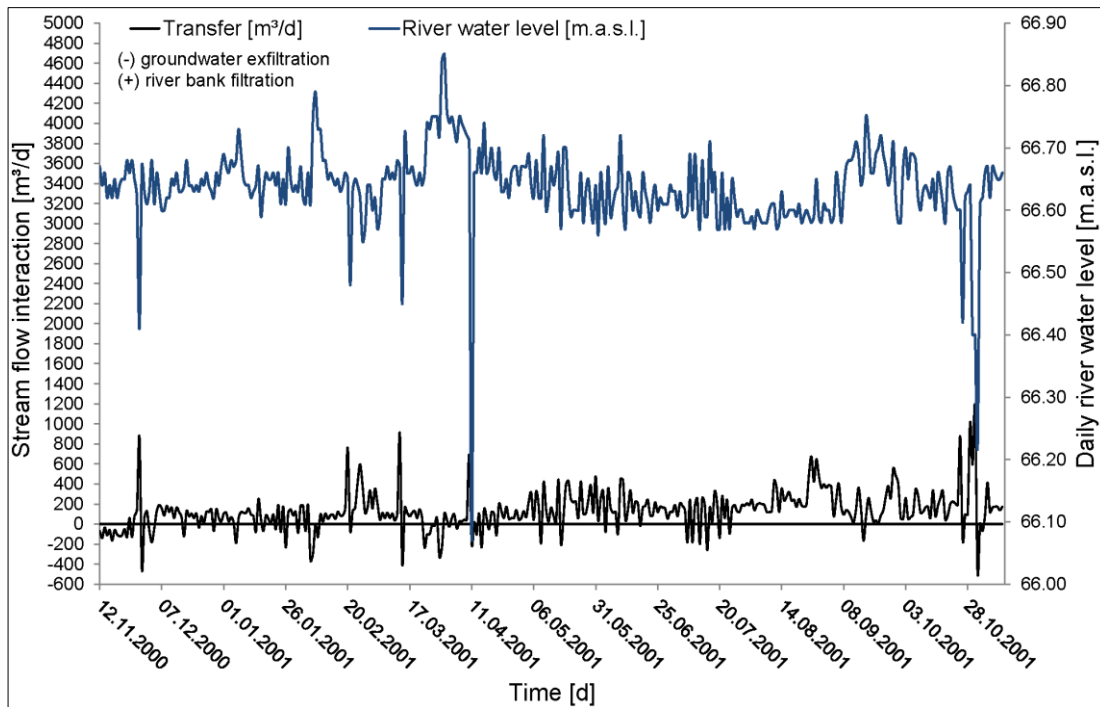


Figure 5-27 Comparison between computed transfer and measured daily river water level of the homogeneous groundwater model for the time period 12/11/2000–12/11/2001 which represents a NQ conditions.

Figure 5-28 shows the results of the fluid flux mass balance of the boundary conditions of the homogeneous transient model of a low flow condition. The maximum water volume is represented by the Neumann boundary condition with $268.8 \text{ m}^3\text{d}^{-1}$ subsurface inflow, which leads to 77.3% water volume inflow. The Dirichlet b. c. (ecosystem lake) has a model inflow of $50.8 \text{ m}^3\text{d}^{-1}$ (13.7% water volume). The minimum model inflow is constituted by the river water (Cauchy b. c.) with $33.5 \text{ m}^3\text{d}^{-1}$, which equates to a model inflow of 9.0%. In contrast, the maximum water volume, which leaves the model is given by the lake water volume with $-645.2 \text{ m}^3\text{d}^{-1}$ (73.8%). Only $-229.2 \text{ m}^3\text{d}^{-1}$ of the model outflow is resulted by the lake condition with 26.2%.

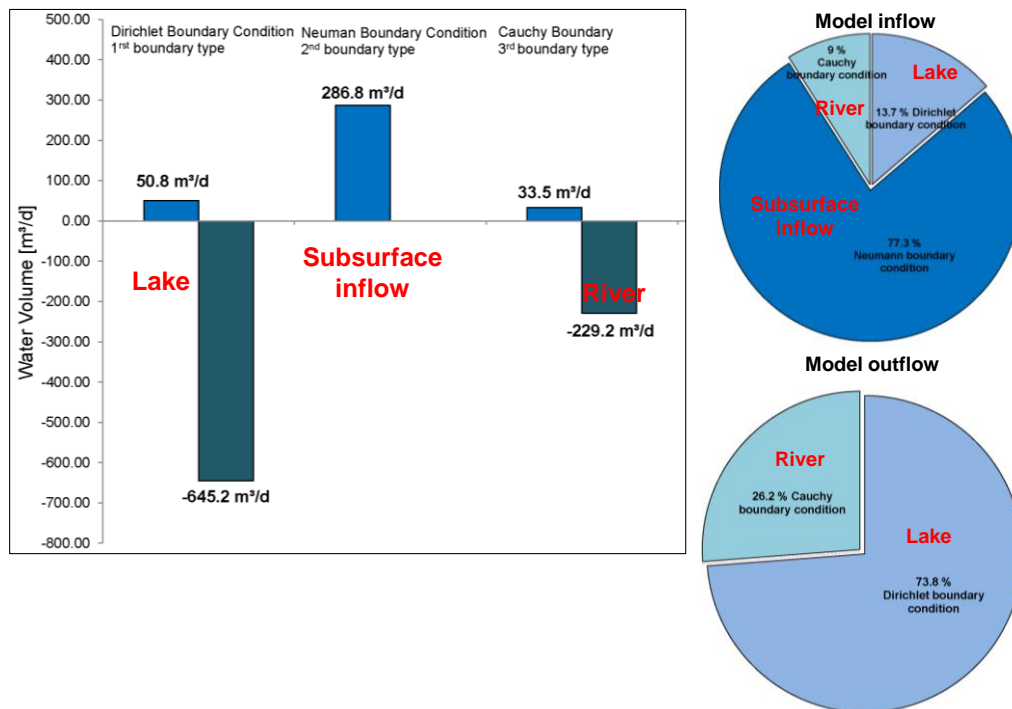


Figure 5-28 Fluid flux mass balance of the homogeneous transient groundwater flow model with percentage of the boundary conditions for inflow and outflow. Simulation of NQ conditions.

Figure 5-29 shows the result of the computed stream flow interaction dependent on the measured river water level from the 12/11/2000 – 12/11/2001 of the heterogeneous subsurface model. 16.6% of the exchange water volume belongs to river bank infiltration which equates to a positive transfer volume. In contrast, 83.4% of the computed stream flow interaction is related to the groundwater exfiltration (negative transfer volume).

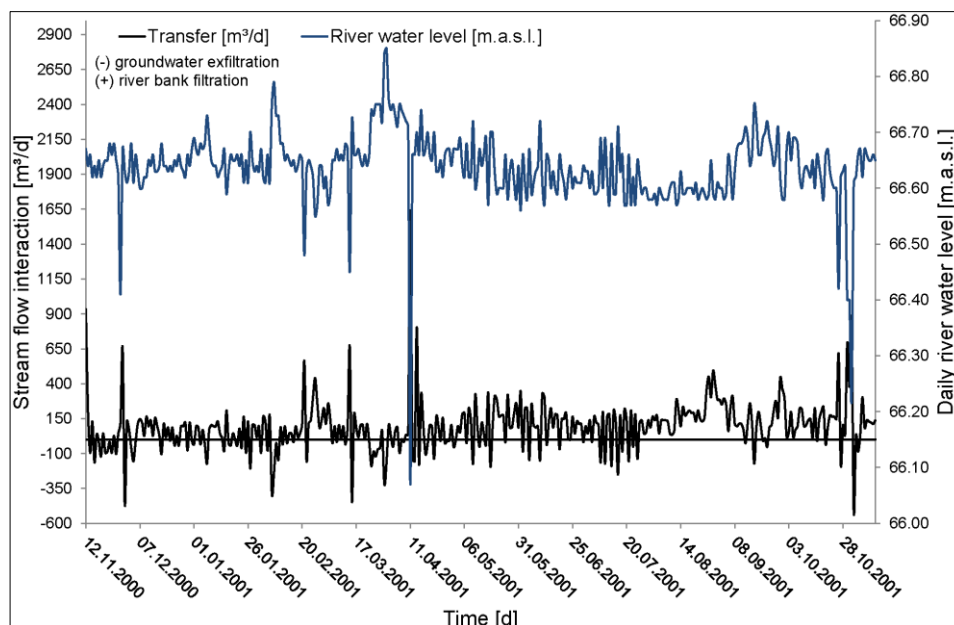


Figure 5-29 Comparison between computed transfer and measured daily river water level of the heterogeneous groundwater model for the time period 12/11/2000–12/11/2001 which represents a NQ conditions.

Figure 5-30 shows the results of the fluid flux mass balance of the boundary conditions of the heterogeneous transient model of a low flow condition. The maximum water volume is represented by the Neumann boundary condition with $238.1 \text{ m}^3\text{d}^{-1}$ subsurface inflow, which leads to 69.3% water volume inflow. The Dirichlet b. c. (ecosystem lake) has a model inflow of $70.7 \text{ m}^3\text{d}^{-1}$ (20.6% water volume). The minimum model inflow is constituted by the river water (Cauchy b. c.) with $37.7 \text{ m}^3\text{d}^{-1}$, which equates to a model inflow of 10.1%. In contrast, the maximum water volume, which leaves the model, is given by the lake water volume with $-575.3 \text{ m}^3\text{d}^{-1}$ (76.7%). Only $-174.5 \text{ m}^3\text{d}^{-1}$ of the model outflow is resulted by the river condition with 23.3%.

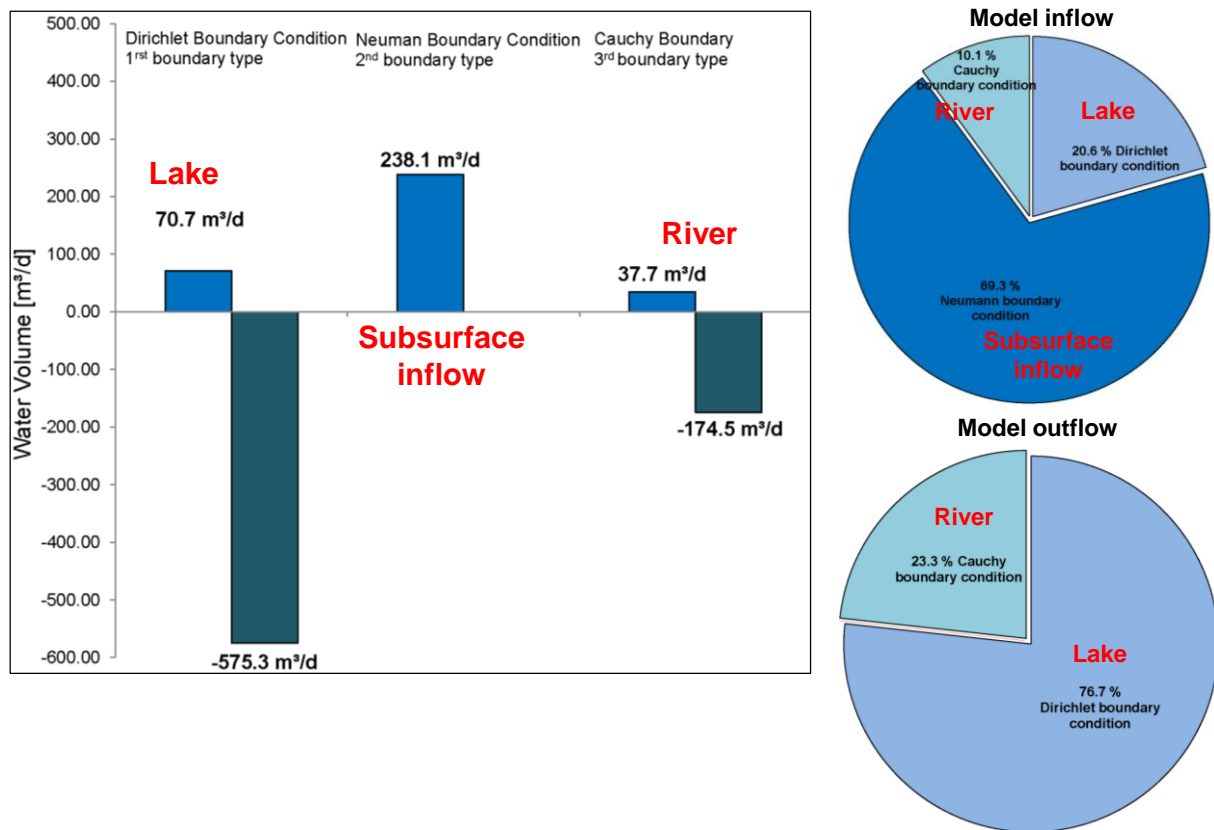


Figure 5-30 Fluid flux mass balance of the heterogeneous transient groundwater flow model with percentage of the boundary conditions for inflow and outflow. Simulation of NQ conditions.

Figure 5-31 represents a summary of the model scenario results related to a risk identification for the bordering ecosystems of the homogeneous and heterogeneous coupled model for a low flow condition, normal flow condition and 20-year flood event. The risk identification is based on the computation of groundwater exfiltration (effluent condition) and river bank filtration (influent conditions). Effluent conditions cause a stream of contaminated groundwater into the adjacent river, which leads into an intensive risk of a potential ecosystem pollution. On the contrary, the influent conditions e.g. during a flood event enable a risk reducing. In this case, the river water flows into the groundwater system.

	Dry year (low flow condition)		Normal year (normal flow condition)		Wet year (20-year flood event)	
	homogen	heterogen	homogen	heterogen	homogen	heterogen
Groundwater exfiltration (m³/d)	- 229.2	- 174.5	- 182.4	- 127.7	- 40.3	- 34.1
River bank filtration (m³/d)	33.5	37.7	190.7	134.9	517.2	410.5

effluent conditions

↓

intensive risk

effluent conditions

↓

normal risk

influent conditions

↓

low risk

Figure 5-31 Results of the 3 different hydrological dynamic scenarios of the coupled homogeneous and heterogeneous groundwater-surface water models including an risk interpretation for the bordering ecosystems based on effluent and influent conditions.

6 Discussion and Outlook

Local-specific knowledge and results relative to the case study

The numerical pollutant dispersion calculation is based on the generation of hydro-geological parameter fields, measurements of groundwater levels and mass concentration in selected observation wells. One goal was the description and simulation of the hydraulic conditions and the species-specific reaction kinetics in the subsurface to obtain a calibrated multi-species transport model. This prognosis model is used for a risk identification with the aim of a prognosis of future pollutant dispersion in the form of spatial probability of pollutant concentration occurrences (spco) in an urban aquifer. The spco of pollutant offers a statement about the contaminant spread in an urban aquifer and the transfer in adjacent ecosystems like surface water bodies. According to Nasiri et al. (2007), these results can be understood as a compatibility analysis which targets the interaction between remediation technologies and specific site characteristics.

The system-related processes could only be solved by an application of a special data preprocessing. The first step was related to the generation of geo-stochastic parameter fields and subsequently a hydrograph analysis to comprehend the hydrological processes. The focus was concentrated on the answer to the question which impulses have an effect on the hydrogeological system and its dynamic behavior. It was not the task to develop new chemical reaction kinetics but the reproduction of groundwater-hydrological influences and therewith the impact quantification on the contamination. Carrier of the information processing was a numerical groundwater code with a flexible mesh generator in z-direction. The numerical groundwater flow and transport calculation were simulated with the program *FEFLOW 6.0x* based on a Finite Element method (cf. chapter 4.4). Especially, the treatment of the free surface by use of the BASD technique (cf. chapter 4.4.1) was essential to solve the complex transient flow and transport conditions and the species mobilization at the boundary between saturated and unsaturated zone. Moreover, the open programming interface offered the possibility to execute a user code at specific stages of the modeling process. This was applied in the PhD research for the Monte Carlo simulation performances (cf. chapter 4.4.4) and the coupling of the groundwater model with the 1D surface water model *MIKE11* (cf. chapter 4.5.3.2). A capable algebraic multigrid solver (cf. chapter 4.4.2) plays an important rule for simulating complex time-dependent multi-species transport problems. The selected software package provides this fast iterative and direct solver. Furthermore, the application of a fully automatic time-stepping procedure using predictor-corrector scheme (cf. chapter 4.4.3) induced a simulation time saving (Diersch, 1988).

Corresponding to the precise number and design of the Finite Elements an accurate ascertainment of the geological structure was required. The reconstruction of the hydro-geological subsurface has been divided into two different techniques. A conventional technique is based on the interpretation of drilling profiles (cf. chapter 4.2.1) and a geo-stochastic indicator simulation (cf. chapter 4.2.2). Based on the complexity of the geological subsurface structure a Direct push method (cf. chapter 4.2.3) was used to verify the generated and interpreted Finite Element model layers and input data. The geo-stochastic technique was adopted to quantify and qualify uncertainties of the aquifer reconstruction according to Dagan (1997). He subjected the hydrogeological variables to a stochastic underground modeling to identify parameter uncertainties and spatial variabilities of the model input data. The uncertainties are manifested in the conceptual model and lead to several scenarios. The validity and solution of a numerical model must be seen with regard to the parameter uncertainties, which are integrated in the structural model. The use of the SIS in this research provides the opportunity to quantify the uncertainty of the reconstructed structure model. Gorelick (1997) successfully operated with a geo-stochastic approach to generate multiple realizations of hydraulic conductivity fields of an aquifer to consider a contaminant capture design problem involving a vinyl chloride plume.

In the following, the subsurface models are classified in a homogeneous (conventional reconstruction) and heterogeneous subsurface (geo-stochastic approach).

The detailed classification of the subsurface structures distributes the physical basis for the spco isolines, whose generation was basically possible through the MCs. Due to the long computing time of each multi-species transport model (13 days for 70 a simulation time), the MC simulations were carried out in cooperation with the University of Siegen, which enabled a cluster computing (cf. chapter 4.4.4).

On a local scale, the uncertainties related to the aquifer reconstruction and estimation of probability of mass concentration occurrences were rigorously evaluated. The described method was successfully applied to a chlorinated ethenes contaminated regional site with all its impacts on the environmental estate, which is located in a city center. The chlorinated ethenes like PCE are common organic contaminants in many urban polluted sites. PCE is subjected to degradation processes in the aquifer system leading to a spectrum of conversion products. According to McKnight et al. (2010), the volatile organic compounds are considered to have the greatest potential to discharge to surface water. On the basis on an ecological engineering framework, the risk assessment is targeted on the identification of the impact of dynamic boundaries on other ecosystems and investigations dealing with the groundwater

quality. A part of the available groundwater is used as drinking water. This fact also underlines the imperative of a risk characterization by of the point source.

The established numerical transient multi-species transport model reflects the condition on the investigation site in an appropriate manner. The transport of pollutants is directed northwestwards and the contamination plume exhibits a pollutant degradation caused by the implemented chemical reaction kinetics (cf. chapter 4.5.2.3). A quantitative pollutant decrease is identifiable (cf. figure 5-15). A transfer from the groundwater into the river of DCE and VC is anticipated after 50 and 70 years simulation time in the range of 10^{-1} – 10^{-2} mg l⁻¹ for the homogeneous and heterogeneous subsurface model. It must be noted that the reproduction of the colmation layer, which is responsible for the interaction of both ecosystems, was carried out only for its hydraulic properties. By use of the 3rd type boundary condition (Cauchy b. c., cf. figure 4-7) the ecosystem coupling was executed. The consideration of the reaction chemistry and environment inside the colmation layer was neglected.

The application of the 3D geo-stochastic indicator simulation has enabled the generation of hydraulic parameter fields, which shows a potential distribution of the hydro-geological aquifer properties. The histogram of the indicator-coded input data presents that the substrate fraction of sand (indicator 2 and 3) has the major portion of the aquifer composition (cf. figure B-6). Clay and silt are the second commonly occurring substrates, stones and gravels constitute the indicator class with the minor portion. The comparison between the distribution of the indicator-coded input data and the geo-stochastic generated parameter fields shows that the conditional SIS reflects the distribution of the input data. Compared to conventional techniques, the indicator simulation provides the opportunity of an uncertainty analysis before the simulation starts. However, this requires a high number of parameter field realizations. According to Wingle et al. (1997), a number of 100 realizations is sufficient for a first uncertainty estimation. This requirement was complied. The results of the uncertainty analysis represents that the highest probabilities of indicator occurrences are located in the near range of the groundwater observation wells (cf. figure B-8). This results because of the use of a conditional simulation, which implies that the hard input data of the drilling profiles are reflected as a part of the simulation results. Consequently, the same indicator is repeatedly assigned near the groundwater well, which resulted in a high probability of occurrence. According to figure B-8, the highest probability indicator occurrences are located between the contamination source and the adjacent ecosystems, which correspond to the principal direction of the groundwater flow. However, probability occurrences are placed in the deeper aquifer areas. In summary, the generated parameter fields of the Sequential Indicator Simulation exhibit high probability occurrences for the area in which input data are available. The considerations of aquifer inhomogeneities are important for a later analysis of spatial

pollutant probability occurrences. Consequently, an adequate prognosis certainty is ensured. For areas with no observation wells available, e.g. in the northeast, this is not guaranteed. An increase of informational value in these areas can only be achieved through an additional installation of groundwater wells. The computed multi-species transport results of both subsurface approaches must be adjusted with the generated uncertainty prognosis of the aquifer reconstruction in all cases. An uncertainty analysis regarding aquifer reconstruction cannot be operated.

The groundwater flow results of both subsurface models for steady-state conditions show a satisfying calibration result (cf. figure 5-1, figure 5-2, figure 5-4). During the calibration, the transfer rate of the 3rd boundary condition and the groundwater recharge were identified as the components with the major influence on the model quality and water balance.

The mass transport results (cf. chapter 5.2) of steady-state flow and transient conditions exhibit that the chosen transport parameter set reflects an appropriate data set, which allows the best fit regarding simulated and measured concentration. Moreover, the contamination degradation and plume spread indicates that most of the simulated data are confirmed with measured data (cf. figure 5-14, figure 5-15). The comparison between measured and computed PCE, TCE, DCE and VC exhibits good agreements (cf. figure 5-10). The deviation of the data points from the regression line is adequate presumed in terms of accuracy. The model results after 50 years of simulation time were considered as current contamination distribution and used for validation purposes. The determined transport data were adopted for the transient multi-species transport model and for the following steps of the parameter variation by use of MC simulations.

The transient groundwater flow results show that both subsurface models reproduce the groundwater hydrograph with its dynamic (cf. figure 5-6, figure 5-8). Therefore, the groundwater model, which built the basis for the transport modeling, provides a true dynamic of the field conditions and data. However, the model results also show that the high increase of the measured data is not well reproduced by the computed hydraulic heads. One reason could be the small selected influence of the gaining stream. Due to the subsurface groundwater inflow through the 2nd boundary condition at the southeastern border of the model domain a counter-current flow is developed to the infiltrating gaining stream. Both multi-species transport models resulted in an adequate spreading of the pollutant PCE and its resulting degradation products TCE, DCE and VC. Depicted in figure 5-15 are the 0.05 mg/l⁻¹ isolines of all existing species of 50 and 70 years simulation time. As shown in this picture, after 50 years the tailing of lower substituted chlorethenes (DCE, VC) tends to be more distinctive than that of higher substituted ethenes (PCE, TCE). In particular, the VC isoline has

a larger distance in comparison to the TCE isoline. This effect can be interpreted by a higher dependency from variation in reaction rates. The occurrence of PCE is only dependent on its own degradation rate, while VC concentration is also dependent on the varying degradation rates of the previous compounds. In consequence, parameter dependency and thus uncertainty is higher for substances at the end of the reaction chain. Additional results for a 70 a simulation time are also shown. Comparison of both simulation periods show, that contamination spectrum changes more towards lower substituted chlorinated ethenes. Respective areas of DCE and VC pollutants are getting more distinctive in the simulation. On the other hand, PCE and TCE affected areas are declining. However, increasing concentrations of pollutants are expected to be washed out into the bordering ecosystems.

The results of the MCs (cf. chapter 5.3) are founded on the basis of the calibrated transient multi-species transport models i.e. the significance of the MC results in this context must be evaluated with the achieved calibration results. The generated spco are not only beheld as isolines but also with its probabilities. Moreover, the probability isolines must be considered in connection with the information content, which was integrated into the Finite Element groundwater model.

The analysis of the spco was performed for 50% (cf. figure C-5 and figure C-6), 80% (cf. figure 5-16 and figure 5-17) and 90% (figure C-7 and figure C-8) probability of exceedance of 0.001 mg l^{-1} , 0.005 mg l^{-1} , 0.01 mg l^{-1} , 0.1 mg l^{-1} , 0.2 mg l^{-1} , 0.5 mg l^{-1} and 1.0 mg l^{-1} concentration of respective compounds. With increasing dynamic, the contamination spreads into the bordering ecosystems. Particularly, lower DCE and VC concentrations ($0.001\text{--}0.01 \text{ mg l}^{-1}$) can be detected with 80% of probability after 50 years simulation time in the river system and lake (cf. figure 5-17). After 70 years almost every selected pollutant concentration thresholds of DCE and VC reach the adjacent ecosystems with 80%. Particularly important is the analysis of the 90% probability isolines (cf. figure C-7 and figure C-8). Based on the high probability calculation discrete contamination zones are identified. Feasible effective remediation activities can now be put into practice. Similar to the 80% probability occurrences the 90% probability isolines show for lower DCE and VC concentration ranges a beginning of contamination passage into the ecosystems after 50 a simulation period. Especially $0.001\text{--}0.01 \text{ mg l}^{-1}$ mass concentration would be detectable in the lake and river after 50 a. After 70 years, the mass concentration of both pollutant increases to 0.1 mg l^{-1} for DCE.

In addition to the probability occurrences, an external coupling between the aquifer and river system was performed (cf. chapter 4.5.3). Under transient conditions, different scenarios were calculated (cf. chapter 5.4) to estimate the water exchange regarding to a potential

contamination exchange. The analysis shows that the normal (2009 – 2010) and drought (2000 – 2001) hydrological years contain a high potential risk for pollutant exchange processes. Figure 5-20 and figure 5-21 display the groundwater exfiltration and river bank filtration days of a normal hydrological year. It is noticeable that 51% of the days belong to effluent conditions, which causes a groundwater stream (contaminated) into the river. During drought seasons like 2000–2001 (figure 5-27 and figure 5-29), the effluent portion is increased to 87% and therefore the risk of river water contamination, as well. In contrast, higher river and groundwater level during a HQ_{20} (2001 – 2002) exhibit an effluent condition portion of 0 - 7.7% (cf. figure 5-23, figure 5-25). Consequently, the risk of a pollutant transfer is minimized. Subsequently, it can be said that one risk-reducing aspect is the river and groundwater level increase (cf. figure 5-31). Representative for all contaminations a risk assessment regarding the occurrence of concentration is performed by using the example of DCE. The evaluation of the spatial probability of pollutant occurrences resulted that 0.01 mg l^{-1} DCE is detectable to 80.0% in the river after 50 a under normal average hydrological conditions (2009 – 2010) with 51% groundwater exfiltration. In case of drought hydrological periods (2000 – 2001), the effluent conditions are intensified to 87%, which leads to an increase of the contaminant, by more than 30.0%. This would imply that 100% of 0.01 mg l^{-1} of DCE achieve the river. On the other hand, a flood event like HQ_{20} (2001 – 2002) causes 92% influent conditions (8% groundwater exfiltration). In comparison to normal hydrological conditions, this is a water volume reduction of 30.0%. Consequently, only 40-50.0% of the pollutants would reach the surface water system. This example should point out that the calculated spatial probability isolines can be used to estimate the extent of pollutants for different scenarios. Such knowledge is a relevant factor in the field of this site characteristic groundwater risk assessment. The significance of this created numerical-stochastic model can be appointed as optimal because of its multi-attribute pre-processing.

Hence, it can be concluded that normal hydrological discharge years possess the trend of a high groundwater risk. In particular, drought hydrological years must be taken under observation due to the inversion of hydraulic gradients between contaminated aquifer and surface water body. In urban areas, a precautionary measure is installed by weirs with locks. Thus, a water management is appropriate to control the water levels.

Briefing of the new aspects of the thesis

The main focus of this present work was a development of more effective ways to constraint multi-species transport models to enhance their accuracy for an application in the risk assessment framework. This involves new kinds of collected field data (aspect 1, cf. chapter 4). For example, the Hydraulic Profiling Technique was used to validate the assumed hydraulic conductivity values of the homogeneous and heterogeneous model. An understanding of the measurement relevant was taken into account through groundwater level -, recharge- and river water level measurements. This was necessary to understand the system-relevant processes of the investigation.

In addition, information like geo-stochastic generated parameter fields by use of a Sequential Indicator Simulation perfected the geological and hydro-geological interpretation. This type of parameter estimation is an important part of the overall monitoring process and should be given proper consideration (Shlomi, 2010). These parameter fields were used to identify uncertainties in the aquifer reconstruction and furthermore they were applied to formulate the hydro-geological structure model, subsurface stress and strain fields. All measured and observed data were integrated into the numerical multi-species transport model to evaluate the exposure of the pathway (aspect 2, cf. chapter 5).

This work shows that the utilization of a MCs were expedient in the field of generating spco isolines which leads into risk characterization (aspect 4, cf. chapter 5.3). The resulted probability isolines reveal that the bordering ecosystems (receptor) are under risk in the near future.

Risk assessment integration

The present thesis can be accepted as a feasible instrument for a groundwater risk assessment contribution based on the probability estimation. Through a systematical application of field investigations and time-series analysis a conclusive multi-species transport model for predicting contamination hotspots was developed. Based on high parameter identification and computational efforts an accurate risk identification by spco isonlines were performed. Interaction analysis of different hydro-systems is of particular importance due to their diversity hydraulics conditions. Therefore, an understanding of the coupled hydro-systems was essential to comprehend the temporal interaction by use of external groundwater-surface water coupling. A decisive point in this regard is an identification of contamination mobilization by water level increase or decrease. Due to this fact, the gained knowledge of the hydrograph analysis must be mentioned just as the detailed hydraulic and lithological subsurface characterization by the HPT technique of a downscaled part of the

investigation area. The numerical simulations of the spco isolines precisely represent that the dynamics and the hydraulics are non-neglected factors at a regional observation scale. Dynamical impacts contributed a major proportion to the pollutant exchange. The risk analysis of this case study has shown that the pollution dispersal is determined by the characteristic site hydraulics. Nonetheless, the reaction kinetics had to be fitted. Further research has to be carried out in respect to parameter identification, because the pollutant transport models still exhibit research and development deficits at a regional site.

The groundwater-surface water studies have demonstrated that the hydraulic conditions have a significant impact on the pollutant dispersal behavior and the contaminant passage to the adjacent ecosystems (cf. figure 6-1). Not only the small-scale reaction kinetics are important for the contamination spread, but also the regional advective-convective transport processes, which are dominated by dynamic boundary conditions.

The researcher, in function as a risk assessment manager, was not interested in every detail of reaction process in the subsurface. Instead a robust solutions is presented, which provides a contributions for a groundwater risk assessment in terms of spatial probability of concentration occurrences.

The computed spco isolines are essential for numerous functions, such as groundwater monitoring, regional pollutant mass estimation, parameter estimation and contaminant source identification. Nevertheless, the prognosticated spco isolines of selected pollutants present a practical and executable indicator for a groundwater risk identification. Those allow, like in the present case study, a development of an effective remediation strategy. An explicit representation of the contamination plume spread is crucial to monitoring the groundwater quality, calculating the extent of groundwater pollutant and planning effective site characteristic remediation strategies.

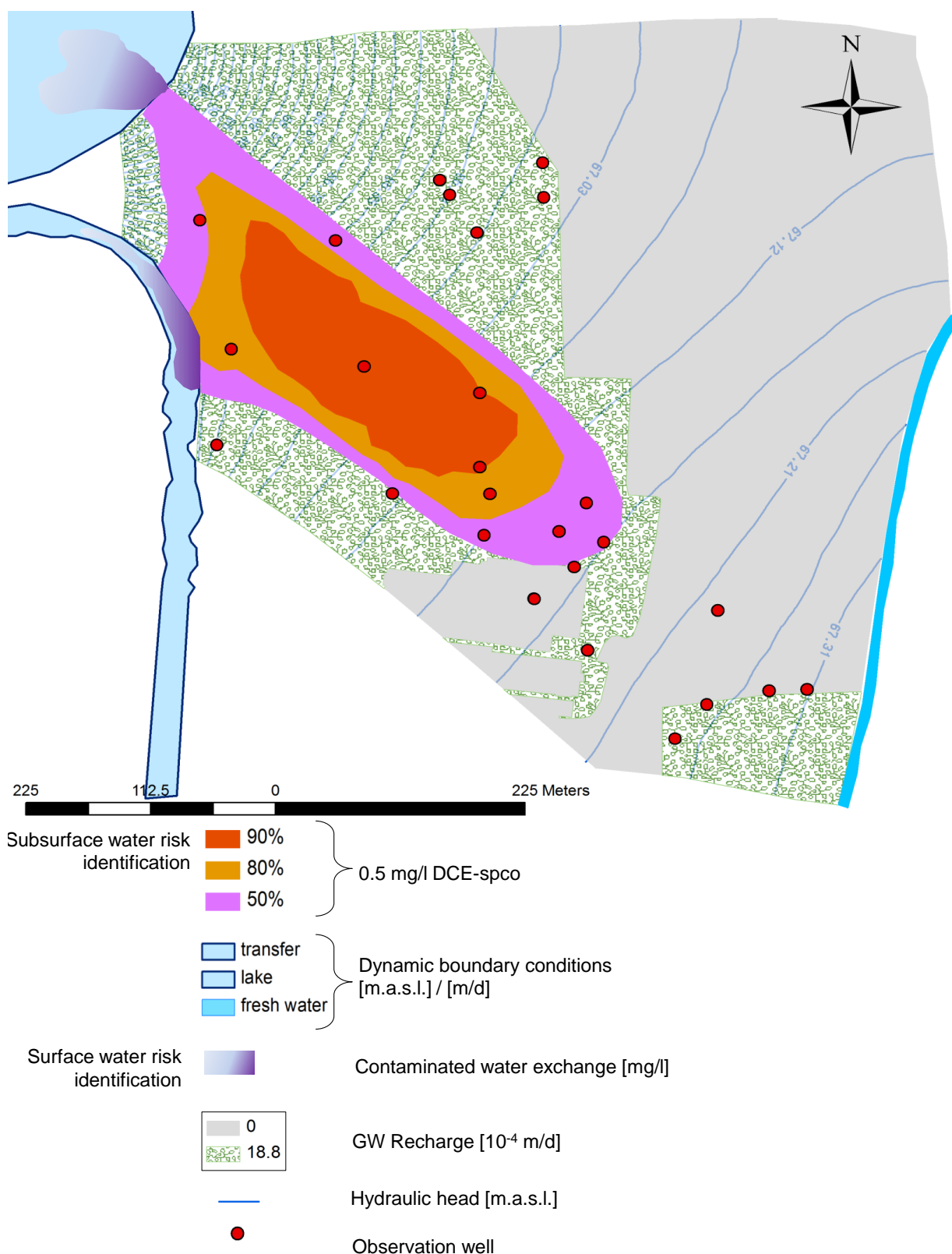


Figure 6-1 Evaluation of spatial probability of 0.5 mg/l DCE concentration occurrences for an advective transport to adjacent hydrosystems based on a Monte Carlo simulation approach with different hydrological boundary conditions (b.c., cf. chapter 4.5) and temporal & spatial assignment of groundwater recharge. Calibrated computed hydraulic heads with available observation wells.

7 List of Literature

- Abbot, M. B.; Refsgaard, J. C. (1996): Distributed hydrological modelling. Dordrecht: Kluwer (Water science and technology library, 22).
- Ad-Hoc-Arbeitsgruppe Boden der Geologischen Landesämter und der Bundesanstalt für Geowissenschaften und Rohstoffe der Bundesrepublik Deutschland; Bundesanstalt für Geowissenschaften und Rohstoffe (1996): Bodenkundliche Kartieranleitung. Mit 91 Tabellen. 4., verb. und erw. Stuttgart: Schweizerbart.
- Aeschbach-Herting, W. (2005/2006): Physika aquatischer Systeme I. Strömung und Transport im Grundwasser. Lehrmaterial, Universität Heidelberg. Umweltphysik.
- Alvarez-Cohen, L.; Speitel, G. E. Jr. (2001): Kinetics of aerobic cometabolism of chlorinated solvents. In *Biodegradation* (12), pp. 105–126.
- Anderman, E. R.; Hill, M. C. (2003): MODFLOW-2000, The U.S. Geological Survey Modular Groundwater-Model-Documentation of Effective-Porosity Parameters in the Advective-Transport Observation (ADV2) Package.
- Andermann, E. R.; Hill, M. C. (2003): MODFLOW-2000, The U.S. Geological Survey modular ground-water-model-documentation of effective-porosity parameters in the advective-transport observation (ADV2) package. Edited by USGS science for a changing world. U.S. Department of Interior. Denver.
- Appelo, C. A. J.; Rolle, M. (2010): PHT3D: A Reactive Multicomponent Transport Model for Saturated Porous Media. In *Ground Water* 48 (5), pp. 627–632.
- Ataie-Ashtiani, B.; Lockington, D. A.; Volker, R. E. (1999): Truncation error in finite difference models for solute transport equation with first-order reaction. In *Journal of Contaminant Hydrology* 1999 (Vol. 35), pp. 409–428.
- Azizian, M.; Istok, J.; Semprini, L. (2007): Evaluation of the in-situ aerobic cometabolism of chlorinated ethenes by toluene-utilizing microorganisms using push–pull tests. In *Journal of Contaminant Hydrology* 90 (1-2), pp. 105–124.
- Baalousha, H. (2006): Groundwater pollution risk using a modified Latin hypercube sampling. In *Journal of Hydroinformatics* (08.3), pp. 223–234.
- Barlebo, H. C.; Hill, M. C.; Rosbjerg, D.; Jensen, K. H. (1998): Concentration Data and Dimensionality in Groundwater Models: Evaluation Using Inverse Modelling. In *Nordic Hydrology* 1998 (Vol. 29 No. 3), pp. 149–178.
- Bear, J.; Beljin, M. S.; Ross, R. R. (1992): Ground Water Issue. Fundamentals of ground-Water Modeling. EPA/540/S-92/005. Edited by EPA Environmental Protection Agency. Office of Research and Development. Washington, D.C.
- Becker, B. P. J. (2010): Zur gekoppelten numerischen Modellierung von unterirdischen Hochwasser. Dissertation. Technische Hochschule Aachen, Aachen. Fakultät für Bauingenieurwesen.
- Bekesi, G.; McConchie, J. (1999): Groundwater recharge modelling using the Monte Carlo technique, Manawatu region, New Zealand. In *Journal of Hydrology* 224 (3-4), pp. 137–148.
- Benekos, I. D.; Shoemaker, C. A.; Stedinger, J. R. (2007): Probabilistic risk and uncertainty analysis for bioremediation of four chlorinated ethenes in groundwater. In *Stochastic Environmental Research and Risk Assessment* 21 (4), pp. 375–390.

-
- Beven, K. (2007): Towards integrated environmental models of everywhere: uncertainty, data and modelling as a learning process. In *Hydrology & Earth System Sciences* 2007 (11(1)), pp. 460–467.
- Bierkens, Marc F. P.; Finke, Peter A.; Willigen, P. de (2000): Upscaling and downscaling methods for environmental research. Dordrecht: Kluwer Academic Publishers (Developments in plant and soil sciences, 88).
- Birk, M. D. (2006): Temporal variability of riverbed hydraulic conductivity at an induced infiltration site, southeast Ohio. Dissertation. Miami University, Oxford, Ohio. Institute of Environmental Sciences.
- Blaschke, A. P.; Steiner, K.-H.; Schmalfuss, R.; Gutknecht, D.; Sengschmitt, D. (2003): Clogging Processes in Hyporheic Interstices of an Impounded River, the Danube at Vienna, Austria. In *International Review of Hydrobiology*. 88 (34), pp. 397–413.
- Blasone, R-S. (2007): Parameter Estimation and Uncertainty Assessment in Hydrological Modelling. Dissertation. Technical University of Denmark, Kgs. Lyngby. Institute of Environmental Resources.
- Boeckenhauer, R. K.; Cox, D. D.; Ensor, K. B.; Bedient, P. B.; Holder, A. W. (2000): Statistical Estimation and Visualization of Ground-Water Contamination Data. EPA/600/R-00/034. Edited by Environmental Protection Agency. Office of Research and Development Washington DC.
- Bradley, P. M. (2000): Microbial degradation of chloroethenes in groundwater systems. In *Hydrogeology Journal* (8), pp. 104–111.
- Bright, J.; wang, F.; Close, M. (2002): Influence of the Amount of Available K Data on Uncertainty About Contaminant Transport Prediction. In *Ground Water* 2002 (Vol. 40, No. 5), pp. 529–534.
- Brown, J. D.; Heuvelink, G. B. M. (2007): The Data Uncertainty Engine (DUE): A software tool for assessing and simulating uncertain environmental variables. In *Computers & Geosciences* 2007 (33), pp. 172–190.
- Carroll, R. W.H; Pohll, G. M.; Hershey, R. L. (2009): An unconfined groundwater model of the Death Valley Regional Flow System and a comparison to its confined predecessor. In *Journal of Hydrology* 2009 (373), pp. 316–328.
- Carsel, R.; Jones, R. L.; Hanse, J. L.; Lamb, R. L.; Anderson, M. P. (1988): A simulation procedure for groundwater quality assessments of pesticides. In *Journal of Contaminant Hydrology* 2 (2), pp. 125–138.
- Christensen, F. M.; Andersen, O.; Duijim, N. J.; Harremoes, P. (2003): Risk terminology—a platform for common understanding and better communication. In *Journal of Hazardous Materials* 2003 (A103), pp. 181–203.
- Christensen, S; Rasmussen, K.R; Moller, K (1998): Prediction of Regional Ground Water Flow to Streams. In *Ground Water* 36 (2), pp. 351–360.
- Clement, T. P.; Johnson, C. D.; Sun, Y.; Klecka, G. M.; Bartlett, C. (2000): Natural attenuation of chlorinated ethene compounds: model development and field-scale application at the Dover site. In *Journal of Contaminant Hydrology* 2000 (42), pp. 113–140.
- Clement, T.P; Sun, Y; Hooker, B.S; Petersen, J.N (1998): Modeling Multispecies Reactive Transport in Ground Water. In *Ground Water Monitor Remediation* 18 (2), pp. 79–92.

- Council of Canadian Academies (2009): The Sustainable Management of Groundwater in Canada. Report of the Expert Panel on Groundwater.
- Dagan, G. (1984): Solute transport in heterogeneous porous formations. In *Journal of Fluid Mechanics*. 145 (-1), p. 151.
- Dagan, G. (1997): Subsurface flow and transport: a stochastic approach. Stochastic modeling of flow and transport: the broad perspective. Digitally printed 1. paperback version 2005. Cambridge: Cambridge University Press.
- Deutsch, C. V.; Journel, A. G. (1998): GSLIB: Geostatistical software library and user's guide. 2nd ed. New York, NY, Berlin: Oxford Univ. Press (Applied geostatistics series).
- DHI-Wasy GmbH (2010): IFMMIKE11 1.1 Coupling the groundwater model FEFLOW and the surface water model MIKE11. User Manual. DHI-Wasy GmbH.
- Diersch, H. (1988): Finite element modelling of recirculating density-driven saltwater intrusion processes in groundwater. In *Advances in Water Resources* 11 (1), pp. 25–43.
- Diersch, H. (1998): Coupled groundwater flow and transport: 2. Thermohaline and 3D convection systems. In *Advances in Water Resources* 21 (5), pp. 401–425.
- Diersch, H.-J. G. (2009): FEFLOW Finite Element Subsurface Flow & Transport Simulation System. White Papers Vol. I. Extended formulation of constraints for Cauchy-type (3rd kind) boundary conditions in FEFLOW. Berlin.
- Diersch, H.-J. G. (2009): FEFLOW Finite Element Subsurface Flow & Transport Simulation System. White Papers Vol. IV. Reactive multi-species transport. DHI-Wasy GmbH. Berlin.
- Diersch, H.-J.G. (2009): FEFLOW Finite Element Subsurface Flow & Transport Simulation System. White Papers Vol. I. The Petrov-Galerkin least square method (PGLS). Berlin.
- Diersch, H.-J.G. (2009): FEFLOW Finite Element Subsurface Flow & Transport simulation System. White Paper Vol. III. Berlin.
- Diersch, H.-J.G. (2009): FEFLOW Finite Element Subsurface Flow & Transport Simulation System. Reference Manual. WASY Software. Berlin.
- England, E.; Sparks, A.; Robinson, M. (1988): Geo—EAS (Geostatistical Environmental Assessment Software). In *Environmental Software* 1988, 1988 (2), pp. 70–75.
- Essaid, H. I.; Bekins, B. A. (1997): BIOMOC, A Multispecies Solute-Transport Model with Biodegradation. Water-resource investigation report. No. 97-4022. Edited by U.S. Geological Survey. Water Resource Division.
- Faunt, C. C.; Provost, A. M.; Hill, M. C.; Belcher, W. R. (2011): Comment on “An unconfined groundwater model of the Death Valley Regional Flow System and a comparison to its confined predecessor” by R.W.H. Carroll, G.M. Pohll and R.L. Hershey [*Journal of Hydrology* 373/3–4, pp. 316–328]. In *Journal of Hydrology* 2011 (397), pp. 306–309.
- Fergusom, C.; Darmendrail, D.; Freier, K.; Jensen, B. K.; Jensen, J.; Kasana, H. et al. (Eds.) (1998): Risk Assessment for Contaminated Sites in Europe. Volume 1. Scientific Basis. With assistance of LQM Press Nottingham.
- Fetter, C. W. (2001): Applied hydrogeology. 4th ed. Upper Saddle River, NJ: Prentice Hall.

-
- Feyen, L.; Caers, J. (2006): Quantifying geological uncertainty for flow and transport modeling in multi-modal heterogeneous formations. In *Advances in Water Resources* 2006 (29), pp. 912–929.
- Figueira, R.; Sousa, A. J.; Pacheco, A. M. G.; Catarino, F. (2001): Use of secondary in space-time statistics for biomonitoring studies of saline deposition. In *Environmetrics* 2001 (12), pp. 203–217.
- Fleckenstein, J.H.; Schmidt, C. (2009): Themenheft: Grundwasser-Oberflächenwasser-Interaktionen. In *Grundwasser* 14 (3), pp. 161–162.
- Flynn, S. J.; Löffler, F. E.; Tiedje, J. M. (2000): Microbial Community Changes Associated with a Shift from Reductive Dechlorination of PCE to Reductive Dechlorination of cis - DCE and VC. In *Environmental Science Technology* 34 (6), pp. 1056–1061.
- Fu, J.; Hernandez, J. G. (2009): Uncertainty assessment and data worth in groundwater flow and mass transport modeling using a blocking Markov chain Monte Carlo method. In *Journal of Hydrology* 364 (3-4), pp. 328–341.
- Gelhar, L. W.; Welty, C.; Rehfeldt, K. R. (1992): A Critical Review of Data on Field-Scale Dispersion in Aquifers. In *Water Resources Research* 1992 (Vol. 28), pp. 1955–1974.
- Geoprobe Systems (2007): Geoprobe Hydraulic Profiling Tool (HPT) System. Standard Operating Procedure. Technical Bulletin No. MK3137. Kejr. Inc.
- Gómez-Hernández, J.; Srivastava, R. M. (1990): ISIM3D: An ANSI-C three-dimensional multiple indicator conditional simulation program. In *Computers & Geosciences* 16 (4), pp. 395–440.
- Gómez-Hernández, J. J.; Wen, X. -H: Probabilistic assessment of travel times in groundwater modeling. In *Stochastic Hydrology Hydraulics* 8 (1), pp. 19–55.
- Goovaerts, P. (1997): *Geostatistics for natural resources evaluation*. New York: Oxford Univ. Press (Applied geostatistics series).
- Gorelick, S. M. (1997): *Subsurface flow and transport: a stochastic approach. Incorporating uncertainty into aquifer management models*. Digitally printed 1. paperback version 2005. Cambridge: Cambridge University Press.
- Grams, S. (2000): *Einsatz geostatistischer Verfahren zur Charakterisierung der Grundwasserbeschaffenheit im Bereich der Rieselfelder südlich Berlins*. Dissertation. TU Berlin, Berlin. Bauingenieurwesen und Angewandter Geowissenschaften.
- Grathwohl, P. (1992): Die molekulare Diffusion als limitierender Faktor. In *UWSF-Z Umweltchemie Ökotoxikologie* 4 (4), pp. 231–236.
- Greis, T. (2011): *Modelling Risk of Groundwater Contaminations in Urban Areas*. Dissertation. TU Braunschweig, Braunschweig. Institut für Bioverfahrenstechnik.
- Greis, T.; Helmholz, K.; Schöniger, H. M.; Haarstrick, A. (2011): Modelling of spatial contaminant probabilities of occurrence of chlorinated hydrocarbons in an urban aquifer. In *Environmental Monitoring Assessment* 2011 (published online), pp. 1–15.
- Gresho, P. M.; Lee, R. L.; Chan, S. T.; Sani, R. L. (1980): Solution of the time-dependent incompressible Navier-Stokes and Boussines equations using the Galerkin finite element method 1980, pp. 203–222.

- Guadagnini, A.; Riva, M.; Neumann, S. P. (2003): Three-dimensional steady state flow to a well in a randomly heterogeneous bounded aquifer. In *Water Resource. Research* 2003 (Vol. 39 (3)), pp. ,
- Gunduz, O.; Aral, M. (2005): River networks and groundwater flow: a simultaneous solution of a coupled system. In *Journal of Hydrology* 301 (1-4), pp. 216–234.
- Hansen, C. (2002): The application of optimization and stochastic methods to analytic transport modeling. Dissertation. Brigham Young University. Department of Civil and Environmental Engineering.
- Harter, T. (1998): Flow in unsaturated random porous media, nonlinear numerical analysis and comparison to analytical stochastic models. In *Advances in Water Resources* 22 (3), pp. 257–272.
- Hassan, A. (2003): A Validation Process for the Groundwater Flow and Transport Model of the Faultless Nuclear Test at Central Nevada Test Area. Nevada Site Office, Desert Research Institute. Las Vegas, Nevada.
- Hattermann, F. F. (1998): Generierung von räumlichen Parameterfeldern zur Grundwassersimulation im regionalen Maßstab in einem Grundwasser-Fördergebiet. Am Beispiel einer Landschaft im norddeutschen Pleistozän (Fuhrberger Feld). Diplomarbeit. TU Braunschweig, Braunschweig. Institut für Geographie und Geoökologie.
- Herrmann, A.; Schöniger, H. M. (1992): Application of Tracer Techniques to Water Balance Determination in Small Catchment Basins. In *Deutsche Gewässerkundliche Mitteilung* (3/4), pp. 94–107.
- Hölting, B.; Coldewey, W. G. (2005): Hydrogeologie. Einführung in die allgemeine und angewandte Hydrogeologie ; 69 Tabellen. 6., überarb. und erw. München: Elsevier Spektrum Akad. Verl.
- Huyakorn, P. S. (1977): Solution of steady-state, convective transport equation using an upwind finite element scheme. In *Applied Mathematical Modelling* 1977 (Vol.1), pp. 187–195,
- Istok, J. D. (1989): Groundwater modeling by the finite element method. Washington, D.C: American Geophysical Union (Water resources monograph, 13).
- Isukapalli, S. S.; Roy, A.; Georgopoulos, P. G. (1998): Stochastic Response Surface Methods (SRSMs) for Uncertainty Propagation: Application to Environmental and Biological Systems. In *Risk Analysis* 1998 (Vol. 18, No. 3), pp. 351–363.
- Jang, W.; Aral, M. M. (2005): Three-dimensional multiphase flow and multispecies transport model TechFlow. Edited by School of Civil and Environmental Engineering. Georgia Institute of Technology. Atlanta, Georgia.
- John, A. K. (2006): Dispersion in large scale permeable media. Dissertation. University of Texas at Austin, Austin, Texas. Department of Petroleum and Geosystems Engineering an.
- Johnson, C. D.; Truex, M. J.; Clement, T. P. (2006): Natural and Enhanced Attenuation of Chlorinated Solvents Using RT3D. Edited by Pacific Northeast National Laboratory. United States Department of Energy.
- Journel, A. G (1983): Nonparametric estimation of spatial distributions 1983, *Mathematical Geology*, Vol. 15, No. 3, pp. 445–468.

-
- Kinzelbach, W.; Siegfried, T. (2002): Conditional first-order second-moment method and its application to the quantification of uncertainty in groundwater modeling. In *Water Resources Research* 2002 (Vol. 38, No. 4), pp. 6-1 - 6-14.
- Kitanidis, P. K. (2003): Introduction to geostatistics. Applications to hydrogeology. Transferred to digital print. Cambridge: Cambridge Univ. Press.
- Koch, C.; Mettke, A.; Heyn, S. (2003/2004): Sanierung von Kippengrundwasser durch Neutralisation und Sulfatreduktion mittels in-situ-Reaktionswänden am Beispiel des Tagebausees Nordrandschlauch (Restseenkette Spreetal-Bluno) Rahmentechnologie. Schriftreihe Siedlungswasserwirtschaft und Umwelt / Rückbau-/Demontagvorhaben Plattenbauten, am Beispiel der Typenserie P2 ; Forschungsprojekt "Rückbau industrieller Bausubstanz-großformatige Betonelemente im ökologischen Kreislauf". Edited by Lehrstuhl Wassertechnik der Universität Cottbus. Cottbus: BTU Fachgruppe Bauliches Recycling (Heft 8).
- Kolditz, O.; Ratke, R.; Diersch, H.-J. G.; Zielke, W. (1998): Coupled groundwater flow and transport: 1. Verification of variable density flow and transport models. In *Advances in Water Resources* 21 (1), pp. 27–46.
- Kolyukhin, D.; Sabelfeld, K. (2005): Stochastic flow simulation in 3D porous media. In *Monte Carlo Methods and Applications* 11 (1), pp. 15–37.
- Krige, D. G. (1951): A statistical approach to some basic mine valuation problems on the Witwatersrand. In *Journal of the Chemical, Metallurgical and Mining Society of South Africa*, 1951, pp. 201–215.
- Lahkim, M. B.; Garcia, L. A. (1999): Stochastic Modeling of Exposure and Risk in a Contaminated Heterogeneous Aquifer. 1: Monte Carlo Uncertainty Analysis. In *Environmental Engineering Science* 16 (5), pp. 315–328.
- Landon, M. K.; Turco, M. J. (2007): Hydrogeologic Setting and Ground-Water Flow Simulations of the Eastern High Plains Regional Study Area, Nebraska. Edited by U.S. Geological Survey.
- Lawrence, A. R.; Macdonald, D. M. J.; Howard, A. G.; Barrett, M. H.; Pedley, S.; Ahmed, K. M.; Nalubega, M. (2001): Guidelines for Assessing the Risk to Groundwater from On-Site Sanitation. Commissioned report CR/01/142.
- Lege, T.; Kolditz, O.; Zielke, W. (1996): Strömungs- und Transportmodellierung. Berlin: Springer (BGR, Bundesanstalt für Geowissenschaften und Rohstoffe ; Bd. 2).
- Lemming, G.; Friis-Hansen, P.; Bjerg, P. L. (2010): Risk-based economic decision analysis of remediation options at a PCE-contaminated site. In *Journal of Environmental Management* 91 (5), pp. 1169–1182.
- Li, J. (2003): Development of an inexact environmental modeling system for the management on petroleum-contaminated sites. Dissertation. University of Regina, Regina. Faculty of Graduate Studies and Research in Partial Fulfillment of the Requirements.
- Ling, M.; Rifai, H. S.: Modeling Natural Attenuation with Source Control at a Chlorinated Solvents Dry Cleaner Site. In *Ground Water Monitoring & Remediation* 2007 (1), pp. 108–121.
- Maniak, U. (1997): Hydrologie und Wasserwirtschaft. Eine Einführung für Ingenieure. 4., überarb. und erw. Berlin: Springer.

- Mao, X.; Prommer, H.; Barry, D.A.; Langevin, C.D.; Panteleit, B.; Li, L. (2006): Three-dimensional model for multi-component reactive transport with variable density groundwater flow. In *Environmental Modelling & Software* 2006 (21), pp. 615–628.
- Marin, C. (1989): Monte Carlo analysis and Bayesian decision theory for assessing the effects of waste sites on groundwater, I: Theory. In *Journal of Contaminant Hydrology* 5 (1), pp. 1–13.
- Massmann, G.; Pekdeger, A.; Dünnebier, U.; Heberer, T.; Richter, D.; Sültenfuß, J.; Tosaki, Y. (2009): Hydrodynamische und hydrochemische Aspekte der anthropogen und natürlich induzierten Uferfiltration am Beispiel von Berlin/Brandenburg. In *Grundwasser* 14 (3), pp. 163–177.
- McKnight, U. S.; Funder, S. G.; Rasmussen, J. J.; Finkel, M.; Binning, P. J.; Bjerg, P. L. (2010): An integrated model for assessing the risk of TCE groundwater contamination to human receptors and surface water ecosystems. In *Ecological Engineering* 36 (9), pp. 1126–1137.
- Metherón, G. (1965): The theory of regionalized variables and its applications (Les Cahiers du Centre de Morphologie Mathématique de Fontainebleau): Masson et Cie Luisant-Chartres, impr. Durand.
- Monninkhoff, B. L. (Ed.) (2004): Kopplung von FEFLOW mit dem 1D-hydrodynamischen Modell MIKE11 (DHI). With assistance of DHI-Wasy GmbH und IDCED Umweltinstitut IWU e.V. International FEFLOW User Conference. Köln. DHI-Wasy GmbH.
- Monninkhoff, B. L.; Kernbach, K. (Eds.) (2006): Coupled surface water- groundwater modeling for planning of flood retention in the Lower Havel area. With assistance of DHI-Wasy GmbH. International FEFLOW User Conference, Berlin.
- Mulligan, C. N.; Yong, R. N. (2004): Natural attenuation of contaminated soils. In *Environment International* 30 (4), pp. 587–601.
- Nasiri, F.; Huang, G.; Fuller N. (2007): Prioritizing groundwater remediation policies: A fuzzy compatibility analysis decision aid. In *Journal of Environmental Management* 82 (1), pp. 13–23.
- Natarajan, N.; Suresh Kumar, G. (2010): Finite difference approach for modeling multispecies transport in porous media. In *International Journal of Engineering Science and Technology* 2010 (Vol. 2 (8)), pp. 3344–3350.
- Ndambuki, J. M.; Otieni, F. A. O.; Stroet, C. B. M.; Terlaky, T.; Veling, E. J. M. (2003): An efficient optimization method in groundwater resource management. In *South African Water Research Commission* 2003, 2003 (Vol. 4), pp. 359–364.
- Neuman, S. P.; di Federico, V. (2003): Multifaceted nature of hydrogeologic scaling and its interpretation. In *Geophysics* 41 (3).
- Nienstedt, D. P. (2011): Geostatistische Rekonstruktion eines urban geprägten Aquifers. Masterarbeit. TU Braunschweig, Braunschweig. Leichtweiß-Institut für Wasserbau.
- Noell, A. L. (2009): Estimation of Sequential Degradation Rate Coefficients for Chlorinated Ethenes. In *Journal of Hazardous* 2009 (13), p. 35.
- Panday, S.; Huyakorn, P. S. (2004): A fully coupled physically-based spatially-distributed model for evaluating surface/subsurface flow. In *Advances in Water Resources* 27 (4), pp. 361–382.

-
- Pannike, S.; Kölling, M.; Schulz, H. D.; Panteleit, B.; Reichling, J.; Scheps, V. (2006): Auswirkung hydrogeologischer Kenngrößen auf die Kältefahren von Erdwärmesondenanlagen in Lockersedimenten. In *Grundwasser-Zeitschrift der Fachsektion Hydrogeologie*, pp. 6–18.
- Partington, D.; Werner, A. D.; Brunner, P.; Simmons, C. T.; Dandy, G. C.; Maier, H. R. (Eds.) (2009): Using a fully coupled surface water-groundwater model to quantify streamflow components. 18th World IMACS/MODSIM Congress. Australia.
- Patelli, E. (2006): Monte Carlo simulation of radioactive contaminant transport in groundwater. Dissertation. Polytechnic of Milan University, Mailand. Department of Nuclear Engineering.
- Perrochet, P.; Diersch, H.-J. G. (2009): White Papers Vol. I. On the primary variable switching technique for simulating unsaturated-saturated flows. Berlin.
- Pickens, J. F.; Grisak, G. E. (1981): Scale-dependent dispersion in a stratified granular aquifer. In *Water Resource Research* 17 (4), p. 1191.
- Piwoni, M. D.; Keeley, J. W. (1990): Ground Water Issue. Basic Concepts of Contaminant Sorption at Hazardous Waste Sites. Edited by EPA Environmental Protection Agency. Office of Research and Development.
- Praamstra, T. F. (1996): The practice of in-situ remediation: biological delay of chlorinated ethenes in ground water. Concept Report IWACO B. V. West, The Netherlands.
- Prommer, H.; Barry, D. A.; Davis, G. B. (2002): Modelling of physical and reactive processes during biodegradation of a hydrocarbon plume under transient groundwater flow conditions. In *Journal of Contaminant Hydrology* 2002 (59), pp. 113–131.
- Rausch, R.; Schäfer, W.; Therrien, R.; Wagner, C. (2005): Solute transport modelling. An introduction to models and solution strategies. Vol. VI Berlin: Borntraeger Verlag.
- Refsgaard, J. C.; Van der Sluijs, J. P.; Højberg, A. L.; Vanrolleghem, P. A. (2007): Uncertainty in the environmental modelling process—A framework and guidance. In *Environmental Modelling & Software* 2007 (22), pp. 1543–1556.
- Riva, M.; Guadagnini, A.; Neuman, S. P.; Franzetti, S. (2001). Radial flow in a bounded randomly heterogeneous aquifer. In *Transport in Porous Media* 45 (1), pp. 139–193.
- Rushton, K. (2007): Representation in regional models of saturated river–aquifer interaction for gaining/losing rivers. In *Journal of Hydrology* 334 (1-2), pp. 262–281.
- Saito, H.; Goovaerts, P. (2001): Accounting for Source Location and Transport Direction into Geostatistical Prediction of Contaminants. In *Environmental Science Technology* 2001 (35), pp. 4823–4829.
- Schaerlaekens, J.; Mallants, D.; Simunek, J.; van Genuchten, M. Th.; Feyen, J. (1999): Numerical simulation of transport and sequential biodegradation of chlorinated aliphatic hydrocarbons using CHAIN_2D. In *Hydrological Processes* (13), pp. 2847–2859.
- Schafmeister, M.-T. (1999): Geostatistik für die hydrogeologische Praxis. Mit 17 Tabellen. Berlin: Springer Verlag.
- Schälchli, U. (1992): The clogging of coarse gravel river beds by fine sediment. In *Hydrobiologia* 235-236 (1), pp. 189–197.

- Scheibe, T. D.; Tartakovsky, A. M.; Tartakovsky, D. M.; Redden, G. D.; Meakin, P. (2007): Hybrid numerical methods for multiscale simulations of subsurface biogeochemical processes. In *Journal of Physics: Conf. Series* 78, p. 12063.
- Schubert, J. (2002): Hydraulic aspects of riverbank filtration-field studies. In *Journal of Hydrology* (266), pp. 145–161.
- Schulze-Makuch, D. (2005): Longitudinal dispersivity data and implications for scaling behavior. In *Ground Water* 43 (3), pp. 443–456.
- Serrano, S. (1992): Semianalytical methods in stochastic groundwater transport. In *Applied Mathematical Modelling* 16 (4), pp. 181–191.
- Shlomi, S. (2009): Combining Geostatistical Analysis and Flow-and-Transport Models to Improve Groundwater Contaminant Plume Estimation. Dissertation. University of Michigan, Michigan. Department of Environmental Engineering.
- Shrestha, S. P.; Loganathan, G. V (1994): Monte Carlo Simulation and Effective Medium Approximation in Subsurface Flow Modeling. In *Ground Water* 32 (6), pp. 929–936.
- Song, J.; Chen, X.; Cheng, C.; Wang, D.; Wang, W. (2010): Variability of streambed vertical hydraulic conductivity with depth along the Elkhorn River, Nebraska, USA. In *Chin. Sci. Bull* 55 (10), pp. 992–999.
- Sophocleous, M. (2002): Interactions between groundwater and surface water: the state of the science. In *Hydrogeology Journal* 10 (1), pp. 52–67.
- Spitz, K.; Moreno, J. (1996): A practical guide to groundwater and solute transport modeling. New York: Wiley Verlag
- Suter, G. W. (2007): Ecological risk assessment. 2nd edition. Boca Raton, Fla: CRC Press.
- Thangarajan, M.; Tiedeman, C. R.; Hill, M. C. (2007): Groundwater. Resource evaluation, augmentation, contamination, restoration, modeling and management. Model Calibration and Issues Related to Validation, Sensitivity Analysis, Post-audit, Uncertainty Evaluation and Assessment of Prediction Data Needs. Dordrecht: Springer.
- The Royal Society (1992): Risk: analysis, perception and management. London: Royal Society.
- Theis, H. J. (2005): Quantifizierung der Prognoseunsicherheiten bei der praktischen Anwendung numerischer Grundwassermodelle. Dissertation. TU Kaiserslautern, Kaiserslautern. Fachbereich Architektur/Raum- und Umweltplanung/Bauingenieurwesen.
- Troldborg, M. (2010): Risk assessment models and uncertainty estimation of groundwater contamination from point sources. Dissertation. Technical University of Denmark, Kgs. Lyngby. Department of Environmental Engineering.
- Vilhelmsen, T. N.; Christensen, S.; Mehl, S. W. (2011): Evaluation of MODFLOW-LGR in Connection with a Synthetic Regional-Scale Model. In *Ground Water*, pp. 1–15.
- Vovelle, F. (1986): EMPWI Monte-Carlo simulation of liquid water. In *Journal of Molecular Structure: THEOCHEM* 139 (1-2), pp. 1–12.
- Wang, M; Zheng, C (1997): Optimal Remediation Policy Selection under General Conditions. In *Ground Water* 35 (5), pp. 757–764.

-
- Wang, T.; McTernan, W. (2002): The development and application of a multilevel decision analysis model for the remediation of contaminated groundwater under uncertainty. In *Journal of Environmental Management* 2002 (64), pp. 221–235.
- Weatherill, D.; Simmons, C. T.; Voss, C. I.; Robinson, N. I. (2004): Testing density-dependent groundwater models: two-dimensional steady state unstable convection in infinite, finite and inclined porous layers. In *Advances in Water Resources*.
- Weber, K. C. (2002): Bilanzierung und Modellierung des BTEX-Austrages aus dem Grundwasser eines Gaswerkgeländes. Fakultät für Bio- und Geowissenschaften, Karlsruhe. Geologisches Institut.
- Webster, R.; Oliver, M. A. (2007): *Geostatistics for environmental scientists*. 2nd edition. Chichester: Wiley Verlag.
- Wiedermeier, T. H.; Swanson, M. A.; Moutoux, D. E.; Gordon, E. K.; Wilson, J. T.; Wilson, B. H. et al. (1998): Technical Protocol of Evaluating the Natural Attenuation of Chlorinated Solvents in Ground Water. Edited by United States Environmental Protection Agency. Office of Research and Development Washington DC.
- Wingle, W. L.; Poeter, E. P.; McKenna, S. A. (Eds.) (1997): *A Geostatistical Uncertainty Analysis Package Applied to Groundwater Flow and Contaminant Transport Modeling. UNCERT User's Guide (Version 1.16)*. Colorado School of Mines.
- Wouters, P.; Schaftingen, J. J. Van; Crochet, M. J.; Geyling, F. T (1987): Numerical simulation of the horizontal Bridgman growth. Part III: Calculation of the interface. In *International Journal for Numerical Methods in Fluids* 7 (2), pp. 131–153.
- Zadeh, L. A. (2005): Toward a generalized theory of uncertainty (GTU)—an outline. In *Information Sciences* 172 (1-2), pp. 1–40.
- Zairi, M.; Rouis, M. J (2000): Numerical and experimental simulation of pollutants migration in porous media. In *Bulletin of Engineering Geology and the Environment* 59 (3), pp. 231–238.
- Zheng, C. (1990): MT3D A Modular Three-Dimensional Transport Model for Simulation of Advection, Dispersion and Chemical Reaction of Contaminants in Groundwater systems. Edited by United States Environmental Protection Agency. Robert S. Kerr Environmental Research Laboratory. Ada, Oklahoma.
- Zheng, L.; Apps, J. A.; Zhang, Y.; Xu, T.; Birkholzer, J. T. (2008): Reactive Transport Simulations to Study Groundwater Quality Changes in Response to CO₂ Leakage from Deep Geological Storage. In *Physics Procedia* 2008 (published online).

Appendix

A Appendix Simulation settings of the different groundwater flow and transport models

Finite-Element flow and transport simulation types for the urban groundwater risk assessment

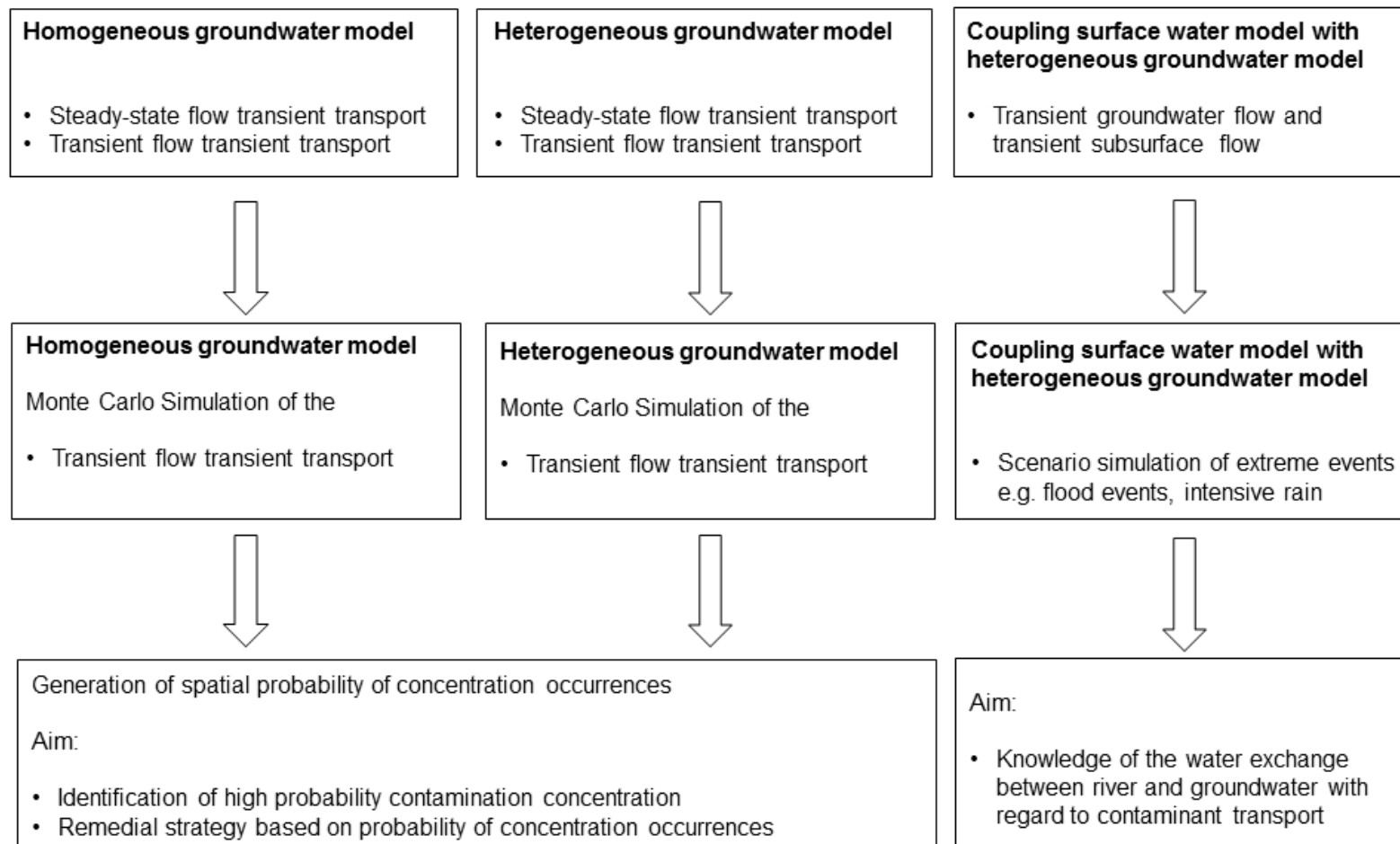


Table A-1 Model setup of the homogeneous steady-state flow transient transport groundwater model.

No.	Homogeneous steady-state flow transient transport model	options
1	type of simulation	3D steady flow and transient transport Multi-species transport for 6 species. Unconfined and saturated aquifer.
2	type of Finite Element generation	Triangle mesh generation algorithm. 6-noded triang. Prism Mesh elements: 502,801 Mesh nodes: 273,672
3	Iterative equation solver:	No upwinding (best-accurate Galerkin-based formulation).
4	Free surface treatment	Best adaption to stratigraphic data: free & movable surface definition. The top slice will simulate a free water table and therefore change its vertical position.
5	Hydro-geological treatment	Implementation of 10 layers. Layer definition based on borehole information. Regionalization of slice z-coordinates with Inverse Distance Interpolation Method.
6	Flow boundaries	1 st boundary condition (Dirichlet type): constant lake water table of 65.98 – 66.89 m.a.s.l for all slices at the west boundary border. 2 nd boundary condition (Neumann type): constant flux of -0.050046 md ⁻¹ for all slices at the east boundary border. Equivalent to an inflow of subsurface water at element faces. 3 rd boundary condition (Cauchy type): constant river water level of 66.83 m.a.s.l. for slice 1 – 3 at the west boundary border.
7	Flow materials	Hydraulic conductivity: A global Kf-value was set for each layer. Kf _{zz} amounts tenth part of Kf _{xx} and Kf _{yy} . Groundwater recharge: Performed with automatic parameter association. The attribute parameters are divided into free surface with a time constant data of 18.79 E-4 md ⁻¹ and a compacted area with 0 md ⁻¹ .

		<p>Storativity (drain/fillable): A global porosity for each geological material was set as a function of the hydraulic conductivity.</p> <p>Transfer rate (in/out): The hydraulic property of the clogging layer was set in slice 1 – 3. In and out rate was defined as $99.360001 \text{ E-4 } 1\text{d}^{-1}$.</p>
8	Biochemical treatment	Implementation of 6 species (PCE, TCE, DCE, VC, ethene and Cl) which are transported by advection and dispersion (fluid phase).
9	Transport boundaries	A fresh water condition with 0 mg l^{-1} of each species is defined at the east boundary border. A power-function for PCE was defined in layer 5 – 6. This represents a contamination in the 1970s.
10	Transport materials	<p>Porosity: A global value for each layer and each species was defined as 0.2779.</p> <p>Longitudinal dispersivity: Different values were set for each layer according to the geological material.</p> <p>Transversal dispersivity: Different values were set for each layer according to the geological material.</p> <p>Sorption: The sorption coefficient was defined for each species after HENRY.</p> <p>Multi-reaction rate: The reaction rate was defined for each species.</p> <p>Molecular diffusion: The molecular diffusion was set as a global value of $28.7216 \text{ E-9 } \text{m}^2\text{s}^{-1}$.</p> <p>Reaction equation: The degradation of the chlorinated hydrocarbons follows a first order law.</p>

Table A-2 Model setup of the heterogeneous steady-state flow and transient transport groundwater model.

No.	Heterogeneous steady-state flow transient transport model	options
1	type of simulation	3D steady flow and transient transport Multi-species transport for 6 species. Unconfined and saturated aquifer.
2	type of Finite Element generation	Triangle mesh generation algorithm. 6-noded triang. Prism Mesh elements: 502,801 Mesh nodes: 273,672
3	Iterative equation solver: Solver settings	No upwinding (best-accurate Galerkin-based formulation).
4	Free surface treatment	Best adaption to stratigraphic data: free & movable surface definition. The top slice will simulate a free water table and therefore change its vertical position.
5	Hydro-geological treatment	Implementation of 13 layers. Each layer has a thickness of 1 m. The topographic shape of the slices results from the DGM. A total aquifer thickness of 23 m is defined.
6	Flow boundaries	1 st boundary condition (Dirichlet type): constant lake water table of 65.98 – 66.89 m.a.s.l. for all slices at the west boundary border. 2 nd boundary condition (Neumann type): constant flux of $-0.050046 \text{ md}^{-1}$ for all slices at the east boundary border. Equivalent to an inflow of subsurface water at element faces. 3 rd boundary condition (Cauchy type): constant river water level of 66.83 m.a.s.l. for slice 1 – 3 at the west boundary border.
7	Flow materials	Hydraulic conductivity: The geo-stochastic generated $K_{f_{xx}}$ parameter fields were imported as trp.-files for each layer and regionalized by Inverse Distance Method. The $K_{f_{xx}}$ values were copied into y- and z-direction. Groundwater recharge: Performed with automatic parameter association. The attribute parameters

		<p>are divided into free surface with a time constant data of $18.79 \text{ E-4 md}^{-1}$ and a compacted area with 0 md^{-1}.</p> <p>Storativity (drain/fillable): The geo-stochastic generated porosity fields were imported as trp.-files for each layer and regionalized by Inverse Distance Method. The porosity values are a function of the hydraulic conductivity.</p> <p>Transfer rate (in/out): The hydraulic property of the clogging layer was set in slice 1 – 3. In and out rate was defined as $99.360001 \text{ E-4 1d}^{-1}$.</p>
8	Biochemical treatment	Implementation of 6 species (PCE, TCE, DCE, VC, ethene and Cl) which are transported by advection and dispersion (fluid phase).
9	Transport boundaries	A fresh water condition with 0 mg l^{-1} of each species is defined at the east boundary border. A power-function for PCE was defined in layer 7 – 10. This represents a contamination in the 1970s.
10	Transport materials	<p>Porosity: A global value for each layer and each species was defined as 0.2779.</p> <p>Longitudinal dispersivity: The geo-stochastic generated longitudinal dispersivity parameter fields were imported as trp.-files for each layer. The transformation of the long. dispersivity values was done according to the hydraulic conductivity.</p> <p>Transversal dispersivity: The geo-stochastic generated longitudinal dispersivity parameter fields were imported as trp.-files for each layer. The transformation of the long. dispersivity values was done according to the hydraulic conductivity.</p> <p>Sorption: The sorption coefficient was defined for each species after HENRY.</p> <p>Multi-reaction rate: The reaction rate was defined for each species.</p> <p>Molecular diffusion: The molecular diffusion was set as a global value of $28.7216 \text{ E-9 m}^2\text{s}^{-1}$.</p> <p>Reaction equation: The degradation of the chlorinated hydrocarbons follows a first order law.</p>

Table A-3 Model setup for the homogeneous transient flow transient transport groundwater model.

No.	Homogeneous transient flow transient transport model	options
1	type of simulation	3D steady flow and transient transport Multi-species transport for 6 species. Unconfined and saturated aquifer.
2	type of Finite Element generation	Triangle mesh generation algorithm. 6-noded triang. Prism Mesh elements: 502,801 Mesh nodes: 273,672
3	Iterative equation solver:	No upwinding (best-accurate Galerkin-based formulation).
4	Free surface treatment	Best adaption to stratigraphic data: free & movable surface definition. The top slice will simulate a free water table and therefore change its vertical position.
5	Hydro-geological treatment	Implementation of 10 layers. Layer definition based on borehole information. Regionalization of slice z-coordinates with Inverse Distance Interpolation Method.
6	Flow boundaries	1 st boundary condition (Dirichlet type): constant lake water table of 65.98 – 66.89 m.a.s.l for all slices at the west boundary border. 2 nd boundary condition (Neumann type) time-varying flux (12/11/09-12/11/10) for all slices at the east boundary border. Equivalent to an inflow of subsurface water at element faces. 3 rd boundary condition (Cauchy type): time-varying river water level (12/11/09–12/11/10) for slice 1 – 3 at the west boundary border.
7	Flow materials	Hydraulic conductivity: A global Kf-value was set for each layer. $K_{f_{zz}}$ amounts tenth part of $K_{f_{xx}}$ and $K_{f_{yy}}$. Groundwater recharge: Performed with automatic parameter association. The attribute parameters are divided into free surface with a time constant data of $18.79 \text{ E-4 md}^{-1}$ and a compacted area with 0 md^{-1} .

		<p>Storativity (drain/fillable): A global porosity for each geological material was set as a function of the hydraulic conductivity.</p> <p>Transfer rate (in/out): The hydraulic property of the clogging layer was set in slice 1 – 3. In and out rate was defined as $99.360001 \text{ E-4 } 1\text{d}^{-1}$.</p>
8	Biochemical treatment	Implementation of 6 species (PCE, TCE, DCE, VC, ethene and Cl) which are transported by advection and dispersion (fluid phase).
9	Transport boundaries	A fresh water condition with 0 mg l^{-1} of each species is defined at the east boundary border. A power-function for PCE was defined in layer 5 – 6. This represents a contamination in the 70ties.
10	Transport materials	<p>Porosity: A global value for each layer and each species was defined as 0.2779.</p> <p>Longitudinal dispersivity: Different values were set for each layer according to the geological material.</p> <p>Transversal dispersivity: Different values were set for each layer according to the geological material.</p> <p>Sorption: The sorption coefficient was defined for each species after HENRY.</p> <p>Multi-reaction rate: The reaction rate was defined for each species.</p> <p>Molecular diffusion: The molecular diffusion was set as a global value of $28.7216 \text{ E-9 } \text{m}^2\text{s}^{-1}$.</p> <p>Reaction equation: The degradation of the chlorinated hydrocarbons follows a first order law.</p>

Table A-4 Model setup of the heterogeneous transient flow transient transport groundwater model:

No.	Heterogeneous steady-state flow transient transport model	options
1	type of simulation	3D steady flow and transient transport Multi-species transport for 6 species. Unconfined and saturated aquifer.
2	type of Finite Element generation	Triangle mesh generation algorithm. 6-noded triang. Prism Mesh elements: 502.801 Mesh nodes: 273.672
3	Iterative equation solver: Solver settings	No upwinding (best-accurate Galerkin-based formulation).
4	Free surface treatment	Best adaption to stratigraphic data: free & movable surface definition. The top slice will simulate a free water table and therefore change its vertical position.
5	Hydro-geological treatment	Implementation of 13 layers. Each layer has a thickness of 1 m. The topographic shape of the slices results from the DGM. A total aquifer thickness of 23 m is defined.
6	Flow boundaries	1 st boundary condition (Dirichlet type): constant lake water table of 65.98 – 66.89 m.a.s.l for all slices at the west boundary border. 2 nd boundary condition (Neumann type) time-varying flux (12/11/09-12/11/10) for all slices at the east boundary border. Equivalent to an inflow of subsurface water at element faces. 3 rd boundary condition (Cauchy type): time-varying river water level (12/11/09–12/11/10) for slice 1 – 3 at the west boundary border.
7	Flow materials	Hydraulic conductivity: The geo-stochastic generated $K_{f_{xx}}$ parameter fields were imported as trp.-files for each layer and regionalized by Inverse Distance Method. The $K_{f_{xx}}$ values were copied into y- and z-direction. Groundwater recharge: Performed with automatic parameter association. The attribute parameters

		<p>are divided into free surface with a time constant data of $18.79 \text{ E-4 md}^{-1}$ and a compacted area with 0 md^{-1}.</p> <p>Storativity (drain/fillable): The geo-stochastic generated porosity fields were imported as trp.-files for each layer and regionalized by Inverse Distance Method. The porosity values are a function of the hydraulic conductivity.</p> <p>Transfer rate (in/out): The hydraulic property of the clogging layer was set in slice 1 – 3. In and out rate was defined as $99.360001 \text{ E-4 1d}^{-1}$.</p>
8	Biochemical treatment	Implementation of 6 species (PCE, TCE, DCE, VC, ethene and Cl) which are transported by advection and dispersion (fluid phase).
9	Transport boundaries	A fresh water condition with 0 mg l^{-1} of each species is defined at the east boundary border. A power-function for PCE was defined in layer 7 – 10. This represents a contamination in the 1970s.
10	Transport materials	<p>Porosity: A global value for each layer and each species was defined as 0.2779.</p> <p>Longitudinal dispersivity: The geo-stochastic generated longitudinal dispersivity parameter fields were imported as trp.-files for each layer. The transformation of the long. dispersivity values was done according to the hydraulic conductivity.</p> <p>Transversal dispersivity: The geo-stochastic generated longitudinal dispersivity parameter fields were imported as trp.-files for each layer. The transformation of the long. dispersivity values was done according to the hydraulic conductivity.</p> <p>Sorption: The sorption coefficient was defined for each species after HENRY.</p> <p>Multi-reaction rate: The reaction rate was defined for each species.</p> <p>Molecular diffusion: The molecular diffusion was set as a global value of $28.7216 \text{ E-9 m}^2\text{s}^{-1}$.</p> <p>Reaction equation: The degradation of the chlorinated hydrocarbons follows a first order law.</p>

Table A-5 Model setup of the transient surface water model

No.	Homogeneous steady-state flow transient transport model	options
1	type of simulation	3D steady flow and transient transport Multi-species transport for 6 species. Unconfined and saturated aquifer.
2	type of Finite Element generation	Triangle mesh generation algorithm. 6-noded triang. Prism Mesh elements: 502,801 Mesh nodes: 273,672
3	Iterative equation solver:	No upwinding (best-accurate Galerkin-based formulation).
4	Free surface treatment	Best adaption to stratigraphic data: free & movable surface definition. The top slice will simulate a free water table and therefore change its vertical position.
5	Hydro-geological treatment	Implementation of 10 layers. Layer definition based on borehole information. Regionalization of slice z-coordinates with Inverse Distance Interpolation Method.
6	Flow boundaries	1 st boundary condition (Dirichlet type): constant lake water table of 65.98 – 66.89 m.a.s.l for all slices at the west boundary border. 2 nd boundary condition (Neumann type): constant flux of -0.050046 md ⁻¹ for all slices at the east boundary border. Equivalent to an inflow of subsurface water at element faces. 3 rd boundary condition (Cauchy type): constant river water level of 66.83 m.a.s.l. for slice 1 – 3 at the west boundary border.
7	Flow materials	Hydraulic conductivity: A global Kf-value was set for each layer. Kf _{zz} amounts tenth part of Kf _{xx} and Kf _{yy} . Groundwater recharge: Performed with automatic parameter association. The attribute parameters are divided into free surface with a time constant data of 18.79 E-4 md ⁻¹ and a compacted area with 0 md ⁻¹ .

		<p>Storativity (drain/fillable): A global porosity for each geological material was set as a function of the hydraulic conductivity.</p> <p>Transfer rate (in/out): The hydraulic property of the clogging layer was set in slice 1 – 3. In and out rate was defined as $99.360001 \text{ E-4 } 1\text{d}^{-1}$.</p>
8	Biochemical treatment	Implementation of 6 species (PCE, TCE, DCE, VC, ethene and Cl) which are transported by advection and dispersion (fluid phase).
9	Transport boundaries	A fresh water condition with 0 mg l^{-1} of each species is defined at the east boundary border. A power-function for PCE was defined in layer 5 – 6. This represents a contamination in the 1970s.
10	Transport materials	<p>Porosity: A global value for each layer and each species was defined as 0.2779.</p> <p>Longitudinal dispersivity: Different values were set for each layer according to the geological material.</p> <p>Transversal dispersivity: Different values were set for each layer according to the geological material.</p> <p>Sorption: The sorption coefficient was defined for each species after HENRY.</p> <p>Multi-reaction rate: The reaction rate was defined for each species.</p> <p>Molecular diffusion: The molecular diffusion was set as a global value of $28.7216 \text{ E-9 } \text{m}^2\text{s}^{-1}$.</p> <p>Reaction equation: The degradation of the chlorinated hydrocarbons follows a first order law.</p>

PCE

TCE

DCE

VC

Figure A-1 First order degradation equation for the used species (PCE, TCE, DCE and VC) of the transport models. Implementation in the Finite Element program via a kinetic reaction editor.

$f(x) =$ **Reaction Kinetics** Ok Cancel Help

Degradation type kinetics, species 5 of 6.

$$R_5 = +k_1 \text{Rate}_1 C_1^{n_1} + k_2 \text{Rate}_2 C_2^{n_2} + k_3 \text{Rate}_3 C_3^{n_3} + k_4 \text{Rate}_4 C_4^{n_4} \\ + k_5 \text{Rate}_5 C_5^{n_5} + k_6 \text{Rate}_6 C_6^{n_6} + k_7 \text{Rate}_7 C_7^{n_7} + k_8 \text{Rate}_8 C_8^{n_8}$$

$k_1 = 0$	$n_1 = 1$
$k_2 = 0$	$n_2 = 1$
$k_3 = 0$	$n_3 = 1$
$k_4 = 0.4488$	$n_4 = 1$
$k_5 = 0$	$n_5 = 1$
$k_6 = 0$	$n_6 = 1$
$k_7 = 0$	$n_7 = 1$
$k_8 = 0$	$n_8 = 1$

ethene

$f(x) =$ **Reaction Kinetics** Ok Cancel Help

Degradation type kinetics, species 6 of 6.

$$R_6 = +k_1 \text{Rate}_1 C_1^{n_1} + k_2 \text{Rate}_2 C_2^{n_2} + k_3 \text{Rate}_3 C_3^{n_3} + k_4 \text{Rate}_4 C_4^{n_4} \\ + k_5 \text{Rate}_5 C_5^{n_5} + k_6 \text{Rate}_6 C_6^{n_6} + k_7 \text{Rate}_7 C_7^{n_7} + k_8 \text{Rate}_8 C_8^{n_8}$$

$k_1 = 0.20768$	$n_1 = 1$
$k_2 = 0.2622$	$n_2 = 1$
$k_3 = 0.3553$	$n_3 = 1$
$k_4 = 0.5512$	$n_4 = 1$
$k_5 = 0$	$n_5 = 1$
$k_6 = 0$	$n_6 = 1$
$k_7 = 0$	$n_7 = 1$
$k_8 = 0$	$n_8 = 1$

Cl

Figure A-2 First order degradation equation for the used species (ethane and Cl) of the transport models. Implementation in the Finite Element program via a kinetic reaction editor.

B Appendix Geostochastic reconstruction technique – theoretical background

B.1 Theory of the spatial-dependent variables

The spatial structure of soil and groundwater system properties is based on the theory of the spatial-dependent variables (*ReV*) (Schafmeister, 1999), (Grams, 2000). (Krige, 1951) used this theory, which was advanced by (Metherón, 1965), for the first time. All hydro-geological and pedological data are among to the spatial-dependent variables after (Schafmeister, 1999) because of the parameter varying affected by the location. The *ReV* is considered as a random variable Z_{x_i} which can receive values at a defined measure point x_i of an area D . These values are given by a probability function. Therefore, a realization is measured for the amount of the observed locations x_i . All existing random variables Z_{x_i} of the area are defined as random function ZF . It is not possible to generate more than one realization z_{x_i} of the random function $Z(x)$ at the same location x_i . Each random function is characterized by stationary criteria. (Schlittgen et al. 1999) differentiate a low and a strict stationary criterion. A low stationary criterion of a random function is given if the mean is independent of the location:

$$E Z(x) = m \quad \text{Eq. B-1}$$

E Mean

m Mean value

The covariance Cov has to be dependent on the distance to but not from the measure point:

$$Cov \ h = Z(x) \cdot Z(x+h) - m^2 \text{ for all } x \quad \text{Eq. B-2}$$

Cov Covariance

h Distance m

If the conditions of the low stationary criteria are complied, the semi-variogram can be used to calculate the spatial correlation (Goovaerts, 1997).

The simplified form of the low stationary criteria is the intrinsic hypothesis. Thereby, the mean of the first moment and the semi-variogram are independent of the location x .

A random function $Z(x)$ complies with the intrinsic hypothesis if the mean of the increments is zero:

$$E[Z(x+h) - Z(x)] = 0 \quad \text{Eq. B-3}$$

Furthermore, the increment has to exhibit a finite variance independent of zero for all distance vectors:

$$\text{Var}[Z(x+h) - Z(x)] = E[(Z(x+h) - Z(x))^2] = 2\gamma(h) \quad \text{Eq. B-4}$$

Var Variance

$\gamma(h)$ Semi-variogram function

B.2 Calculation of the spatial variance

The most frequently applied method for calculating the spatial variance is the computation of the experimental variogram (semi-variogram). The measured spatial-dependent variables were divided by a fixed distance h into pair of values $z(x_i), z(x_i + h)$. The available data were arranged into distance classes to provide an adequate data set (Grams, 2000). The semi-variogram is calculated according to equation B-5 (Schafmeister, 1999):

$$\gamma(h) = \frac{1}{2n(h)} \sum_{i=1}^{n(h)} [z(x_i) - z(x_i + h)]^2 \quad \text{Eq. B-5}$$

$N(h)$ Number of measured value with distance h

In addition to the distance h the maximal search-radius has to be defined. The amount and the length of the distance classes (lag distance) result from the quotient of the maximal search-radius and the distance h . The length of the first distance class relates to the semi distance length to include small scale variances. A definition of the search-parameter is necessary, too. Further parameters are the direction vector, bandwidth and the tolerance (Nienstedt, 2011). Several parameters are often used in calculation the experimental semi-variogram. These parameters are shown diagrammatically in figure B-1.

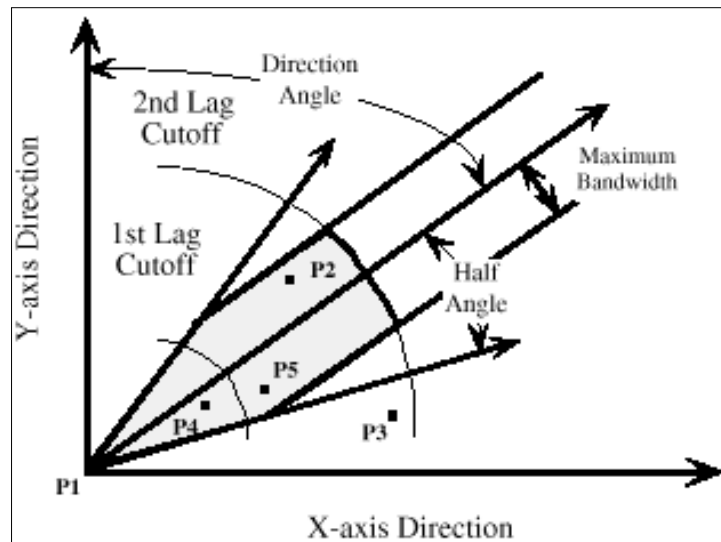


Figure B-1 Parameter used to calculate semi-variogram. Source: England et al. (1988).

Different model functions are available to determine the experimental semi-variogram which is defined by the range, sill and nugget. The model parameters require as input parameters for the SIS. The appropriate model function selection is based on the shape of the experimental semi-variogram. Common functions are spherical, Gaussian, and exponential (cf. figure B-2). A hole-effect model is used in special cases, when the samples exhibit a cyclic nature. When the nugget is less than about 10% of the variance, Gaussian models are typically unstable (Wingle et al., 1997).

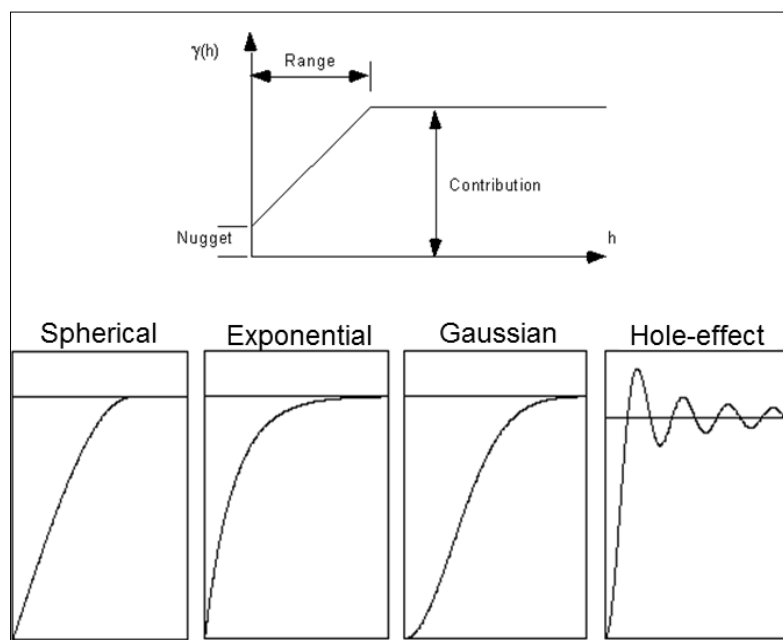


Figure B-2 Shape of the spherical, exponential, Gaussian and Hole-effect model equations. Source: (Wingle et al. 1997). Modified.

The spherical model is one of the most frequently used model function (Grams, 2000):

$$\gamma(h) = C \cdot \frac{3}{2} \cdot \frac{h}{a} - \frac{3}{2} \cdot \frac{h^3}{a^3} \text{ for } h \leq a \text{ or rather } \gamma(h) = C \text{ for } h \geq a \quad \text{Eq. B-6}$$

C Sill

a Range

The model function increases linear in the origin and reaches asymptotic in the range a the sill C .

The exponential model function continues curved near the origin and reaches the sill only asymptotically:

$$\gamma(h) = C \cdot 1 - \exp\left(-\frac{3h}{a}\right) \quad \text{Eq. B-7}$$

The Gaussian model function continues a parabolic trend and reaches the sill asymptotically. This model is used to describe a random function of variable with high spatial coherence:

$$\gamma(h) = C \cdot 1 - \exp\left(-\frac{3h^2}{a^2}\right) \quad \text{Eq. B-8}$$

The hole-effect model has a non-monotonic decay of the covariance function with distance:

$$\gamma(h) = C \cdot 1 - \frac{h}{a} \exp\left(-\frac{h}{a}\right) \quad \text{Eq. B-9}$$

B.3 Anisotropy

In general, variogram models were signified as isotropic but anisotropic conditions can be identified at the site. Anisotropy can simply be determined when experimental variograms are calculated with different spatial directions with a small angle of beam. Three-dimensional distributed data present a significant anisotropy in the majority of cases. A *geometric anisotropy* exists if the range of the variogram is varying in different space directions. Generally, the ranges of the vertically stratifications are smaller than the ranges of the horizontal stratification. (Schafmeister, 1999) propose the application of an upsetting or extending of the spatial coordinates to regard the geometric anisotropy. In case of an *affine anisotropy* the variogram shows different sills in different space directions. The application of a nested variogram enables the consideration of this type of anisotropy.

B.4 Histogram

The resulting set of frequencies constitutes the frequency distributions of the input parameter, and its graph is the histogram. The input parameter set will be divided into several classes and the number of individuals in each class is counted. The number of classes is influenced by the number of individuals and the spread of parameters (Webster

and Oliver, 2007). The data set which includes the number of measured realizations of a random variable is plotted with increasing order. The total interval is divided by the number m of points into fragment intervals which exhibit the same size. A realization of a random variable belongs to a specific fragment interval if (Kitanidis, 2003):

$$r_{s-1} \leq Z < r_s \quad \text{Eq. B-10}$$

r Points of a fragment interval
 s Fragment interval

B.5 Kriging technique

Kriging techniques are used to reproduce the temporal and spatial correlation structure of the variogram. This technique is applied to estimate the spatial-dependent variable as well as the determination of their reliability bound in form of a Kriging estimator standard deviation. A further important aspect is the consideration of the individual spatial arrangement of the monitoring network related to the interpolation mesh. The input data are implemented and reproduced according to their location in the interpolation mesh (Schafmeister, 1999).

The procedure of a conditioned SIS is presented in the following section and taken from (Kitanidis, 2003).

The Kriging estimator is simply a procedure that uses data to find a representative value. It represents a linear combination of weighted samples z_i from neighboring measuring points n .

$$z_0 = \sum_{i=1}^n \lambda_i z(x_i) \quad \text{Eq. B-11}$$

z_i Kriging estimator

λ_i Weighting factor

The Kriging estimator of the unknown parameter z_0 must fulfill the following condition:

- z_0 must be unbiased if $E z_0 - z_0 = 0$
- The root-mean-square error $E z_0 - z_0^2$ must be minimum

In consideration of a stationarity the mean is $E z x_i = m$ and for $z_0 = m$. Out of it, the unbiasedness is formulated as:

$$E \sum_{i=1}^n \lambda_i z x_i - z_0 = \sum_{i=1}^n \lambda_i m - m = m \sum_{i=1}^n \lambda_i - 1 = 0 \quad \text{Eq. B-12}$$

The result of equation B-12 is that the sum of the weights λ_i must be 1. The mean of the squared error can be expressed by the variogram:

$$E z_0 - z_0^2 = \text{Var } z_0 - z_0 = 2 \sum_{i=1}^n \lambda_i \gamma x_i - x_0 - \sum_{i=1}^n \sum_{j=1}^n \lambda_i \lambda_j \gamma(x_i - x_j) \quad \text{Eq. B-13}$$

The error variance can be minimized by use of a Lagrange-Multiplier. The function

$\varphi = \varphi(\lambda_1, \dots, \lambda_n, \mu)$ will be minimized instead of equation B-13. It is required that:

$$\varphi = \text{Var } z_0 - z_0 - 2\mu \sum_{i=1}^n \lambda_i - 1 \quad \text{Eq. B-14}$$

φ Langrange-Multiplicator

By equating the partial derivative to zero $\frac{\partial \varphi}{\partial \lambda_i}, i = 1, \dots, n$ and $\frac{\partial \varphi}{\partial \mu}$ the minimum is received. This results into a linear Kriging system of equation with +1 :

$$\sum_{j=1}^n \lambda_j \gamma(x_i - x_j) + \mu = \gamma(x_i - x_0) \text{ for } i=1,2,\dots,n \text{ with } \sum_{j=1}^N \lambda_j = 1 \quad \text{Eq. B-15}$$

The matrix of equation B-15 is written as follows:

$$\begin{bmatrix} \gamma(x_1 - x_1) & \gamma(x_1 - x_2) & \dots & \gamma(x_1 - x_n) & 1 \\ \gamma(x_2 - x_1) & \gamma(x_2 - x_2) & \dots & \gamma(x_2 - x_n) & 1 \\ \vdots & \vdots & \ddots & \vdots & \vdots \\ \gamma(x_n - x_1) & \gamma(x_n - x_2) & \dots & \gamma(x_n - x_n) & 1 \\ 1 & 1 & \dots & 1 & 1 \end{bmatrix} \cdot \begin{bmatrix} \lambda_1 \\ \lambda_2 \\ \vdots \\ \lambda_n \\ \mu \end{bmatrix} = \begin{bmatrix} \gamma(x_1 - x_0) \\ \gamma(x_2 - x_0) \\ \vdots \\ \gamma(x_n - x_0) \\ 1 \end{bmatrix} \quad \text{Eq. B-16}$$

It is applied: $\gamma(x_i - x_i) = \gamma(0) = 0$ in case of investigation of punctual distributed data. The result of the diagonal of the linear system of equations is zero.

B.6 Pre-processing of the data set

The drilling profiles of 35 groundwater wells were digitalized and indicator-coded related to their geological compound. The histogram shows the frequency distribution of the indicator classes.

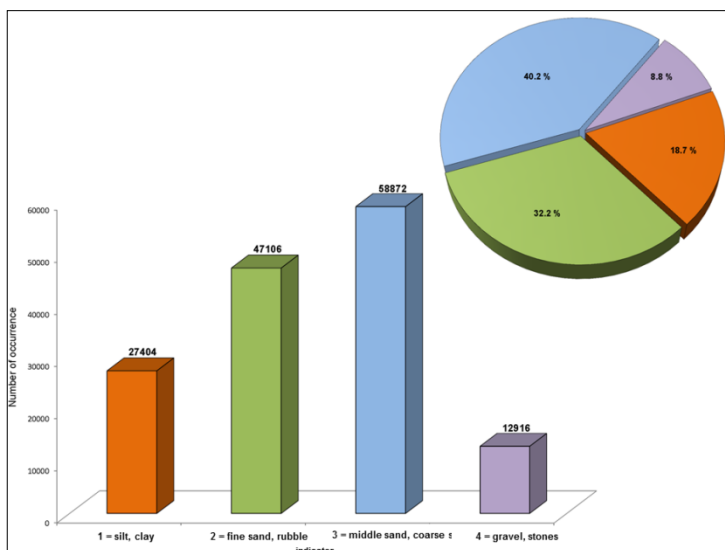


Figure B-3 Illustration of the histogram of the input parameter of indicator class.

The spatial correlation was determined by generating experimental variograms and the adaption of variogram functions (cf. chapter B.2). A variogram was calculated for each indicator in horizontal and vertical direction. The used geo-stochastic search-parameters are given in table B-1.

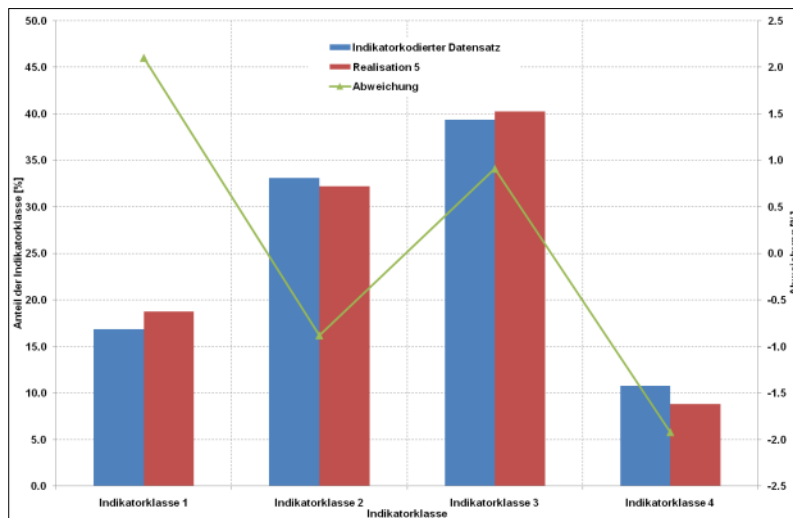


Figure B-4 Illustration of the histogram of the input data (blue) and the geo-stochastic generated realization number five (red) as well as the percentage deviation. Source: (Nienstedt 2011).

Figure B-4 shows the frequency distribution of the realization of the SIS and the frequency distribution of the original input parameters. The comparison of both histograms demonstrated that the frequency distribution of the original input data set is conserved during the SIS. The deviation amounts approx. two percent for the indicator

class 1 and 4, as well as ca. one percent for the indicator class 2 and 3. The cumulative frequency distribution of the original input parameter is integrated as input parameter during the SIS. The partial frequency distribution of the indicator-coded data set is given in table B-1.

Table B-1 Cumulative portion of the indicator classes of the original data set. Calculated by (Nienstedt 2011).

Indicator class	Cumulative portion [1]
1	0.17
2	0.5
3	0.89
4	1

Table B-2 Search-parameter for generating the experimental variogram of the geo-stochastic models. Investigated by (Nienstedt 2011).

Search-parameter	Horizontal variogram	Vertical variogram
Lag distance	60 m	2 m
Max search distance	600 m	20 m
Direction bandwidth	300 m	10 m
Plunge bandwidth	1 m	1 m
Hor. search direction	0°	0°
Vert. search direction	0°	90°
Hor. half-angle	90°	90°
Vert. half-angle	10°	90°

The distances of the adapted model function are used to calculate the anisotropy factor. The generation of the horizontal variograms in different space directions enables anisotropy

verification. The SIS was performed based on the calculated distances, sills and nuggets as well as the anisotropy factors. Furthermore, a definition of the interpolation mesh was necessary to limit the area where the geo-stochastic analysis is carried out. An area of 760 m x 770 m was selected on horizontal plane (cf. figure B-5).

The vertical extension of the interpolation mesh based on the digital terrain model (DTM) and the geological profile of the groundwater wells. The highest point of the DTM is located in the southeastern corner of the investigation area with an elevation of 77 m.a.s.l., the deepest point is located close to the lake in the north-western corner with an elevation of 66 m.a.s.l. An elevation-difference of 11 m is the result. The groundwater observation wells have different drilling depths, therefore the amount of available data for the Sequential Indicator Simulation is decreasing with increasing depth. Because of this fact, a depth of 53 m.a.s.l. was selected as the lowest limitation at the northwestern corner of the model area. In this depth 8 groundwater wells are still available. Moreover, this elevation value matches to the aquifer depth of the homogeneous model. The vertical discretization is carried out with a defined layer-thickness of 1 m. The layer-chronology was selected surface-parallel to the DTM.

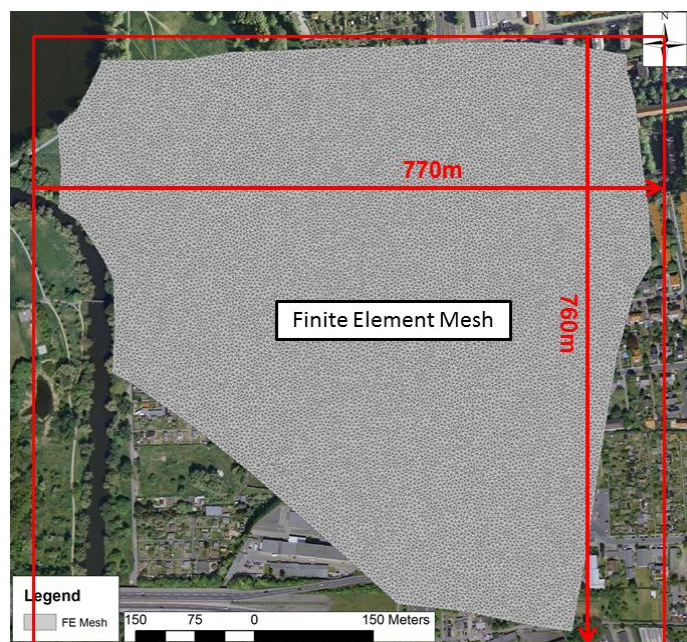


Figure B-5 Finite Element mesh of the investigation area and corresponding discretization of 770 m x 760 m of the geo-stochastic interpolation mesh.

Two experimental variograms were computed for each indicator (in horizontal and vertical direction, figure B-6 and figure B-7) to quantify the spatial correlation.

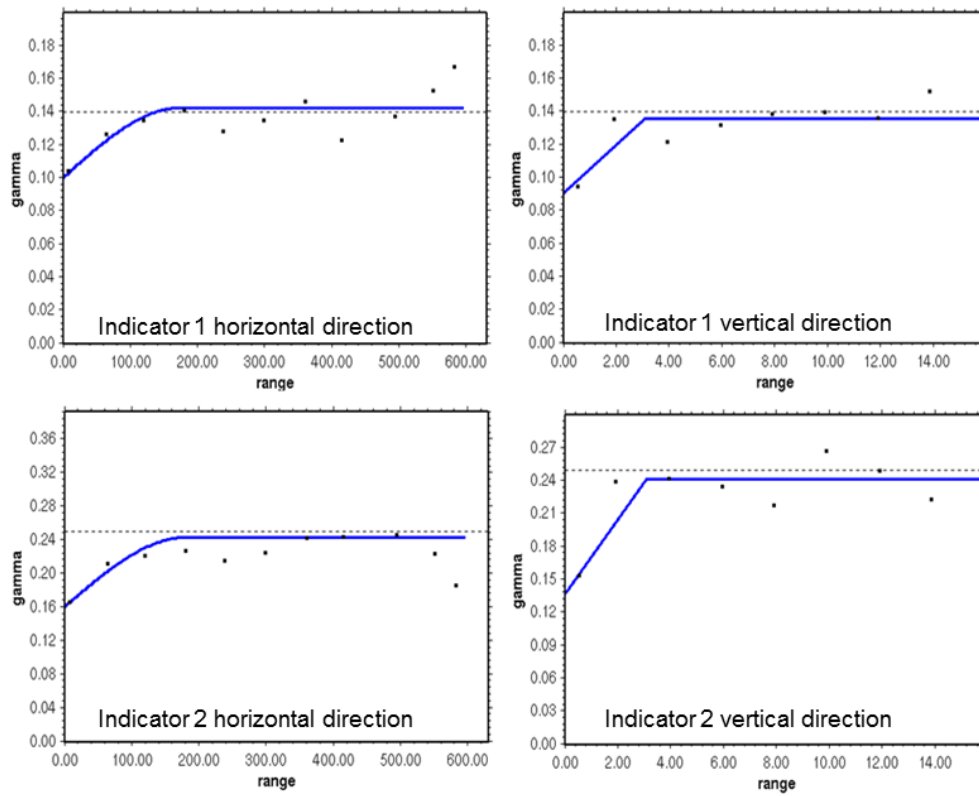


Figure B-6 Experimental indicator variogram in horizontal and vertical direction for indicator 1 and 2.

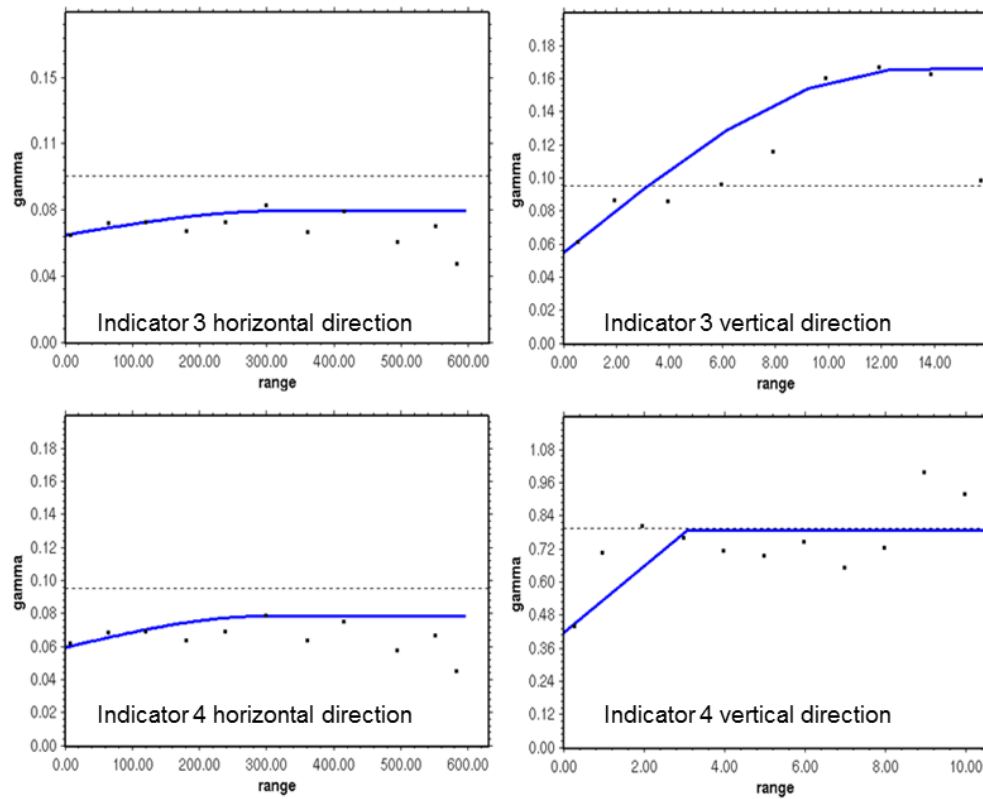


Figure B-7 Experimental indicator variogram in horizontal and vertical direction for indicator 3 and 4.

The same model function was used to calculate the anisotropy factor, which is integrated in the SIS. Table B-3 presents the adapted parameters of the variogram model.

Table B-3 Parameter of the adapted variogram model as well as the calculated mean-squared error and the anisotropy factor.

Indicator	Direction	Range	Sill	Nugget	MSE	Anisotropy factor
1	horizontal	174.0	0.04	0.10	$2.91 \cdot 10^{-4}$	116
	Vertical	1.5	0.04	0.09	$2.66 \cdot 10^{-4}$	
2	Horizontal	180.0	0.08	0.16	$1.30 \cdot 10^{-4}$	120
	Vertical	1.5	0.10	0.13	$4.60 \cdot 10^{-4}$	
3	Horizontal	324.0	0.01	0.06	$1.42 \cdot 10^{-4}$	25.3
	Vertical	12.8	0.11	0.05	$7.34 \cdot 10^{-4}$	
4	Horizontal	300.0	0.01	0.06	$1.89 \cdot 10^{-4}$	142.8
	Vertical	2.1	0.36	0.42	$9.84 \cdot 10^{-4}$	

Different initial values, which appropriate the grid cell where the SIS begins, were assigned for each realization. For each further simulation the values were added by 1001 the initial value of the first simulation was 1001. The fifth parameter realization was selected for the heterogeneous groundwater model.

100 realizations of a heterogeneous parameter field of the subsurface by use of the SIS were computed. The uncertainties of the probability of the indicator occurrence were generated from the 100 realization. Figure B-8 exhibits the percentage probability of occurrence of the most frequency generated indicator for each grid cell.

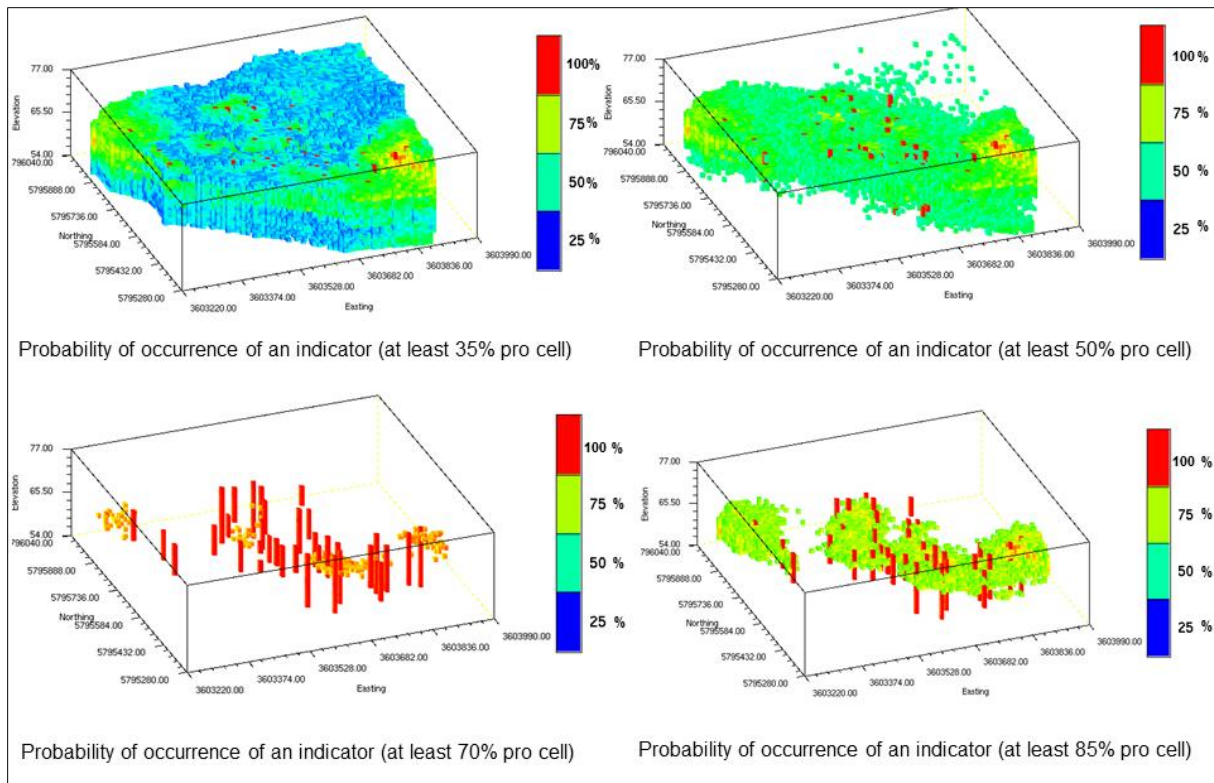


Figure B-8 *Probability of occurrence of the most frequency generated indicator pro grid element from 100 realizations for the range 35% up to 85%.*

The lower two pictures represent a high probability of indicator occurrence 70-85%. The probability of occurrences reveals that just a small part of the investigation area is acceptably reconstructed. The upper two pictures reflect an average and low probability of indicator occurrence. In consideration of the object target can be assumed that the subsurface parameter fields are sufficiently reconstructed.

Figure B-9 shows the probability of occurrence of the individual indicators based on 100 Monte Carlo simulations. A comparison of the indicator results shows that indicator 2 and 3 are mostly occurred. This corresponds to a medium up to a high substrate hydraulic conductivity.

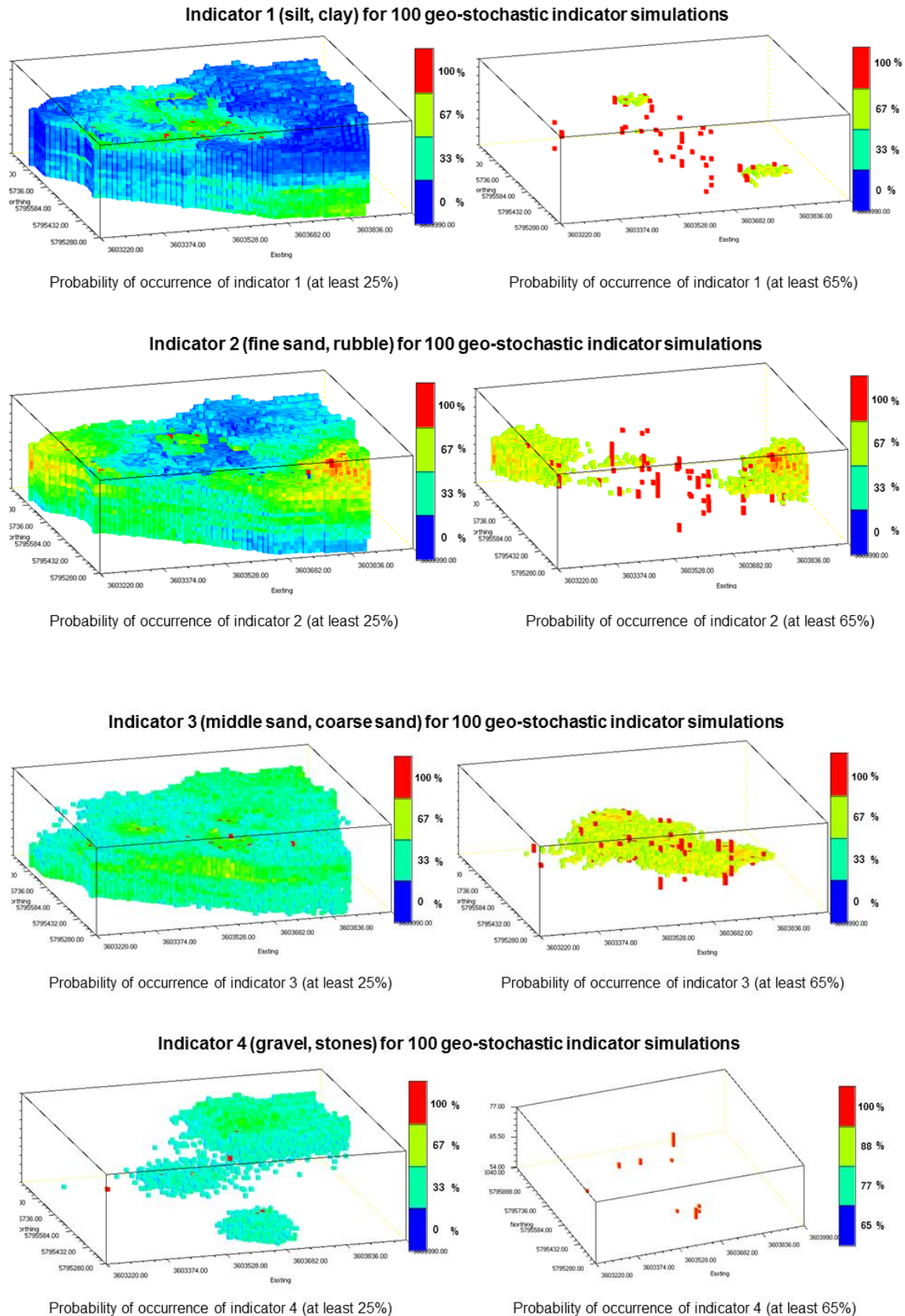


Figure B-9 Demonstration of the probability of indicator 1, 2, 3 and 4 from 100 Monte Carlo simulations with a probability of occurrence of at least 25% and at least 65%.

C Appendix Model scenario outputs of selected boundary conditions

C.1 Mass transport results of the steady-state flow and transient transport conditions

Figure C-1 presents the multi-species transport results for steady-state flow and transient transport condition of the homogeneous and heterogeneous subsurface models. The upper two pictures show the 0.5 mg/l^{-1} concentration isolines of PCE, TCE, DCE and VC for 70 years simulation time. The comparison of both model types shows that the pattern of the contaminant plume is approximately equal however the length of the homogeneous plume amounts to 262 m and of the heterogeneous plume to 288 m. Both plume types are expanded over the whole site and are directed to the bordering river. It can be observed that the 0.5 mg/l^{-1} PCE isoline of the homogeneous model is decomposed in the course of degradation.

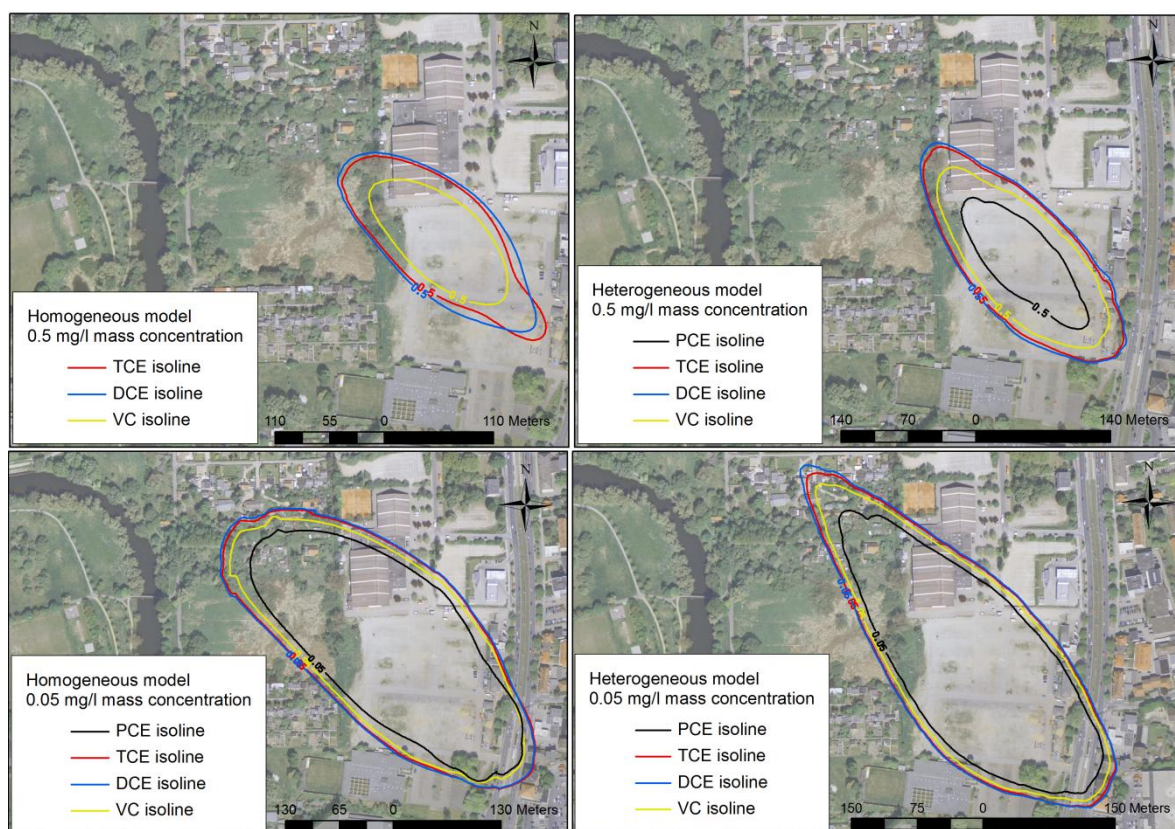


Figure C-1 Contaminant isolines (0.5 mg/l^{-1} and 0.05 mg/l^{-1}) of the homogeneous and heterogeneous steady-state flow and transient transport model for PCE, TCE, DCE and VC.

The lower two pictures present the 0.05 mg/l^{-1} concentration isolines of both models. In this case, the isoline pattern and the length differ from each other. The homogeneous plume amounts to 467 m and the heterogeneous to 508 m. In addition, the adjustments vary. The

homogeneous plume is directed to the river and the heterogeneous contamination streams northwards to the lake.

C.2 Mass transport results of the transient flow and transient transport conditions

Figure C-2 shows simulation results of the com 1.0 mg/l^{-1} concentration isolines of PCE, TCE, DCE and VC for the homogeneous and heterogeneous multi-species transport model after 50 a and 70 a simulation time. The upper two pictures present the results of the homogeneous aquifer. As it is shown the 1.0 mg/l^{-1} isolines are closed-formated with a length of 213 m and have the approx. equal pattern with the exception of VC with a length of 93 m and a smaller diameter as the other ones. After 50 a simulation time, only DCE and TCE still occurs with a concentration of 1.0 mg/l^{-1} . As it is noticeable the contamination plume is advanced and the width is reduced. The two lower pictures show the results of the heterogeneous aquifer. Different from the homogeneous model, the VC concentration of 1.0 mg/l^{-1} does not occur and the DCE isoline is larger than the isolines of PCE and TCE. The latter contaminant isolines have an extent of 187 m. DCE has a length of 421 m and is directed to the river. After 70 a simulation time, only 1.0 mg/l^{-1} of DCE is residual and the pattern of the isoline is modified in comparison the 50a simulation result. In this case, the contamination plume of DCE impacts the bordering lake and river as well as wide parts of the planted area.

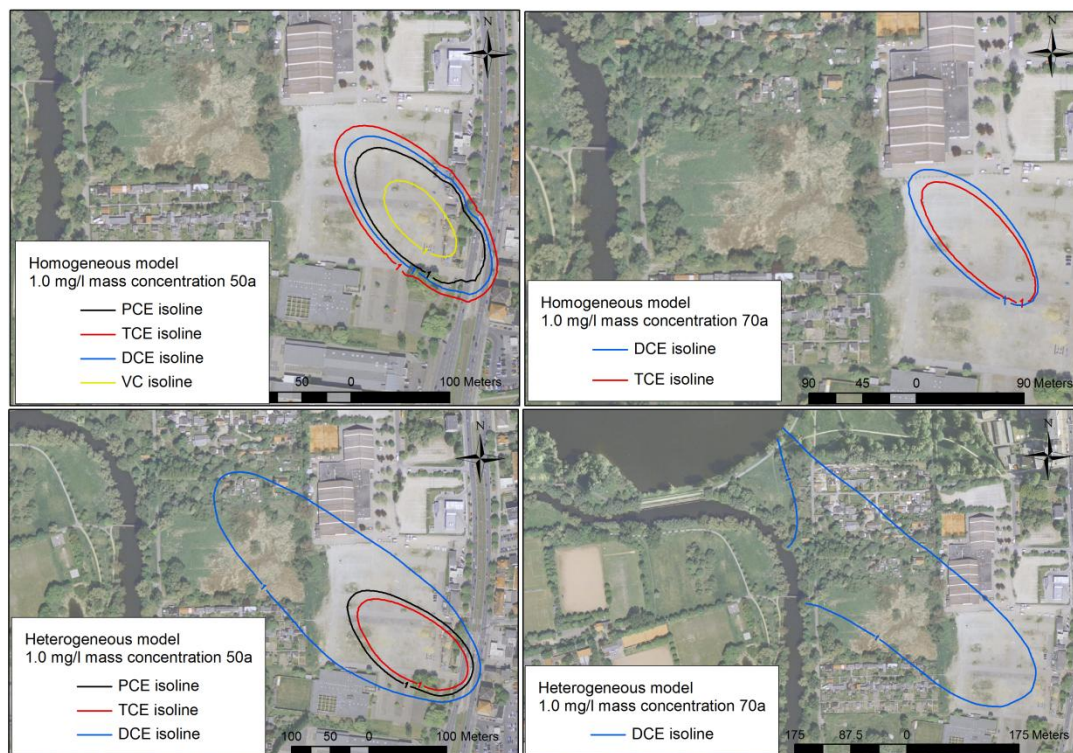


Figure C-2 Computed 1.0 mg/l^{-1} concentration isolines of the transient homogeneous and heterogeneous multi-species transport model for 50 a and 70 a simulation time.

Figure C-3 represents the 0.5 mg/l^{-1} mass concentration isolines of PCE, TCE, DCE and VC of the homogeneous and heterogeneous aquifers for 50 a and 70 a simulation time. The two upper images refer to the homogeneous multi-species transport model results. The left image presents the occurrence of 0.5 mg/l^{-1} after 50 years. As it is noticeable, all isolines are closed-located and have approx. the same shape and length of 263 m. An exception is VC with 180 m. After 70 years simulation time, the extent of VC and PCE differ in comparison to DCE and TCE. The latter two species have the same plume shape and length of 258 m. In contrary, VC has a length of 191 m and PCE is reduced to a length of 64 m. The two lower pictures document the 0.5 mg/l^{-1} isoline occurrences of the heterogeneous aquifer. Only PCE, TCE and DCE are shown after 50 years simulation time. PCE and DCE are calculated with the same length (216 m) and shape of isolines. DCE deviates from the other concentrations with a length of 484 m and a wider plume dimension. After 70 years simulation time, the PCE and TCE 0.5 mg/l^{-1} concentration is decreased to a length of 168 m for PCE and 116 m for TCE. In contrast, the contamination spread of 0.5 mg/l^{-1} of DCE is advanced in the length and width. It impacts the river, the lake and wide parts of the planted area.

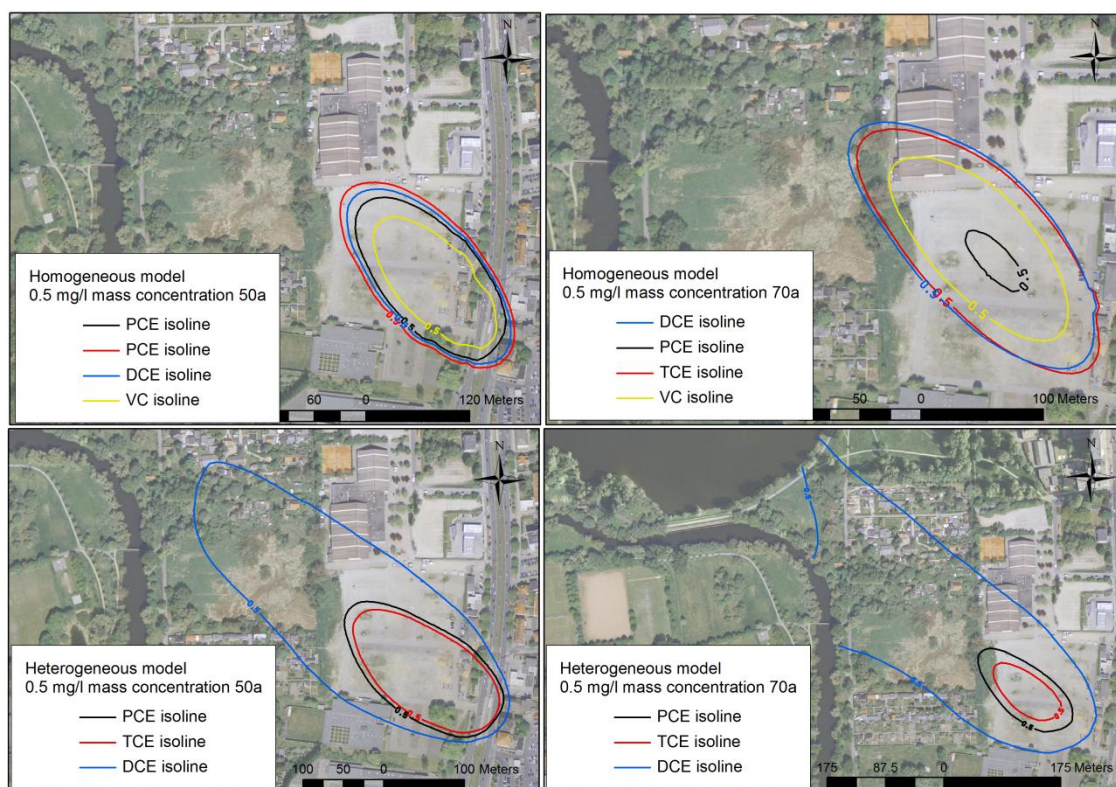


Figure C-3 Computed 0.5 mg/l^{-1} concentration isolines of the transient homogeneous and heterogeneous multi-species transport model for 50 a and 70 a simulation time.

Figure C-4 illustrates the 0.2 mg/l^{-1} mass concentration isolines of the homogeneous and heterogeneous aquifers after 50 a and 70 a simulation run. The upper images refer to the homogeneous multi-species transport model. As it is noticeable that the PCE, TCE, DCE and

VC isolines are closed-located and have an equal shape and length with approx. 312 m for PCE, TCE and DCE and 261 m for VC. After 70 years simulation time, the isolines differ from each other. DCE and TCE have an equal appearance in shape and length (375 m). The VC isoline is advanced of 320 m and PCE with 320 m. The lower images are related to the heterogeneous model. The 50 year simulation shows that PCE and TCE have approx. the same extent and length of 265 m. VC is spatially staggered to the other isolines and has a smaller extent of 142 m. The maximum spread is given by DCE with 560 m. After 70 years computation, the DCE 0.2 mg/l⁻¹ concentration isoline is advanced and connected with the river and lake as well as wide parts of the green area. PCE and TCE appear with the same length (276 m) and shape.

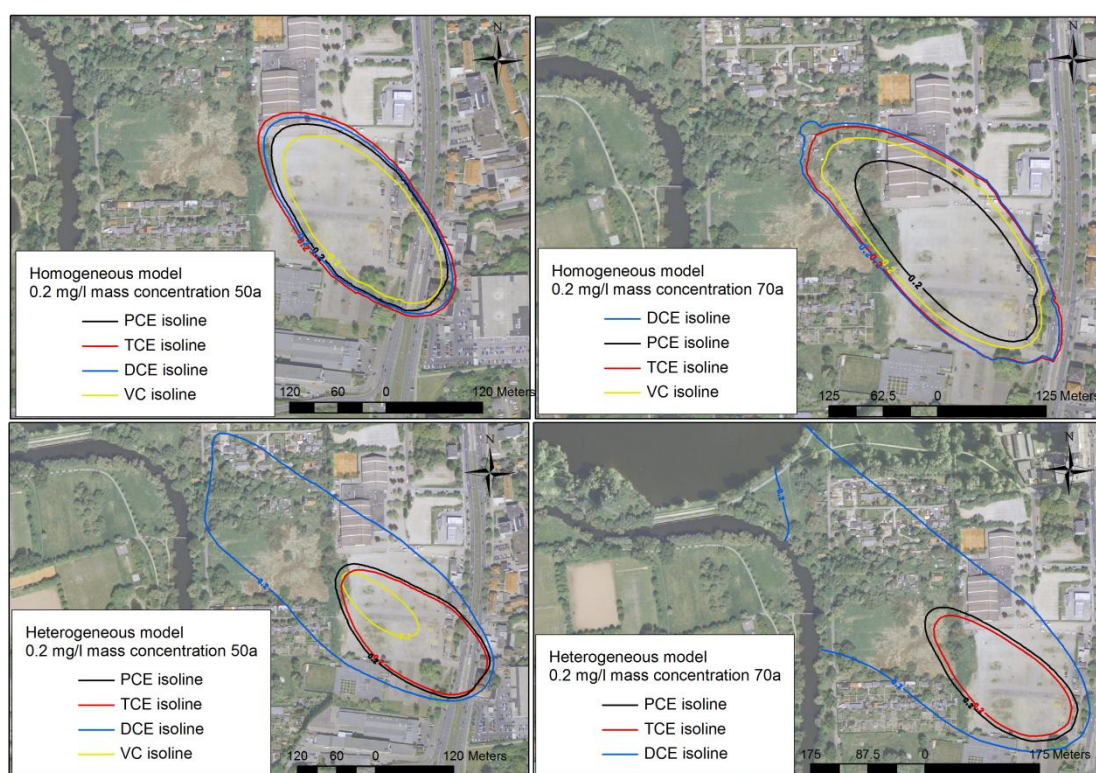


Figure C-4 Computed 0.02 mg/l⁻¹ concentration isolines of the transient homogeneous and heterogeneous multi-species transport model for 50 a and 70 a simulation time.

C.3 Results of the Monte Carlo simulation of the homogeneous aquifer

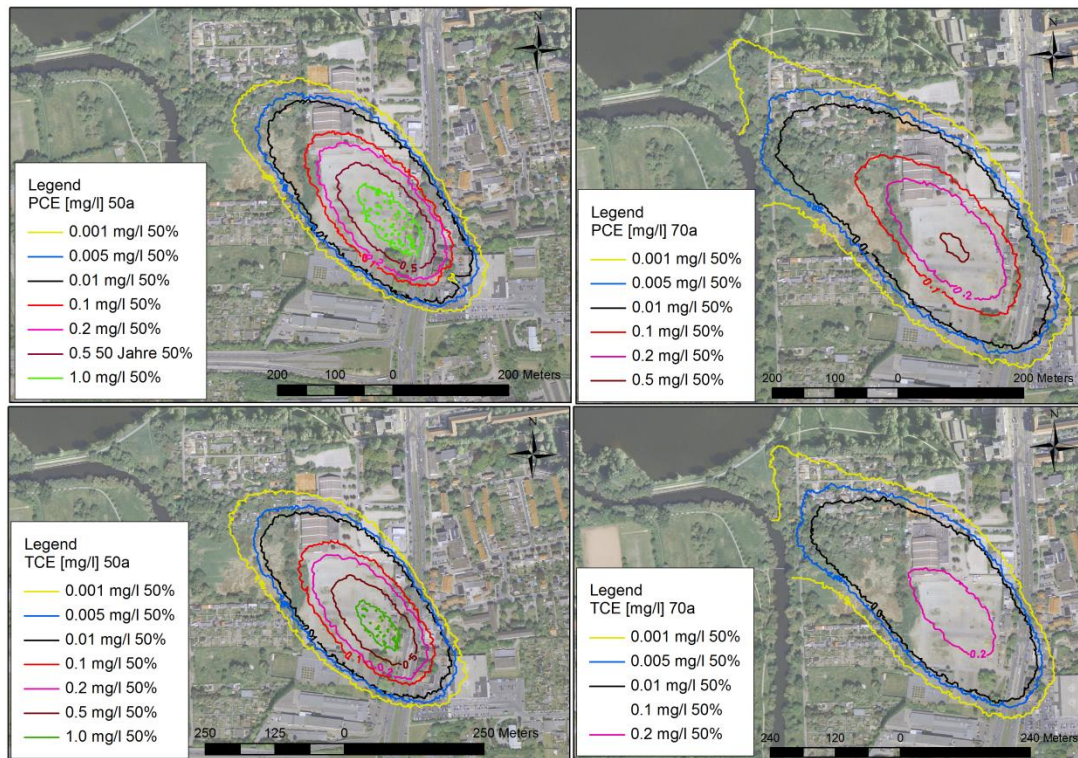


Figure C-5 Computed 50% PCE and TCE probability of concentration isoline of the homogeneous subsurface model of 50 a and 70 a simulation time based on a Monte Carlo simulation.

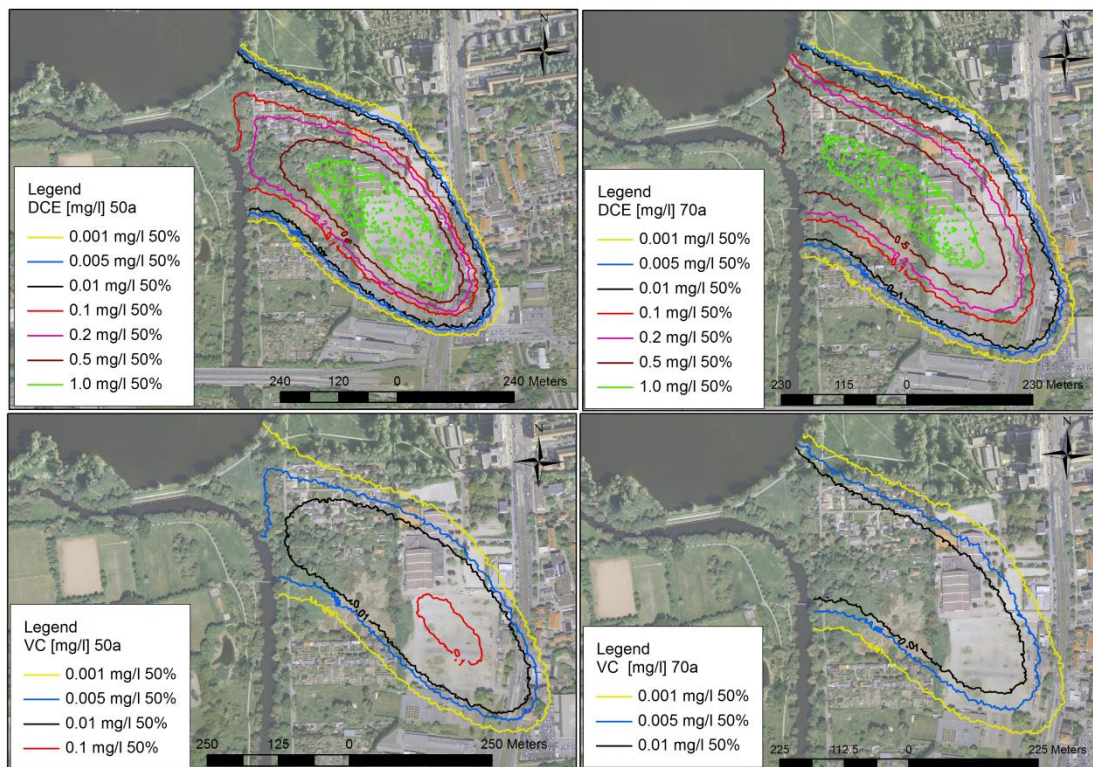


Figure C-6 Computed 50% DCE and VC probability of concentration isoline of the homogeneous subsurface model of 50 a and 70 a simulation time based on a Monte Carlo simulation.

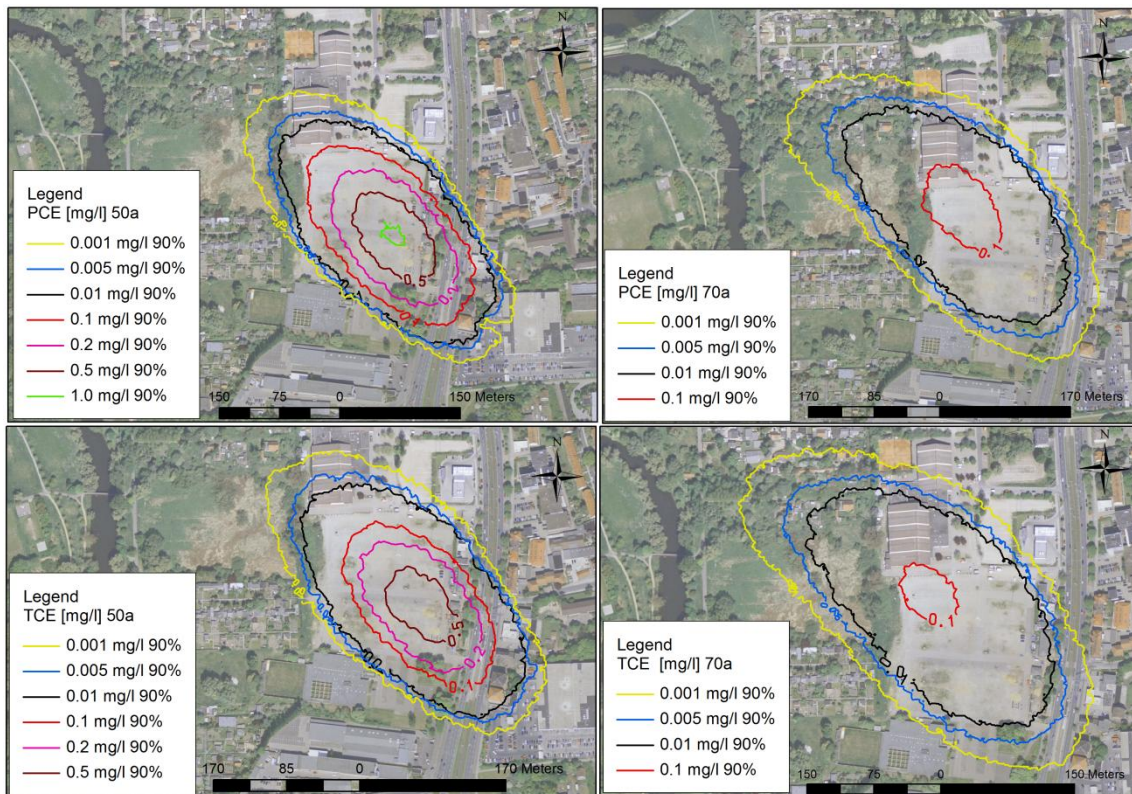


Figure C-7 Computed 90% PCE and TCE probability of concentration isoline of the homogeneous subsurface model of 50 a and 70 a simulation time based on a Monte Carlo simulation.

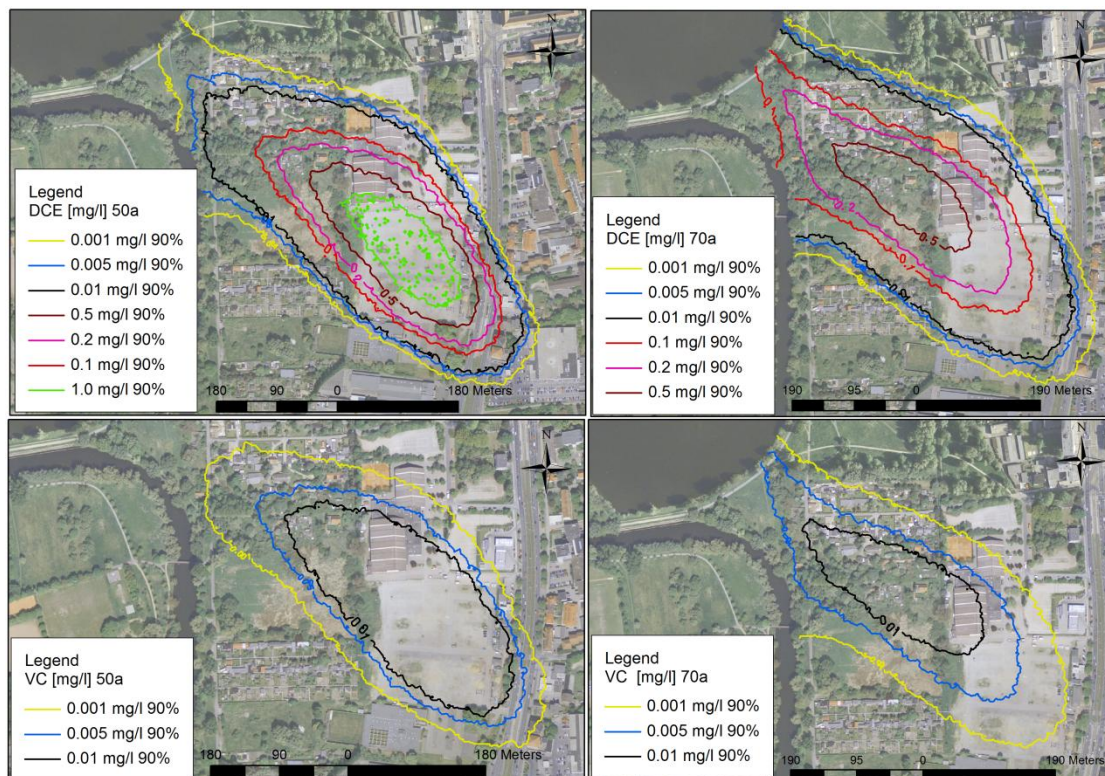


Figure C-8 Computed 90% DCE and VC probability of concentration isoline of the homogeneous subsurface model of 50 a and 70 a simulation time based on a Monte Carlo simulation.

C.4 Results of the Monte Carlo simulation of the heterogeneous aquifer

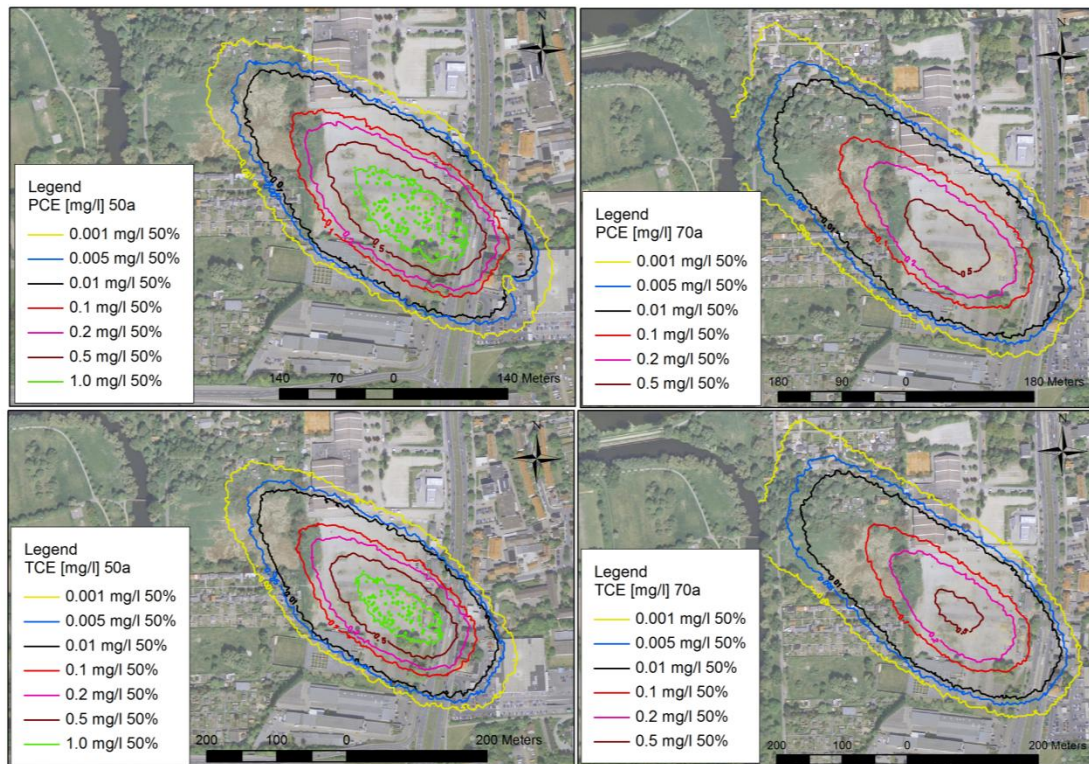


Figure C-9 Computed 50% PCE and TCE probability of concentration isoline of the heterogeneous subsurface model of 50 a and 70 a simulation time based on a Monte Carlo simulation.

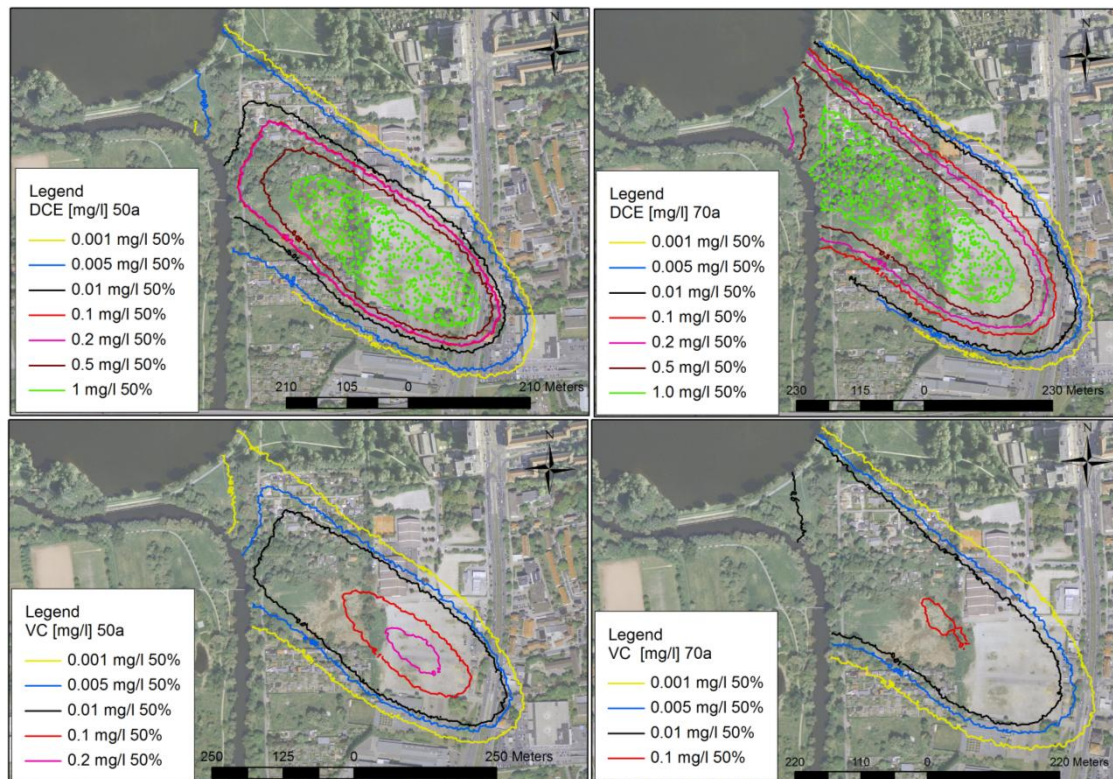


Figure C-10 Computed 50% DCE and VC probability of concentration isoline of the heterogeneous subsurface model of 50 a and 70 a simulation time based on a Monte Carlo simulation.

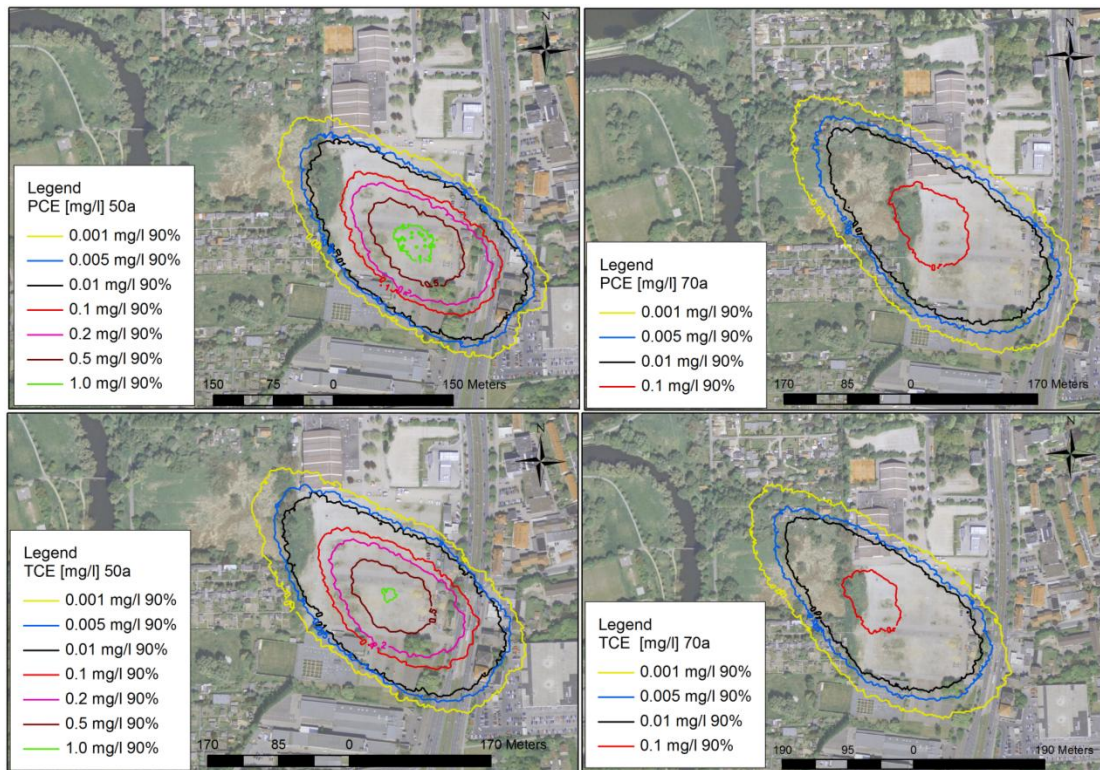


Figure C-11 Computed 90% PCE and TCE probability of concentration isoline of the heterogeneous subsurface model of 50 a and 70 a simulation time based on a Monte Carlo simulation.

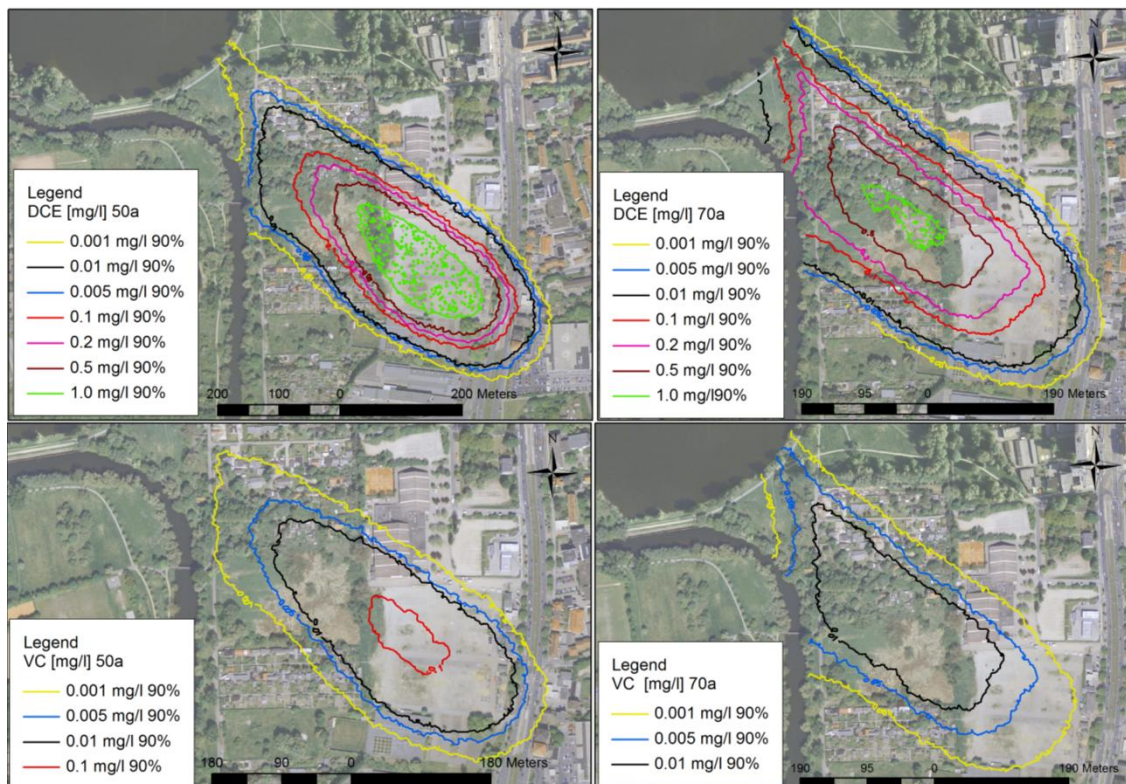


Figure C-12 Computed 90% DCE and VC probability of concentration isoline of the heterogeneous subsurface model of 50 a and 70 a simulation time based on a Monte Carlo simulation.